ISSN 2079-1372 *DOI: 10.31891/2079-1372*

THE INTERNATIONAL SCIENTIFIC JOURNAL

PROBLEMS OF TRIBOLOGY

Volume 31 ***No 2/120-2026***

МІЖНАРОДНИЙ НАУКОВИЙ ЖУРНАЛ

ПРОБЛЕМИ ТРИБОЛОГІЇ

PROBLEMS OF TRIBOLOGY

INTERNATIONAL SCIENTIFIC JOURNAL

Published since 1996, four time a year

Volume 31 No 2/120-2026

Establishers:

Khmelnytskyi National University (Ukraine)
Lublin University of Technology (Poland)

Associated establisher:
Vytautas Magnus University (Lithuania)

Editorial board address:
International scientific journal "Problems of Tribology",
Khmelnytskyi National University,
Instytutska str. 11, Khmelnytskyi, 29016, Ukraine
phone +380975546925

Indexed: CrossRef, DOAJ, Ulrichsweb, ASCI, Google Scholar, Index Copernicus

E-mail: tribology@khmnu.edu.ua

Internet: https://tribology.khmnu.edu.ua/

ПРОБЛЕМИ ТРИБОЛОГІЇ

МІЖНАРОДНИЙ НАУКОВИЙ ЖУРНАЛ

Видається з 1996 р. ***Виходить 4 рази на рік***

Том 31 **№ 2/120-2026**

Співзасновники:
Хмельницький національний університет (Україна)
Університет Люблінська Політехніка (Польща)

Асоційований співзасновник:

Університет Вітовта Великого (Литва)

Адреса редакції:
Україна, 29016, м. Хмельницький, вул. Інститутська 11, к. 4-401
Хмельницький національний університет, редакція журналу “Проблеми трибології”

тел. +380975546925, **E-mail**: tribology@khmnu.edu.ua

Internet: https://tribology.khmnu.edu.ua/

Зареєстровано Міністерством юстиції України
Свідоцтво про держреєстрацію друкованого ЗМІ: Серія КВ № 1917 від 14.03. 1996 р.
(перереєстрація № 24271-14111ПР від 22.10.2019 року)

Входить до переліку наукових фахових видань України
(Наказ Міністерства освіти і науки України № 612/07.05.19. Категорія Б)

Індексується в МНБ: CrossRef, DOAJ, Ulrichsweb, ASCI, Google Scholar, Index Copernicus

Рекомендовано до друку рішенням вченої ради ХНУ, протокол № 18 від 14.05.2026 р.

ISSN 2079-1372 Problems of Tribology, V. 31, No 2/120-2026

Problems of Tribology
Website: http://tribology.khnu.km.ua/index.php/ProbTrib
E-mail: tribosenator@gmail.com

CONTENTS

***ISSN 2079-1372 Problems of Tribology**, V. 31, No 2/120-2026*

Problems of Tribology
Website: http://tribology.khnu.km.ua/index.php/ProbTrib
E-mail: tribosenator@gmail.com

ЗМІСТ

ISSN 2079-1372 Problems of Tribology, V. 31, No 2/120-2026, 6-15

Problems of Tribology
Website: http://tribology.khnu.km.ua/index.php/ProbTrib
E-mail: tribosenator@gmail.com

DOI: https://doi.org/10.31891/2079-1372-2026-120-2-6-15

Kinetics of heterogeneous chemical reactions, initiated by metal deformation

V.V. Shevelya[0000-0002-5462-3524], **V.P. Oleksandrenko** *[0000-0002-2404-2104], **M.S. Stechyshyn** [0000-0001-5780-2790], **K.S. Sokolan** [0000-0002-3513-8312], **V.M. Fedoriv**[0000-0002-4499-0910], **Y.M. Nelyubin** [0009-0004-2579-158X]

Khmelnytskyi National University, Ukraine
**E-mail: oleksandrenkovp@khmnu.edu.ua*

Received: 20 March 2026: Revised 10 April 2026: Accept: 15 April 2026

Abstract

Topochemical processes in the air environment initiated by plastic deformation of the metal of various intensities and types were investigated : cyclic bending of the sample, rolling friction, sliding friction, cutting. It was established that during the cyclic loading of the metal, the concentration and composition of the air components in the test chamber change: a decrease in the content of the reagent - molecular oxygen and the appearance of the interaction product - hydrogen. The influence of the type of plastic deformation of the metal and the processes that occur during this on the kinetic dependences of the topochemical processes was revealed: damped, rectilinear and exponential. The dependence of the speed of topochemical processes on the intensity of plastic deformation was established. An indicator for assessing the competing effect of metal oxidation on the active centers of the surface subjected to plastic deformation was proposed. The results obtained reveal the nature of the friction and wear process and ways to increase the durability of friction units.

Keywords : topochemical reactions, kinetics, rate, plastic deformation, intensity, oxygen, hydrogen

Introduction

The widespread use of low-, medium-, and high-strength metals requires new nonlinear approaches to ensure their long-term strength, which take into account elastic-plastic deformation and physicochemical factors of the interaction of the environment with the stressed metal [1].

Deformation of a metal is its reaction to the influence of external mechanical forces. The external change in the shape and dimensions of a part made of metal is the result of a change in the arrangement of atoms, that is, the structure of a solid body during the development of deformation. Internal changes in the metal depend on the characteristics of its structure and the conditions of external mechanical loading. They can cause an increase or decrease in interatomic distances, and therefore a change in the shape and type of the crystal lattice , the nucleation, movement and propagation of structural defects: point, linear, coplanar [2,3,4]. Changes in the structure of the metal cannot but affect its structurally sensitive property - reactivity. First of all, this concerns reactions between the metal and components of the environment, which are heterogeneous, that is, those that occur at the interface of the phases: metal - gas medium (air), metal - liquid.

The initial components – metal and components of the environment that take part in the chemical interaction, the intensity of the reactions and the products that are formed in this process affect the formation of the long-term strength of metals [5,6]. The study of heterogeneous chemical reactions in the process of plastic deformation of metals and their influence on the long-term strength of metals is given considerable attention [1,7,8]: in the process of friction and wear, - in connection with the formation on the contacting conjugate surfaces of products of the interaction of the metal with oxygen in the surrounding air [9,10], and the development of hydrogen wear [11,12,13], under static and cyclic loads, - the influence of metal hydrogenation on its strength [14,15]. In most cases, the studies concern the qualitative analysis of products of heterogeneous chemical transformations: oxide films, metal hydrides by X-ray structural analysis, OGE spectroscopy, etc. , the presence of the release of gaseous components (primarily hydrogen ions) by mass spectrometric analysis. However, not enough attention is paid in scientific research to the measured, quantitative analysis of the presence and intensity of heterogeneous reactions that occur under the influence of deformation of metals with components of the

environment. In view of this, the aim of this work is to study the kinetics of topochemical reactions under the influence of various mechanical loads, which will allow to expand the understanding of the nature of chemical processes that are the response of a solid to its plastic deformation and the key to a controlled effect on the long-term strength of metals from the point of view of relaxation processes.

Equipment and Materials

During plastic deformation of a metal, conditions arise for the realization of its chemical interaction with the components of the surrounding environment. As a result of the course of heterogeneous chemical reactions, the composition of the environment will change - reactants will disappear and products will appear. By quantitative dependencies, one can judge the nature of the reactions, that is, study the mechanism of interaction of the environment with the metal during plastic deformation.

To ensure not only qualitative, but also quantitative control over the change in the content of environmental components due to their participation in chemical interaction with the activated solid, the unit in which the metal undergoes plastic deformation must be placed in an isolated, hermetic chamber .

To study the chemical processes that occur during plastic deformation of metal by bending, a device was manufactured (Fig. 1), consisting of a sealed chamber made of a vacuum rubber hose, which is closed at both ends by sample holders.

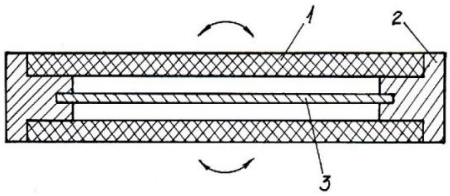

Fig. 1. Device for studying the kinetics of heterogeneous chemical reactions during cyclic bending of metal: 1 – chamber; 2 – sample holder; 3 – sample

The study of the change in the composition of the gas medium due to the course of chemical processes was carried out after a certain number of cycles of bending the sample. For this, an air sample was taken from the chamber using a medical syringe, which was used to pierce the wall of the vacuum hose. The selected sample of the gas medium was subjected to chromatographic analysis.

A common drawback of most friction machines is the lack of sealed chambers for housing the friction unit, which makes it impossible to study the physicochemical processes occurring between the surrounding environment and the contacting surfaces, to investigate the influence of gaseous media and gases dissolved in liquids on their tribotechnical properties.

To conduct studies of heterogeneous chemical reactions during friction, installations were used that allow testing under rolling and sliding friction conditions in a closed, hermetic volume (Fig. 2, 3) [1].

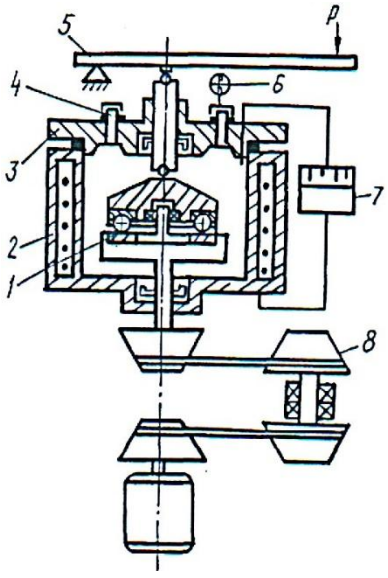

Fig. 2. Friction installation rolling : 1 – friction unit; 2 – chamber; 3 – cover; 4 – sampler; 5 – loading device; 6 – pressure gauge; 7 – temperature block; 8 – drive

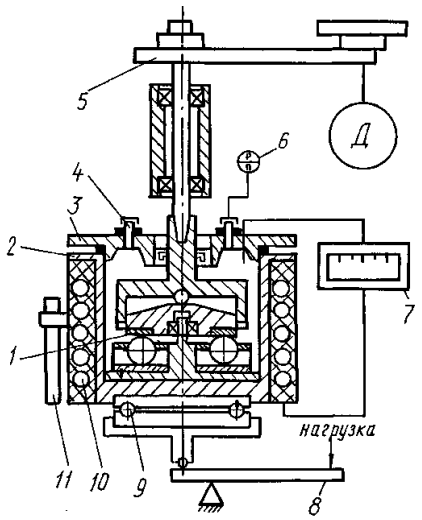

Fig. 3. Sliding friction setting (3 balls – plane) : 1 – friction unit; 2 – chamber; 3 – cover; 4 – sampler; 5 – drive; 6 – pressure gauge; 7 – temperature block; 8 – loading device; 9 – thrust bearing; 10 – heating element; 11 – tensile beam

The devices were equipped with lids with samplers, through which, using a medical syringe, samples of the medium surrounding the friction unit were taken from the chamber for chromatographic analysis of the changes that occur in it during friction. To ensure control of changes in the composition of the gas environment during cutting, the cutting unit was also placed in a sealed chamber. In all test chambers, an excess pressure was created to ensure the possibility of sampling the medium for subsequent chromatographic analysis. To determine the component composition and concentration of gases, gas chromatographs " Chromatec -Crystal 5000" and " Gazochrom 3101" were used, which have a sensitivity threshold for hydrogen, respectively, 4×10^{-10} g/ml and 1×10^{-4} % by volume. Cyclic bending was tested on samples made of St3 steel, made in the form of a plate with dimensions: $l \times b \times h = 80 \times 6.0 \times 0.3$ (mm). Rolling friction experiments were carried out at contact stresses of 2300 MN/m^2, the speed was 850 min^{-1}. The conditions for testing sliding friction on the installation had the following parameters: sliding speed 1.18 m/s, speed 450 s^{-1}, axial load 150 N, to ensure the registration of changes in the air environment, the test time was 30 min. The test specimens were made of ShKh15 steel.

Cutting of metal – steel 45 by drilling was carried out with a drill with a diameter of 5.8 mm made of steel P6M5 at an axial load of 500 N, a cutting speed of 0.45 m/s, and a productivity of 5×10^{-5} m/s for 5 min.

Results and Discussion

Cyclic deformation of a sample of St3 steel in an air environment leads to the initiation of heterogeneous chemical processes (Fig. 4) and with an increase in the number of cycles, the amount of released hydrogen increases, the oxygen content decreases, and the nitrogen content remains unchanged. The loading frequency was 1 bend per second.

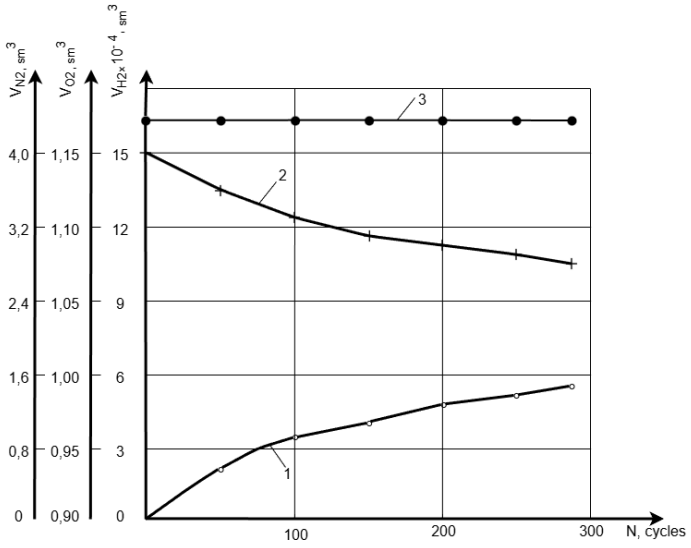

Fig. 4. Kinetics of heterogeneous reactions during cyclic bending of the sample (St3): 1 – hydrogen (H_2); 2 – oxygen (O_2); 3 – nitrogen (N_2)

In the conducted studies, the release of hydrogen is the result of the interaction of water vapor present in the air surrounding the zone of influence of mechanical loads on the metal, with activated plastic deformation of the steel. The chemical nature of the processes can be depicted by the following schemes:

$$Fe + H_2O \rightarrow FeO(FeOH) + H_2 \uparrow; \qquad (1)$$
$$Fe + 2H^{\bullet} \rightarrow Fe^{2+} + H_2 \uparrow.$$

The absorption of molecular oxygen and the corresponding reduction in its volume in the test chamber is due to the topochemical reaction of the interaction of O_2 with the activated metal, in our case steel, which mainly consists of iron, its oxidation with the formation of oxides on the surface:

$$3\,Fe + 2\,O_2 \downarrow = Fe_3O_4 \qquad (2)$$

Mechanochemical transformations have the character of a complex multi-stage process, which includes stages of metal deformation under the influence of mechanical loads with the supply , accumulation and dissipation of mechanical energy, direct chemical interaction of the metal with the components of the environment and solid-phase transformations, the implementation of various secondary processes associated with electron emission, quantum radiation and others. In the kinetics of topochemical processes under the influence of mechanical load, two extreme cases can be distinguished [16]: the first corresponds to the conditions under which the speed of the entire process is determined by the speed of the primary mechanochemical stage, and the second - when the limiting stage is the supply or absorption of mechanical energy. Thus, the criterion for dividing heterogeneous chemical reactions caused by mechanical loading of a solid body by kinetic features is the ratio between the rates of absorption of elastic energy and directly mechanochemical reactions. The first case concerns conditions when a solid is in a constant field of mechanical stresses. The conditions of our research relate to the second case, when heterogeneous reactions occur under variable metal loading and the rate of elastic energy input is much lower than the rate of the chemical reaction initiated by the absorption of this energy by the solid.

With a steady-state cyclicity of mechanical energy supply under steady-state conditions, the average mechanical power supplied to a solid body over time remains constant. For each unit load cycle, a part of the mechanical energy is absorbed by the metal and over a certain number of cycles, the average steady-state degree of material deformation and the corresponding average energy level ΔE_{def} that was absorbed are established. The rate of energy absorption is directlyproportional to the supplied power W , *and the rate of dissipation is proportional to the average level* ΔE_{def}. In steady-state mode:

$$\alpha W = \frac{1}{\tau_p}\Delta E_{\text{деф}} \qquad \text{or} \qquad \Delta E_{\text{деф}} = \alpha \tau_p W, \qquad (3)$$

where α is a coefficient that is close in magnitude to the efficiency of the metal deformation process, and therefore lies within the efficiency range $< \alpha < 1$, τ_p – stress relaxation time.

The nature of the distribution of deformation energy in a metal depends on many factors [1]: the heterogeneity of the structure, the presence of impurities and alloying elements, the damping properties of the system, the speed of load application and is unknown, but it can be suggested that it is quite steep and can be described by an exponential law, that is, the part of the bonds that acquire deformation energy is proportional to the value exp. $(-\frac{\text{E}_{\text{деф}}}{\Delta \text{E}_{\text{деф}}})$. Also, it should be taken into account that the external load on the metal is applied periodically and in the system there is a constant redistribution of deformation energy between the bonds with a speed A (s^{-1}) or, accordingly, with a characteristic time 1/A (s), which depends on both the intensity of the force load and the inherent relaxation time of the material. In the case when the kinetics of a chemical process initiated by the application of mechanical energy is limited by its redistribution in the metal, the rate constant should be proportional to the rate of redistribution of the strain energy between the bonds A (s^{-1}) and the probability of accumulation on a certain bond of the critical strain energy $E^{\text{i}}_{\text{деф}}$ sufficient to initiate a topochemical reaction under the influence of mechanical loading and the deformation caused by it. Therefore, in this case, the dependence of the rate constant of the heterogeneous reaction on the intensity of the application of mechanical energy in variable load fields will have, taking into account equation (3), the following form:

$$k_{mech} \sim A\, exp\,(-\frac{E^{i}_{\text{деф}}}{\Delta E_{\text{деф}}}) = A\, exp\,(-\frac{E^{i}_{\text{деф}}}{\alpha \tau_p W}) \qquad (4)$$

From the above equation it is clear that under loads the rate of heterogeneous chemical processes should be directly proportional to the intensity of the mechanical energy supply and the metal deformation caused by it, the processes of accumulation and dissipation of elastic energy.

Plastic deformation of the metal, and therefore the disordering of the structure with the formation, propagation and migration of structural defects as centers of catalysis , initiates the course of topochemical reactions, the result of which is a change in the composition of the surrounding gaseous medium - the release of hydrogen in the volume of 5.1×10^{-4} cm ^{3} , and the absorption of oxygen in the volume of 6.4×10^{-2} cm ^{3} . If the metal is thermodynamically unstable, in the air environment a film of solid products of interaction with components is formed on the surface, most often oxide [17], which inhibits the further course of chemical processes. However, cyclic bending of the sample leads to cracking and destruction of this film, and therefore contributes to the exposure of the metal. At the initial stage of deformation, processes of intensive propagation and movement of dislocations occur in the metal, their emergence to the surface, and this contributes to a significant activation of the course of topochemical reactions with the participation of active components in the air. At the same time, there is intensive dissipation of the supplied mechanical energy into heat due to internal friction processes, as evidenced by the heating of the sample.

Further deformation of the sample leads to an increase in the density of dislocations, complication of their movement, interaction between themselves and with impurity atoms , i.e. contributes to the exhaustion of both physical and chemical processes of dissipation of the supplied energy. This is manifested in the slowing down of the course of topochemical reactions and, ultimately, the development of damaging phenomena, the appearance of microcracks in the places of accumulation of dislocations , which grow, merge and cause the destruction of the sample under conditions of low-cycle fatigue ($N_p = 280$ cycles).

The kinetics of heterogeneous chemical reactions of the interaction of components of the surrounding gas environment with activated plastic deformation metal at different intensities of contact load were studied: during rolling friction, sliding friction and during metal cutting. As can be seen from the obtained experimental data (Fig. 5,6,7,8), in the process of friction, as well as during metal cutting, regardless of the materials studied, hydrogen is also released and oxygen is absorbed. The nitrogen content remained unchanged. However, the nature of topochemical processes, depending on the conditions of mechanical impact on the metal, is significantly different. This is due to the intensity of plastic information, which is also the initiator of the increase in the reactivity of the metal and the conditions of the presence on the metal surface of solid products of its interaction with active components of the environment.

The load intensity during rolling friction (Fig. 5), which is formed by the angular velocity of the sample ($\omega = 14.2$ s $^{-1}$) and six balls in the separator, increases to 85.4 s $^{-1}$ of deformations per unit surface per second. This causes acceleration of heterogeneous reactions between the activated metal and air components and, as a result, a change in the component and quantitative composition of the environment - the amount of released hydrogen is 132.4×10^{-4} cm ^{3} , i.e. it increases 25.9 times compared to the cyclic bending of the sample, and the absorbed oxygen is 29.4×10^{-2} cm ^{3} , which is 4.6 times higher than the previous test (Fig. 4).

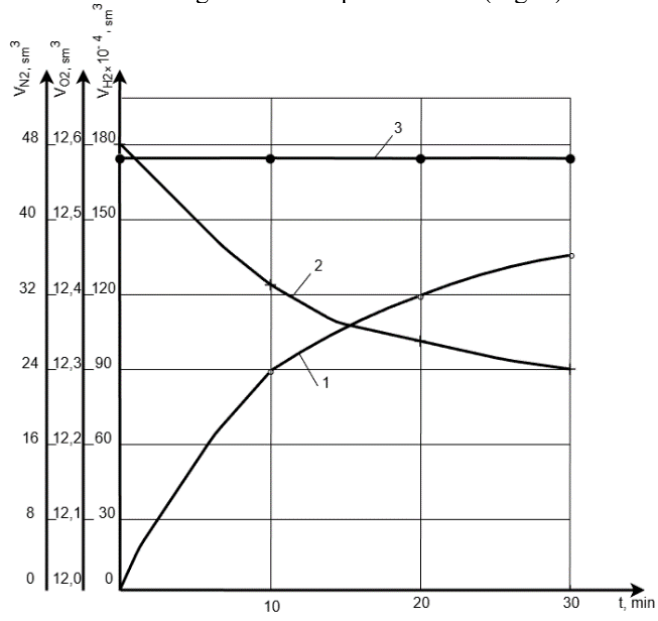

Fig. 5. Kinetics of heterogeneous reactions during rolling friction (ShKh15 – ShKh15): 1 – hydrogen (H_2); 2 – oxygen (O_2); 3 – nitrogen (N_2)

During sliding friction on the friction pair "3 balls - plane" the angular velocity of the moving sample was 7.5 s $^{-1}$, and taking into account 3 balls, the number of re-deformations per unit surface was 22.5 s $^{-1}$, i.e. it was significantly less than the value during rolling friction, but the intensity of topochemical reactions significantly increased (Fig. 6): 2570.0×10^{-4} cm ^{3} of hydrogen was released and 470.0×10^{-2} cm $^{3\text{ of oxygen was consumed}}$, which, respectively, is 19.4 and 16 times higher than the result during rolling friction. This is due to the peculiarities of the sliding friction process.

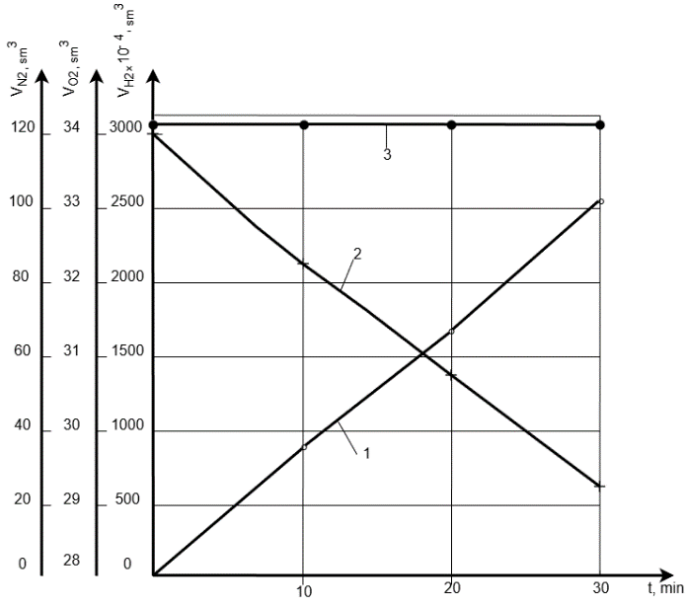

Fig. 6. Kinetics of heterogeneous reactions under sliding friction (3 balls – plane, ShKh15 – ShKh15): 1 – hydrogen (H_2); 2 – oxygen (O_2); 3 – nitrogen (N_2)

During bending tests and friction rolling, plastic fatigue deformation of the metal surface occurs, but the solid products of the interaction of active air components with the activated metal - oxides (hydroxides) - crack, in small quantities collapse, but remain on the surface and thus shield it from the access of reagents. At the same time, during friction sliding, solid products of the interaction are removed from the friction surface, and therefore its constant renewal, the formation of a juvenile surface, which has an exceptionally high reactivity, which leads to the intensification of hydrogen release and oxygen absorption as components of heterogeneous chemical processes and their kinetics is characterized by linearity.

The friction pair "3 balls – plane" is open for access of active components of the environment to the plastically deformed metal. To study the influence of the closedness of the friction pair on the course of topochemical reactions, experiments were conducted on the plane-plane friction pair (Fig. 7). As a result, it was found that the closedness of the activated surface of the friction pair by the counterbody for access of water vapor and oxygen does not affect the nature of the chemical interaction and the linearity of the kinetic dependence. During the friction process, 1170.0×10^{-4} cm ^{3} of hydrogen was released and 185.0×10^{-2} cm ^{3} of oxygen was consumed , which is comparable in order, but somewhat lower than the results obtained with sliding friction on the pair "3 balls – plane", but significantly exceeds the results with cyclic bending and rolling friction.

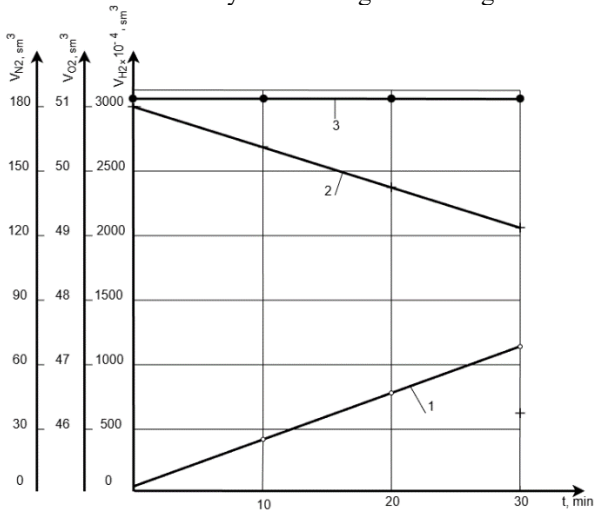

Fig. 7. Kinetics of heterogeneous reactions under sliding friction (plane – plane, ShKh15 – ShKh15): 1 – hydrogen (H_2); 2 – oxygen (O_2); 3 – nitrogen (N_2)

If sliding friction mechanically removes solid compounds from the friction track topochemical interaction, which are relatively weakly connected to the surface, then during cutting the cutting edge of the tool cuts off the base metal layer with the products present on it, which leads to intensive plastic deformation of the juvenile surface and acceleration of tribochemical processes. At an angular velocity cutting ω = 28 s $^{-1}$ In 5 minutes of the

experiment, 1200.0×10 $^{-4}$ cm ^{3} of hydrogen was released and 114.0×10 -2 cm ^{3} of oxygen was consumed (Fig. 8). The kinetic dependence of topochemical reactions has an exponential form, which is due to the nature of the drilling process, namely, the increase in the contact area of the cutting tool with the sample, and therefore the increase in the intensity of plastic deformation of the metal as the drill is deepened.

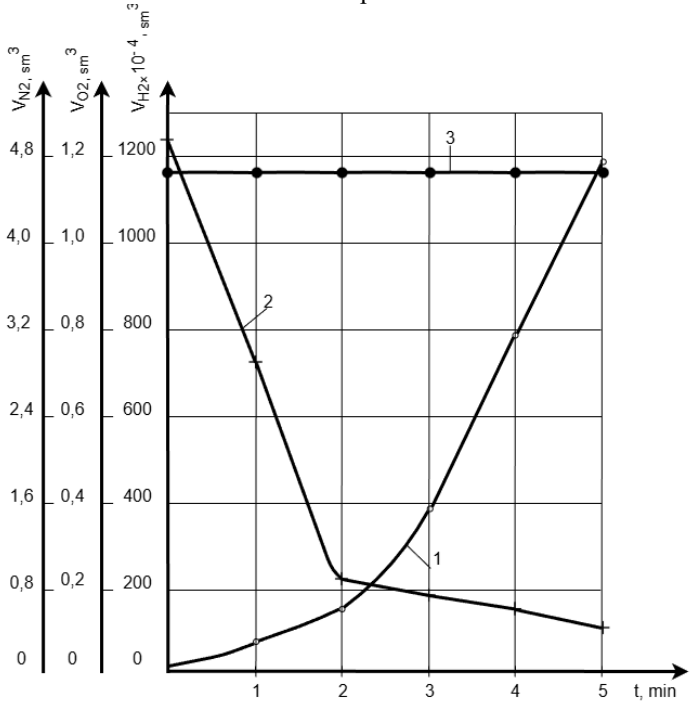

Fig. 8. Kinetics of heterogeneous reactions during cutting (steel 45 – steel P6M5): 1 – hydrogen (H $_2$); 2 – oxygen (O $_2$); 3 – nitrogen (N $_2$)

More complete information about the features of topochemical reactions is provided by the analysis of the speed (cm ^{3} /s) of the processes of hydrogen evolution $(\upsilon_{H_2})$and oxygen absorption (υ_{O_2})(Table 1). The intensity of chemical oxidation reactions initiated by mechanical loading of the metal increases in the following order: cyclic bending of the metal → rolling friction → sliding friction (plane-plane pair) → sliding friction (pair "3 balls-plane") → cutting. At the same time, the speed of the surface oxidation reaction by water vapor, which causes the release of hydrogen, increases by 222 times: from $\upsilon_{H_2} = 1{,}8 \times 10^{-6}$cm ^{3} /s during cyclic bending to $\upsilon_{H_2} = 400{,}0 \times 10^{-6}$cm ^{3} /s during cutting, and by oxygen by 16 times, respectively, from $\upsilon_{O_2} = 2{,}3 \times 10^{-4}$ cm ^{3} /s to $\upsilon_{O_2} = 38{,}0 \times 10^{-4}$cm ^{3} /s.

Table 1

Influence of the type of metal deformation on the rate of hydrogen evolution (υ_{H_2}), oxygen absorption $(\upsilon_{O_2})$and their ratio$(\upsilon_{H_2}/\upsilon_{O_2})$

Type of deformation	Speed, cm ^{3} /s		The ratio of the rates of hydrogen evolution and oxygen absorption, $(\upsilon_{H_2}/\upsilon_{O_2})$
	Selection hydrogen, $\upsilon_{H_2} \times 10^{-6}$	Oxygen absorption, $\upsilon_{O_2} \times 10^{-4}$	
Cyclic distillation	1.8	2.3	0.0078
Rolling friction	7.3	1.6	0.0456
Sliding friction pair: plane – plane	65.0	10.3	0.0631
Sliding friction pair: 3 balls – plane	142.7	26.1	0.0547
Cutting	400.0	38.0	0.1053

The simultaneous presence of oxygen and water molecules in the air environment causes the emergence of a competing effect of metal oxidation on the active centers of the surface, which is subject to plastic deformation. An idea of the possible prevailing course of chemical reactions is indirectly given by the value of their activation energy [17]. Studies [18] have established that for the reaction of iron with water vapor, the calculated activation energy is 28±3 kJ /mol. This value is close to the activation energy of iron oxidation by oxygen (32±6 kJ /mol), which indicates a similar limiting step of the process, which consists in the exchange of metal atoms and adsorbed

oxygen or water. With increasing temperature and thickness of the oxide film, the mechanism can change to diffusion or electric field-controlled. The energies of chemical bond breaking in the oxygen (O_2) and water (H_2O) molecules are similarly close , that is, splitting of the substance into free atoms , as a prerequisite for their activation to enter into chemical interaction with the metal, which is, respectively, 498 kJ / mol (O = O) and 463 kJ / mol (H - O) [19]. The proximity of both activation and dissociation energies indicates a comparable possibility and speed of the processes of metal oxidation by oxygen and water vapor and the expected preservation of the constancy of the ratio of their rates under stationary conditions.

An idea of the activation of characteristic oxidation reactions is given by the ratio of the rates of hydrogen release and oxygen absorption: $\upsilon_{H_2}/\upsilon_{O_2}$. The faster hydrogen is released, the more the metal is oxidized by water vapor, and, accordingly, the faster the oxygen present in the atmosphere is absorbed, the more intensively it oxidizes the metal. Analysis of the results obtained (Table 1) The ratio $\upsilon_{H_2}/\upsilon_{O_2}$of the rates of hydrogen release (υ_{H_2})and oxygen absorption (υ_{O_2})during dynamic plastic deformation of the metal indicates a significant differentiated influence of the supplied mechanical energy on the activation of chemical reactions of metal oxidation by water vapor and oxygen. The lowest value of the ratio $\upsilon_{H_2}/\upsilon_{O_2}$is observed at the least intense cyclic loading of the sample - cyclic bending and is 0.0078. With an increase in the intensity of the supplied mechanical energy and, accordingly, the plastic deformation of the metal, the ratio increases $\upsilon_{H_2}/\upsilon_{O_2}$: with rolling friction it is 0.0456, with sliding friction: for the pair "3 balls - plane" - 0.0547, for the pair plane - plane - 0.0631, with cutting - 0.1053. Thus, an increase in the ratio is observed $\upsilon_{H_2}/\upsilon_{O_2}$ by 13.5 times, which indicates the prevailing influence of the intensity of plastic deformation on the activation of the reaction of metal oxidation by water vapor, which is accompanied by the release of hydrogen.

In all cases of dynamic loading of steel, as shown by the research results (Fig. 4,5,6,7,8), the nitrogen content in the test chamber remains unchanged, which indicates its inertness in relation to the activated metal.

Conclusions

Installations and methods for studying heterogeneous chemical reactions in the process of plastic deformation of metals have been developed. The kinetics of the topochemical interaction of active air components initiated by plastic deformation of the metal have been established: during bending and rolling friction, there is a damped dependence, for sliding friction, both for an open pair (3 balls – plane) and a closed pair (plane – plane) – it is rectilinear, and during cutting – exponential. Regardless of the type of plastic deformation, the openness of the friction pair, the same type of topochemical reactions occur with the absorption of the reacting component – oxygen and the release of the interaction product – hydrogen, nitrogen is inert and does not participate in chemical processes. It was found that the intensity of topochemical reactions depends on the type of plastic deformation and increases in the order: cyclic bending of the metal → rolling friction → sliding friction (plane-plane pair) → sliding friction (pair "3 balls-plane") → cutting. At the same time, the rate of the surface oxidation reaction by water vapor, which causes the release of hydrogen, increases by 222 times, and by oxygen by 16 times. An indicator of the activation of characteristic oxidation reactions in the air environment depending on the type of plastic deformation is proposed: the ratio of the rates of hydrogen release and oxygen absorption - $\upsilon_{H_2}/\upsilon_{O_2}$. An increase in the ratio $\upsilon_{H_2}/\upsilon_{O_2}$in the revealed order of increasing the intensity of mechanochemical reactions from the type of plastic deformation by more than 13 times was established, which indicates the prevailing influence of the intensity of plastic deformation and substructural processes that occur in this case on the activation of the metal oxidation reaction by water vapor, which is accompanied by the release of hydrogen. The results revealed reveal the essence of the influence of metal deformation on the kinetics and nature of mechanochemical processes and the principles of regulating their intensity in order to ensure the increase in long-term strength and durability of machine parts.

References

1. Tribochemistry and rheology of wear resistance: Monograph / VV Shevelya , VP Oleksandrenko . – Khmelnitsky, KhNU . 2006. – 278 p.

2. Tsang- Tse Fang Elements of Structures and Defects of Crystalline Materials. 2018. - 230 https://doi.org/10.1557/mrs.2018.312

3. Wolfer , WG (2012). Fundamental Properties of Defects in Metals. Comprehensive Nuclear Materials. DOI: 10.1016/B978-0-08-056033-5.00001-X

4 . Faisal, Nadimul & Cora, Ömer Necati & Bekci , Muhammed & Sliwa , RE & Sternberg, Yehuda & Pant, Shashank & Degenhardt , Richard & Prathuru , Anil. (2021). Defect Types. DOI: 10.1007/978-3-030-72192-3_3

5. Shevelya VV, Oleksandrenko VP Dissipative properties of frictional contact taking into account the processes of mechanical and tribochemical relaxation // Friction and Wear. - 2005. - No. 5. - P.471-480.

6. Shevelya VV, Orlovich V., Oleksandrenko VP On the role of inelastic phenomena in friction of solid bodies // Friction and wear. - 2005. - No. 4. - P. 367-374.

7. Recent Progress on Wear-Resistant Materials: Designs, Properties, and Applications / Wenzheng Zhai , Lichun Bai , Runhua Zhou , Xueling Fan , Guozheng Kang , Yong Liu , Kun Zhou // Advanced Science. – Volume 8, Issue 11, 2021. https://doi.org/10.1002/advs.202003739

8. Ganzyuk AL, Oleksandrenko VP Development of the foundations of the evolutionary model of fretting corrosion from the position of physical chemistry and solid state chemistry from the balance of external influx factors // Khmelnitsky National Newsletter university. - Khmelnitsky, 2018. - No. 2 (259). - P.20-28. https://journals.khnu.km.ua/vestnik/pdf/tech/pdfbase/2018/2018_2/(259)%202018-2-t.pdf

9. Kengesbekov , A.; Sagdoldina , Z.; Torebek , K.; Baizhan , D.; Kambarov , Y.; Yermolenko , M.; Abdulina , S.; Maulet , M. Synthesis and Formation Mechanism of Metal Oxide Compounds. Coatings 2022, 12 , 1511. https://doi.org/10.3390/coatings12101511

10. Micromechanical modeling of mechanochemical processes in heterogeneous materials / M Poluektov , AB Freidin , Ł Figiel // Modeling and Simulation in Materials Science and Engineering , - Volume 27 , Number 8 , 2019 DOI: 10.1088/1361-651X/ab3b3a

11. Shchepetov , V. , Bys , S. , Byalik , M. , Medvedchuk , V. , & Bys , Y. (2025). The influence of hydrogen saturation on the wear mechanism of steel. Problems of Tribology , 30 (2/116), 84–89. https://doi.org/10.31891/2079-1372-2025-116-2-84-89

12. Effect of hydrogen charging on the wear resistance of CrN -coated Al alloy for hydrogen valve of fuel cell electric vehicles / Dong-Ho Shin, Seong-Jong Kim // International Journal of Hydrogen Energy . – Volume 89 , 4 November 2024, Pages 279-292 https://doi.org/10.1016/j.ijhydene.2024.09.251

13. Hutsaylyuk , V., Student, M., Dovhunyk , V., Posuvailo , V., Student, O., Maruschak , P., & Koval'chuck , I. (2019). Effect of hydrogen on the wear resistance of steels upon contact with plasma electrolytic oxidation layers synthesized on aluminum alloys. Metals , 9 (3), 280. https://doi.org/10.3390/met9030280

14. Sobola , D., & Dallaev , R. (2024). Exploring Hydrogen Embrittlement: Mechanisms, Consequences, and Advances in Metal Science. Energies , 17 (12), 2972. https://doi.org/10.3390/en1712297

15. Chen, YS; Huang, C.; Liu, PY; Yen, HW; Niu , R.; Burr, P.; Moore, KL; Martínez-Pañeda , E.; Atrens , A.; Cairney , JM Hydrogen trapping and embrittlement in metals - A review. Int. J. Hydrogen Energy 2024, in press https://doi.org/10.1016/j.ijhydene.2024.04.076

16. Heinike , G. (1984) Tribochemistry . Akademie-Verlag , Berlin.

17. Cicek , V., & Al- Numan , B. (2011). Corrosion chemistry . John Wiley & Sons. 744 e01_978-1-119-28375-1_01.pdf

18. Grosvenor AP, Kobe BA, McIntyre NS Activation energies for the oxidation of iron by oxygen gas and water vapor . Surface Science , Volume 574, Issues 2–3, 2005, Pages 317-321, ISSN 0039-6028, https://doi.org/10.1016/j.susc.2004.10.043 .

19. Luo, YR (2007). Comprehensive handbook of chemical bond energies . Boca Raton: CRC Press. ISBN 978-0-8493-7366-4 . OCLC 76961295

Шевеля В.В., Олександренко В.П., Стечишин М.С., Соколан К.С., Федорів В.М., Нелюбін Ю.М. Кінетика гетерогенних хімічних реакцій, ініційованих деформацією металів

Досліджено топохімічні процеси в середовищі повітря, які ініціюються пластичною деформацією металу різної інтенсивності та виду: циклічний перегин зразка, тертя кочення, тертя ковзання, різання. Встановлено, що в процесі циклічного навантаження металу відбувається зміна концентрації і складу компонентів повітря, яке знаходиться у випробувальній камері: зниження вмісту реагенту – молекулярного кисню та поява продукту взаємодії – водню. Виявлено вплив виду пластичної деформації металу та процесів, що при цьому відбуваються на кінетичні залежності топохімічних процесів: затухаючі, прямолінійні та експоненціальні. Встановлено залежність швидкості топохімічних процесів від інтенсивності пластичної деформації. Запропоновано показник оцінки конкуруючого ефекту окиснення металу на активних центрах поверхні, що піддається пластичній деформації. Отримані результати розкривають природу процесу тертя та зношування та шляхи підвищення довговічності вузлів тертя.

Ключові слова: топохімічні реакції, кінетика, швидкість, пластична деформація, інтенсивність, кисень, водень

ISSN 2079-1372 Problems of Tribology, V. 31, No 2/120-2026, 16-22

Problems of Tribology
Website: http://tribology.khnu.km.ua/index.php/ProbTrib
E-mail: tribosenator@gmail.com

DOI: https://doi.org/10.31891/2079-1372-2026-120-2-16-22

Increasing the durability of the Ti-GFRP/CFRP contact with a layer of wear-resistant polymer composite coatings under vibration load conditions

A. Khimko[1]0009-0009-8059-880X, **O. Mikosyanchyk[1]**0000-0002-2438-1333, **M. Khimko[2]**0009-0005-4364-5444, **V. Klipachenko[2]**0009-0003-3750-4421

[1]National University "Kyiv Aviation Institute", Ukraine
[2]Air Company LLC "H3Operations", Ukraine
E-mail: andreykhimko@ukr.net

Received: 22 March 2026: Revised 14 April 2026: Accept: 19 April 2026

Abstract

The development of aviation and the improvement of the flight characteristics of aircraft and helicopters requires the use of CFRP carbon fibers and GFRP fiberglass in power structures. The vibration load factor is an integral part of the aircraft design. With vibrations, a contact that we thought was nominally stationary begins to move at the micro level over time. Movement between parts is sufficient for the catastrophic development of fretting-corrosion wear of contacting parts, followed by the development of fatigue cracks and structural failure. Therefore, it is very important to pay attention to increasing the durability of contact made of Ti-GFRP/CFRP materials under vibration loads, since as a rule, these are power parts of aircraft, damage to which significantly reduces the reliability of the structure and increases the risk of fatigue cracks, especially in parts made of titanium alloys. One method of increasing the durability of the Ti-GFRP/CFRP contact is the use of intermediate "sacrificial" materials that are triggered during operation and replaced during repairs, but protect the contact from damage. The paper analyzes wear-resistant composite materials and determines what materials F4K15M5 and ZX550 are most suitable for this. It was found that during tests in the Ti-F4K15M5-GFRP system, the metal surface is completely protected by spreading an intermediate material on the surface. The mechanisms of wear of intermediate materials and their effect on contact under vibration loads have been determined.

Keywords: vibrations, titanium alloys, wear-resistant polymer materials, CFRP carbon fiberglass, GFRP fiberglass, durability, analysis, fretting corrosion.

Introduction

Ti-GFRP/CFRP material contact is increasingly common in modern aircraft where ultra-light and heavy-duty materials are used. The development of aviation and the improvement of the flight characteristics of aircraft and helicopters requires the use of CFRP carbon fibers and GFRP fiberglass in power structures. These parts are used to make wing panels, fuselage power elements, brackets and levers, etc. At the same time, the tendency to replace all steel parts in aircraft with titanium alloy is realized on modern Boeing and Airbus aircraft. Even power fasteners in modern aircraft are made of titanium alloys. Therefore, the contact of titanium alloys with power composite materials is increasingly found both in aircraft and in technology, where high strength characteristics are required with a low weight of the structure [1, 2].

At the same time, the factor of vibration loads is an integral part of the aircraft design. With vibrations, a contact that we thought was nominally stationary begins to move at the micro level over time. A movement between parts of a few microns is already sufficient for the catastrophic development of fretting-corrosive wear of contacting parts, followed by the development of fatigue cracks and structural failure. Therefore, it is very important to pay attention to increasing the durability of contact made of Ti-GFRP/CFRP materials under vibration loads, since as a rule, these are power parts of aircraft, damage to which significantly reduces the reliability of the structure and increases the risk of fatigue cracks, especially in parts made of titanium alloys.

Taking into account the latest trends in aviation tribology to replace metal parts and friction pairs operating at specific loads up to 300 MPa with tribological polymer composite materials, the issue of contact protection of

structural Ti-GFRP/CFRP can be considered using modern wear-resistant composite materials with high tribological characteristics.

Literature review

Wear-resistant composite materials, in turn, can be divided into those that operate at increased loads of up to 300 MPa with reinforced fibers [3] and replace the metal friction pair according to their characteristics and into those that do not have reinforcement [4] and act as a lubricating layer on friction surfaces. The latter have PTFE and functional additives in the form of solid lubricants and reinforcing nanoparticles for the required physical and mechanical characteristics and operate in load ranges up to 50 MPa. It is such composite materials that are advisable for use in the Ti-GFRP/CFRP contact under vibration loads or under the development of fretting-corrosion processes. The undoubted advantage of wear-resistant composite materials is their flexibility in obtaining a certain composition with different fillers to obtain the necessary characteristics that allow replacing traditional liquid or paste-like lubricant when rubbing under conditions of fretting development. The composition of wear-resistant polymer composite materials, as a rule, includes the following types [4]: PEEK+PTFE+graphite+MoS_2 (high wear resistance under dry friction), UHMWPE+graphite+PTFE (low coefficient of friction in wet environment), PA6/PA66+graphite+PTFE (bushings and gears when working with pulsations), RI+graphite+PTFE (low coefficient of friction and heat resistance up to 250 ºC), polyoxymethylene+PTFE+MoS_2 (high tribological characteristics under dry friction), POM+graphite+PTFE (bushings and bearings up to 0.1 m/s, vibration loads), etc.

Thus, in the work [5], the authors, studying PTFE-based coatings during fretting corrosion, found that an increase in the normal load to 600 N increases the destruction of tribological films of polymeric composite materials without reinforcement. Studies show that the process of degradation of the coating under the influence of mechanical and chemical influences occurs due to the breaking of molecular chains and the emergence and spread of microcracks that cause the separation of PTFE coating particles.

The authors of the work [6] found that the lowest coefficient of friction under vibration loads of 0.091 was established with a mixture of PEEK and PTFE (70 %) with the addition of 10 % carbon fibers and 20 % graphite. It is also determined that the use of carbon fibers 20 % together with graphite 10 % allows obtaining the smallest wear value of 1.9 · 10-7 mm^3/Nm in the same matrix.

The authors note an increase in the wear resistance of the POM material with the addition of graphite and molybdenum disulfide under fretting conditions [7]. It has been determined that the addition of graphite and MoS_2 has a positive effect on impact strength in fretting corrosion tests. Microstructural study shows that the addition of 2-6 % solid lubricants increases the tribological characteristics of POM by 2 times.

The author of the work [8], studying polymeric composite materials based on PTFE, found that the addition of tin bronze microparticles in the composition of 30 % show excellent tribological characteristics at a load of 33 N and a frequency of 1 Hz or at a load of 81 N and a frequency of 0.75 Hz. The authors found that when tested under vibration conditions, the load and frequency become inversely proportional to the coefficient of friction.

The analysis of literature sources [3-8] showed that the most common are wear-resistant polymer composite material, which in their composition replace tribological films, materials with the addition of PTFE, graphite and MoS_2 in certain proportions, and functional additives (carbon nanotubes, talc, metal particles, PEEK) to obtain the necessary strength characteristics. PTFE and MoS_2 form a thin tribological layer on the surface, reducing adhesion and wear, while graphite stabilizes friction at moderate temperatures and retains properties under high loads. Thus, the analysis shows that fillers (PTFE+graphite+MoS_2) in PEEK matrices provide maximum wear resistance and self-lubrication over a wide range of friction modes.

Purpose

The purpose of the work is to increase the durability of the Ti-GFRP/CFRP contact by using modern wear-resistant composite materials under vibration load conditions.

Objects of research and experimental conditions

When choosing wear-resistant polymer composite materials for the protection of the Ti-GFRP/CFRP contact, first of all, you need to pay attention to the fact that most materials are used in techniques with certain strength characteristics, for which reinforcing fibers are introduced into the composition of polymers or more durable plastic is used as a matrix. In the case of T-GFRP/CFRP contact, only a layer of wear-resistant polymer composite materials is required between the power structural elements of aircraft, therefore, only materials with high tribological characteristics should be selected for protection.

In the paper [4], the author noted that wear-resistant polymer composite materials F4K15M5 are the basic tribological layer for many articulated bearings. The material F4K15M5, which consists of PTFE material (fluoroplastic-4) with 15 % graphite and 5 % MoS_2, has increased wear resistance, which is 1000 times higher than unfilled PTFE and a lower coefficient of friction [9]. Among the filled grades of PTFE-4, it has the most favorable friction and wear characteristics, and the material F4K15M5 is the best among them in terms of

tribological parameters. Its analogues are Dyneon TFM-1600 G5, Ecoflon 2 (SKF), F4G15M5, as well as materials using another base PEEK+15%C+5%MoS_2, PI+15%C+5%MoS_2, UHMPE+15%C+5%MoS_2.

Among the commercial wear-resistant polymer composite materials that are widely used in mechanical engineering and have similar characteristics is the ZX550 material from Zedex. The ZX550 composite material has the best wear resistance characteristics among the materials of this company and consists of a PTFE base with the addition of 15 % graphite, 5 % MoS_2, 10 % glass fibers (E-glass) and 10 % fluorides (BaF_2, CaF_2) or bronze powder. The addition of glass fibers provides an increase in the strength and shape retention of polymer composite materials, while fluorides and bronzes expand the operating temperature range and increase the damping properties of the polymer during cyclic movements (vibration, fretting processes).

Thus, for testing the increase in the durability of the contact wear resistance contact Ti-GFRP/CFRP under vibration loads, we use materials F4K15M5 and ZX550. In Table. 1. Some physical and mechanical characteristics of wear-resistant polymer composite materials are presented.

Since the surface roughness of GFRP/CFRP materials is greater on titanium alloys, it is logical to assume that if there is a layer of materials F4K15M5 and ZX550 between the Ti-GFRP/CFRP contact, there will actually be a slippage between the selected polymer composite materials and the titanium alloy.

Table 1

Physical and Mechanical Characteristics of Wear-Resistant Polymer Composite Coatings Tested in Experiments

№	Indicators	F4K15M5 PTFE +15% Graphite +5 % MoS_2	Zedex ZX-550 PTFE +15% Graphite +5% MoS_2 +10–20% E-glass +5–10% BaF_2/CaF_2/bronze
1	Density, g/cm^3	2,20-2,24	2,25-2,230
2	Hardness Shore D	58-62	60-65
3	Dry friction coefficient	0,05-0,08	0,05-0,12
4	Tensile strength, MPa	18-22	20-25
5	Compressive strength, MPa	60-75	80-100
6	Operating temperature range, ºC	-100…+260	-250…+240
7	Bending modulus, MPa	500-600	800-1000

So, for the test, discs were made of ZX550 and F4K15M5 materials with a thickness of 0.5 mm and glued to GFRP material. The counter-sample was the Ti5Al5V5Mo1Cr1Fe material, which is the most common titanium alloy for the power parts of Antonov aircraft.

The conditions for conducting resource tests were as follows:

1. The test base for contact was determined at 300 thousand km. cycles.
2. The damage assessment was determined by determining the arithmetic mean of eight sections of friction tracks according to the scheme according to GOST 23.211-80.
4. The frequency of oscillations was 30 Hz.
5. The amplitude of oscillations was 125 μm and was determined from accelerated test conditions to intensify processes under vibrations.
6. The load for all subjects was 10 MPa.
7. All tests were carried out at a temperature of 16 to 20 °C.

Analysis of the tests performed and evaluation of the durability of the Ti-GFRP/CFRP contact

The test results are presented in Fig. 1, taking into account the wear of polymer composite materials. The analysis of the wear resistance of materials shows that wear-resistant polymer composite materials perfectly protect the friction surface of titanium alloy Ti5Al5V5Mo1Cr1Fe. When tested in the Ti-F4K15M5-GFRP system, the metal surface is completely protected by smearing on the surface of the composite material (Fig. 2 a). Ti-ZX550-GFRP is 30 % lower than in tests with a layer of material F4K15M5, but on the surfaces of the titanium alloy we have damage from the action of reinforced E-glass fibers.

Chemical analysis of the surface of the tribological film F4K15M5 (Fig. 2 b) shows the presence of areas with dark spots on the surface. The analysis shows that there is a gradual operation of polymeric composite materials due to the constant processes of smearing and tearing of the polymer and the action (Table 2) of oxygen on the composition of the film. Increased activation of the tribological layer is also shown by the total wear of friction surfaces (Fig. 1).

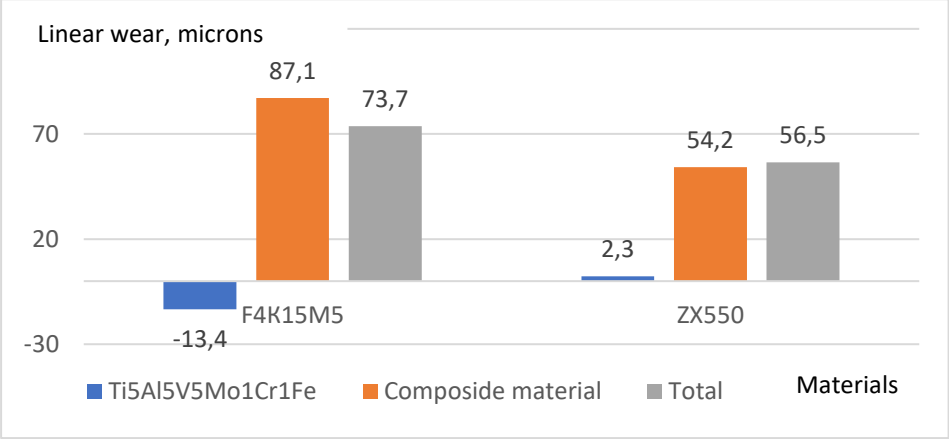

Fig. 1. Wear resistance of polymer composite materials paired with Ti5Al5V5Mo1Cr1Fe when tested under vibration load conditions

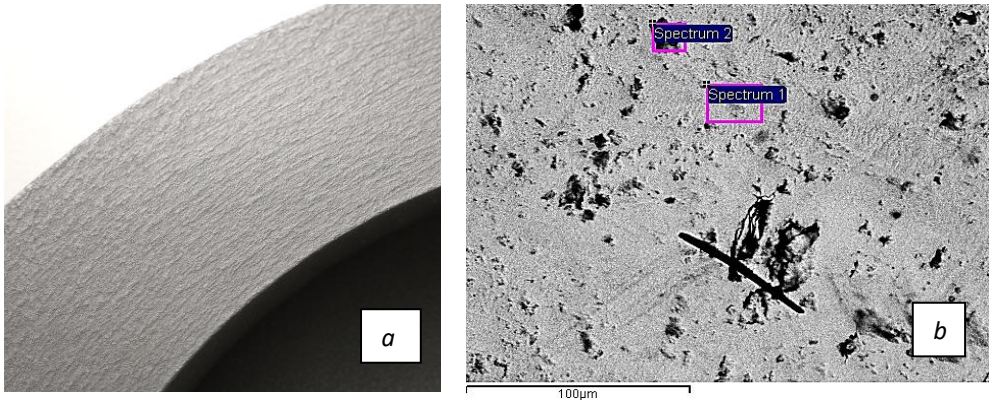

Fig. 2. Topographies of friction surfaces of titanium alloy Ti5Al5V5Mo1Cr1Fe (a) and chemical composition of tribological film sections (b) on the surface after vibration tests with F4K15M5 material.

Table 2

Chemical analysis of the friction surface with F4K15M5 material after vibration tests (Fig. 2 b), %

Spectrum	S	F	O	Mo	S	Ti	Si
Spectrum 1	38,2	26,7	11,3	6,5	5,1	7,8	1,2
Spectrum 2	25,4	16,4	20,3	4,5	4,2	21,1	5,8

During the sliding friction of materials Ti5Al5V5Mo1Cr1Fe with F4K15M5 under vibration conditions, micro irregularities of the titanium alloy come into contact with the PTFE-based material that is part of the composition and its introduction into the metal surface by cutting and adhering a softer surface to a harder surface of the alloy. Under loads and reverse movements, particles of polymer material F4K15M5 set with their subsequent rupture during stretching, which leads to the formation of a tribological film on the surface of the titanium alloy (Fig. 3a). The tribological film protects the surface of the titanium alloy from the contact of the reinforcing fibers of the GFRP material [10]. It includes wear particles of the material F4K15M5 (PTFE, MoS_2, graphite), which are mixed with each other and smeared on the surface of the titanium alloy with the addition of oxygen and the formation of additional structures. PTFE material provides a coefficient of friction in the range of 0.04-0.07, and graphite and MoS_2 petals stabilize friction, fill voids and absorb vibration loads from fretting processes and energy conversion into temperature. When the tribological layer that is self-lubricating is formed, friction goes into a mode with a chaotic breakdown and repeated growth of micro welds without sudden changes in the coefficient of friction. In the process of friction, the tribological layer is triggered by oxygen and periodic contact of oxygen with the surface of titanium. There is abrasive-adhesive wear of the metal surface and in the future contact of reinforced fibers on the surface of the titanium alloy. In general, properly selected materials of wear-resistant polymer composite materials stabilize the operation of the Ti-GFRP/CFRP contact with the intermediate layer and minimize the wear of Ti5Al5V5Mo1Cr1Fe and GFRP materials.

When Ti5Al5V5Mo1Cr1Fe materials come into contact with ZX550, the wear mechanism is almost the same, but increased physical and mechanical characteristics (greater hardness and modulus of elasticity) and the

presence of E-glass and fluoride-bronze complex in the composition of reinforced fibers contribute to a more active action of oxygen on the surface of the titanium alloy with the formation of additional TiO_2 oxides as part of the tribological film. Fiberglass increases the strength of the tribological layer, reduces the depth of secondary plastic deformation and inhibits the increase in cracks in the film. Fluorides increase physical and mechanical characteristics for stress damping during vibration loads, and bronze particles stabilize tribological characteristics when the temperature in the friction zone rises [11].

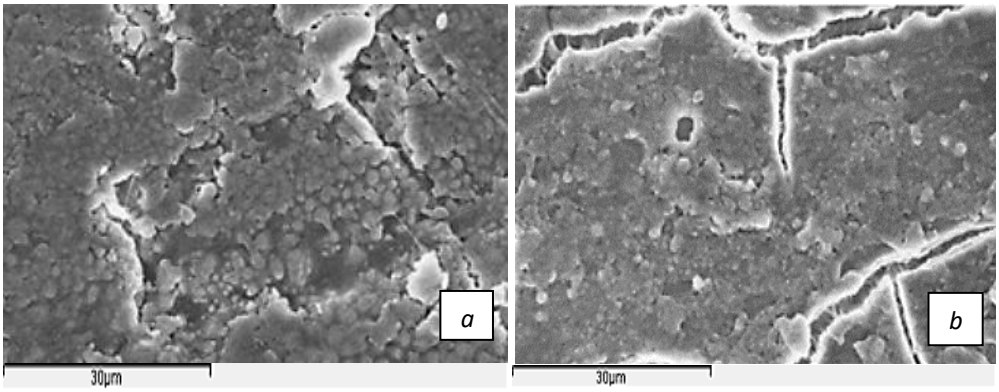

Fig. 3. Topography of the tribological layer formed on the surface of the titanium alloy Ti5Al5V5Mo1Cr1Fe by friction with polymer wear-resistant composite materials F4K15M5 (a) and ZX550 (b) under vibration loads

Due to the increased strength characteristics of the tribological layer, cracks appear on the surface (Fig. 3b), and the wear of the titanium alloy (Fig. 1) and the coefficient of friction increases to 0.05-0.08 in comparison with friction with the material F4K15M5, where the coefficient of friction was 0.04-0.07.

Conclusions

Thus, the analysis of test results and wear mechanisms of Ti-GFRP/CFRP contacts with intermediate layers of wear-resistant polymer composite materials under vibrations shows that the F4K15M5 material protects the contact of titanium alloys in contact by 30% more than the use of ZX550 material under fretting conditions at a load of 10 MPa, but is triggered faster. When exposed to vibration loads on the aircraft structure of about 10 MPa, we can recommend the material F4K15M5 in the contact system Ti-F4K15M5-GFRP/CFRP, which will give guaranteed protection of materials for some time, and in case of long-term operation or exposure to vibrations with a load of more than 20 MPa, we can recommend Zedex ZX550, which will be a kind of balance in damage and tripping of all contact materials Ti-ZX550-GFRP/CFRP. In addition, it is possible to carry out additional protection of the surface of titanium alloy or non-metallic coatings (oxidation, phosphating, passivation) or increase the wear resistance of the surface, for example, by chemical heat treatment (nitriding, carburizing), which showed excellent results in terms of wear resistance to fretting corrosion in the contact protection system Ti-GFRP/CFRP.

The work was carried out in accordance with contracts No. 2023/39/UA, No. 2024/139/UA between «H3OPERATIONS» Airlines LLC, No. 2025/88/UA between «KSENA» Airlines LLC and No. 2025/101/UA between Private joint-stock company «Constanta Airlines» and National University «Kyiv Aviation Institute».

The team of authors expresses its deep gratitude to the Director of Airlines LLC «H3OPERATIONS» Vladyslav Klipachenko and the Director of Private joint-stock company «Авіакомпанія константа» Vadim Vdovychenko, for their support and assistance in obtaining materials for testing the Ti-GFRP/CFRP contact and analyzing damage sites of modern Boeing and Bell Helicopter aircraft.

References

1. Tareq M.A. Al-Quraan, Andrii Khimko, Margaryta Khimko, Oksana Mikosianchyk, Rudolf Mnatsakanov, Oleksandr Yakobchuk Increasing the Wear Resistance of Titanium Alloys in Plain Bearings with Galvanic and Vacuum-Arc Coatings. *Tribology in Industry.* Vol. 48, 1 (2026), p. 72-82. https://doi.org/10.24874/ti.2043.10.25.11 [English]

2. Chernets M.V., Romanenko E.O., Kornienko A.O., Chernets Yu.M. Methodological Foundations of Calculation of Metal and Metal-Polymer Plain Bearings: Contact Strength, Wear, Durability. Tom. 3. *Metal-polymer transmissions.* – Kyiv: NAU, 2022. – 250 p. [Ukrainian]

3. Chen Y. L., Lei Y. L., Zhang Y. Aircraft Composite Structures Fatigue Durability Test Method. *Advanced Materials Research.* 2014. Vol. 941-944. P. 1558–1561. URL: https://doi.org/10.4028/www.scientific.net/amr.941-944.1558 [English]

4. Khimko M., Khimko A., Mnatsakanov R., Mikosyanchyk O. Resource testing of modified plain bearings for the aviation industry. *Problems of tribology.* V.29, № 2/112-2024, P.16-22. URL: https://doi.org/10.31891/2079-1372-2024-112-2-16-22 [English]

5. Xu, M.H. Zhu, Z.R. Zhou, Fretting wear behavior of PTFE-based bonded solid lubrication coatings. *Thin Solid Films,* V. 457, Issue 2, 2004, Pages 320-325, https://doi.org/10.1016/j.tsf.2003.10.008 [English]

6. Li, Y.; Chen, Y.; Guo, Y.; Bian, D.; Zhao, Y. Tribological Behavior of PEEK/PTFE Composites Reinforced with Carbon Fibers and Graphite. *Materials* 2022, 15, 7078. https://doi.org/10.3390/ma15207078 [English]

7. Ramanjaneyulu, G., and Rajendran, R., Study of Wear Behaviour of POM/Graphite and POM/MoS_2 Composites, *SAE Technical Paper* 2017-28-1988, 2017, https://doi.org/10.4271/2017-28-1988 [English]

8. Charfi A, Neili S, Kharrat M, Dammak M. Tribological behaviors of PTFE-based composites filled with bronze microparticles. *Journal of Thermoplastic Composite Materials.* 2019. 34(12): 1639-1653. https://doi.org/10.1177/0892705719875203 [English]

9. Zygmunt R. Adhesion and wear in miniature plastic bearings. *Wear* 1991. 142, no. 1 185–93. http://dx.doi.org/10.1016/0043-1648(91)90160-v [English]

10. Khimko A., Popov O., Khimko M. Efect of temperature on the wear resistance TI6AL4V-CFRP/GFRP contact under vibration conditions. *Friction and wear problems.* 2026. No 1 (110). Pp. 4-12. URL: https://doi.org/10.18372/0370-2197.1(110).20915 [English]

11. Khimko A. M., Khimko M. S., Popov O. V., Klipachenko V. V. Estimation of the stress-strain state of composite materials for hinged bearings. *Problems of friction and wear.* 2025. № 1 (106). Pp. 4-16. URL: https://doi.org/10.18372/0370-2197.1(106).19819 [Ukrainian]

Хімко А.М., Мікосянчик О.О., Хімко М.С., Кліпаченко В.В. Підвищення довговічності контакту Ti-GFRP/CFRP прошарком зносостійких полімерних композиційних покриттів в умовах вібраційного навантаження

Розвиток авіації та підвищення льотно-технічних характеристик літаків та вертольотів вимагає застосування вуглепластиків CFRP та склопластиків GFRP в силових конструкціях. Фактор вібраційних навантажень є невід'ємною частиною конструкції повітряного судна. При вібраціях контакт який ми вважали номінально нерухомим починає з часом рухатись на мікрорівні. Переміщення між деталями достатньо для катастрофічного розвитку фретинг-корозійного зношування контактуючих деталей із наступним розвитком втомних тріщин та руйнування конструкції. В роботі проведено аналіз зносостійких композиційних матеріалів та визначено, що найбільше підходять для цього матеріали Ф4К15М5 та ZX550. Встановлено, що при випробуваннях в системі Ti-Ф4К15М5-GFRP поверхня металу захищена повністю за рахунок намазування на поверхню проміжного матеріалу. При випробуваннях із матеріалом ZX550 сумарний захист контакту Ti-ZX550-GFRP на 30 % нижче ніж при випробуваннях із прошарком матеріалу Ф4К15М5 але на поверхнях титанового сплаву маємо пошкодження від дії армованих волокон E-glass. Визначено механізми зношування проміжних матеріалів та їх вплив на контакт при вібраційних навантаженнях. Встановлено, що при впливі вібраційних навантажень до 10 МПа можна рекомендувати матеріал Ф4К15М5 в системі контактів Ti-Ф4К15М5-GFRP/CFRP, який дасть гарантований захист матеріалів на деякий час, а при довготривалої роботи та навантаженні більше 20 МПа можна рекомендувати фірми Zedex ZX550, який буде своєрідним балансом в пошкодженнях та спрацюваннях всіх матеріалах контакту Ti-ZX550-GFRP/CFRP.

Ключові слова: вібрації, титанові сплаві, зносостійкі полімерні матеріали, вуглепластик CFRP, склопластик GFRP, довговічність, аналіз, фретинг-корозія

ISSN 2079-1372 Problems of Tribology, V. 31, No 2/120-2026, 23-33

Problems of Tribology
Website: http://tribology.khnu.km.ua/index.php/ProbTrib
E-mail: tribosenator@gmail.com

DOI: https://doi.org/10.31891/2079-1372-2026-120-2-23-33

Technological features of forming regular micro reliefs on conical surfaces

V.O. Dzyura, * 0000-0002-1801-2419, **S.S. Kyryk** 0009-0002-6649-7649

Ternopil Ivan Puluy National Technical University, Ukraine
**E-mail: volodymyrdzyura@gmail.com*

Received: 28 March 2026: Revised 25 April 2026: Accept: 04 May 2026

Abstract

The paper examines the technological features of schemes for forming regular micro reliefs on conical surfaces. A classification of these formation schemes is proposed according to the regularity of the generated micro relief and its geometric parameters. A set of possible groove configurations of the formed micro relief has been obtained, comprising 54 variants of geometric property combinations that integrate the shape of the axial line of the micro relief grooves, the pattern of variation of the groove geometric parameters, and the groove profile itself. The specific characteristics of each technological scheme are analyzed, and the principal analytical relationships are derived that determine the interdependence between the geometric parameters defining the shape of the micro relief groove elements-namely the pitch (T_k) and the amplitude (A_g); the groove arrangement parameter – the center-to-center spacing (S_o); and the parameters of the conical surface, including the cone angle (α_c) and the length of the axial line of the regular micro irregularities formed on the conical surface. The obtained relationships make it possible to ensure the regularity of the micro relief groove elements and to form a micro relief with the required geometric parameters. It has been established that the determination of the length of the helical line on the conical surface forms the basis for further calculations of the groove elements arranged along this line. An analytical expression for determining the length of this line has been obtained, which serves as a foundation for ensuring the regularity of micro relief grooves formed along a helical line according to the method of geometric similarity.

Keywords: regular micro reliefs, grooves, conical surfaces, geometric parameters.

Introduction

Modern mechanical engineering increasingly relies on the concept of the "functional surface," where the condition of the subsurface layer determines a component's service life, energy efficiency, and reliability as significantly as material strength or geometric precision. This is particularly critical for machine parts designed as "bodies of revolution," as they operate in high-precision friction pairs involving rolling or sliding contact: shafts and bushings, bearing journals, rollers, liners, plunger and spool pairs, sealing elements, and the working surfaces of vibration and pumping units. In such systems, contact pressures, cyclic loads, local temperature spikes, and complex lubrication regimes—ranging from hydrodynamic to boundary lubrication—create stress concentration zones and potential reductions in durability. Consequently, the controlled formation of micro-reliefs to enhance surface performance characteristics remains a vital challenge for contemporary mechanical engineering.

Literature review

Surface engineering involves a significant volume of scientific research aimed at developing innovative technological solutions in mechanical engineering to meet the growing demands of the industry. The use of traditional surface treatment methods is approaching its technical limits, restricting the possibilities for enhancing and imparting the necessary performance characteristics to the surfaces of machine parts.

Modern mechanical engineering actively employs methods such as surface plastic deformation, chemical, and thermochemical treatment to improve the functional properties of surfaces. These methods are well-studied and widely applied to ensure the specified characteristics of the working surfaces of components [1, 2, 3]. They guarantee the stability of the physicochemical, mechanical, and operational properties of the formed surfaces throughout their entire service life.

The feasibility of forming regular micro-reliefs on the functional surfaces of machine parts is primarily driven by the ability to purposefully control the functional properties of the surface layer at the micro-geometric level. Unlike stochastic roughness, a regular texture ensures a predictable contact nature, stable lubrication conditions, and a controlled load distribution within the friction zone. This facilitates a transition from empirical parameter selection to the engineering design of surfaces with predetermined tribological, hydrodynamic, and wear-resistant characteristics. Research in the field of surface plastic deformation has demonstrated that ordered micro-grooves or cellular structures act as lubricant micro-reservoirs, reduce the real contact area, and promote the formation of a stable lubricant film, leading to a reduction in the friction coefficient and contact zone temperature [4]. Generally, it can be asserted that textured surfaces produced via burnishing and rolling exhibit enhanced wear resistance and contact endurance due to the strengthening of the surface layer and the formation of a favorable micro-topography. For surfaces with regular micro-reliefs, one of the most critical parameters is the relative area of the micro-relief—a value indicating the ratio of the projected area of the micro-relief grooves to the total surface area on which they are located [5]. The formation of regular micro-reliefs on flat surfaces does not present significant difficulties and is easily implemented at the current level of technological development. On flat surfaces, it is possible to realize any micro-relief shape and ensure complete regularity. Regularity is defined as the stability of the micro-relief's geometric parameters in two mutually perpendicular directions. Micro-reliefs on flat surfaces can be formed on standard milling or drilling machines without the use of specialized devices [6].

A more complex case involves the formation of regular micro-reliefs on internal or external cylindrical surfaces, particularly stepped ones. In this instance, the profile of the micro-relief grooves is somewhat distorted, with the magnitude of this distortion depending on the curvature of the surface being textured. Even more challenging is the formation of regular micro-reliefs on the face surfaces of bodies of revolution. Such surfaces are found on variator transmission discs, rod ends, face flanges, and other machine components. Analytical dependencies for determining the geometric parameters of triangular-profile micro-relief grooves are defined in [7]. A specific feature of forming micro-relief grooves on the face surfaces of bodies of revolution is that the linear velocity of a point decreases as it approaches the center of rotation, necessitating constant correction of the processing regimes. Furthermore, it is impossible to form a completely regular micro-relief on such a surface because the circumference decreases toward the center of rotation. Consequently, grooves located on this inner circumference will have a smaller circular pitch than those located on a circumference with a larger radius. The most complex case involves intricate profiled surfaces: involute, spherical, conical, and other complex geometries. The difficulty lies in the fact that the geometric parameters of the grooves (amplitude, axial pitch) change continuously. Consequently, the relative area of the micro-relief will vary across different sections, leading to discrepancies in the surface's operational properties. However, the application of three- or five-axis CNC machine tools enables the reproduction of grooves in practically any configuration, while stepless feed regulation guarantees high geometric precision and texture parameter stability. This results in a fully regular structure with cells of the required, even highly complex, shape.

Typically, the tool used for forming micro-relief grooves allows for the regulation of the deforming force, utilizing a ball as the deforming element. The proposed tool facilitates the generation of various texture types with grooves of arbitrary configurations, where the design process involves preliminary mathematical modeling in the MathCAD environment. Such modeling determines the coordinates of characteristic profile points used to prepare the CNC control program. This allows for the pre-standardization of micro-relief geometric parameters, evaluation of its relative area, and prediction of the textured surface's operational properties. The advantages of this approach include versatility regarding groove shape and size, as well as the ability to purposefully form the required physical and mechanical characteristics of the surface layer. The primary limitations remain the high cost of equipment and tooling, alongside relatively low productivity.

Another approach is based on the copying or rolling method [8], where the decisive role is played by a tool with forming elements whose geometry directly corresponds to the configuration of the intended grooves. In this case, the surface structure is reproduced through the mechanical transfer of the tool profile onto the workpiece material, where the relationship between the feed rate and the rotational speed of the working unit determines the spatial arrangement of the grooves and the shape of their lateral flanks.

The most effective technical solutions for forming various types of regular micro-reliefs involve the use of tools and equipment described in [9]. Experimental studies demonstrate that such technological systems enable the formation of regular micro-reliefs of varying complexity on virtually any surface. Software-controlled processing ensures high geometric precision of the formed grooves and, consequently, maintains a stable relative area of the micro-relief.

In study [10], the influence of the arrangement of triangular regular micro-irregularities on the friction coefficient between the end surfaces of bodies of revolution was investigated, both with and without the use of L-AN-46 lubricant. The experiments were conducted with a clamping force of 20 N and a relative sliding velocity of 0.4 m/s. The authors found that the arrangement of micro-relief elements significantly affects the friction coefficient values. The lowest friction coefficient was observed during the interaction of end surfaces with a micro-relief featuring a central angle of 90° oriented toward the outer edges of the end surface.

The mechanisms of regular micro-relief formation and their positive impact on enhancing performance properties are also detailed in [11].

The aim of this work is to derive fundamental analytical dependencies that describe the regularities of regular micro-relief distribution on the conical surfaces of bodies of revolution.

Research materials and methodology

For bodies of revolution, the requirement for regularity takes on additional significance due to the specific kinematics of relief formation. Most technologies used to create micro-reliefs on cylindrical surfaces rely on a combination of workpiece rotation and tool feed, resulting in relief elements formed along helical trajectories or their combinations. Any instability within this kinematic pair – such as runout, synchronization errors between feed and rotation, elastic deformations of the technological system, fluctuations in contact force, or tool wear and micro-slippage – immediately translates into a disruption of the pattern's periodicity. This manifests as variations in pitch and depth, distortion of element geometry, or local rarefaction and oversaturation of the texture. In turn, an irregular micro-relief generates non-homogeneous pressure and temperature fields within the contact zone, impairs the repeatability of the tribological effect, and may facilitate local zones of accelerated wear or the initiation of fatigue damage. Thus, for components designed as bodies of revolution, micro-relief regularity is a fundamental prerequisite for the controllability and functional reliability of the surface. There are three principal schemes for forming regular and partially regular micro-reliefs on conical surfaces (Fig. 1), one of which comprises two subtypes.

The first scheme involves the formation of micro-reliefs with grooves arranged in concentric circles with uniform geometric parameters. In this case, the grooves form a system of closed circles whose centers coincide with the axis of the conical surface. The geometric characteristics of the grooves – width, depth, and the spacing between them – remain constant across all concentric trajectories. This scheme ensures a uniform distribution of micro-asperities across the surface and is utilized when homogeneous tribological properties are required throughout the entire contact area.

The second scheme involves the formation of micro-reliefs with grooves arranged in concentric circles based on the principle of geometric similarity. In this instance, the grooves also form a system of concentric circles; however, their geometric parameters vary proportionally to the distance from the cone's vertex. This approach ensures the scale similarity of micro-relief elements across the entire surface and accounts for the varying local radius of the conical surface.

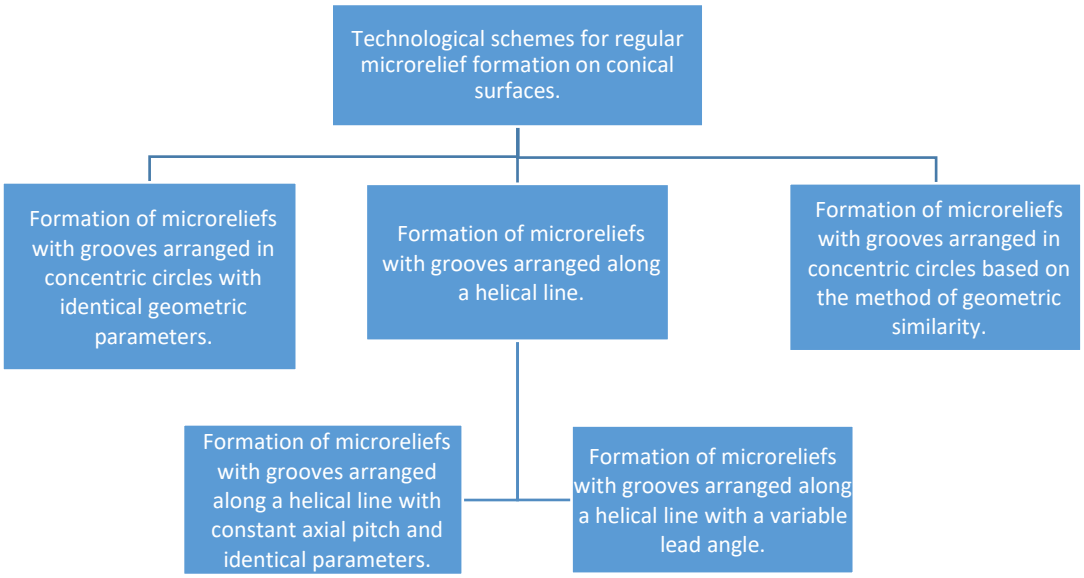

Fig. 1. Classification of technological schemes for regular micro relief formation on conical surfaces

The third scheme involves the formation of micro reliefs with grooves arranged along a helical line. In this case, the groove forms a continuous spiral trajectory on the conical surface. This type of micro relief is generated through a combination of the part's rotational motion and the tool's translational movement. The helical arrangement of the grooves creates a directional surface structure, which can improve lubricant drainage or facilitate the formation of a hydrodynamic lubrication wedge. This scheme is characterized by the formation of grooves along a helical line with a constant axial pitch and groove amplitude. This allows for the adjustment of groove density across different sections of the conical surface, which may be necessary to compensate for changes in contact conditions or loading along the cone.

The fourth scheme shares common features with the second and third schemes; however, the micro relief grooves are formed using the method of geometric similarity. This allows for the maintenance of the ratio between the primary geometric parameters of the groove element, ensuring a proportional change in the shape of the micro

relief grooves as the diameter of the conical surface decreases. These schemes provide for the creation of a set of possible micro relief groove variants formed on conical surfaces (Fig. 2), which includes 54 variants of geometric property sets. These sets combine the shape of the groove centerline, the law governing the change in geometric parameters of the grooves, and the groove shape itself. At the first parameter level, the shape of the groove centerline is defined: it can be in the form of a concentric circle, a helical line with a constant pitch, or a helical line with a constant lead angle. At the second level, the law governing the change in the geometric parameters of the micro relief grooves is specified: constant geometric parameters T_g and A_g allow for the formation of identical micro relief groove elements; parameters determined by the method of geometric similarity in the axial direction ensure a gradual reduction of the groove without losing the ratio between the axial pitch T_g and the groove amplitude A_g; parameters determined by the method of geometric similarity in the inter-axis direction provide partial regularity of the micro relief with a gradual reduction of the axial pitch.

At the third level, the alignment of the micro relief grooves is established, which is determined by the relationship between the symmetry lines of the groove elements. They can be coaxial, where the symmetry axes of the groove elements located on circles (coils) of different diameters coincide; shifted by $0.5T_k$, which is a condition for creating micro reliefs with grooves whose peaks may touch; and other so-called "creeping" displacements, where the displacement value Δ is within the range $0 < \Delta < 0.5T_k$.

At the final level, the shape of the micro relief groove is selected. The most common are sinusoidal and triangular shapes of continuous micro relief grooves.

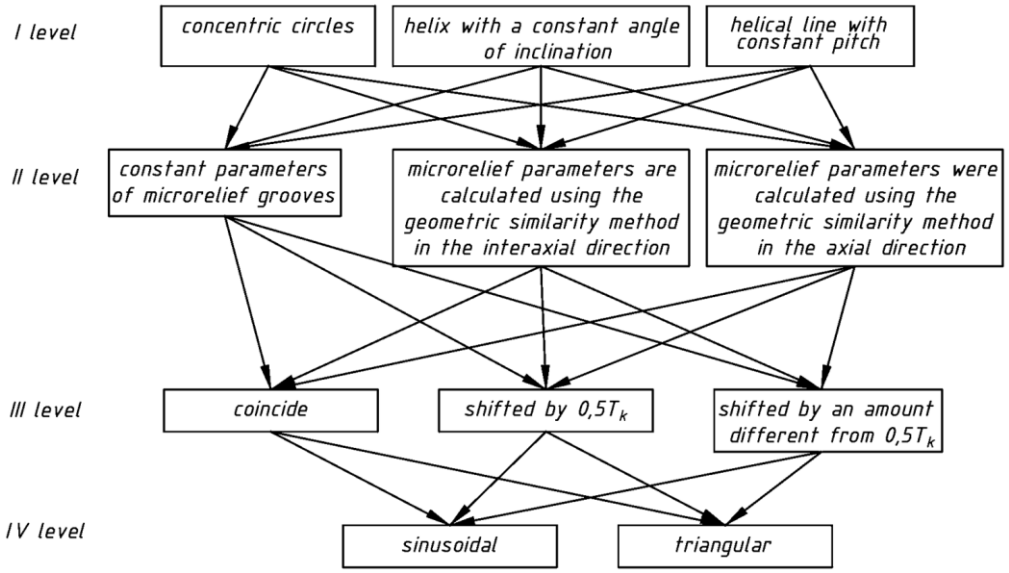

Fig. 2. Set of possible variants for micro relief grooves formed on conical surfaces

The parameterization of the geometric properties of regular micro relief grooves formed on a conical surface is quite complex (Fig. 3); it differs significantly from grooves formed on flat surfaces and more closely resembles grooves formed on the end faces of bodies of revolution [12].

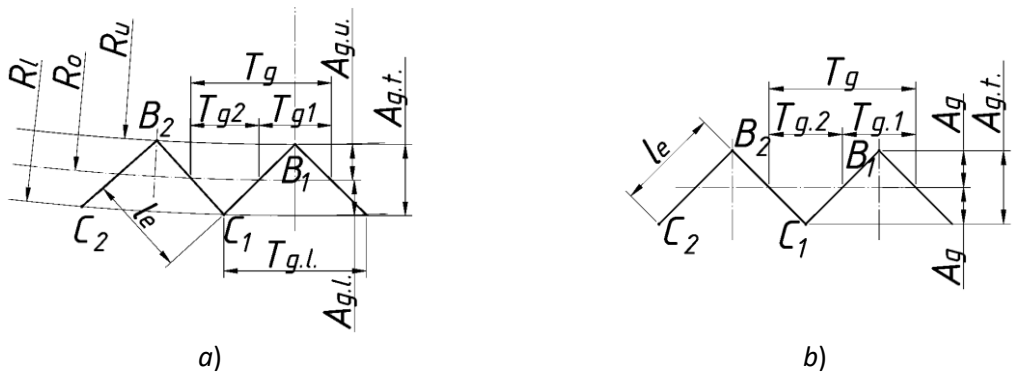

a) *b*)

Fig. 3. Parameters of triangular profile microrelief grooves: (*a*) formed on a conical surface according to the scheme of groove arrangement in concentric circles with identical geometric parameters; (*b*) formed on a flat surface

As seen in (Fig. 3*a*), the simplest triangular profile micro relief grooves formed on a conical surface are described by a greater number of geometric parameters due to the asymmetry of the groove profile relative to the longitudinal axis R_o.

The amplitude value $A_{g.u.}$, defined from the groove centerline described by a circle of radius R_o to the peaks lying on a circle of radius R_l, and the amplitude value $A_{g.l.}$, defined from the centerline to the peaks lying on a circle of radius R_u, are not identical, i.e., $A_{g.u.} \neq A_{g.l.}$ Collectively, these values determine the total groove height $A_{g.t.} = A_{g.u.} + A_{g.l.}$ The corresponding parameter for grooves formed on flat surfaces (Fig. 3b) is identical and equals A_g.

The parameter T_g, which describes the axial pitch of the micro relief grooves formed on flat surfaces (Fig. 3b), is defined as the distance between periodically repeating parts of the groove profile and represents the sum of the segments intersecting the groove profile along the centerline, i.e., $T_g = T_{g1} + T_{g2}$.

For grooves formed on conical surfaces (Fig. 3a), the axial pitch T_g is also defined as the distance between periodically repeating parts of the groove profile; however, the segments that constitute it are non-identical, i.e. $T_{g.1} \neq T_{g.2}$. This occurs because the outer and inner peaks of the micro relief grooves are located on circles of different radii, R_l and R_u. Consequently, the distance between the profile peaks BB_1 will be smaller than the distance between the profile bases CC_1. Thus, for the analytical description of the geometric parameters of regular micro relief grooves formed on conical surfaces, it is appropriate to employ modified notation for the primary geometric parameters: the axial pitch T_g and the amplitude A_g.

The formation scheme of regular micro reliefs with grooves arranged on concentric circles of a conical surface (Fig. 4) ensures uniform geometric parameters A_g, T_g, which remain constant regardless of the circumference (the centerline of the micro relief grooves) on which the groove elements are located. A distinctive feature of this formation scheme is that the number of groove elements positioned at different levels is non-identical and decreases as they approach the apex of the conical surface. The center-to-center distance S_o between micro relief grooves at adjacent levels is determined by the groove pitch T_g and the inclination angle of the conical surface α_c. The resulting micro relief is partially regular. Regularity is maintained for parameters A_g and T_g, however, given the specific characteristics of the conical surface, the center-to-center pitch S_o of the micro relief grooves is inconsistent. Furthermore, the coaxiality of the micro relief grooves is not maintained. The specific characteristics of forming such micro relief grooves are illustrated in Figure 3.

The method for forming the grooves is implemented as follows. By combining the rotation movement D_n of the workpiece with a conical surface at a rotational speed n_g with the simultaneous reciprocating movement D_i of a ball-shaped deforming element – using an amplitude A_g and an oscillation frequency i_g – grooves are formed with a pitch $T_g = \pi \cdot D_1/m$, where D_1 is the cross-sectional diameter of the surface of the body of revolution and m is the number of groove elements formed per single revolution of the workpiece.

Upon completing one full revolution of the workpiece with the conical surface about its axis, the rotational movement D_n and the oscillatory movement D_i are deactivated. The deforming element is withdrawn from contact with the conical surface and is moved along the workpiece axis by the center-to-center distance S_o using a discrete movement D_s. Subsequently, the deforming element is reintroduced into engagement with the conical surface of the workpiece, the movements D_i and D_n are reactivated, and the formation of the micro relief grooves proceeds.

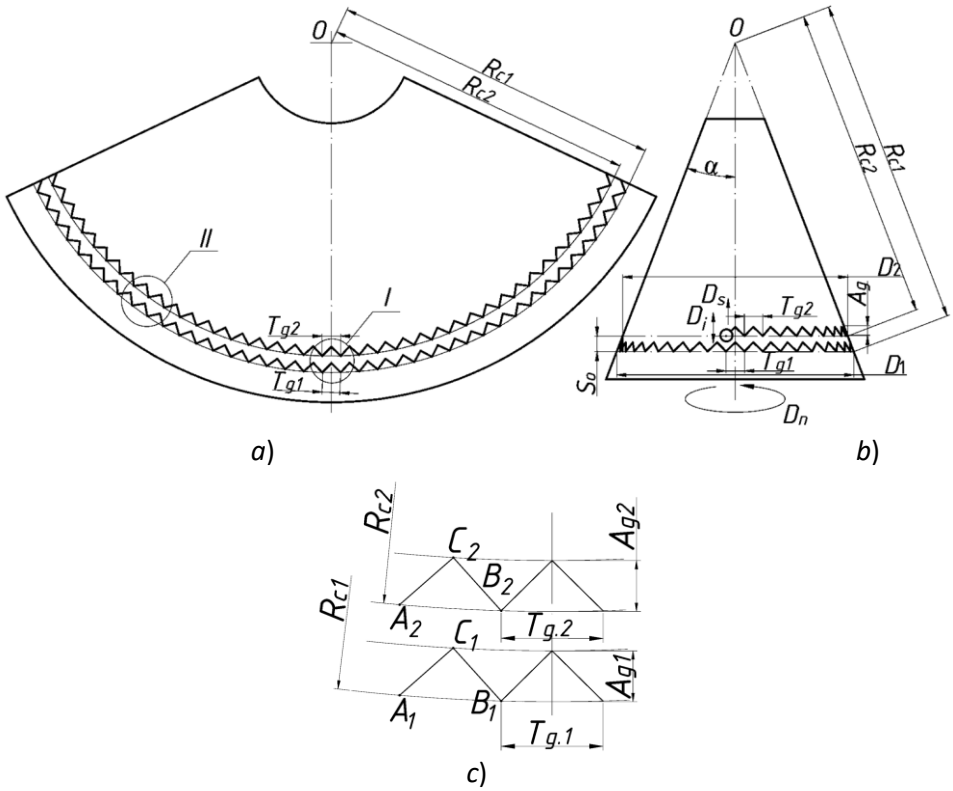

Fig. 4. The formation scheme of a regular micro relief on a conical surface with grooves arranged in concentric circles with identical geometric parameters: (*a*) development of the conical surface; (*b*) general view of the conical surface; (*c*) – parameterization of the micro relief grooves.

The absence of distortion in the profile of a groove formed with uniform geometric parameters is achieved by reducing the number of groove elements on the surface. A disadvantage of this scheme is that, despite ensuring identical primary geometric parameters for the grooves (A_g, T_g), the resulting microrelief will be irregular. This is clearly observed when comparing the coaxiality of grooves located at different levels (Fig. 4a). This occurs because the circular arcs on which the grooves are positioned have different surface curvatures.

The core of the method for forming grooves with uniform geometric parameters involves determining a circle diameter D_2 on the conical surface that can accommodate an integer number of groove elements with the pitch T_g used on a circle of a different diameter D_1 (Fig. 4c). Consequently, the oscillation frequency of the deforming element on circles of different diameters will vary and depends on the number of groove elements.

Analytical dependencies that establish the relationship between the geometric parameters defining the groove shape – specifically the pitch T_k and amplitude A_g the groove placement parameters (center-to-center distance S_o), and the surface parameters (inclination angle α and the length of the axial line of the regular micro-irregularities) will facilitate ensuring the regularity of the micro relief grooves and the formation of a micro relief with the required specifications.

The length of the arc on which the micro relief groove elements are positioned is determined by the following formula:

$$L_1 = \frac{\pi \cdot R_1 \cdot \alpha}{180^\circ} \tag{1}$$

where R_1 is the radius of a circle with diameter D_1, мм;
α is the cone apex angle, deg.

On an arc of radius R_1, n_1 groove elements are positioned; therefore, the arc length corresponding to a single groove element is defined as:

$$l_{g1} = \frac{\pi \cdot R_1 \cdot \alpha}{n_1 \cdot 180^\circ} \tag{2}$$

Since linear dimensions are used during the design of the grooves, and in order to eliminate the distortion caused by the placement of groove elements along a circular arc, the groove pitch is defined as:

$$T_g = 2 \cdot R_1 \cdot \sin\left(\frac{l_g \cdot 90^\circ}{R_1 \cdot \pi}\right) = 2 \cdot R_1 \cdot \sin\left(\frac{\alpha}{2 \cdot n_1}\right) \tag{3}$$

The radius of the circle on which the groove containing n_2 elements is positioned shall be determined by the following dependency:

$$R_2 = \frac{l_g \cdot n_2 \cdot 180^\circ}{\pi \cdot \alpha} = \frac{R_1 \cdot n_2}{n_1} \tag{4}$$

The center-to-center pitch S_o of the micro relief grooves is determined by the following dependency:

$$S_o = \frac{m \cdot T_g}{2 \cdot \pi \cdot tg\alpha} \tag{5}$$

where T_g is the axial pitch of the micro relief grooves, mm;
m – an integer indicating how much smaller the number of micro relief groove elements located on a concentric circle of diameter D_2 is compared to those on a concentric circle of diameter D_1.

The scheme for forming micro reliefs with grooves arranged in concentric circles using the method of geometric similarity assumes the geometric similarity of the axial pitch T_g, while the groove amplitude A_g remains constant (Fig. 5).

A key feature of this scheme is that the oscillation frequency of the deforming element will remain the same during the formation of micro relief groove elements on each concentric circle of diameter D_2 on the conical surface. Micro relief grooves positioned on concentric circles of different diameters D_1 and D_2 on the conical surface will have an identical amplitude A_g but different axial pitches T_{g2}. The latter is determined via the method of geometric similarity based on the ratio of the diameters of the concentric circles where the micro relief grooves are formed, using the formula: $T_{g2} = T_{g1} \times D_2/D_1$.

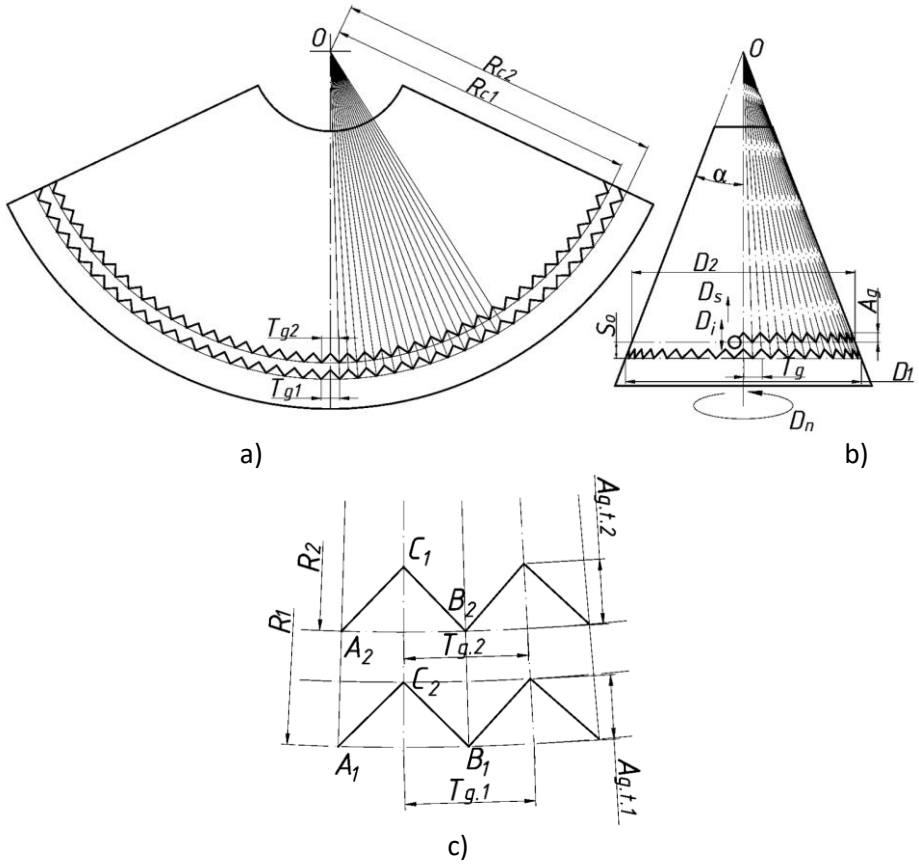

Fig. 5. The formation scheme of a regular microrelief on a conical surface with grooves arranged in concentric circles using the method of geometric similarity (*a*) development of the conical surface; (*b*) general view of the conical surface; (*c*) parameterization of the microrelief grooves.

Technologically, the simplest approach for forming a regular microrelief on a conical surface is a scheme in which the microrelief grooves are arranged along a helical line. This scheme can be implemented in two variants: where the microrelief grooves are positioned along a helical line with a uniform pitch (Fig. 6), and where they are positioned along a helical line with a constant inclination angle but uniform pitch. Considering the technological aspects of implementation, the scheme with a uniform pitch is simpler, as it is ensured by the stability of the machine tool feed rate.

At the same time, this scheme is one of the most complex in terms of determining the geometric parameters of the microrelief grooves, as the grooves are positioned along a helical line described on a conical surface rather than a circular arc (Fig. 6).

The precise determination of the helical line length is a necessary prerequisite for ensuring the regularity of the formed microrelief. A helical line on a conical surface has a complex shape because its radius changes along the axis. Its length is most accurately determined through parametric specification and the integration of an arc element.

The coordinates of a point on a helical line on a cone can be specified as follows:

$$\begin{cases} x = z \cdot \tan(\alpha) \cdot \cos(\varphi) \\ y = z \cdot \tan(\alpha) \cdot \sin(\varphi) \\ z = \dfrac{S_o \cdot \varphi}{2\pi} \end{cases} \tag{6}$$

where α – angle between the axis and the generator of the conical surface, deg;
φ – angle of rotation around the axis, deg;
S_o – pitch of the helical line (Fig. 6), mm.
From this, the radius on the cone is determined by the formula:

$$r(\varphi) = \frac{S_o}{2\pi} \varphi \cdot \tan(\alpha) \tag{7}$$

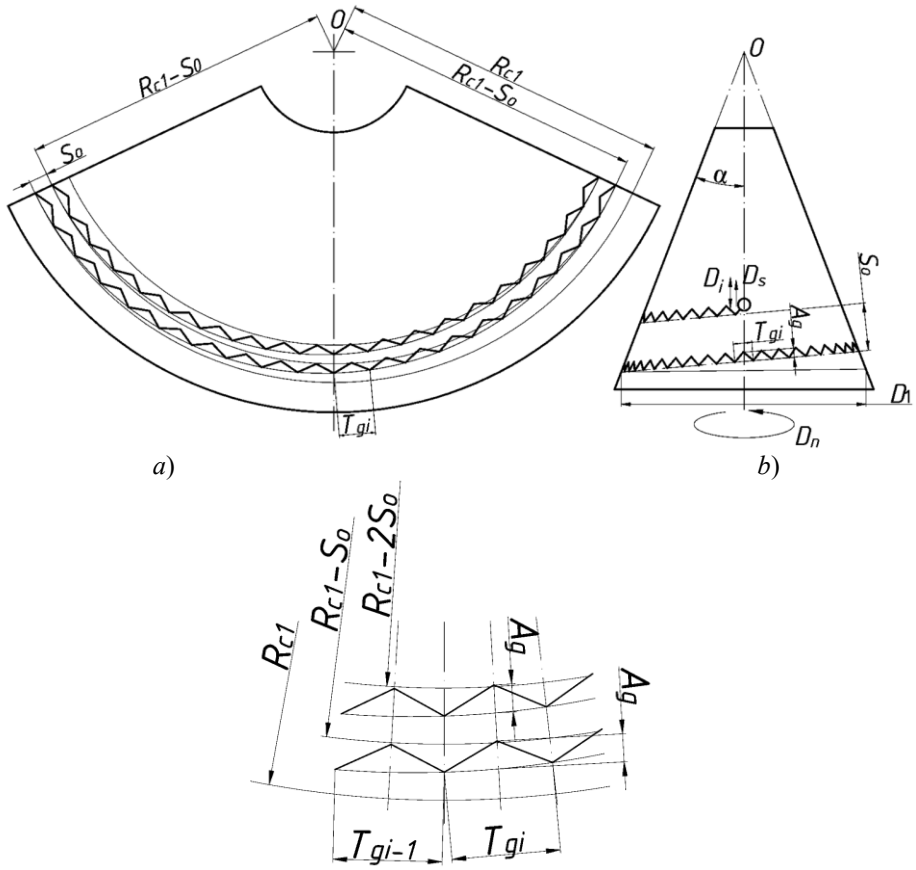

Fig. 6. The formation scheme of a regular micro relief on a conical surface with grooves arranged along a helical line using the method of geometric similarity (*a*) development of the conical surface; (*b*) general view of the conical surface; (*c*) parameterization of the micro relief grooves.

The length of the helical line is determined through the arc element of a spatial curve:

$$ds = \sqrt{\left(\frac{dx}{d\varphi}\right)^2 + \left(\frac{dy}{d\varphi}\right)^2 + \left(\frac{dz}{d\varphi}\right)^2}\, d\varphi \tag{8}$$

After substitution, we obtain the formula for the length of the helical line from φ_1 to φ_2

$$L = \int_{\varphi_1}^{\varphi_2} \sqrt{\left(\frac{S_o}{2\pi}\right)^2 + \left(\frac{S_o}{2\pi}\cdot\tan(\alpha)\right)^2 \cdot \left(1+\varphi^2\right)}\, d\varphi \tag{9}$$

To determine the length of a single turn, the angle values are as follows: $\varphi_1=0$ and $\varphi_2=2\pi$.

However, for practical application, it is more convenient to derive an analytical dependency for determining the helical line length that incorporates the geometric parameters of the conical surface – specifically, the larger *R* and smaller *r* radii of the cone.

A precise parametric description of a single turn: if $\varphi\in[0,2\pi]$, then the radius varies from *r* to *R*.

$$\rho(\varphi) = r + \frac{R-r}{2\pi}\varphi \tag{10}$$

Then the spatial curve is defined as:

$$\begin{cases} x = \rho(\varphi)\cdot\cos(\varphi) \\ y = \rho(\varphi)\cdot\sin(\varphi) \\ z = \dfrac{p\cdot\varphi}{2\pi} \end{cases} \tag{11}$$

where ρ – the current radius of a point on the helical line, i.e., the distance from the cone axis to a point on the curve.

The length of a single turn is determined by the formula:

$$L=\int_0^{2\pi}\sqrt{\left(\frac{dx}{d\varphi}\right)^2+\left(\frac{dy}{d\varphi}\right)^2+\left(\frac{dz}{d\varphi}\right)^2}\,d\varphi \tag{12}$$

Since

$$\rho'(\varphi)=\frac{R-r}{2\pi} \tag{13}$$

then after differentiation, we obtain the standard result:

$$\left(\frac{dx}{d\varphi}\right)^2+\left(\frac{dy}{d\varphi}\right)^2=(\rho'(\varphi))^2+\rho^2(\varphi) \tag{14}$$

Therefore

$$L=\int_0^{2\pi}\sqrt{\left(\frac{R-r}{2\pi}\right)^2+\left(r+\frac{R-r}{2\pi}\varphi\right)^2+\left(\frac{S_o}{2\pi}\right)^2}\,d\varphi \tag{15}$$

For convenience, we introduce the notation

$$a=\frac{R-r}{2\pi};\qquad b=\frac{S_o}{2\pi}; \tag{16}$$

Then

$$L=\int_0^{2\pi}\sqrt{a^2+b^2+(r+a\varphi)^2}\,d\varphi \tag{17}$$

Making a replacement

$$u=r+a\varphi\qquad du=ad\varphi; \tag{18}$$

At φ=0: $u=r$, at φ=2π: $u=R$.
Then

$$L=\frac{1}{a}\int_r^R\sqrt{u^2+a^2+b^2}\,d\varphi \tag{19}$$

Let us denote

$$c^2=a^2+b^2 \tag{20}$$

That is

$$c^2=\left(\frac{R-r}{2\pi}\right)^2+\left(\frac{S_o}{2\pi}\right)^2=\frac{(R-r)^2+S_o^{\,2}}{4\pi^2} \tag{21}$$

Given the formula for the original indefinite integral

$$\int\sqrt{u^2+c^2}\,du=\frac{u}{2}\sqrt{u^2+c^2}+\frac{c^2}{2}\ln\left(u+\sqrt{u^2+c^2}\right)+C \tag{22}$$

where C – arbitrary constant of integration.
Formula (19) will take the form

$$L=\frac{1}{a}\left[\frac{u}{2}\sqrt{u^2+c^2}+\frac{c^2}{2}\ln\left(u+\sqrt{u^2+c^2}\right)\right]_r^R \tag{23}$$

Because

$$\frac{1}{a}=\frac{2\pi}{R-r} \tag{24}$$

Then formula (23) will take the form

$$L=\frac{\pi}{R-r}\left[R\sqrt{R^2+c^2}-r\sqrt{r^2+c^2}+c^2\ln\left(\frac{R+\sqrt{R^2+c^2}}{r+\sqrt{r^2+c^2}}\right)\right] \tag{25}$$

where

$$c^2=\frac{(R-r)^2+S_o^{\,2}}{4\pi^2}; \tag{26}$$

Taking into account (26), formula (25) takes the following form:

$$L=\frac{\pi}{R-r}\left[R\sqrt{R^2+\frac{(R-r)^2+S_o^{\,2}}{4\pi^2}}-r\sqrt{r^2+\frac{(R-r)^2+S_o^{\,2}}{4\pi^2}}+\frac{(R-r)^2+S_o^{\,2}}{4\pi^2}\ln\left(\frac{R+\sqrt{R^2+\frac{(R-r)^2+S_o^{\,2}}{4\pi^2}}}{r+\sqrt{r^2+\frac{(R-r)^2+S_o^{\,2}}{4\pi^2}}}\right)\right] \quad (27)$$

Both formula (25) and formula (26) are convenient for engineering use. They include only the values of the conical surface dimensions and the center-to-center pitch S_o. An accurate value for the length of the helical line will allow for the calculation of the axial pitch T_g to ensure the required microrelief parameters.

Conclusions

Technological schemes for forming a regular micro relief with continuous grooves on the conical surfaces of bodies of revolution have been considered. The technological features of forming a regular micro relief with triangular-shaped grooves on the conical surfaces of bodies of revolution have been established. A condition for the regularity of such grooves has been obtained depending on their geometric parameters, placement parameters, and the parameters of the conical surface. It has been established that when ensuring the regularity of the micro relief grooves, the center-to-center distance S_o is a discrete parameter proportional to the pitch of the micro relief grooves T_k.

References

1. Gurey, V., Hurey, I., Hurey, T., Wojtowicz, W. (2023). Fatigue Strength of Steel Samples After Friction Treatment. In: Tonkonogyi, V., Ivanov, V., Trojanowska, J., Oborskyi, G., Pavlenko, I. (eds) Advanced Manufacturing Processes IV. InterPartner 2022. Lecture Notes in Mechanical Engineering. Springer, Cham. https://doi.org/10.1007/978-3-031-16651-8_26

2. Hurey, I., Hurey, T., Gurey, V. (2020). Wear Resistance of Hardened Nanocrystalline Structures in the Course of Friction of Steel-Grey Cast Iron Pair in Oil-Abrasive Medium. In: Ivanov, V., et al. Advances in Design, Simulation and Manufacturing II. DSMIE 2019. Lecture Notes in Mechanical Engineering. Springer, Cham. https://doi.org/10.1007/978-3-030-22365-6_57

3. Swirad, S. Influence of Ball Burnishing on Lubricated Fretting of the Titanium Alloy Ti6Al4V. Lubricants 2023, 11, 341. https://doi.org/10.3390/lubricants11080341

4. Pawlus, P., Reizer, R., & Wieczorowski, M. (2025). Improvement of wear scar volume estimation in reciprocating motion. Wear, 572-573, Article 205615. https://doi.org/10.1016/j.wear.2024.205615.

5. Pawlus, P., Koszela, W., & Reizer, R. (2022). Surface texturing of cylinder liners: A review. *Materials, 15*, 8629. https://doi.org/10.3390/ma15238629

6. Zhan, X., Yi, P., Liu, Y., Xiao, P., Zhu, X., & Ma, J. (2020). Effects of single- and multi-shape laser-textured surfaces on tribological properties under dry friction. *Proceedings of the Institution of Mechanical Engineers, Part C: Journal of Mechanical Engineering Science, 234*(7), 1382–1392. https://doi.org/10.1177/0954406219892294

7. Slavov, S., & Dimitrov, D. (2018). A study for determining the most significant parameters of the ball-burnishing process over some roughness parameters of planar surfaces carried out on CNC milling machine. In *MATEC Web of Conferences, 178*, 02005. https://doi.org/10.1051/matecconf/201817802005

8. Dzyura, V., Maruschak, P., & Prentkovskis, O. (2021). Determining optimal parameters of regular microrelief formed on the end surfaces of rotary bodies. *Algorithms, 14*, 46. https://doi.org/10.3390/a14020046

9 S. Slavov, I. Iliev, Design and FEM static analysis of an instrument for surface plastic deformation of non-planar functional surfaces of machine parts, Fiability & Durability, ISSN 1844 – 640X, 2016, Nov 1(2) DOI: 10.13140/RG.2.2.23594.21447.

10 S. Wos, W. Koszela, P. Pawlus. Comparing tribological effects of various chevron-based surface textures under lubricated unidirectional sliding. Tribology International 146 (2020) 106205 : (веб-сайт). URL: https://doi.org/10.1016/j.triboint.2020.106205

11 Jianfei Wang, Weihai Xue, Siyang Gao, Shu Li, Deli Duan. Effect of groove surface texture on the fretting wear of Ti–6Al–4V alloy. Wear. Vol. 486–487, 2021, 204079, https://doi.org/10.1016/j.wear.2021.204079.

12 Stępień, P. (2009). Regular surface texture generated by special grinding process. *Journal of Manufacturing Science and Engineering, 131*(1), 011015. https://doi.org/10.1115/1.3070511

Дзюра В.О., Кирик С.С. Технологічні особливості формування регулярних мікрорельєфів на конічних поверхнях

В статті розглянуто особливості технологічних схем формування регулярних мікрорельєфів на конічних поверхнях. Проведено класифікацію цих схем формування за регулярністю створюваного мікрорельєфу та його геометричними параметрами. Отримано множину можливих варіантів канавок сформованого мікрорельєфу, яка передбачає 54 варіанти наборів геометричних параметрів, які поєднують форму осьової лінії канавок мікрорельєфу, закономірність зміни геометричних параметрів канавок та власне їх форму. Розглянуто особливості кожної з технологічних схем та отримано основині аналітичні залежності, що визначаються взаємозв'язок між геометричними параметрами, що визначають форму елементів канавок мікрорельєфу – кроком T_k та амплітудою A_g, параметрами розміщення канавок – міжосьовою відстанню S_o, параметрами поверхні – кутом нахилу α_c та довжиною осьової лінії регулярних мікронерівностей, що сформовані на конічній поверхні. Отримані залежності допоможуть забезпечити регулярність елементів канавок мікрорельєфу та сформувати мікрорельєф із необхідними геометричними параметрами. Встановлено, що основою подальших розрахунків елементів канавок розміщених по гвинтовій лінії конусної поверхні є визначення довжини цієї лінії. Отримано аналітичну залежність для визначення довжини гвинтової лінії конусної поверхні, як основи забезпечення регулярності канавок мікрорельєфу сформованого на гвинтовій лінії за методом геометричної подібності.

Ключові слова: регулярні мікрорельєфи, канавки, конічні поверхні, геометричні параметри

ISSN 2079-1372 Problems of Tribology, V. 31, No 2/120-2026, 34-43

Problems of Tribology
Website: http://tribology.khnu.km.ua/index.php/ProbTrib
E-mail: tribosenator@gmail.com

DOI: https://doi.org/10.31891/2079-1372-2026-120-2-34-43

Effect of composition modification and heat treatment on the microstructure and wear resistance of plasma-sprayed nickel-based coatings for engine valves

O.V. Dykha* 0000-0003-3020-9625, **A.A. Vychavka** 0009-0009-1467-9337, **O.P. Babak** 0000-0002-1068-0631, **M.O. Dykha** 0000-0002-6075-1549, **V.O. Dytyniuk** 0000-0001-6377-524X

[1]*Khmelnytskyi national University, Ukraine*
**E-mail: tribosenator@gmail.com*

Received: 04 April 2026: Revised 05 May 2026: Accept: 10 May 2026

Abstract

The work investigated the microstructure, phase composition and wear resistance of plasma coatings based on self-fluxing nickel alloys obtained from PG-10N-01 powder and intended for strengthening internal combustion engine valves. It was established that due to high heating and cooling rates during plasma spraying, a lamellar structure with the presence of amorphous and crystalline phases, oxide inclusions and pores is formed. It was shown that heat treatment provides partial crystallization of the amorphous phase, a decrease in porosity and an increase in the microhardness of the coating. The distribution of microhardness along the depth of the layer was studied, which is characterized by relative stability within the coating and a gradual decrease in the transition zone to the base. The effect of composition modification (introduction of ferrosilicon) on the structure formation and porosity of the coating was established. According to the results of tribological tests, an increase in wear resistance and a decrease in the coefficient of friction after heat treatment were determined. The adhesive wear mechanism caused by the structural heterogeneity of the coating is substantiated.

Keywords: plasma spraying, NiCrBSi, microstructure, wear resistance, microhardness, heat treatment, phase composition, porosity, friction coefficient, internal combustion engine valve

Introduction

Increasing the durability and reliability of machine parts operating under conditions of intense friction and wear is one of the key tasks of modern mechanical engineering and materials science. This problem is of particular relevance for friction units of vehicles, energy and technological equipment, where the combination of high contact loads, temperature effects and aggressive environments leads to accelerated destruction of surface layers. Such critical elements include valves of internal combustion engines, which operate under conditions of cyclic thermomechanical loads, elevated temperatures, gas corrosion and intensive wear of contact surfaces. Destruction or premature wear of valves leads to a decrease in the efficiency of the engine and a reduction in its resource.

In this regard, technologies for forming protective coatings are becoming widely used, among which plasma spraying occupies a leading place due to its high versatility, productivity and the ability to obtain coatings with specified functional properties. The use of plasma coatings to strengthen the working surfaces of valves allows to increase their wear resistance, heat resistance and corrosion resistance, which directly affects the operational characteristics of the engine.

Plasma coatings based on self-fluxing nickel alloys are characterized by high hardness, resistance to corrosion and abrasive wear and the ability to form dense protective layers with good adhesion to the base. The formation of the microstructure of such coatings occurs under conditions of extremely high heating and cooling rates of powder particles, which leads to the formation of a lamellar structure with the presence of amorphous and crystalline phases, oxide inclusions, pores and interparticle boundaries. It is these structural features that determine the mechanical and tribological characteristics of the coatings, in particular their hardness, wear resistance and resistance to fracture under contact interaction conditions.

Analysis of modern research shows that improving the operational properties of plasma coatings is achieved by optimizing their phase composition, reducing porosity, forming strengthening carbide and boride phases, as

well as using additional technological operations, in particular heat treatment or remelting. Thermal stabilization of the structure contributes to the transition of the amorphous component to a more stable crystalline state, reducing residual stresses and increasing the cohesive strength of the coating. Another promising direction is the modification of the composition of powder materials, which allows for targeted influence on the formation of the structure and properties of coatings.

However, despite a significant amount of scientific research in this area, the relationship between the microstructure of plasma coatings, their phase composition and wear mechanisms remains poorly understood, especially for coatings used to restore and strengthen internal combustion engine valves. The influence of technological parameters of spraying, heat treatment and modification of the powder composition on the formation of structural heterogeneity and its role in the processes of friction and fracture needs to be clarified.

In this regard, the purpose of this work is to study the microstructure and wear resistance of plasma coatings based on self-fluxing nickel alloys, establish the regularities of the formation of their structural state, and evaluate the influence of composition modification and heat treatment on the performance characteristics of coatings intended for strengthening internal combustion engine valves.

Literature review

The microstructure of plasma coatings is formed as a result of the impact of molten or semi-molten powder particles on the surface of the substrate, their rapid cooling, deformation and layering. As a result, a typical lamellar structure is formed from individual flattened particles, interlamellar boundaries, pores, oxide inclusions and local areas of incomplete fusion. It is this heterogeneity that largely determines the hardness, wear resistance and corrosion behavior of coatings. NiCrBSi coatings are characterized by a combination of a hard metal matrix with boride, carbide and silicide phases, which increase microhardness and resistance to abrasive wear [2], [5], [7]. At the same time, excessive porosity or weak interlamellar bonding can reduce the cohesive strength of the coating and contribute to fracture under contact loads [7], [8].

An important way to improve the structure of plasma coatings is heat treatment or remelting. Short-term heat treatment of NiCrBSi coatings promotes relaxation of residual stresses, partial compaction of the structure, formation of more stable crystalline phases and increase of microhardness, which positively affects wear resistance [6], [8]. Laser or automatic remelting provides a denser structure with fewer pores and cracks, improves metallurgical bond with the base and increases the mechanical characteristics of the coatings [2], [9]. Such changes are especially important for self-fluxing NiCrBSi alloys, since boron and silicon lower the melting point, facilitate surface wetting and promote the formation of a dense wear-resistant layer [11].

Increasing the wear resistance of plasma coatings is often achieved by introducing hard reinforcing phases, in particular WC–Co. With an increase in the WC–Co content in NiCrBSi-composite coatings, the proportion of hard carbide inclusions increases, which counteract microcutting and plastic deformation of the surface during friction [3], [10]. However, excessive content of hard particles can increase the brittleness of the coating, promote the formation of microcracks and worsen the uniformity of the structure. Therefore, optimal wear resistance is ensured not only by high hardness, but also by a balanced combination of hard phases, a plastic matrix, low porosity and sufficient adhesion to the base [3], [10].

Amorphous and nanocrystalline coatings based on Fe and Ni alloys are characterized by increased structural homogeneity, the absence of large crystal grains, and high hardness, which contributes to increased resistance to wear and corrosion failure [1], [5], [6]. Nanocrystallization of amorphous NiCrBSi alloy after spraying can improve operational properties due to the formation of finely dispersed strengthening phases [5]. However, the corrosion resistance and durability of such coatings depend on the condition of the substrate surface, the quality of preparation before spraying, the coating density, and the presence of defects that can be penetration paths for aggressive media [1], [4], [12].

Thus, the analysis of literature sources shows that the wear resistance of plasma coatings is determined by a complex of structural factors: lamellar structure, porosity, phase composition, the presence of solid boride and carbide phases, the quality of interparticle bonding and the state of the “coating–base” interface. The most effective directions for increasing their performance are optimization of spraying parameters, use of composite powders, heat treatment, laser remelting and formation of a dense finely dispersed or nanocrystalline structure [2], [6], [8], [9].

Purpose and objectives of the study

The purpose of this work is to establish the regularities of microstructure formation and study the wear resistance of plasma coatings based on self-fluxing nickel alloys, as well as to assess the influence of powder composition modification and heat treatment on their physicomechanical and tribological properties.

To achieve the goal, the work performed a microstructural analysis of plasma coatings, determined their phase composition and features of structure formation depending on the deposition conditions, investigated the distribution of microhardness across the coating cross-section, and established the effect of heat treatment on its structural state and mechanical properties. Special attention was paid to assessing the effect of modifying the powder composition, in particular the introduction of ferrosilicon, on the porosity and structural characteristics of

the coating, as well as conducting tribological tests to establish wear patterns and determine the mechanisms of surface destruction under friction conditions.

Analysis of the structure of plasma coatings

During plasma spraying of PG-10N-01 powder on 40X steel, a hardened layer is formed, which evenly covers the surface of the part. The coating thickness is 300–350 μm and is characterized by uniformity over the entire area (Fig. 1a). The average hardness of the coating does not exceed HV 550. The resulting layer is characterized by a fine-grained structure and uniform distribution of structural components after melting with the formation of a transition zone between the coating and the base.

The formation of the coating structure occurs under conditions of high rates of heating and cooling of particles (10^6–10^8 K/s), which is accompanied by their complete or partial melting. The starting powder contains nickel, chromium, boron, silicon, iron and carbon, which causes the formation of a significant proportion of the amorphous phase in the coating. During the deposition process, the molten and semi-molten particles are deformed and form a lamellar (plate-like) structure of the surface layer, which determines the main physical, mechanical and tribological properties of the coating.

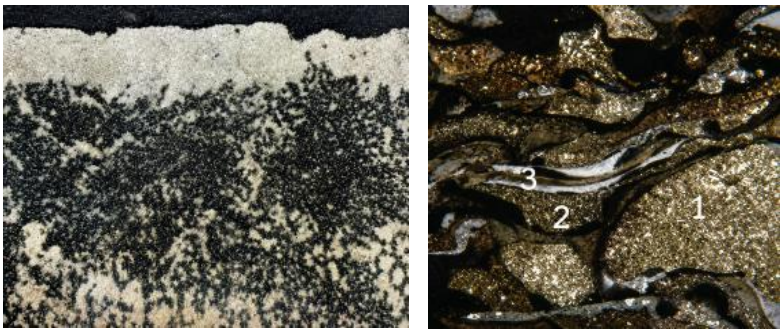

a) b)

Fig. 1. Microstructure of plasma coating and structural components of the deposited layer

The formed coatings are characterized by a complex heterogeneous structure (Fig. 1b), in which three main types of particles are distinguished: unmelted and undeformed (1), unmelted but plastically deformed (2), and completely molten particles (3). The proportion of unmelted particles is insignificant and does not exceed 10%. The main operational properties of the plasma coating are determined by particles of type 3, since it is they that form a dense structure with increased hardness, reaching 1000 HV, during crystallization.

It was found that the choice of spraying modes significantly affects the quality of the formed coating. High cooling rates of molten particles contribute to the occurrence of residual tensile stresses. If these stresses exceed the adhesion strength to the base, the coating may peel off. Important factors determining the morphology and specific surface area of the coating are the size and shape of the powder particles: a decrease in size and an increase in their irregularity lead to an increase in the specific surface area and affect the features of structure formation. The results of the analysis of the morphology of the coating obtained from the PG-10N-01 powder are shown in Fig. 2a.

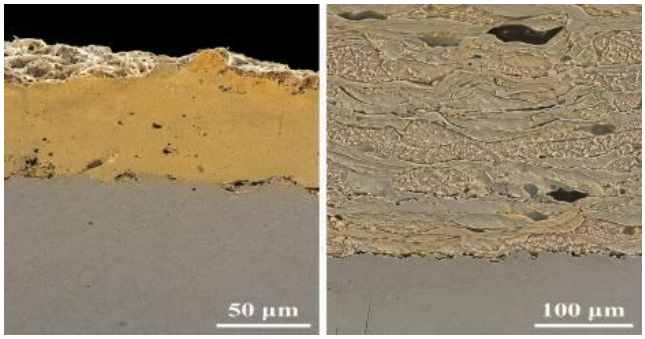

a) b)

Fig. 2. Morphology of the cross-section of the PG-10N-01 powder coating.

The coating is characterized by a uniform thickness without pronounced macrodefects, such as cavities or cracks, which indicates the stability of the deposition process and sufficient adhesion to the substrate. At the same time, individual spherical inclusions are detected in the structure, which correspond to semi-molten or unmolten particles of the starting powder that have not undergone full thermal action in the plasma jet. The reason for their formation is insufficient thermal input or limited duration of the particles in the high-temperature zone, which makes it impossible to form an amorphous phase. Such solid inclusions are evenly distributed in the amorphous-

crystalline matrix of the coating (Fig. 2b) and can act as local stress concentrators.

Microstructural analysis showed that the vast majority of structural elements of the coating have sizes up to 200 μm, while the fine component is represented by grains with a size of 3–8 μm. The morphology of the grains is heterogeneous and includes leaf-like and dendritic forms (Fig. 3), which indicates non-equilibrium crystallization conditions. The formation of such a structure is due to high cooling rates of molten particles, which leads to the development of dendritic growth and the formation of fine phases, which determine the mechanical and tribological properties of the coating.

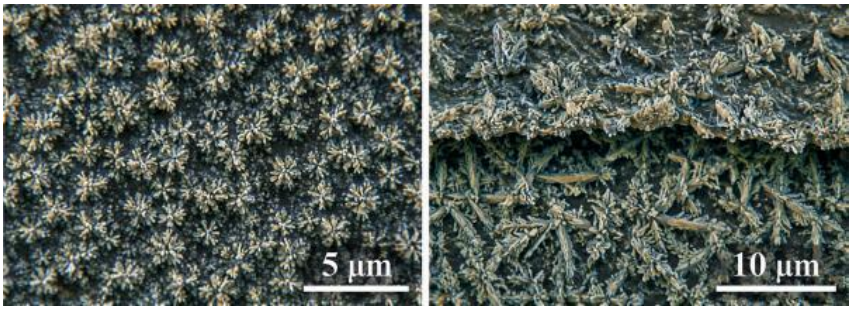

a) b)

Fig. 3. Grain structure of the applied coating from PG-10N–01 powder

During spraying, a significant number of sprayed particles are produced, which settle on the surface of the part in a semi-molten or molten state, cool and deform into flat particles. As a result, a layered coating surface is formed. The surface roughness Ra is 0.224 μm.Stabilization of the structure of the resulting coating occurs during the following heat treatment, which involves annealing at temperatures below the Trek temperature (recrystallization) to convert the amorphous structure into a crystalline one. Annealing was carried out at a temperature of 863 K (590 °C) with a holding time of 1 hour. Heat treatment improves the functional properties of the coating: the structure is stabilized due to the transition of the amorphous component to a crystalline one, crystals of the strengthening phases CrNi3 and Fe3Ni appear; the cohesive forces of adhesion of the coating to the base increase and porosity decreases. In the X-ray diffraction pattern taken after heat treatment [1-5], a wide peak indicates the transition of the amorphous phase to a crystalline one Fig. 4.

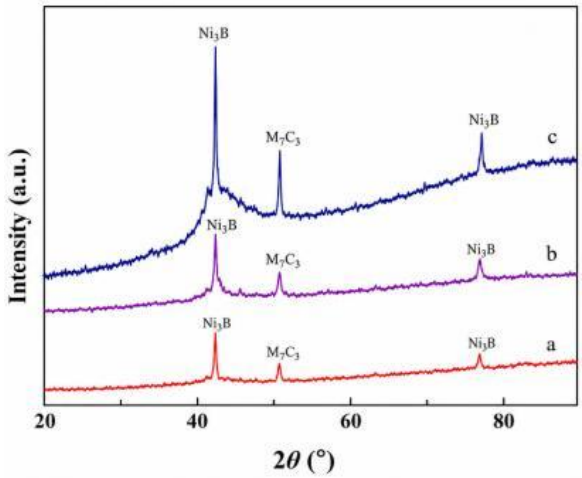

Fig. 4. X-ray diffraction patterns of NiCrBSi powder: a – in the initial state; b – powder after sputtering; c – powder after sputtering and heat treatment

The X-ray diffraction patterns of the NiCrBSi powder (Fig. 4) indicate phase transformations occurring during spraying and subsequent heat treatment.

In the as-received condition (curve a), the diffraction pattern is characterized by pronounced peaks corresponding to the Ni_3B phase (in the regions of ~2θ = 40–45° and ~75–80°), which is typical for boride constituents in self-fluxing nickel-based powders. In addition, a peak of the carbide phase M_7C_3 (~2θ ≈ 50°) is observed, indicating the presence of chromium-rich carbides in the structure. After spraying (curve b), a decrease in intensity and noticeable broadening of the Ni_3B peaks are observed, suggesting partial dissolution or amorphization of the boride phase due to rapid solidification of the molten material. The M_7C_3 peaks are still present but become less pronounced, indicating dispersion and refinement of the carbide phase. Following spraying and heat treatment (curve c), recrystallization of the structure occurs, as evidenced by the increased intensity and sharper peaks of Ni_3B. At the same time, the carbide phases M_7C_3 become more clearly defined, and additional carbides (such as those of the $M_{23}C_6$ type) may also be detected based on peak positions in the corresponding 2θ ranges. This suggests the formation of a more equilibrium and strengthened

microstructure with a higher fraction of hard phases.

Thus, the analysis of the diffraction patterns (Ni_3B, M_7C_3) demonstrates that spraying leads to partial amorphization and phase dispersion, whereas heat treatment promotes recrystallization and phase stabilization, which are key factors contributing to increased hardness and wear resistance of the coating.

Fig. 5 shows that the sputtered surface has two types of grains (Fig. 5, a and b): larger crystals in the form of dendrites (a) – Ni3B, smaller (b) – grains up to 1 μm in size, almost spherical in shape, which corresponds to chromium carbides Cr7C3, Cr7C23.

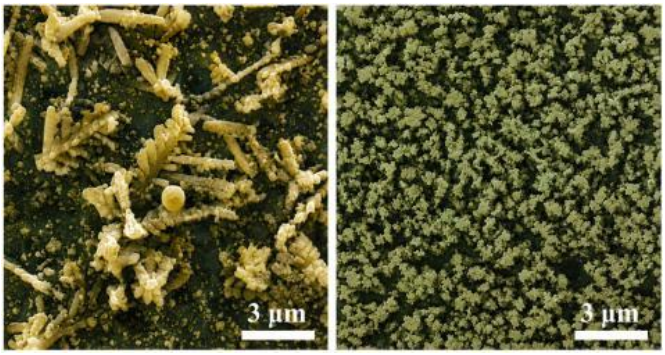

a) b)

Fig. 5. Morphology of two types of grains in the cross-section of the PG-10N-01 powder coating.

The results of spectral analysis showed that after heat treatment, the content of the chromium carbide phase in the coating structure increases, and the content of the Ni3B phase decreases.

Microhardness study of the deposited layer

Hardness is one of the important operational characteristics of the material. The analysis of microhardness along the cross-section of the coating was carried out to assess the mechanical properties of the formed microstructure. The features of the plasma spraying technological process (high powder heating temperature, high cooling rate of the applied coatings) cause an uneven distribution of the components of the powder material over the surface of the part, as a result of which the applied coating has a heterogeneous chemical composition and structure, as well as a different number of pores and oxides. Usually, a significant proportion of the amorphous phase with a special structure and properties is found in the structure of plasma coatings. All this provides an ambiguous nature of the change in hardness along the cross-section of the coating. The microhardness of the coating applied to the surface of the part and the coating, which after application was subjected to stabilizing heat treatment - annealing at 590°C, was determined. The results are presented in Fig. 6.The average hardness of the coating is within 500 - 550 MPa, the thickness of the coating does not exceed 300 - 350 microns. Between the hardness of the coating and the hardness of the base, there is a fairly smooth decrease in values to the average values of the hardness of the base. As can be seen from the graphs, the microhardness varies depending on the distance from the surface of the part, but within the applied layer it does not change significantly.

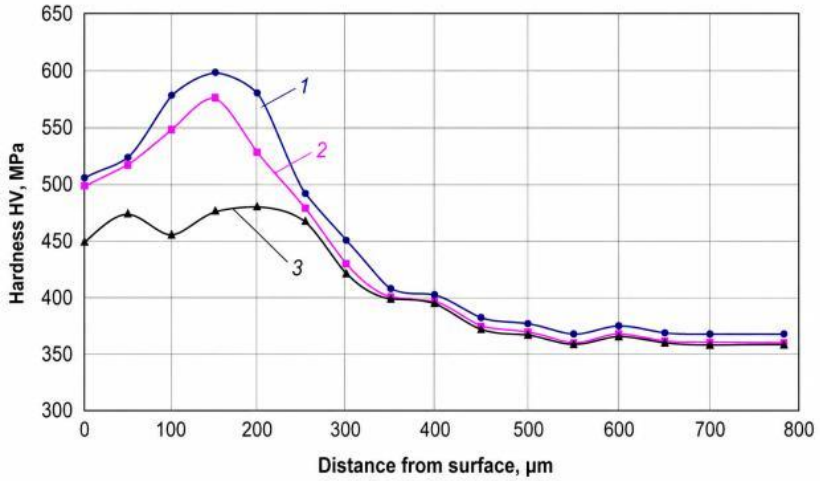

Fig. 6. Microhardness of plasma coatings of the Ni-Cr-B-Si system: 1 - coating of the Ni-Cr-B-Si system from PG-10N-01 powder after heat treatment; 2 - coating without annealing; 3 - Steel 40X without coating.

Fluctuations in microhardness values are due to the heterogeneous structure of the applied coating.

The presence of hard phases such as boron nitrides or chromium carbides in individual zones increases the hardness of these zones. Areas of the coating where an amorphous structure has formed have lower hardness values. Heat treatment contributes to the formation of a more uniform and stable structure, increasing the hardness of the applied coating (up to HV 600) due to the separation of the carbide phase – Cr3C7 and intermetallics Fe3Ni from the γ-solid solution (Fig. 6).

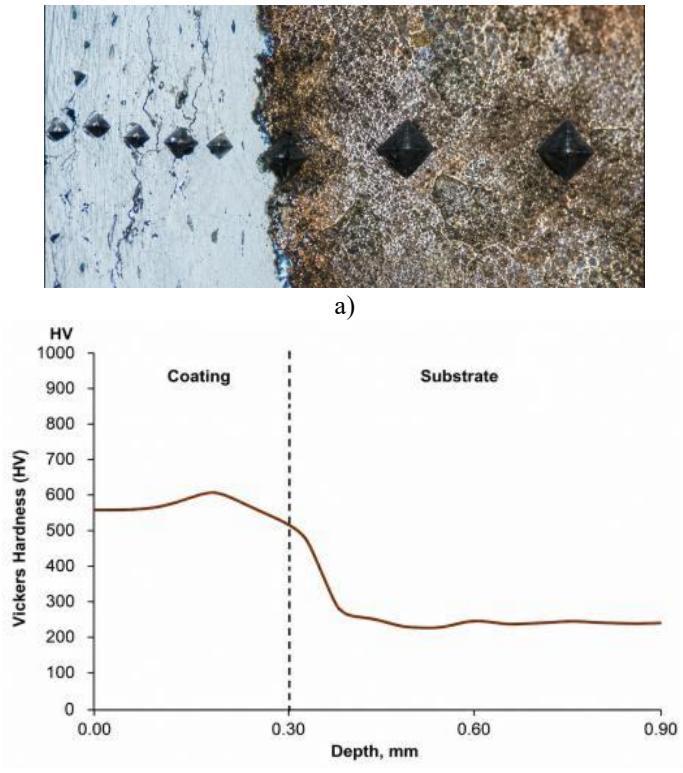

Fig. 7. Hardness along the depth of the plasma coating: a) impressions from the indentation of a tetrahedral pyramid; b) hardness distribution along the depth of the coating [3-8]

The Vickers microhardness profile versus depth clearly reveals the interface between the coating and the substrate, as well as the variation of mechanical properties across these regions (fig. 7). In the near-surface region (0–0.25 mm), corresponding to the coating, the hardness remains high and relatively stable at ~550–600 HV, with a slight maximum (~600 HV) in the middle of the layer. This indicates the formation of a strengthened structure due to the presence of hard phases (borides and carbides) and rapid solidification during spraying. Near the coating–substrate interface (~0.30 mm), a noticeable drop in hardness to ~500 HV is observed, indicating a transition (diffusion) zone characterized by gradual changes in phase composition and microstructure. Within the substrate (beyond 0.30 mm), the hardness decreases sharply to ~250–300 HV and then stabilizes at ~230–250 HV with minor fluctuations. These values correspond to the base material without strengthening phases. Thus, the hardness profile exhibits a gradient behavior: high hardness in the coating, a sharp transition at the interface, and consistently lower values in the substrate, confirming the effectiveness of the coating as a strengthening layer.

Adding ferrosilicon (from 2 to 5%) to PG-10N-01 powder contributes to the formation of a greater thickness of the applied layer and its porosity (Fig. 8).

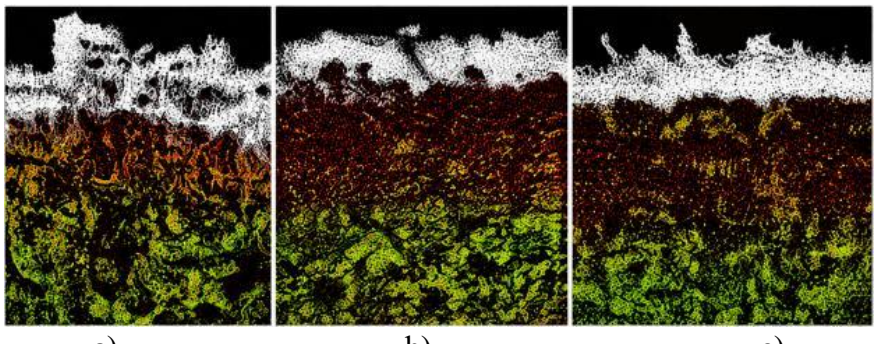

Fig. 8. Microstructure of the valve surface: a - - coating of PG-10N-01 powder with the addition of 5% ferrosilicon; b - coating of PG-10N-01 powder with the addition of 2% ferrosilicon, c) - coating of PG-10N-01 powder without the addition of ferrosilicon.

Table 1

Dependence of coating porosity on ferrosilicon content

Powder composition	Layer depth, μm	Porosity, %
PG-10N-01	290	0…1
PG-10N–01 + 2% ferrosilicon	330	10…15
PG-10N–01 + 5% ferrosilicon	350	20…30

When ferrosilicon is added to the powder, macrovoids are formed on the surface (Fig. 8, a, b). An increase in the amount of silicon in the composition of the PG powder contributes to the formation of chromium silicides (Cr3Si, Cr5Si3), which contribute to an increase in the hardness of the resulting layer. An increase in porosity when forming a coating with the addition of ferrosilicon has almost no effect on the microhardness, since chromium silicides appear in the structure, the hardness of which is not inferior to the hardness of chromium carbides (HV 1600). The porosity of the surface layer of the part significantly affects its oil capacity and lubricating properties, therefore determining the durability of the friction surface under conditions of insufficient lubrication. The changes that occur after the introduction of the powder into the coating significantly affect the formation and growth of transition layers. This, in turn, leads to changes in the mechanical properties of composite materials. Due to the short duration of the reflow process, the transition zone has an insignificant length of 10–15 μm. However, this length is sufficient to remove residual stresses, increase density and ensure fusion of the coating with the base, which is manifested in the penetration of the applied material into the surface layers. As a result of coagulation processes, the shape of the pores in the coating becomes rounded. Results of microanalysis of the chemical composition of molten plasma coatings of the Ni-Cr-B-Si system from PG-10N-01 powder with the addition of ferrosilicon, carried out using a microanalyzer PEM 106 i.

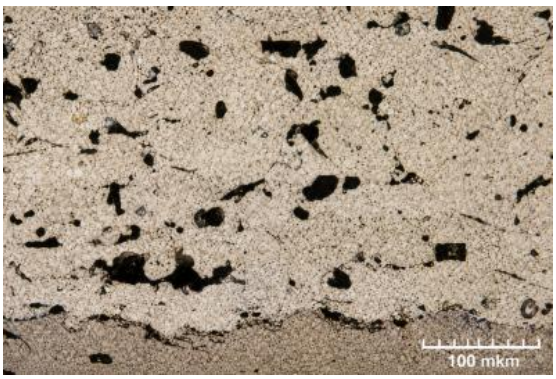

Fig. 9. Microstructure of the Ni-Cr-B-Si system coating

Table 2

Chemical composition of Ni-Cr-B-Si powder coating

Elements	Mass fraction in volume percent, %					
	Transition zone	1	2	3	4	5
Ni		83.7	48.3	64.4	87.7	71.9
Cr	5.49	12.4	33.3	20.2	7.36	20.6
Fe	94.00	2.8	16.4	12.1	4.58	4.3
Yes	0.33	0.9	0.75	1.64	0.26	1.06

As a result of chemical analysis of the distribution of elements in the structural coating, it can be concluded that silicon inclusions are mainly concentrated in dark areas of the coating (Fig. 9).

Study of wear resistance of valves after plasma spraying

The study of the wear resistance of valves was carried out on the friction machine SMC-2 according to the roller-flat counterbody scheme, which made it possible to establish the influence of nanodispersed inclusions on the level of increase in the wear resistance of self-flux coatings of the Ni-Cr-B-Si system (PG-10N-01) (Fig. 10). The dependencies that were obtained as a result of laboratory studies made it possible to analyze the kinetics of wear of self-flux coatings, as well as the level of their wear resistance. The composition of the Ni-Cr-B-Si system powder allows, after spraying onto the steel surface of a part made of Steel 40X, to obtain an increase in microhardness and bond strength due to physicochemical processes that ensure an increase in operational indicators (wear resistance, corrosion resistance). Wear tests conducted on SMC-2 showed that samples with a coating that was subjected to heat treatment have higher wear resistance.

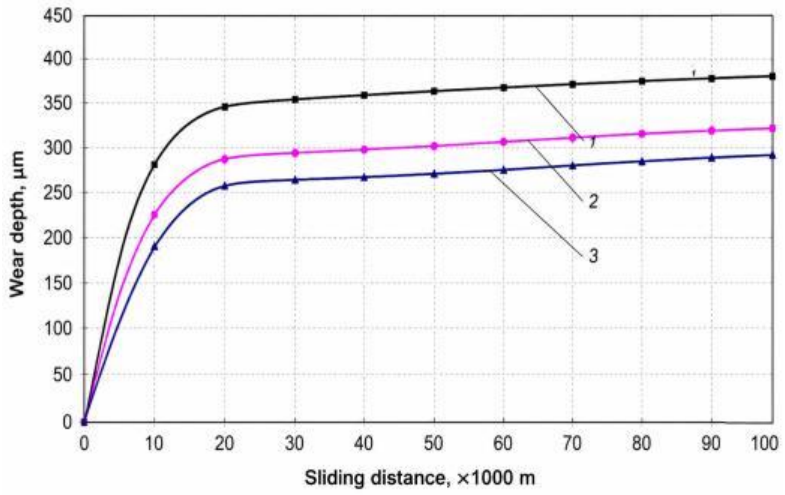

Fig. 10. Wear resistance of plasma coatings from Ni-Cr-B-Si powder system: 1 – Steel 40X without coating; 2 – Ni-Cr-B-Si coating from PG-10N-01 powder without annealing; 3 – coating after heat treatment.

Heat treatment has a positive effect on the tribological characteristics of the coating: it contributes to a decrease in the friction coefficient and its greater stability during friction [2-7] (Fig. 10).

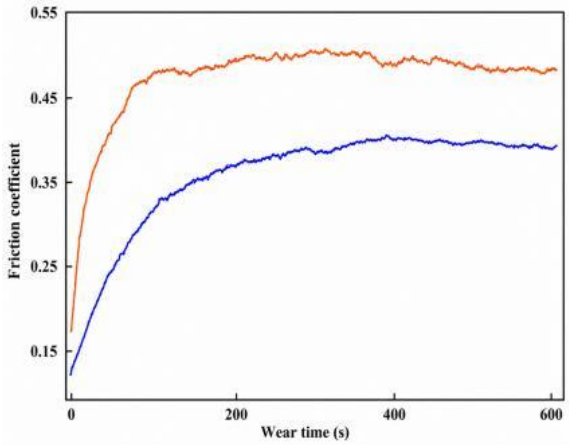

Fig. 11. Character of change in the friction coefficient of the NiCrBSi coating after application to the surface of the part (red curve) and after heat treatment (blue curve)[2-7]

Fig. 11 shows a comparison of the friction coefficient between the sprayed coating and the coating that was subjected to heat treatment. The friction coefficient of the sprayed coating gradually stabilizes, starting from 60 s, reaching values of 0.45. The friction coefficient fluctuated greatly, which negatively affects the wear resistance of the material. For the coating that was subjected to heat treatment, the stabilization of the friction coefficient was detected later - after 250 s, but its values are lower - 0.38. The higher values of the friction coefficient for the applied coating are explained by the rather inhomogeneous structure that was formed during spraying and the rather high surface roughness. The coating that was subjected to heat treatment has a more homogeneous structure, so the friction coefficient undergoes smaller fluctuations. To describe the wear mechanism of the sprayed coating, the morphology of the wear surface of the coating that was subjected to heat treatment was investigated. The worn surface consists of both relatively smooth particles, with a small number of cracks and an almost round shape, and areas where cracks have expanded due to friction, the particles are displaced relative to each other and overlap. Amorphous nickel-based coating is a typical brittle material with a large number of protruding particles on the surface, so the friction force and compressive stresses cause cracks in the defects under the oxide layer during wear. The boundaries of flat particles have a high content of oxides, which are prone to wear and delamination. The reciprocating motion causes fatigue damage to the surface structure of the coating and creates fatigue cracks. Under the action of a periodic tangential force, the fatigue crack expands and causes volume delamination. The presence of multiple cracks in the middle and surrounding areas of an individual particle also indicates that particles with poor flattening or insufficient fusion exist independently in the coating. A significant amount of wear products was found in the friction zone (Fig. 12)

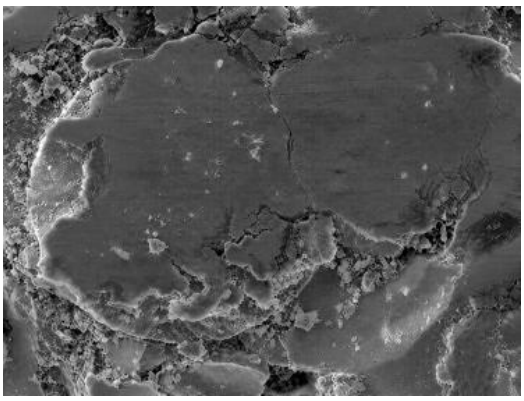

Fig. 12. The coating surface is contaminated with wear products

In Fig. 11, a large amount of fine debris adhering to the coating surface can be seen. This indicates that, unlike the wear mechanism of amorphous material, the wear mechanism of nanocrystals is predominantly adhesive. Debris that accumulates on the surface of the part can significantly increase wear. Cracks occur during friction, which are mainly caused by the presence of pores and oxides. The crack nuclei are powder particles with a defective surface (incompletely melted particles).

Conclusions

1. The effectiveness of the use of plasma coatings based on self-fluxing nickel alloys to increase the wear resistance of heavily loaded parts, in particular internal combustion engine valves, is shown. Based on the planning of a factorial experiment, the optimal spraying parameters were determined according to the microhardness criterion: current strength 244 A, distance 100 mm, powder consumption 0.48 g/s.

2. It was found that the microstructure of the coatings is heterogeneous and includes amorphous and crystalline phases. Heat treatment (annealing at 590 °C) promotes crystallization of the amorphous component, formation of strengthening phases (Cr_7C_3, Ni_3B, Cr_3Si) and increase of the microhardness of the coating by 100–120 HV.

3. According to the results of microstructural and tribological analysis, it was established that the wear of the coating is predominantly adhesive in nature and is caused by its structural heterogeneity, the presence of pores and oxide inclusions, which act as stress concentrators and centers of crack initiation.

4. It has been proven that modification of the coating composition by introducing up to 5% ferrosilicon has a positive effect on its operational properties: the porosity and oil capacity of the surface increase, which contributes to a decrease in the intensity of wear under friction conditions.

References

1. Jiang, C., Liu, W., Wang, G., Chen, Y., Xing, Y., Zhang, C., & Dargusch, M. (2017). The corrosion behaviors of plasma-sprayed Fe-based amorphous coatings. Surface Engineering, 34, 634–639.https://doi.org/10.1080/02670844.2017.1319647

2. Serres, N., Hlawka, F., Costil, S. et al. Microstructures of Metallic NiCrBSi Coatings Manufactured via Hybrid Plasma Spray and In Situ Laser Remelting Process. J Therm Spray Tech 20, 336–343 (2011). https://doi.org/10.1007/s11666-010-9565-1

3. Guo, H., Li, B., Lu, C., Zhou, Q., & Jia, J. (2019). Effect of WC–Co content on the microstructure and properties of NiCrBSi composite coatings fabricated by supersonic plasma spraying. Journal of Alloys and Compounds, 789, 966–975.https://doi.org/10.1016/j.jallcom.2019.02.290

4. Ghaziof, S., Raeissi, K., & Golozar, MA (2010). Improving the corrosion performance of Cr–C amorphous coatings on steel substrate by modifying the steel surface preparation. Surface and Coatings Technology, 205, 2174–2183.https://doi.org/10.1016/j.surfcoat.2010.08.082

5. Li, C.-J., Wang, Y.-Y., & Li, H. (2004). Effect of nano-crystallization of high velocity oxy-fuel-sprayed amorphous NiCrBSi alloy on properties of the coatings. Journal of Vacuum Science & Technology A, 22, 2000–2004.https://doi.org/10.1116/1.1776183

6. Bacha, N.-E. (2003). Characterization of amorphous plasma sprayed coatings of FeCrPC and NiCrBSi. Journal of Metastable and Nanocrystalline Materials, 18, 1–8.https://www.scientific.net/JMNM.18.1

7. Chen, L.-Y., Xu, T., Lu, S., Wang, Z.-X., Chen, S., & Zhang, L.-C. (2018). Improved hardness and wear resistance of plasma sprayed nanostructured NiCrBSi coating via short-time heat treatment. Surface and Coatings Technology, 350, 436–444.https://doi.org/10.1016/j.surfcoat.2018.07.037

8. Planche, MP, Liao, H., Normand, B., & Coddet, C. (2005). Relationships between NiCrBSi particle characteristics and corresponding coating properties using different thermal spraying processes. Surface and Coatings Technology, 200, 2465–2473. https://doi.org/10.1016/j.surfcoat.2004.08.224

9. Liu, L., Xu, H., Xiao, J., Wei, X., Zhang, G., & Zhang, C. (2017). Effect of heat treatment on structure and property evolutions of atmospheric plasma sprayed NiCrBSi coatings. Surface and Coatings Technology, 325, 548–554.https://doi.org/10.1016/j.surfcoat.2017.07.011

10. Chen, L.-Y., Wang, H., Zhao, C., Lu, S., Wang, Z.-X., Sha, J., Chen, S., & Zhang, L.-C. (2019). Automatic remelting and enhanced mechanical performance of a plasma sprayed NiCrBSi coating. Surface and Coatings Technology, 369, 31–43.https://doi.org/10.1016/j.surfcoat.2019.04.052

11. Shieh, Y.-H., Wang, J.-T., Shih, HC, & Wu, S.-T. (1993). Alloying and post-heat treatment of thermal sprayed coatings of self-fluxing alloys. Surface and Coatings Technology, 58, 73–84.https://doi.org/10.1016/0257-8972(93)90176-O

12. Cha, SC, Gudenau, HW, & Bayer, GT (2002). Comparison of corrosion behavior of thermal sprayed and diffusion-coated materials. Materials and Corrosion, 53, 195–205. https://doi.org/10.1002/1521-4176(200203)53:33.0.CO;2-G

Диха О.В., Вичавка А.А., Бабак О.П., Диха М.О., Дитинюк В.О. Вплив модифікації складу та термічної обробки на мікроструктуру і зносостійкість нікелевих плазмових покриттів для клапанів ДВЗ

У роботі досліджено мікроструктуру, фазовий склад і зносостійкість плазмових покриттів на основі самофлюсівних нікелевих сплавів, отриманих із порошку ПГ-10Н-01 та призначених для зміцнення клапанів двигунів внутрішнього згоряння. Встановлено, що внаслідок високих швидкостей нагріву і охолодження під час плазмового напилення формується ламелярна структура з наявністю аморфних і кристалічних фаз, оксидних включень і пор. Показано, що термічна обробка забезпечує часткову кристалізацію аморфної фази, зниження пористості та підвищення мікротвердості покриття. Досліджено розподіл мікротвердості по глибині шару, який характеризується відносною стабільністю в межах покриття та поступовим зменшенням у зоні переходу до основи. Встановлено вплив модифікації складу (введення феросиліцію) на структуроутворення та пористість покриття. За результатами трибологічних випробувань визначено підвищення зносостійкості та зниження коефіцієнта тертя після термічної обробки. Обґрунтовано адгезійний механізм зношування, зумовлений структурною неоднорідністю покриття.

Ключові слова: плазмове напилення, NiCrBSi, мікроструктура, зносостійкість, мікротвердість, термічна обробка, фазовий склад, пористість, коефіцієнт тертя, клапан ДВЗ

ISSN 2079-1372 Problems of Tribology, V. 31, No 2/120-2026, 44-51

Problems of Tribology
Website: http://tribology.khnu.km.ua/index.php/ProbTrib
E-mail: tribosenator@gmail.com

DOI: https://doi.org/10.31891/2079-1372-2026-120-2-44-51

Construction and application of the limit strain surface for evaluating the plasticity of porous bodies

R. Sivak[1] 0000-0002-7459-2585, **L. Polishchuk[1]** 0000-0002-5916-2413, **V. Shenfeld[1]*** 0000-0002-5548-6971, **A. Ormanbekova[2]** 0000-0001-8663-006X, **N. Zhumakhan[2]** 0000-0002-9548-6896

Vinnytsia National Technical University, Vinnytsia, Ukraine
Almaty Technological University, Almaty, Kazakhstan
**E-mail: leravntu@gmail.com*

Received: 10 April 2026: Revised 25 April 2026: Accept: 14 May 2026

Abstract

Traditional failure criteria for solid materials are not applicable to powder materials due to the presence of porosity, which acts as a sink for dislocations, alters defect accumulation kinetics, and slows structural degradation. This study presents a comprehensive analysis of the deformation behavior of cylindrical porous iron-based samples. The deformed state on the sample surface was determined using the coordinate grid method, while displacement measurements were performed with a high-precision instrumental microscope, enabling the calculation of strain rate components at each stage up to macrocrack formation. To ensure a wide variation of the stress state index and the Nadai–Lode parameter, eight loading paths were implemented, including free upsetting under different friction conditions and deformation in steel shells. The parameters η_0 and μ_σ were calculated considering porosity functions, ensuring an adequate representation of void effects on the stress state. Experimental data were processed using successive approximation methods to identify key model parameters. As a result, an analytical expression for the limit deformation surface was obtained, describing the failure condition of the material. A significant finding is the confirmation of the invariance of the plasticity resource of the base material with respect to initial porosity, provided the matrix composition and structure remain unchanged. This enables the obtained surface to be considered a universal characteristic of sintered iron. The developed approach provides a reliable tool for predicting defect formation and optimizing powder metallurgy processes such as pressing, calibration, and bulk forming.

Keywords: destruction, porosity, damage accumulation, stress-strain state, stress state index

Introduction

The importance of researching porous structures stems from their unique ability to combine low specific gravity with high functional capabilities. The development of accurate computational models for predicting the physico-mechanical properties of materials resulting from plastic processing critically depends on changes in porosity and becomes a primary task for ensuring the required technological heredity of products.

The transition to the analysis of 3D environments has allowed for the identification of the influence of cell shape and cross-sectional heterogeneity of struts on plasticity, emphasizing the insufficiency of simplified 2D approaches for an adequate description of micro-scale effects. An important step in this direction was the work [1], which proposed a methodology for generating 3D open-cell porous materials based on space partitioning into regions, where each region contains points closer to one center than to others. The authors demonstrated that the anisotropy of such structures is determined by the pore growth trajectory along the z-axis, while the randomness of pore size and their spatial distribution in the xy-plane creates a complex effect of weakening the mechanical properties.

These microstructural studies establish the foundation for transitioning from the analysis of individual structural elements to a phenomenological description at the macroscale. The development of macroscopic yield models has progressed from the criterion [2], which is based solely on the first and second stress invariants and is limited to circular deviatoric cross-sections, to more complex surfaces. An attempt to expand this framework was the flexible criterion [3] for granular media; however, it proved incapable of describing the change in the

orientation of the triangular cross-section along the hydrostatic axis. In the study [4], a modification of the Ehlers model was proposed, allowing for the correct orientation of the triangular deviatoric cross-sections of the yield surface depending on the sign of the hydrostatic pressure.

Despite significant progress, a substantial gap remains regarding the description of plastic behavior under large hydrostatic loading components and the inclusion of Lode angle dependence [5]. Existing models often ignore the influence of the third invariant of the stress deviator, which is critical for porous bodies where the shape of the yield surface transforms from tension to compression [6]. Neglecting these effects leads to significant errors in predicting the onset of plastic flow under conditions of complex triaxial stress states [7]. The lack of a holistic approach that combines the random nature of 3D microstructure with refined phenomenological criteria hinders the design of high-reliability products operating under critical loading regimes.

The aim of this study is to develop a methodology for constructing limit strain surfaces for porous bodies $\Gamma_{op}(\eta_0,\mu_\sigma)$ depending on the stress state index of the base material η_0 and the Nadai-Lode parameter μ_σ. This is based on experimental studies of the upsetting process of cylindrical specimens under various contact friction conditions and within shells, as well as obtaining the limit strain surface for an iron-based porous material, which will allow for the prediction of the technological heredity indicators of products.

Object and Methods of Research

During the plastic deformation of porous bodies, the damage accumulation process is more complex than during the same deformation of solid bodies, as in this case, plastic loosening occurs simultaneously with the material compaction process. The determining factor during fracture is not "loosening" in general (i.e., overall porosity), but the development and accumulation of micropores and microcracks within the skeleton material. Furthermore, pores act as sinks for dislocations, which slows down the rate of damage accumulation. In macroscopic experiments, it is impossible to separate the processes of material compaction and loosening. Therefore, to evaluate the plasticity of porous bodies, the strain accumulated in the base material at the moment of fracture was adopted as the measure of plasticity [8, 9].

$$\Gamma_{OP} = \int_0^{t_p} \dot{\gamma}_0 d\tau, \tag{1}$$

where t_p – is the deformation time until fracture;

$$\dot{\gamma}_0^2 = \frac{f_2(\theta)\dot{e}^2}{(1-\theta)} + \frac{f_1(\theta)\dot{\gamma}^2}{(1-\theta)};$$

$$\dot{\gamma} = \sqrt{\left(\dot{e}_{ij} - \frac{1}{3}\dot{e}\delta_{ij}\right)\left(\dot{e}_{ij} - \frac{1}{3}\dot{e}\delta_{ij}\right)},$$

$\dot{\gamma}$ is the intensity of the strain rate deviator;
$\dot{\gamma}_0\ is$ the intensity of the strain rate deviator in the base material;
$\dot{e}_{ij}$ is the components of the strain rate tensor;
$\dot{e} = \delta_{ij}\dot{e}_{ij}$ is the rate of relative volume change;
$f_1(\theta), f_2(\theta)$ are the porosity functions;
θ - porosity.
In general, the cold plastic limit strain of the base material depends on a number of factors:

$$\Gamma_{op} = f(x_i,c_j,\eta,\mu_\sigma,\theta), \tag{2}$$

where x_i is parameters that account for the influence of chemical composition and sintering conditions;
c_j is the influence of structure;
η, μ_σ are the influence of the stress state scheme.

Chemical composition and structure characterize the inherent plasticity of the material. The influence of the latter is established during experimental studies conducted according to specific programs. As a result, dependency (2) takes the following form:

$$\Gamma_{op} = f[\eta(\Gamma_o,\theta),\mu_\sigma(\Gamma_o,\theta)], \tag{3}$$

where Γ_o is the strain accumulated in the base material at a given moment in time.

Thus, during the cold plastic deformation of porous bodies, the primary factors determining plasticity are the stress state scheme and porosity. The dependence of plasticity on the stress state scheme is

described by the limit strain surface $\Gamma_{op}(\eta_0,\mu_\sigma)$. In this dependency, one of the arguments is the stress state index of the base material [8, 9].

$$\eta_0 = \eta \sqrt{\frac{f_1(\theta)}{(1-\theta)\left(\frac{1f_1(\theta)}{6f_2(\theta)}\eta^2+1\right)}}, \tag{4}$$

where $\eta = \frac{I_1(T_\sigma)}{\sqrt{J_2(D_\sigma)}} = \sqrt{6}\frac{p}{\tau}$ - the stress state index of a porous body;

$p = \frac{1}{3}\sigma_{ij}\delta_{ij}$ – average stress;

$\tau = \sqrt{(\sigma_{ij} - p\delta_{ij})(\sigma_{ij} - p\delta_{ij})}$ - the stress deviator intensity;

σ_{ij} - Components of the stress tensor.

To construct the limit strain surface $\Gamma_{op}(\eta_0,\mu_\sigma)$ for a porous body, it is necessary to ensure conditions where η_0 = const and μ_σ = const throughout the entire deformation process. During the plastic deformation of porous bodies, realizing such conditions is practically impossible. Therefore, to obtain the $\Gamma_{op}(\eta_0,\mu_\sigma)$ relationship, tests were conducted under loading conditions close to simple loading. In this case, the hypothesis of a linear damage accumulation law is valid [10, 11]. Thus, the fracture condition can be written as [8]:

$$\psi = \int_0^{\Gamma_{op}} \frac{d\Gamma_0}{\Gamma_{op}(\mu_\sigma,\eta_0)} = 1, \tag{5}$$

where ψ - used plasticity resource;

Γ_{op} - accumulated strain of the base material at the onset of a macrocrack.

$\Gamma_{op}(\eta_0,\mu_\sigma)$ - limit strain surface.

Based on the analysis of experimental results, the following relationship was adopted to approximate $\Gamma_{op}(\eta_0,\mu_\sigma)$

$$\Gamma_{op}(\eta_0,\mu_\sigma) = \Gamma_{op}(0,0)\exp(\lambda_2\mu_\sigma - \lambda_1\eta) \tag{6}$$

where $\lambda_1 = ln\left(\frac{\Gamma_{op}(-1,0)}{\Gamma_{op}(0,0)}\right)$, $\lambda_2 = ln\left(\frac{\Gamma_{op}(0,1)}{\Gamma_{op}(0,0)}\right)$, $\Gamma_{op}(0,0)$, $\Gamma_{op}(-1,0)$, $\Gamma_{op}(0,1)$ - Limit strains of the base material at η_0=0, μ_σ=0, η_0=-1, μ_σ=0, η_0=0, μ_σ=1 respectively.

The following methodology was used to construct the $\Gamma_{op}(\eta_0,\mu_\sigma)$ relationship. At the first stage, a plasticity diagram was constructed. During the construction of plasticity diagrams, a plane stress state occurs, where σ_2 = 0 i, and, as shown in [8], in this case η = -μ. Therefore, formula (6) is reduced to the form:

$$\Gamma_{op}(\eta_0,\mu_\sigma) = \Gamma_{op}(0,0)\exp(-\lambda\eta), \tag{7}$$

where $\lambda=\lambda_1+\lambda_2$. (8)

Problem Statement

Based on experimental studies of the upsetting process of cylindrical specimens under various contact friction conditions and within cladding, it is necessary to develop a methodology for constructing the limit strain surfaces $\Gamma_{op}(\eta_0,\mu_\sigma)$ for porous bodies and to obtain the limit strain surface for an iron-based porous material.

Results and Discussion

To determine the limit strain Γ_{op} for various deformation paths, free upsetting tests were conducted on cylindrical specimens made of iron-based porous material with three initial porosities: θ_0=0.27, θ_0=0.214, θ_0=0.128. The initial dimensions of the specimens were h=15.5 mm, d=11.3 mm. Upsetting was performed under various contact friction conditions, as well as with constrained (clamped) ends.

The strain state on the free surface of the specimens was determined using the grid method (coordinate-measuring grid method). For this purpose, marks were applied in the axial and tangential directions in the middle-height section of the specimen using a Vickers hardness tester, spaced circumferentially at 120^0. The initial distance between the marks was a_0=2mm. Initial and current values of a were measured using a toolmaker's microscope with an accuracy of 0.005 mm. To ensure identical deformation paths, determined by consistent friction conditions at the specimen-tool contact interface, 5 to 6 specimens were selected for each initial porosity. The variation in porosity within a batch did not exceed $\Delta\theta_0$ = 0.005. Each specimen was then upset in stages $\left(\frac{\Delta h_i}{h} = 0.05\ldots0.07\right)$ until a macrocrack with a length of 0.5...1.0 мм appeared. At each stage, the strain components e_z, e_φ were determined. The degree of strain at the moment of fracture was refined by upsetting a control specimen

until failure, which was conducted in 1...3 stages. After determining the limit strain, one specimen from the batch was upset to various degrees of reduction. From the resulting 5 to 6 upset specimens, a half-ring was cut from the "barrel" region, and its density was determined by hydrostatic weighing.

Since a model of a strain-hardening plastic porous body is being considered, real time can be excluded from the physical equations. Therefore, for the upsetting process, the parameter adopted as the time substitute (or time-like parameter) was [9].

$$t = 2\,ln\frac{D}{D_0}. \tag{9}$$

Taking into account the chosen parameter t, the strain rates and the volumetric strain rate were determined.

$$\dot{e} = \frac{\dot{\theta}}{1-\theta} \tag{10}$$

The intensity of the strain rate deviator was determined using the formula:

$$\dot{\gamma} = \sqrt{\left(\dot{e}_z - \frac{1}{3}\dot{e}\right)^2 + \left(\dot{e}_\phi - \frac{1}{3}\dot{e}\right)^2 + \left(e_r - \frac{1}{3}\dot{e}\right)^2}. \tag{11}$$

The accumulated intensity of the strain deviator was determined by numerical integration.

$$\Gamma = \int_0^t \dot{\gamma}\,d\tau. \tag{12}$$

The stress state index η was calculated using the formula:

$$\eta = -\sqrt{6}\frac{\dot{e}_r - \frac{1}{3}\dot{e}}{\dot{\gamma}}, \tag{13}$$

in the derivation of which it was taken into account that $\sigma_r = 0$ i on the free surface, and the flow theory relations [12] were utilized. The accumulated strain of the base material was calculated using the formula $\Gamma_0 = \int_0^t \dot{\gamma}_0 d\tau$, while the stress state index η_0 was determined by (4). During free upsetting under various contact friction conditions and upsetting with constrained ends, the relations $\sigma_\varphi = \sigma_1$, $\sigma_2 = 0$ and $\sigma_3 = \sigma_z$ hold in the equatorial region; therefore, the Nadai-Lode parameter is equal to:

$$\mu_\sigma = \frac{2\sigma_2 - \sigma_1 - \sigma_3}{\sigma_1 - \sigma_3} = \frac{2\dot{e}_r - \dot{e}_\phi - \dot{e}_z}{\dot{e}_\phi - \dot{e}_z}. \tag{14}$$

The deformation paths in the Γ_0 - η_0, μ_σ coordinates, obtained after processing the experimental data, are shown in Fig. 1.

It was hypothesized that the limit strain Γ_{op} during the cold plastic deformation of porous materials depends only on the base material and the parameters η_0 and μ_σ independent of the initial porosity θ_0.

The constants $\Gamma_{op}(0,0)$, λ of the porous sintered material, which depend on the powder particle size distribution, its chemical composition, pressing and sintering conditions, etc., are subject to experimental determination.

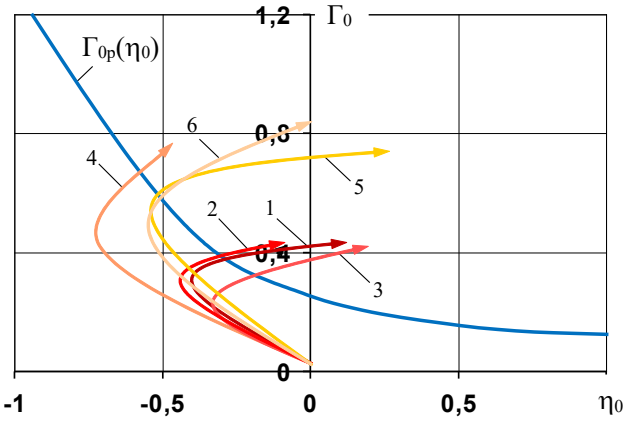

Fig. 1. Plasticity diagram and deformation paths in η_0-Γ_0 coordinates

Taking into account (7), the fracture criterion (5) takes the form:

$$\int_0^{\Gamma_{op}^*} exp(\lambda,\eta)\, d\Gamma_0 = \Gamma_{op}(0,0), \tag{15}$$

where Γ_{op}^* - the limit strain of the base material for a given deformation path.

Equations (15) were formulated for 8 deformation paths. By equating the left-hand sides of (15), four equations were obtained, from which the value λ=1.55 was determined using the method of successive approximations. Given the known value of λ, the value $\Gamma_{op}(0,0) = 0.28$ was found from (15).

Thus, for the dependence $\Gamma_{op}(\eta_0)$ under the condition $\eta = -\mu_\sigma$ the following was obtained:

$$\Gamma_{op}(\eta_0) = 0.28\exp(-1.55\eta_0). \tag{16}$$

The resulting plasticity diagram for the porous material, $\Gamma_{op}(\eta_0)$ is shown in Fig. 1, as well as in Fig. 2 as a curve obtained from the intersection of the plane $\eta_0 = -\mu_\sigma$ with the surface $\Gamma_{op}(\eta_0,\mu_\sigma)$.

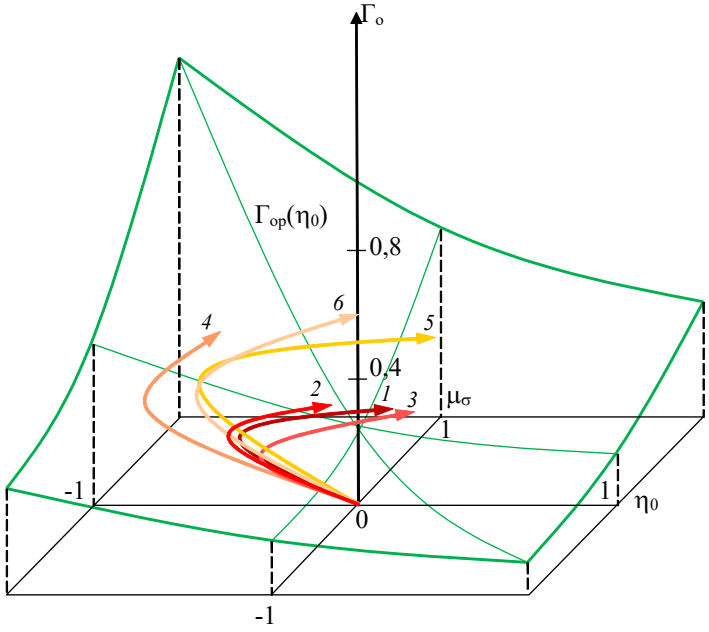

Fig. 2. Limit strain surface and deformation paths in η_0 - μ_σ - Γ_0 coordinates for a sintered iron-based porous material

To obtain other points on the limit strain surface $\Gamma_{op}(\eta_0,\mu_\sigma)$, cylindrical specimens with three initial porosities $\theta_0 = 0.27$, $\theta_0 = 0.214$, $\theta_0 = 0.128$ were upset in jackets. In doing so, it was assumed that the condition on the specimen surface is fulfilled:

$$\sigma_r = \sigma_{r0}, \tag{17}$$

where σ_{r0} - is the radial stress on the specimen surface and σ_r - is the radial stress on the inner surface of the jacket, which was determined according to the procedure [13]. Upsetting was performed in jackets with an inner diameter $d_{вн} = 8$ mm, $d_{н1} = 12$ mm, $d_{н2} = 16$ mm, $d_{н3} = 20$ mm.

The stress state index of the base material, η_0 in the critical zone (from a fracture perspective) was determined using formula (4). Meanwhile, the stress state index of the porous body, η , was determined by formula (18), which was derived using the relations of flow theory:

$$\eta = \sqrt{6}\frac{p}{\tau} = \sqrt{6}\left(\frac{\sigma_{r0}}{\tau} + \frac{\frac{1}{3}\dot{e} - \dot{e}_r}{\dot{\gamma}}\right). \tag{18}$$

In deriving (18), it was taken into account that

$$\frac{\dot{\gamma}}{\tau}p = \frac{\dot{\gamma}}{\tau}\sigma_{r0} - \dot{e}_r - \frac{1}{3}\dot{e}. \tag{19}$$

In the "barrel" region, it can be assumed that $\sigma_1 = \sigma_\varphi$, $\sigma_2 = \sigma_{r0}$, $\sigma_3 = \sigma_z$, then, the following formula for calculating the Lode parameter is obtained:

$$\mu_\sigma = \frac{2\sigma_{r0} - \sigma_\phi - \sigma_z}{\sigma_\phi - \sigma_z}. \tag{20}$$

The values of $\dot{e}_r$, $\dot{e}_\phi$, $\dot{e}_z$ were determined by the distortion of the dividing grid applied to the specimen surface. The stresses were found according to the procedure [13]. By analogy with (15) and taking into account (9), the fracture criterion (5) takes the form:

$$\int_0^{\Gamma_{op}^*} exp(-\lambda_2\mu_\sigma + (\lambda - \lambda_2)\eta)\, d\Gamma_0 = \Gamma_{op}(0,0). \tag{21}$$

Equations (21) were formulated for six deformation paths. By equating the left-hand sides of (21), three equations were obtained, from which the value λ_2=0.857 was determined using the method of successive approximations.

As a result, the following formula for the limit strain surface was obtained:

$$\Gamma_{op}(\eta_0, \mu_\sigma) = 0{,}28\, exp(-0.857\mu_\sigma - 0.69\eta_0) \tag{22}$$

in which λ_1 = 0,69. The resulting limit strain surface $\Gamma_{op}(\eta_0,\mu_\sigma)$ is shown in Fig. 2.

Conclusions

The processes of plastic deformation in porous bodies are determined by a complex combination of macroscopic densification and strain-induced loosening mechanisms. The significance of the study lies in establishing fundamental laws of fracture based on the analysis of damage accumulation directly within the material skeleton. The obtained results demonstrate alignment with the stated objectives, proving that the state of the base material is the decisive factor in the exhaustion of the plasticity resource. In the course of the study, it was substantiated and confirmed that the mathematical model of the limit strain surface fully validates the theoretical assumptions regarding the dependence of the limit state on the stress state index of the base material η_0 and the stress state type parameter μ_σ (Lode parameter). The results achieved provide a solid foundation for transitioning from empirical estimations to the analytical prediction of limit forming. The methodological integrity of the work is ensured by strict adherence to the sequential stages of experimental research and the precision of measurement procedures. The study is based on a comprehensive analysis of the deformation of sintered iron under various loading paths. The implementation of the research included the following stages: specimen preparation, deformation, measurement of the coordinates of the dividing grid nodes, and determination of the moment of fracture (macro-crack initiation). This methodological approach allowed for the transformation of primary experimental data into a verified physico-mathematical model. Consequently, the article proposes a methodology for constructing the limit strain surface of porous bodies in the following coordinates: the limit strain of the base material Γ_{op}, the stress state triaxiality (index) of the base material η_0, and the Lode parameter μ_σ. The methodology enables the derivation of the limit strain surface of a porous body $\Gamma_{op}(\eta_0,\mu_\sigma)$ based on compression tests of cylindrical specimens under various contact friction conditions and within jackets.

References

1. Chen, K., Qin, H. & Ren, Z. (2023). *Establishment of the microstructure of porous materials and its relationship with effective mechanical properties.* Sci Rep 13, 18064. https://doi.org/10.1038/s41598-023-43439-6

2. Zepeda-Ruiz, Luis A. and Stukowski, Alexander and Oppelstrup, Tomas and Bulatov, Vasily V. (2017). *Probing the limits of metal plasticity with molecular dynamics simulations.* Nature. Volume 550, number 7677, pages 492–495. https://doi.org/10.1038/nature23472

3. Yang, Yangyiwei and Bharech, Somnath and Finger, Nick and Zhou, Xiandong and Schröder, Jörg and Xu, Bai-Xiang. (2024). *Elasto-plastic residual stress analysis of selective laser sintered porous materials based on 3D-multilayer thermo-structural phase-field simulations*. npj Computational Materials. Volume 10, number 1. https://doi.org/10.1038/s41524-024-01296-5

4. Abendroth, Martin, Malik, Alexander, Kiefer, Björn. (2023). *A Modified Ehlers Model for the Description of Inelastic Behavior of Porous Structures.* Institut for Mechanics and Fluid Dynamics, TU Bergakademie Freiberg. https://doi.org/10.2139/ssrn.4651521

5. H. A. Bahliuk, S. F. Kyryliuk. (2023). Evoliutsiia protsesu ushchilnennia ta deformovanoho stanu poruvatykh zahotovok pry yikh hariachomu shtampuvanni u vidkrytomu shtampi. Mech. Adv. Technol. Vol. 7, No. 3, pp. 350–355. https://doi.org/10.20535/2521-1943.2023.7.3.292713

6. Patnaik, S., Jokar, M., Ding, W. et al. (2022) *On the role of the microstructure in the deformation of porous solids*. npj Comput Mater 8, 152. https://doi.org/10.1038/s41524-022-00840-5

7. Lindqwister, Winston, Peloquin, Jacob, Dalton, Laura, Gall, K. (2025). *Predicting compressive stress-strain behavior of elasto-plastic porous media via morphology-informed neural networks*. Communications Engineering. VL 4. https://doi.org/10.1038/s44172-025-00410-9

8. Sivak I. O. (1996). *The evaluation of deformability of the porous bodies*. The Bulletin of the Polytechnic Institute of Jassy. XLII (XLVI), № 3(4). P. 607– 611.

9. Ogorodnikov V. A., Derevenko I. A., Sivak R. I. (2018). *On the influence of curvature of the trajectories of deformation of a volume of the material by pressing on its plasticity under the conditions of complex loading*. Materials science. 54, № 3. P. 326–332. https://doi.org/10.1007/s11003-018-0188-x

10. O. V. Hrushko, V. A. Ohorodnikov, Yu. O. Slobodianiuk. (2019). Deformovnist malovuhletsevoho drotu v protsesi yoho bahatostupinchastoho kholodnoho volochinnia, Visnyk Vinnytskoho politekhnichnoho instytutu, № 3, S. 103-110. https://doi.org/10.31649/1997-9266-2019-144-3-103-110

11. Mirzaei, A. M., Mirzaei, A. H., Sapora, A. et al. (2025). *Strain based finite fracture mechanics for fatigue life prediction of additively manufactured samples*. Int J Fract 249, 44. https://doi.org/10.1007/s10704-025-00855-1

12. Shtern, M.B., Mikhailov, O.V. (2003). *Numerical Modelling of the Compaction of Powder Articles of Complex Shape in Rigid Dies: Effect of Compaction Scheme on Density Distribution. Part 2. Modelling Procedure and Analysis of Forming Schemes*. Powder Metall. Met. Ceram. 42, 114–121. https://doi.org/10.1023/A:1022928118809

13. Laptiev, A. V. (2024). *New Die-Compaction Equations for Powders as a Result of Known Equations Correction: Part 1–Review and Analysis of Various Die-Compaction Equations*. Powders, 3(1), 111-135. https://doi.org/10.3390/powders3010008

14. Bernard-Granger, Guillaume and Benameur, Nassira and Addad, Ahmed and Nygren, Mats and Guizard, Christian and Deville, Sylvain. (2009). *Phenomenological analysis of densification mechanism during spark plasma sintering of MgAl2O4*. Journal of Materials Research. Volume 24, number 6. Pages 2011–2020. https://doi.org/10.1557/jmr.2009.0243

15. Manière, Charles and Olevsky, Eugene A. (2017). *Porosity dependence of powder compaction constitutive parameters: Determination based on spark plasma sintering tests*. Scripta Materialia. Volume 141. Pages 62–66. https://doi.org/10.1016/j.scriptamat.2017.07.026

16. Al-Qureshi, H.A.; Soares, M.R.F.; Hotza, D.; Alves, M.C.; Klein, A.N. (2008). *Analyses of the fundamental parameters of cold die compaction of powder metallurgy*. J. Mater. Process. Technol. 199, 417–424. https://doi.org/10.1016/j.jmatprotec.2007.08.030

17. Aryanpour, G.; Farzaneh, M. (2015). *Application of a piston equation to describe die compaction of powders*. Powder Technol. 277, 120–125. https://doi.org/10.1016/j.powtec.2015.02.032

18. Molinari, A., Cristofolini, I., Pederzini, G., Rambelli, A. (2018). *A densification equation derived from the stress-deformation analysis of uniaxial cold compaction of metal powder mixes*. Powder Metall. 61, 210–218. https://doi.org/10.1080/00325899.2018.1466501

19. Haim Kalman. (2020). *Phenomenological study of particulate materials compression – From individual through bed compression to tableting*. Powder Technology. Volume 372, pages 161-177. https://doi.org/10.1016/j.powtec.2020.05.115

20. Montes, J.M.; Cuevas, F.G.; Cintas, J.; Ternero, F.; Caballero, E.S. (2018). *On the compressibility of metal powders*. Powder Metall. 61, 219–230. https://doi.org/10.1080/00325899.2018.1467074

Сивак Р.І., Поліщук Л.К., Шенфельд В.Й., Орманбекова А.А., Жумакхан Н. Побудова та застосування поверхні граничних деформацій для оцінки пластичності пористих тіл

Традиційні критерії руйнування суцільних матеріалів є непридатними для порошкових систем через наявність пористості, яка виступає стоком для дислокацій, змінює кінетику накопичення дефектів і уповільнює процеси структурної деградації. У роботі виконано комплексний аналіз деформування циліндричних зразків пористого матеріалу на основі заліза. Деформований стан на поверхні визначали методом координатних сіток, а переміщення міток вимірювали за допомогою високоточного інструментального мікроскопа, що дозволило розрахувати компоненти швидкостей деформацій на всіх стадіях навантаження до утворення макротріщин. Для охоплення широкого діапазону індексу напруженого стану та параметра Надаї–Лоде реалізовано вісім траєкторій навантаження, включаючи вільне осадження за різних умов тертя та деформування в сталевих оболонках. Розрахунок параметрів η_0 та $\mu\sigma$ виконано з урахуванням функцій пористості, що забезпечило коректне врахування впливу пор на напружений стан матеріалу. Експериментальні дані узагальнено методом послідовних наближень, що дозволило визначити ключові параметри моделі. У результаті отримано аналітичну залежність поверхні граничних деформацій, яка описує умову руйнування матеріалу. Підтверджено інваріантність ресурсу пластичності базового матеріалу відносно початкової пористості за умови незмінності складу та структури матриці. Практична цінність полягає у створенні інструменту прогнозування дефектоутворення та оптимізації процесів порошкової металургії.

Ключові слова: руйнування, пористість, накопичення пошкоджень, напружено-деформований стан, показник напруженого стану

ISSN 2079-1372 ***Problems of Tribology****, V. 31, No 2/120-2026, 52-59*

Problems of Tribology
Website: http://tribology.khnu.km.ua/index.php/ProbTrib
E-mail: tribosenator@gmail.com

DOI: https://doi.org/10.31891/2079-1372-2026-120-2-52-59

The effect of load and sliding speed on the wear rate of a metal-polymer composite containing an Al-Co filler

K.A. Mykyta 0009-0001-1307-4434

Dniprovsk State Technical University, Kamyanske, Ukraine
E-mail: mikita2703@gmail.com

Received: 12 April 2026: Revised 25 April 2026: Accept: 15 May 2026

Abstract

The paper presents the results of a study on the tribotechnical behaviour of a polymer composite material based on ultra-high-molecular-weight polyethylene, filled with 25 wt.% of a rapidly quenched binary alloy of the Al–10 wt.% Co system. The relevance of the study is due to the need to improve the wear resistance of tribological joints operating under conditions of intensive wear, high loads, and insufficient lubrication. The aim of the study is to develop a mathematical model describing the influence of sliding speed and applied load on the intensity of linear wear of the composite under dry friction conditions using a disk–pad configuration. The study was carried out using a full factorial experiment and a first-order regression model, which made it possible to quantitatively evaluate the influence of the experimental factors and their interaction. It was established that with increasing load, the intensity of linear wear increases significantly, while the influence of sliding speed is less pronounced and becomes evident in interaction with load. A synergistic effect of the combined action of the investigated factors on the linear wear intensity of the polymer composite was identified. The developed mathematical model was validated using statistical criteria and adequately describes the experimental data. The obtained results can be used to predict the wear resistance of the material and to determine rational operating conditions for tribological joints, thereby improving their durability and reliability.

Keywords: ultra-high-molecular-weight polyethylene, binary alloy of the Al-Co system, sliding speed, applied load, linear wear rate, mathematical model

Introduction

The development of modern technology directly depends on the stable and efficient operation of lightly and heavily loaded tribological components of equipment. Under aggressive operating conditions, particularly in the presence of abrasive particles (e.g. sand and crop-processing products) and moisture, as well as under friction conditions with insufficient or no lubrication, bearings and other friction elements are subject to severe wear. This leads to loss of performance, equipment downtime, and significant financial costs associated with the repair and replacement of machine components. One common solution to this problem is using polymer composite materials (PCMs) based on thermoplastics containing dispersed fillers (FLs) of various types, including graphite, aluminosilicate microspheres, carbides, and metal powders. Using them as an alternative to traditional materials reduces manufacturing labour intensity, including for components of complex geometry, as well as reducing operating costs associated with the maintenance of tribological systems [1, 2].

Literature Review

The main factors affecting the wear resistance of polymer composite materials are the sliding speed (υ, m/s) and the applied load (P, MPa). Knowledge [3] of the critical values of these parameters makes it possible to determine rational operating conditions for PCM-based components, predict their tribological behaviour, and extend the service life of tribological systems [4]. The application of design of experiments methods and the development of a mathematical model make it possible to determine these critical parameters without conducting a large number of resource-intensive experiments, including bench and full-scale tests, while ensuring high informativeness and reliability of the obtained results [5]. One of the most widely used materials for PCM production is ultra-high molecular weight polyethylene (UHMWPE), which is characterized by a low coefficient

of friction and high resistance to wear and aggressive environments. Studies have shown that the incorporation of dispersed metallic nanoparticles [6], in particular aluminium-based binary alloys [7, 8], can significantly improve its functional properties by increasing stiffness, wear resistance, and thermal conductivity of UHMWPE. Despite the large number of studies, the combined effect of sliding speed and load on the wear rate of PCMs filled with such nanoparticles remains insufficiently investigated. In particular, there is a lack of generalized mathematical models capable of predicting the tribological behaviour of these materials over a wide range of operating conditions.

In works [7, 8] it was established that the PCM containing 25 wt.% of a rapidly quenched binary alloy of the Al-10 wt.%Co system exhibits an effective combination of tribological properties. A rapidly quenched binary alloy of the Al–Co system containing 10 wt.% Co was selected as a dispersed filler (particle size 50–100 μm) for the polymer matrix. As shown by X-ray diffraction studies, the structure of these alloys contains single-phase highly supersaturated substitutional solid solutions based on Al, which provide these binary alloys with unique functional properties. These properties are caused by a high level of crystal lattice microstrains in the alloys. The difference in the atomic radii of the elements (r_{Al}=0,143 nm, r_{Co}=0,143 nm) causes lattice microstrain ($\Delta a/a$) at the level of $2{,}7\cdot10^{-3}$. In particular, the introduction of this FL contributes to an increase in the wear resistance of UHMWPE (manufactured by Jiujiang Zhongke Xinxing New Material Co., Ltd., China) under various operating conditions, including the action of firmly embedded abrasive particles and friction without lubrication, as well as to improved heat dissipation from the contact zone, which is critically important for tribological materials.

At the same time, an analysis of the literature indicates that the combined effect of sliding speed and applied load on the wear rate of such materials remains insufficiently studied, particularly in terms of quantitative description and prediction of their tribological behaviour. In this regard, there is a need to apply mathematical modeling approaches that make it possible to establish relationships between friction regime parameters and material wear resistance. With this in mind, the present study employs a full factorial design with subsequent development of a first-order regression model to investigate the effect of sliding speed and load on the linear wear rate of the PCM. This approach makes it possible not only to evaluate the individual contributions of these parameters, but also to identify the synergistic effects of their interaction [7, 8].

In study [7], it was established that the coefficient of friction of the composite changes insignificantly. Therefore, the linear wear rate was selected as the main optimization parameter, since it directly characterizes the durability and performance of tribological joints.

The purpose of the work

In view of the above, the aim of this work is to develop a mathematical model describing the effect of load and sliding speed on the linear wear rate of a polymer composite based on ultra-high molecular weight polyethylene containing 25 wt.% of a rapidly quenched binary alloy of the Al-10 wt.% Co system as a filler.

Objects and methods of research

The tribological properties of the developed PCM under dry contact conditions were investigated using an SMC-2 testing machine in a «disk–pad» configuration. This configuration was selected because it simulates real friction conditions in tribological systems across various engineering applications The samples were fabricated in the form of cylinders with a diameter of 30 mm and a height of 10 mm. The counterbody was made of medium-carbon steel (grade 45) with a diameter of 25 mm, a hardness of 45–48 HRC, and a surface roughness of R_a=0,32 μm. To ensure the reliability of the results, error estimation was performed based on the variance of parallel measurements using the Cochran, Student's t-, and Fisher's F-tests. This made it possible to confirm the reproducibility of the experiments, the statistical significance of the model coefficients, and the adequacy of the developed model. The linear wear rate was calculated using the following equation:

$$I_h = \frac{\lambda}{\rho_{exp}} \cdot \frac{\Delta m}{S \cdot L},$$

where λ=1 indicates that all points of the friction surface of the specimen are in contact with the counterbody;

ρ_{exp} is the experimental density of the specimen, determined by hydrostatic weighing, g/cm^3;

Δm is the mass loss, g;

S is the contact area between the specimen and the counterbody, cm^2;

L is the sliding distance (friction path) of the specimen [8].

The morphology of the friction surfaces was investigated using a BIOLAM-M binocular microscope.

Results analysis and discussion

For PCMs with an effective content of 25 wt.% of the FL in the Al-Co system, the linear wear rate (I_h) was selected as the optimisation parameter. This parameter depends on two factors: sliding speed (x_1) and load (x_2):

$$I_h = f(x_1, x_2),$$

To simplify the calculations, the experimental factor values were transformed to a coded scale (−1, 0, +1) using the following formula:

$$x_i = \frac{X_i - X_{io}}{n},$$

where X_i is the current value of the factor, X_{i0} is the baseline level, and n is the variation step [9]. The transformation from natural factor values to coded variables was performed as follows:

$$x_1 = \frac{v - v_0}{\Delta v},$$
$$x_2 = \frac{P - P_0}{\Delta P},$$

where υ is the sliding velocity, m/s; P is the applied load, MPa; υ_0=1,0 m/s and P_0=1,0 MPa are the baseline factor levels; Δυ=0,5 m/s and ΔP=0,5 MPa are the variation intervals. The coded values of the experimental factors are presented in Table 1. The selected ranges of load and sliding speed were determined taking into account the expected operating conditions of lightly and moderately loaded tribological joints of agricultural machinery, in which UHMWPE-based composites can be used.

Table 1

Initial data for experiment design

Factors	Symbol, unit of measurement	Conventional symbol	Variation step (n)	Level of variation		
				-1	0	+1
Sliding speed	υ, m/s	x_1	0,5	0,5	1,0	1,5
Load	P, MPa	x_2	0,5	0,5	1,0	1,5

In accordance with the experimental design, N = 9 experiments were conducted, each repeated three times (k=3), thereby increasing the reliability of the results and minimising the influence of random measurement errors (Table 2).

Table 2

Experimental design matrix with calculated factor interaction terms

№ of the experiment	Variable values on the coded scale				Variable values on the natural scale	
	x_0	x_1	x_2	x_1x_2	υ, m/s	P, MPa
1	+1	+1	+1	+1	1,5	1,5
2	+1	+1	0	0	1,5	1
3	+1	+1	-1	-1	1,5	0,5
4	+1	0	+1	0	1	1,5
5	+1	0	0	0	1	1
6	+1	0	-1	0	1	0,5
7	+1	-1	+1	-1	0,5	1,5
8	+1	-1	0	0	0,5	1
9	+1	-1	-1	+1	0,5	0,5

To describe mathematically the influence of the studied factors on the linear wear rate, a first-order regression equation was used:

$$y = b_0 + b_1x_1 + b_2x_2 + b_{12}x_{12},$$

where y is the calculated value of the optimisation parameter; b_0 is the intercept term corresponding to the value of the response function at the center of the experiment; b_1, b_2 are coefficients describing the effects of sliding velocity and load, respectively; b_{12} is a coefficient accounting for the interaction between the factors. The mean values of the response function ($\bar{y}_j$) were determined from the results of parallel experiments [10, 11]:

$$\bar{y}_j = \frac{1}{k}\sum_{i=1}^{k} y_{ji}, \qquad j=1,2,\ldots,N$$

where k = 3 is the number of repetitions and N = 9 is the total number of experiments according to the experimental design (Table 3). The mean square errors of the parallel experiments were calculated using the following expressions:

$$S_j^2 = \frac{S_r^2}{\sum_{j=1}^{N} x_i},$$
$$S_j^2 = \frac{\sum_{j=1}^{N}(y_i - \bar{y}_j)}{k-1}.$$

The homogeneity of variances obtained in the parallel experiments was assessed using Cochran's criterion:

$$G_p = \frac{\max S_j^2}{\sum_{i=1}^{k} S_j^2}.$$

A comparison between the calculated value of Cochran's criterion and the tabulated value was conducted for the number of degrees of freedom $f_1=k-1$ and the number of experiments N, at a confidence level of P=0,95. Since the calculated value of Cochran's criterion G_p is lower than the tabulated value G_{tab}, the dispersions are considered homogeneous. The error in determining the regression coefficients was estimated using the following expression:

$$S_{bi} = \frac{S_y}{\sqrt{N \cdot k}}.$$

Table 3

Experimental and calculated values of linear wear rate

№ of the experiment	y_1	y_2	y_3	mean	calculated
				$\tilde{y}_j$	$y_j{}^p$
1	$4{,}86\cdot10^{-6}$	$5{,}00\cdot10^{-6}$	$5{,}12\cdot10^{-6}$	$4{,}99\cdot10^{-6}$	$3{,}68\cdot10^{-6}$
2	$4{,}58\cdot10^{-6}$	$4{,}63\cdot10^{-6}$	$4{,}52\cdot10^{-6}$	$4{,}58\cdot10^{-6}$	$2{,}50\cdot10^{-6}$
3	$1{,}8\cdot10^{-7}$	$3{,}57\cdot10^{-7}$	$5{,}72\cdot10^{-7}$	$3{,}7\cdot10^{-7}$	$1{,}76\cdot10^{-6}$
4	$2{,}79\cdot10^{-6}$	$2{,}85\cdot10^{-6}$	$2{,}74\cdot10^{-6}$	$2{,}79\cdot10^{-6}$	$2{,}28\cdot10^{-6}$
5	$3{,}56\cdot10^{-7}$	$3{,}59\cdot10^{-7}$	$3{,}6\cdot10^{-7}$	$3{,}58\cdot10^{-7}$	$1{,}52\cdot10^{-6}$
6	$1{,}91\cdot10^{-8}$	$1{,}1\cdot10^{-8}$	$1{,}05\cdot10^{-8}$	$1{,}35\cdot10^{-8}$	$7{,}60\cdot10^{-7}$
7	$1{,}26\cdot10^{-7}$	$2{,}89\cdot10^{-7}$	$1{,}61\cdot10^{-7}$	$1{,}26\cdot10^{-7}$	$9{,}20\cdot10^{-7}$
8	$9{,}75\cdot10^{-9}$	$1{,}35\cdot10^{-8}$	$9{,}82\cdot10^{-9}$	$1{,}16\cdot10^{-8}$	$5{,}40\cdot10^{-7}$
9	$9{,}74\cdot10^{-9}$	$9{,}6\cdot10^{-9}$	$9{,}74\cdot10^{-9}$	$9{,}69\cdot10^{-9}$	$2{,}00\cdot10^{-7}$

The regression coefficients were calculated using analytical dependencies derived from the full factorial experiment results.

$$b_0 = \sum_{i=1}^{N} \frac{\bar{y}_j x_0}{N},$$
$$b_i = \sum_{i=1}^{N} \frac{\bar{y}_j x_i}{N},$$
$$b_{ij} = \sum_{i=1}^{N} \frac{\bar{y}_j x_{ij}}{N}.$$

Based on the calculated data, a first-order regression equation was obtained. It describes the influence of the studied factors on the response function.

$$y(I_h) = 1{,}47 \cdot 10^{-6} + 1{,}08 \cdot 10^{-6} x_1 + 8{,}35 \cdot 10^{-7} x_2 + 5{,}00 \cdot 10^{-7} x_{12}.$$

To obtain the regression equation in natural variables, the coded variables were substituted using the following relationships:

$$x_1 = \frac{v - 1{,}0}{0{,}5},$$
$$x_2 = \frac{P - 1{,}0}{0{,}5}.$$

Substituting these expressions into the regression equation, the following equation in natural variables (P, υ) was obtained:

$$I_h = (-0{,}36 + 0{,}16 \cdot \upsilon - 0{,}33 \cdot P + 2{,}00 \cdot \upsilon \cdot P) \cdot 10^{-6}.$$

The analysis of the obtained coefficients shows that an increase in sliding velocity and load is accompanied by an increase in wear intensity, as confirmed by the positive values of coefficients b_1 and b_2. The positive value of the interaction coefficient b_{12} indicates the presence of a synergistic effect, whereby the simultaneous action of both factors intensifies the wear process.The statistical significance of the regression coefficients was assessed using Student's t-criterion by constructing confidence intervals, taking into account the corresponding degrees of freedom and a confidence level of 0,95.

$$|b_{cr}| = t_{cr} \cdot S_{bi}.$$

A coefficient was considered statistically significant if its absolute value exceeded the critical value. The results of the analysis showed that all coefficients were significant according to Student's criterion and were therefore retained in the mathematical model. As a result, a regression equation was obtained. It adequately describes the influence of the studied factors on the response function. The adequacy of the developed model was evaluated by comparing the experimental and calculated values of the response function [12, 13]. For this purpose, the dispersion of adequacy was determined:

$$S_{ad}^2 = \frac{1}{N - B}\sum_{j=1}^{N}\left(\bar{y}_j - y_j^P\right)^2,$$

where B is the number of statistically significant coefficients. Accordingly, the number of degrees of freedom for the adequacy assessment is $f_{ад}$=N – B. The calculated values of wear intensity are presented in Table 4. To assess the adequacy of the mathematical model, Fisher's criterion was applied, defined as the ratio of the adequacy variance to the reproducibility variance [11].

$$F_p = \frac{S_{ad}^2}{S_y^2}.$$

Table 4

Calculated data for assessing model adequacy using Fisher's criterion

S_y^2	Regression coefficients				S_{ad}^2
	b_0	b_1	b_2	b_{12}	
$1{,}07 \cdot 10^{-14}$	$1{,}47 \cdot 10^{-6}$	$1{,}08 \cdot 10^{-6}$	$8{,}35 \cdot 10^{-7}$	$5{,}00 \cdot 10^{-7}$	$3{,}10 \cdot 10^{-14}$

At a confidence level of 0,95 and corresponding degrees of freedom f_1=3 and f_2=5, the calculated value of Fisher's criterion (F_p = 2,89) is lower than the tabulated value (F_{tab} =5,05). This confirms the adequacy of the mathematical model for describing the studied process.

Based on the simplified and statistically significant first-order regression equation, a response surface of the linear wear rate of the PCM was constructed as a function of sliding speed and applied load (Fig. 1).

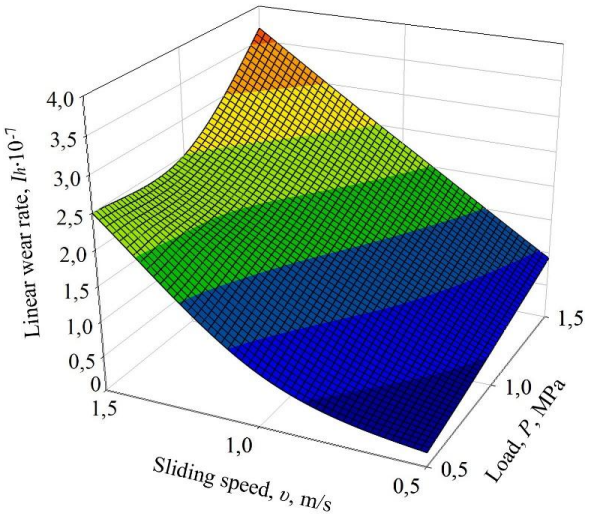

Fig. 1. Response surface of the linear wear rate (I_h) of the composite as a function of sliding speed (υ, m/s) and applied load (P, MPa)

Analysis of the response surface (Fig. 1) shows that the linear wear rate of the PCM is strongly influenced by both sliding speed and applied load. As the load increases, a monotonic increase in wear rate is observed, which can be attributed to higher contact stresses and intensified degradation processes in the surface layer. The effect of sliding speed is nonlinear: as it increases, the wear rate changes less markedly; however, when combined with high loads, a sharp decrease in wear resistance is observed. This indicates the presence of interaction effects between the factors, as evidenced by the shape of the response surface.

The obtained dependences of the linear wear rate on sliding speed and load are determined by the peculiarities of the stress-strain state of the surface layer of the PCM during friction. The introduction of the metallic FL contributes to the redistribution of contact stresses in the surface layer and limits excessive plastic deformation of UHMWPE during friction. Under relatively low loads and sliding speeds, this ensures stabilization of the tribocontact and high wear resistance, which is confirmed by the morphology of the friction surfaces (Fig. 2a), characterized by a less damaged surface relief and insignificant traces of plastic deformation. This indicates that an adhesive-fatigue wear mechanism is realized between the tested specimen and the steel counterbody. At the same time, an increase in the applied load leads to an increase in the real contact area and contact stresses, which is accompanied by intensified deformation and destruction processes in the surface layer of the PCM. Under such conditions, friction-induced heating becomes more pronounced, especially at high sliding speeds. Despite the fact that the Al–Co FL promotes efficient heat dissipation from the contact zone, as confirmed by the increase in the thermal conductivity of the PCM reported in [14], under the simultaneous action of high loads and sliding speeds the amount of generated thermal energy exceeds the ability of the tribosystem to stabilize the friction process. This results in intensified wear processes, which is confirmed by the experimentally established increase in the linear wear rate of the PCM. Analysis of the friction surface morphology showed that at high values of load and sliding speed, pronounced deformation regions, local damage, and traces of material removal are observed on the friction surface of the PCM. This indicates the predominance of mechanical destruction processes in the surface layer (Fig. 2b) and the transition to a pseudoelastic wear mechanism.

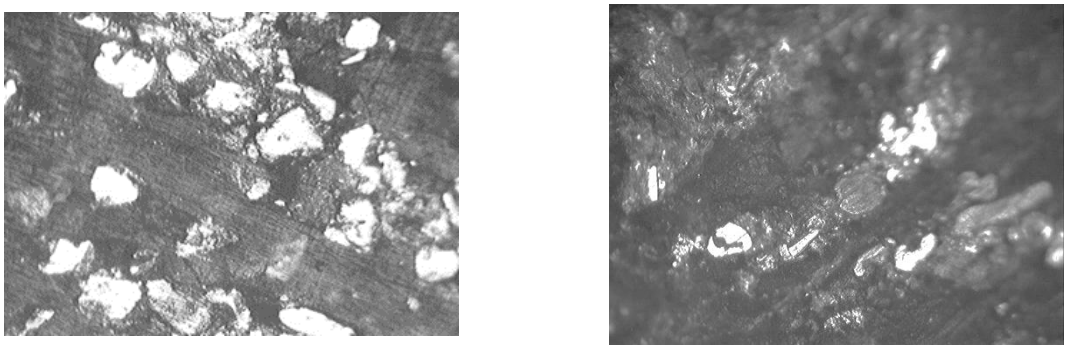

a b

Fig. 2. Morphology of the friction surface (×150) of the polymer composite containing 25 wt.% of the binary alloy under friction conditions: P = 1,0 MPa and υ = 1,0 m/s (a), and P = 1,5 MPa and υ = 1,5 m/s (b)

The positive interaction coefficient obtained in the regression equation indicates a synergistic effect of the applied load and sliding speed on damage accumulation in the surface layer of the PCM. This indicates that the simultaneous increase in these parameters promotes intensification of degradation processes compared with their individual influence. Such behaviour is consistent with current concepts of dry friction of PCMs, according to which the applied load primarily determines the stress state of the tribological interaction, whereas the sliding speed significantly affects the thermal conditions of friction.

Moreover, the presence of highly supersaturated substitutional solid solutions and a high level of crystal lattice microstrains in the Al–Co binary alloy may contribute to increasing the resistance of the PCM surface layer to microcutting and local plastic deformation during friction. In addition, the metallic nature of the binary alloy promotes more efficient heat dissipation from the friction zone, which partially suppresses the development of thermally activated wear processes under dry friction conditions. Minimum values of the linear wear rate are observed in the region of low sliding speeds and low applied loads, whereas the maximum values occur under their simultaneous increase.

Analysis of the results shows that the minimum wear rate values are achieved at lower load levels, whereas an increase in load leads to a rise in wear rate, which is consistent with the result of regression analysis. Thus, the obtained experimental results and the developed regression model consistently describe the influence of sliding speed and applied load on the linear wear rate of the investigated polymer composite. The model adequately reflects both the individual effects of the factors and their interaction, which is confirmed by statistical analysis and graphical interpretation of the response surface.

Therefore, the relationships established in this study regarding the increase in wear intensity with increasing applied load are consistent with the results of other studies on PCMs [4, 9], which demonstrate the decisive role of contact stresses in the wear process. It was also found that the less pronounced effect of sliding speed and its interaction with the load are in agreement with current understanding of PCM wear mechanisms, where sliding

speed determines the thermal conditions at the contact, while the applied load governs the intensity of surface layer degradation. Similar approaches to analyzing the influence of these factors and to developing mathematical models using design of experiments methods are presented in [12]. Thus, the obtained results not only confirm previously reported data but also extend them by providing a quantitative description of the interaction between factors affecting the linear wear intensity of PCM based on UHMWPE containing 25 wt.% of a binary Al–Co alloy as a filler.

Conclusions

1.In this study, quantitative relationships describing the effect of sliding speed and applied load on the linear wear rate of a UHMWPE-based PCM filled with 25 wt.% of a rapidly quenched Al–10 wt.% Co alloy were established for the first time.

2.Based on the experimental data and using a full factorial design, an adequate mathematical model of the wear process was developed, accounting for both the individual effects of the studied factors and their interaction. A synergistic effect of the combined action of sliding speed and load on the linear wear rate was identified, which has not been sufficiently reported previously for this class of materials.

3.The developed mathematical model made it possible to determine the range of rational operating parameters at which minimum values of the linear wear rate of the PCM are achieved. The model can be used to predict the wear resistance of the composite and to substantiate optimal operating conditions under various friction regimes in tribological systems.

4.Semi-helical moldboards made of the developed PCM were manufactured and tested at LLC «Dnipro Metal Structures Plant». The field test results demonstrated increased wear resistance, reduced soil adhesion, and improved plow efficiency. These results support the recommendation of this PCM for implementation in industrial production.

References

1. A.S. Kobets Application of polymer composites in the agricultural industry. Monograph. Dnipro: Zhurfond, 2022. 356 p. https://dspace.dsau.dp.ua/handle/123456789/7031

2. O. Ponomarenko, N. Yevtushenko, K. Berladir,; Zapolovskyi, M.; Krmela, J.; Krmelová, V.; Artyukhov, A. Modeling and optimization of properties of the environmentally clean molds based on oligofurfuryloxysiloxanes for the production the metal castings. Polymers. 2022. Vol.14. P. 1883. https://doi.org/10.3390/polym14091883

3. O. Kabat, V. Sytar, O. Derkach, K. Sukhyy Polymeric composite materials of tribotechnical purpose with a high level of physical, mechanical and thermal properties. Chemistry & Chemical Technology. 2021. Vol. 15, No 4. P. 543–550. https://doi.org/10.23939/chcht15.04.543

4. B.P. Chang, H. Md Akil, R. Nasir, A. Khan Optimization on wear performance of UHMWPE composites using response surface methodology. Tribology International. 2015. Vol. 88. P. 158–167. https://doi.org/10.1016/j.triboint.2015.03.028

5. O.V. Dykha, T.V. Gedzuk. Rated and experimental modeling of tribological properties of constructional and lubri-cating materials. Problems of Tribology. 2014. Vol.71, No 1. P. 84–87. https://tribology.khmnu.edu.ua/index.php/ProbTrib/article/view/94

6. L. Wang, S. Gao, J. Wang, W. Wang, L. Zhang, M. Tian Surface modification of UHMWPE fibers by ozone treatment and UV grafting for adhesion improvement. The Journal of Adhesion. 2018. Vol. 94. P.30–45. https://doi.org/10.1080/00218464.2016.1229603

7. V. Bashev, K. Mykyta, A.-M. Tomina The Influence of a Rapidly Quenched Binary Alloy of the Al–Co System on the Wear Resistance of Ultra-High-Molecular-Weight Polyethylene. In: Aikin, M., et al. Advanced and Novel Technologies – Interdisciplinary Collaboration in Materials Science. ANTICM 2025. Advances in Science, Technology & Innovation. Springer, Cham. 2025. P. 205–208. https://doi.org/10.1007/978-3-032-00373-7_27

8. V.F. Bashev, A.-M.V. Tomina, K.A. Mykyta, T.V. Kalinina, S.I. Riabtsev, O.I. Kushnerov The influence of a rapidly-quenched filler on the wear resistance of ultrahigh molecular weight polyethylene. Functional Materials. 2024. Vol.31, No 3. P. 387–390. http://functmaterials.org.ua/contents/31-3/387

9. T. Brink, L. Frérot, J.-F. Molinari A parameter-free mechanistic model of the adhesive wear process of rough surfaces in sliding contact. J. Mech. Phys. Solids. 2021. Vol. 147. P. 104238. https://doi.org/10.1016/j.jmps.2020.104238

10. S. Colonna, M.M. Bernal, G. Gavoci, J. Gomez, C. Novara, G. Saracco, A. Fina Effect of processing conditions on the thermal and electrical conductivity of poly (butylene terephthalate) nanocomposites prepared via ring-opening polymerization. Materials & Design. 2017. Vol. 119. P. 124-132. https://doi.org/10.1016/j.matdes.2017.01.067

11. Kalinichenko S.V., Yeriomina Ye., Burya A.I., Dašić P. Optimization of Polychlorotrifluoroethylene Processing Technology by the Response Surface Methodology. Lecture Notes in Networks and Systems. 2020. Vol. 128. P. 322–330. https://doi.org/10.1007/978-3-030-46817-0_37

12. O. Yeromenko, Y. Yeriomina, A.-M. Tomina, P. Dašić Optimization of the Processes of Operation of Basalt Plastic Friction Unit. Lecture Notes in Networks and Systems. 2024, Vol. 926 LNNS. P. 118–128. 10.1007/978-3-031-54664-8_12

13. O.O. Naberezhna, K.A. Yeriomina Optimization of technological parameters of organoplastic pressing using experimental design. Metinvest Polytechnic Scientific Journal. Series: Technical Sciences. 2025. No. 4. P. 167–173. https://doi.org/10.32782/3041-2080/2025-4-22

14. K. Mykyta, A.-M. Tomina, V. Bashev, Ye. Yeriomina, S. Ryabtsev The effect of a rapidly quenched Al-Co alloy on the thermophysical characteristics of ultra-high-molecular-weight polyethylene. Molecular Crystals and Liquid Crystals. 2025. P. 210-215. https://doi.org/10.1080/15421406.2025.2584299

Микита К.А. Вплив навантаження та швидкості ковзання на інтенсивність зношування металополімерного композиту з наповнювачем системи Al-Co

У роботі наведено результати дослідження триботехнічної поведінки полімерного композиційного матеріалу на основі надвисокомолекулярного поліетилену, наповненого 25 мас.% швидкозагартованого бінарного сплаву системи Al-10 мас.% Co. Актуальність дослідження обумовлена необхідністю підвищення зносостійкості трибологічних з'єднань, що працюють в умовах інтенсивного зношування, підвищених навантажень і недостатнього змащення. Метою дослідження є розробка математичної моделі впливу швидкості ковзання та прикладеного навантаження на інтенсивність лінійного зношування композити в умовах тертя без змащення за схемою «диск-колодка». Дослідження виконано із застосуванням методу повного факторного експерименту з використанням регресійного рівняння першого порядку, що дозволило кількісно оцінити вплив дослідних факторів та їх взаємодії. Встановлено що зі зростанням навантаження інтенсивність лінійного зношування суттєво підвищується, тоді як вплив швидкості ковзання є менш вираженим і проявляється при взаємодії з навантаженням. Виявлено синергетичний ефект спільної дії дослідних факторів на інтенсивність лінійного зношування даного полімерного композиту. Побудована математична модель перевірена за статистичними критеріями та адекватно описує експериментальні дані. Отримані результати можуть бути використані для прогнозування зносостійкості матеріалу та визначення раціональних режимів експлуатації трибологічних з'єднань, що сприяє підвищенню їх довговічності та надійності.

Ключові слова: надвисокомолекулярний поліетилен, бінарний сплав системи Al-Co, швидкість ковзання, прикладене навантаження, інтенсивність лінійного зношування, математична модель

ISSN 2079-1372 Problems of Tribology, V. 31, No 2/120-2026, 60-65

Problems of Tribology
Website: http://tribology.khnu.km.ua/index.php/ProbTrib
E-mail: tribosenator@gmail.com

DOI: https://doi.org/10.31891/2079-1372-2026-120-2-60-65

New anti-corrosion pigment based on natural aluminosilicate with a layered structure

M.-O.M. Danyliak*0000-0003-0688-8146, **S. A. Korniy** 0000-0003-3998-2972

Karpenko Physico-Mechanical Institute of the NAS of Ukraine, Lviv, Ukraine
E-mail: danyliak-olena@ukr.net

Received: 15 April 2026: Revised 28 April 2026: Accept: 15 May 2026

Abstract

Eco-friendly anti-corrosion pigments based on the natural ion-exchange montmorillonite mineral with a layered structure was obtained by mechanochemical modification. It is shown that due to modification with zinc monophosphate, montmorillonite is enriched with zinc cations and phosphate anions. According to scanning electron microscopy results the montmorillonite particles are in the form of curved plates that tend to agglomerate. Using EDX analysis, it was established that the initial montmorillonite was Ca, Mg – form of montmorillonite. Due to the mechanochemical modification of montmorillonite, intercalation of Zn^{2+} cations into the layered structure of natural montmorillonite occurred, and phosphate anions were able to form surface adsorption complexes with positively charged edge surfaces of montmorillonite through the acidic environment of the crystal hydrate of the salt $Zn(H_2PO_4)_2 \cdot 2H_2O$, while the content of zinc and phosphorus is ~5 wt. % and ~ 4 wt. %, respectively. It was established that the obtained pigment based on mechanochemically modified montmorillonite increases the corrosion resistance of the aluminium alloy in an acid rain environment with pH = 4.5 by potentiodynamic polarization and electrochemical impedance spectroscopy methods. The inhibitory effect of mechanochemically modified montmorillonite consists in the release of Zn^{2+} cations from montmorillonite containers, which, interacting with OH^- anions, form zinc hydroxides at the cathode sites, and the slowing down of electrochemical corrosion occurs due to the formation of phosphates at the anode sites of the aluminium alloy. It was established that the protection degree of the aluminium alloy in the acid rain environment with mechanochemically modified montmorillonite was above 90 %. Thus, montmorillonite, an aluminosilicate mineral of natural origin, is a promising material for obtaining new eco-friendly anti-corrosion pigments in paint and varnish coatings to ensure long-term protection of metal products.

Key words: corrosion, montmorillonite, ion-exchange minerals, anti-corrosion pigment, clay, aluminium alloy.

Introduction

One of the most common and effective methods of protecting metallic materials is the use of paint coatings. However, during use, the protective properties of paint coatings diminish under the influence of the environment, which eventually leads to the formation of an active corrosion cell beneath the coating. Therefore, the long-term effectiveness of such coatings can be enhanced by the adding of anti-corrosion pigments [1, 2]. Chromate-based compounds are the most widely used and effective pigments. However, their harmful effects limit their use in paint and varnish coatings [3]. This necessitates the search for environmentally friendly alternatives that also exhibit high inhibitory effectiveness. Such alternatives include the use of natural minerals with ion-exchange properties, for example, sepiolite, galuzite or bentonite [4–6], etc. Bentonite consists mainly of montmorillonite, which possesses cation-exchange properties, and is therefore a promising natural ion-exchange material for anti-corrosion pigments [7]. Montmorillonite is a 2:1-layered hydrated aluminium silicate with a composition similar to the formula: $(½Ca,Na)(Al,Mg,Fe)_4[(Si,Al)_8O_{20}](OH)_4.nH_2O$. It consists of a central layer of aluminium oxide octahedra, which is sandwiched between two layers of silicon oxide tetrahedra [8, 9]. It can be used as a container for the intercalation of corrosion inhibitors [10]. Anti-corrosion pigments based on ion-exchange minerals can be obtained by mechanochemical modification. Therefore, the aim of this work is to obtain an environmentally friendly anti-corrosion pigment based on montmorillonite through mechanochemical

modification, and to evaluate its inhibitory effectiveness for improving the corrosion resistance of the aluminium alloy in an acid rain environment.

Research materials and methodology

To prepare the anti-corrosion pigment, montmorillonite obtained from bentonite from the Ilnytske deposit in Zakarpattia Oblast (Ukraine), supplied by Lignit+ LLC, was used. The montmorillonite was obtained from the bentonite by sedimentation of the coarse-particle phase. Mechanochemical modification of natural montmorillonite was carried out using zinc monophosphate $Zn(H_2PO_4)_2 \cdot 2H_2O$ in a ball mill for 15 minutes at ambient temperature. The elemental composition and surface morphology of the initial and mechanochemically modified montmorillonite were studied using Zeiss MA10 scanning electron microscope equipped with an AztecLive energy-dispersive microanalysis system (EDX) based on an X Max 50 detector. The aluminium alloy, with the chemical composition (wt.%): Si ≤ 0.5; Cr ≤ 0.1; Mn 0.3–0.9; Cu 3.8–4.9; Mg 1.2–1.8; Fe ≤ 0.5; Ti ≤ 0.15; balance Al, was used in the study. The corrosion resistance of the aluminium alloy was investigated in a model acid rain solution [11] with and without montmorillonite pigments (both in their initial form and after mechanochemical modification), as well as with the addition of zinc monophosphate (at a concentration of 2 g/l) at room temperature using methods of potentiodynamic polarisation and electrochemical impedance spectroscopy (EIS). The Versa STAT 3 frequency response potentiostat was used. The potential scanning rate during potentiodynamic polarisation was 2 mV/s. The three-electrode cell contained an Ag/AgCl reference electrode, a platinum auxiliary electrode and a working electrode made of the aluminium alloy. EIS measurements were performed in the frequency range 10,000–0.01 Hz with an applied signal amplitude of 10 mV. Equivalent circuits are shown in Fig. 1 (R_s, R_c, R_{ct}, CPE_c, and CPE_{dl} – solution resistance, protective film resistance, charge transfer resistance, constant phase element of the protective film and the double layer, respectively), which was used for fitting the EIS data of the aluminium alloy samples after 48 hours of exposure in an acid rain environment. ZView® software was used to fit the EIS data. The inhibitory efficiency (IE, %) was determined using the following formulas [12].

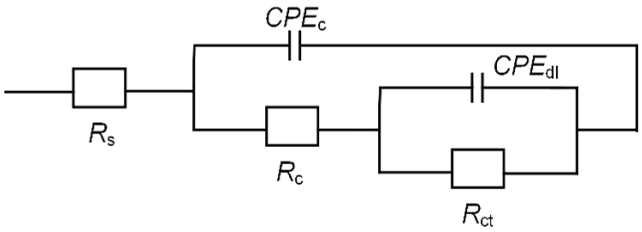

Fig. 1. Equivalent circuits for EIS data fitting after 48 hours of exposure in an acid rain environment without and with anti-corrosion pigment

Research results and discussion

An analysis of the morphology and dispersibility of the initial and mechanochemically modified montmorillonites (Fig. 2) showed that their particles are agglomerates and have the shape of curved plates, and that the modification leads to conglomeration. Their chemical composition was determined using EDX analysis. The initial montmorillonite is the Ca, Mg form of montmorillonite, as Ca and Mg were detected in its composition. As a result of the mechanochemical modification of montmorillonite, Zn^{2+} cations are intercalated into the layered structure of natural montmorillonite, whilst phosphate anions can form surface adsorption complexes with the positively charged edge surfaces of montmorillonite via the acidic environment of the $Zn(H_2PO_4)_2 \cdot 2H_2O$ salt hydrate, with the zinc and phosphorus contents being ~5 wt. % and ~4 wt.%, respectively (Table 1).

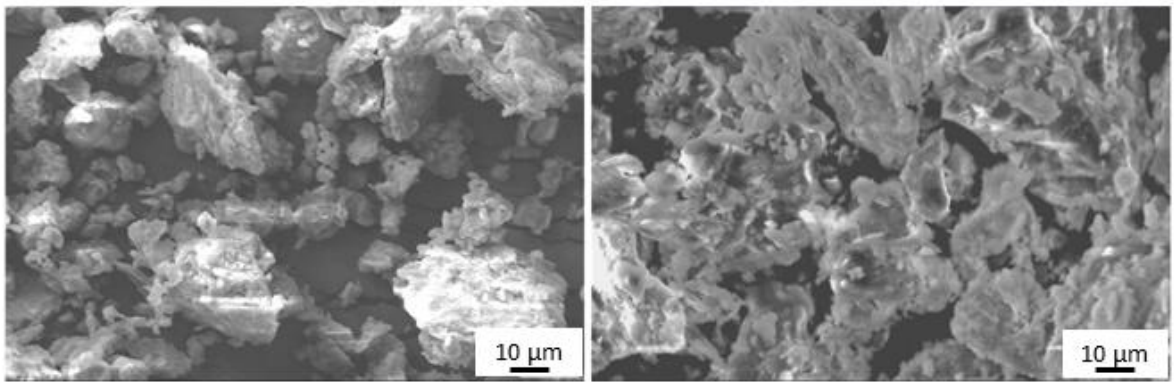

a) ***b)***

Fig. 2. SEM images of the initial (*a*) and mechanochemically modified (*b*) montmorillonites

Table 1

Chemical composition (wt. %) of the initial and mechanochemically modified montmorillonites

Element	O	Na	Mg	Al	Si	Fe	Zn	Ca	P
Initial montmorillonite	45.9	0.3	1.1	11.4	28.7	11.3	-	1.3	-
Mechanochemically modified montmorillonite	46.0	1.2	0.9	8.0	21.7	11.4	5.5	0.9	4.4

Figure 3 shows the polarization curves of the aluminium alloy after 48 hours of exposure to an acid rain environment. Electrochemical parameters obtained by the Tafel method of extrapolation of polarization curves are shown in the Table 2. Zinc monophosphate does not improve corrosion resistance due to the reduction of the environment's pH to 3.1, which promotes the dissolution of the aluminium matrix. Mechanochemically modified montmorillonite reduces the corrosion current density of the aluminium alloy by a factor of ~25 compared to the acid rain environment without it after 48 hours of exposure (Table 2), and the inhibitory effectiveness is ~96%. The protective effect of mechanochemically modified montmorillonite lies in the formation of insoluble $Zn(OH)_2$ hydroxides at the cathodic sites and aluminium phosphates at the anodic sites of the aluminium alloy. A similar inhibitory mechanism is described in [13], where the inhibitory effect of mechanochemically modified zeolite with zinc monophosphate at a 1:1 component ratio on an aluminium alloy in a chloride solution was investigated. It was found that the synthesised anti-corrosion pigment reduces the corrosion rate of the aluminium alloy in a 0.1% NaCl solution, with an inhibitory effectiveness of 83%.

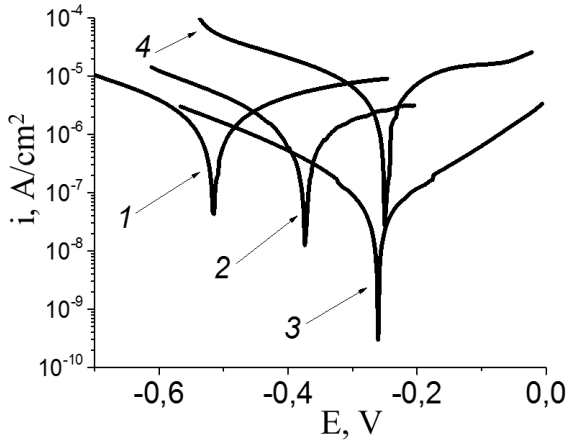

Fig. 3. Polarization curves of the aluminium alloy after48 hours of exposure in an acid rain environment: 1 – without montmorillonite; 2 – with the initial montmorillonite; 3 – with the mechanochemically modified montmorillonite; 4 – with zinc monophosphate

Table 2

Electrochemical characteristics of the aluminium alloy after48 hours of exposure in an acid rain environment

Environment	E_{cor}, V	i_{cor}, A/cm^2
Acid rain environment	-0.51	$9.7 \cdot 10^{-7}$
Acid rain environment + the initial montmorillonite	-0.37	$6.2 \cdot 10^{-7}$
Acid rain environment + the mechanochemically modified montmorillonite	-0.26	$3.9 \cdot 10^{-8}$
Acid rain environment + zinc monophosphate	-0.25	$3.4 \cdot 10^{-6}$

The results of the polarisation and EIS studies correlate with one another (Figs. 4 and 5, Table 3). The pigment based on montmorillonite, mechanochemically modified with zinc monophosphate, increases the charge transfer resistance of the aluminium alloy compared to samples exposed to an acid rain environment and when adding either the initial montmorillonite or zinc monophosphate. The inhibitory effectiveness, as determined by EIS results, is 94.5%. On the Bode diagram corresponding to the aluminium alloy in an acid rain solution without pigment, a peak is present in the low-frequency region, indicating the occurrence of electrochemical reactions resulting in the formation of corrosion products on the surface. The formation of a high-frequency peak following exposure when using mechanochemically modified montmorillonite indicates the formation of a protective film. The Bode plot of the aluminium alloy in an acid rain solution containing zinc monophosphate has a peak with an intensity reaching up to 60°, indicating the formation of a film on the surface; however, due to the acidic environment (pH=3.1) caused by zinc monophosphate, which promotes the dissolution of aluminium, it contains corrosion products.

The Nyquist diagrams are semicircular in shape, indicating that the rate of the electrochemical process is determined by the charge transfer stage. The diameter of these semicircles depends on the presence of modified montmorillonite, which also indicates the formation of a protective film that helps inhibit corrosion.

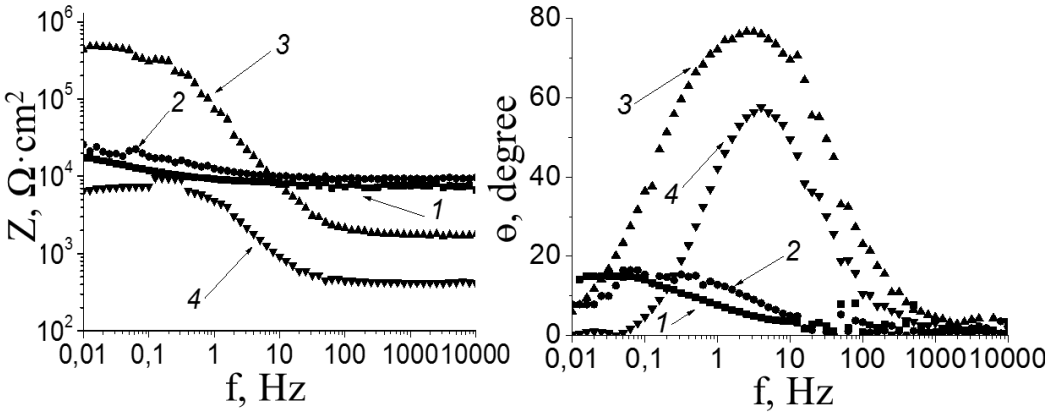

Fig. 4. Bode diagrams of the aluminium alloy after48 hours of exposure in an acid rain environment: 1 – without montmorillonite; 2 – with the initial montmorillonite; 3 – with the mechanochemically modified montmorillonite; 4 – with zinc monophosphate

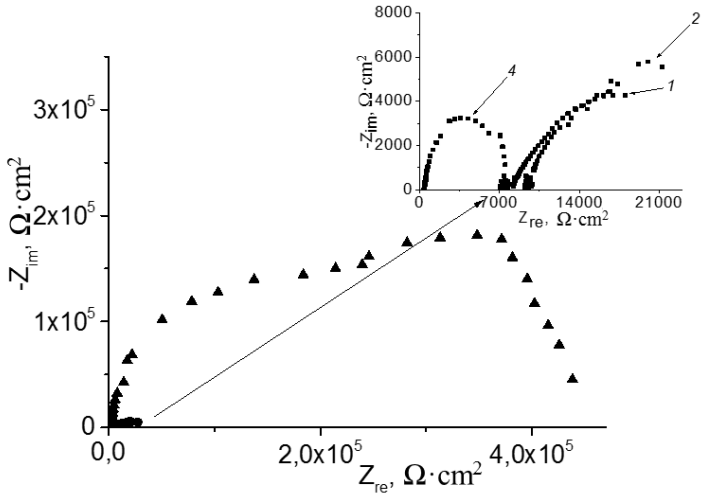

Fig. 5. Nyquist diagrams of the aluminium alloy after48 hours of exposure in an acid rain environment: 1 – without montmorillonite; 2 – with the initial montmorillonite; 3 – with the mechanochemically modified montmorillonite; 4 – with zinc monophosphate

Table 3

EIS characteristics of the aluminium alloy after48 hours of exposure in an acid rain environment

Environment	R_s, Ohm	R_f, Ohm ·cm^2	CPE_f, s^n/ Ohm ·cm^2	R_{ct}, Ohm ·cm^2	CPE_{ct}, s^n/ Ohm ·cm^2
Acid rain environment	6997	890	$1.93\cdot10^{-6}$	23096	$2.22\cdot10^{-4}$
Acid rain environment + the initial montmorillonite	9379	2600	$7.22\cdot10^{-5}$	26000	$1.50\cdot10^{-5}$
Acid rain environment + the mechanochemically modified montmorillonite	1722	2507	$2.40\cdot10^{-6}$	420500	$2.54\cdot10^{-7}$
Acid rain environment + zinc monophosphate	424	1611	$2.17\cdot10^{-5}$	5300	$7.68\cdot10^{-6}$

Conclusions

The use of a pigment based on mechanochemically modified montmorillonite enhances the corrosion resistance of the aluminium alloy in an acid rain environment. The inhibitory effect of mechanochemically modified montmorillonite based on the release of Zn^{2+} cations from montmorillonite containers, which, interacting with OH^- anions, form zinc hydroxides at the cathodic sites, and the slowing down of electrochemical corrosion occurs due to the formation of phosphates at the anodic regions of the aluminium alloy.

According to electrochemical studies, the degree of protection of the aluminium alloy in an acid rain environment with mechanochemically modified montmorillonite is over 90%. Thus, montmorillonite – a naturally occurring aluminosilicate mineral – is a promising material for the production of new, environmentally friendly anti-corrosion pigments in paint and varnish coatings to ensure long-term protection of metal products.

Acknowledgements

The authors gratefully acknowledge the financial support for this work from grant "Development of anti-corrosion pigments based on natural aluminosilicate mineral with laminar structure for polymer coatings on aluminium alloys" (Project of the National Research Foundation of Ukraine No. 2025.05/0001)

References

1. Lyon S.B. Advances in corrosion protection by organic coatings: What we know and what we would like to know / S.B. Lyon, R. Bingham, D.J. Mills // Prog. Org. Coat. – 2017. – Vol. 102. – P. 2–7. – DOI: https://doi.org/10.1016/j.porgcoat.2016.04.030

2. Sorensen P.A. Anticorrosive coatings: A review / P.A. Sorensen, S. Kill, K. Dam-Johansen, C.E. Weinell // J. Coat. Tenchnol. Res. – 2009. – Vol. 6. – P. 135–176. – DOI: https://doi.org/10.1007/s11998-008-9144-2

3. Vander Kloet J. The role of chromate in filiform corrosion inhibition / J. Vander Kloet, W. Schmidt, A.W. Hassel, M. Stratmann // Electrochim. Acta. – 2003. – Vol. 48. – P. 1211–1222. – DOI: https://doi.org/10.1016/S0013-4686(03)00256-1

4. Henriques R. R. Sepiolite modified with phosphonium ionic liquids as anticorrosive pigment for epoxy coatings / R. R. Henriques, B. G. Soares // Appl. Clay Sci. – 2021. – Vol. 200. – P. 105890. – DOI: https://doi.org/10.1016/j.clay.2020.105890

5. Khan A. Hybrid Halloysite Nanotubes as Smart Carriers for Corrosion Protection / A. Khan, A. Hassanein, S. Habib, M. Nawaz, R. A. Shakoor, R. Kahraman // ACS Appl. Mater. Interfaces. – 2020. – Vol. 12(33). – P. 37571–37584. – DOI: https://doi.org/10.1021/acsami.0c08953

6. Williams G. Inhibition of corrosion-driven organic coating disbondment on galvanised steel by smart release group II and Zn(II)-exchanged bentonite pigments / G. Williams, H.N. McMurray, M.J. Loveridge // Electrochim.Acta. – 2010. – Vol. 55. – P. 1740–1748. – DOI: https://doi.org/10.1016/j.electacta.2009.10.059

7. Dantas de Mendonça y Araújo S. E. Bentonite Clay and its Potential Applications / S. E. Dantas de Mendonça y Araújo, A. L. Roberto, J.E. Pereira Farias, J. A. Oshiro Junior // MRF. – 2025. – Vol. 173. – P. 124–144. – DOI: https://doi.org/10.21741/9781644903452-5

8. Williams G. Smart release corrosion inhibitor pigments based on organic ion-exchange resins / G. Williams, S. Geary, H.N. McMurray // Corros. Sci. – 2012. – Vol. 57. – P. 139–147. – DOI: https://doi.org/10.1016/j.corsci.2011.12.024

9. Egloffstein Th. A. Natural bentonites - influence of the ion exchange and partial desiccation on permeability and self-healing capacity of bentonites used in GCLs / Th. A. Egloffstein // Geotext. Geomembr. – 2001. – Vol. 19. P. 427–444. – DOI: https://doi.org/10.1016/S0266-1144(01)00017-6

10. Zhou X. Smart corrosion inhibitors for controlled release: A review / X. Zhou, Q. Dong, D. Wei, J. Bai, F. Xue, B. Zhang, Zh. Ba, Zh. Wang // Corros. Eng. Sci. Technol. – 2023. – Vol. 58(2). P. 190–204. – DOI: 10.1080/1478422X.2022.2161122

11. Korniy S.A. Influence of a phosphate–nitrate composition on the corrosion of mechanically activated aluminum alloy / S.A. Korniy, I.M. Zin, O.P. Khlopyk, M.B. Tymus, M. Ya. Holovchuk // Mater. Sci. – 2022. – Vol. 57. P. 284–290. – DOI: 10.1007/s11003-021-00543-0

12. Shukla S. K., Quraishi M. A., Ebenso E. E. Adsorption and corrosion inhibition properties of cefadroxil on mild steel in hydrochloric acid // International Journal of Electrochemical Science. – 2011. – 6. – P. 2912–2931. – DOI: https://doi.org/10.1016/S1452-3981(23)18228-9

13. Korniy S. Aluminium alloy corrosion inhibition by composite pigment based on nanoporous synthetic zeolite and zinc dihydrogen phosphate / S. Korniy, I. Zin, M. O. Danyliak, O. Khlopyk, B. Datsko, M. Holovchuk // Appl. Nanosci. – 2023. – Vol. 13. P. 7257–7266. – DOI: https://doi.org/10.1007/s13204-023-02888-1

Даниляк М.-О.М., Корній С.А. Новий протикорозійний пігмент на основі природного алюмосилікату шаруватої структури

Екологічно безпечний протикорозійний пігмент на основі природного іонообмінного мінералу монтморилоніту шаруватої структури отримано механохімічною модифікацією. Показано, що при модифікації цинк монофосфатом монтморилоніт збагачується катіонами цинку та фосфат аніонами. За результатами скануючої електронної мікроскопії показано, що частинки монтморилоніту мають вигляд вигнутих пластинок, що схильні до агломерації. За допомогою EDX-аналізу встановлено, що вихідний монтморилоніт є формою Ca, Mg монтморилоніту. Показано, що внаслідок механохімічної модифікації монтморилоніту відбувається інтеркаляція катіонів Zn^{2+} у шарувату структуру природного монтморилоніту, а аніони фосфату утворюють поверхневі адсорбційні комплекси з позитивно зарядженими крайовими поверхнями монтморилоніту через кисле середовище кристалічного гідрату солі $Zn(H_2PO_4)_2 \cdot 2H_2O$, при цьому вміст цинку та фосфору становить ~5мас. % та ~4 мас. % відповідно. За допомогою потенціодинамічної поляризації та електрохімічної імпедансної спектроскопії встановлено, що отриманий пігмент на основі механохімічно модифікованого монтморилоніту підвищує корозійну стійкість алюмінієвого сплаву в умовах кислотного дощу з pH = 4,5. Інгібуючий ефект механохімічно модифікованого монтморилоніту полягає у вивільненні катіонів Zn^{2+} з контейнерів монтморилоніту, які, взаємодіючи з аніонами OH^-, утворюють гідроксиди цинку в катодних ділянках, а уповільнення електрохімічної корозії відбувається завдяки утворенню фосфатів в анодних ділянках алюмінієвого сплаву. Встановлено, що ступінь захисту алюмінієвого сплаву в середовищі кислотного дощу за допомогою механохімічно модифікованого монтморилоніту перевищував 90 %. Таким чином, монтморилоніт, алюмосилікатний мінерал природного походження, є перспективним матеріалом для отримання нових екологічно безпечних протикорозійних пігментів у лакофарбових покриттях з метою забезпечення довготривалого захисту металевих виробів.

Ключові слова: корозія, монтморилоніт, іонообмінні мінерали, глина, протикорозійний пігмент, алюмінієвий сплав

ISSN 2079-1372 Problems of Tribology, V. 31, No 2/120-2026, 66-75

Problems of Tribology
Website: http://tribology.khnu.km.ua/index.php/ProbTrib
E-mail: tribosenator@gmail.com

DOI: https://doi.org/10.31891/2079-1372-2026-120-2-66-75

Hardening protective coatings on niobium alloys, their thermal-cyclic creep and long-term strength

L. Lopata[*1] 0000-0002-2053-9252, **A. Lopata**[1] 0000-0001-5266-6486, **I. Kachynska**[1] 0009-0006-7623-2897, **I. Rybak**[2] 0000-0002-2071-5754, **A. Solovykh**[3] 0000-0002-2071-5754, **S. Katerinich**[3] 0000-0003-3052-0747

[*1]*G. S. Pisarenko Institute for Problems of Strength of National Academy of Sciences of Ukraine*
[2]*National Transport University*
[3]*Central Ukrainian National Technical University*
**E-mail:beryuza@ukr.net*

Received: 20 April 2026: Revised 30 April 2026: Accept: 18 May 2026

Abstract

A solution to the problem of protecting niobium from high-temperature, highly intensive oxidation is considered. The isothermal and thermocyclic creep and long-term strength characteristics of a niobium alloy with three coating variants are determined at temperatures of 1400–250°C in air. A test methodology for niobium alloys with coatings under simultaneous loads, high temperatures, abrupt thermal cycles, and an oxidizing environment with radiant heating and non-contact cooling by focusing radiant energy is presented, ensuring reliable determination of mechanical properties. A comparison of ultimate strains, creep rates, and durability under isothermal and thermocyclic conditions for the three coating variants is conducted, demonstrating the advantage of a combined plasma-diffusion coating over silicide and borosilicide coatings. Differences in creep and long-term strength characteristics of the three coating variants are demonstrated, which are explained by the nature of crack development in the coating. The transition from single "sharp" cracks in the coating to regular cracks in the diffusion sublayer with rounded tops ensures an increase in the strength and durability of the niobium alloy.

Keywords: strengthening protective coatings, niobium alloys, thermocyclic creep, plasma diffusion coatings, long-term strength, durability.

Introduction

High heat resistance and moderate density, approximately equal to that of alloy steels, allow niobium alloys to be considered as a replacement for nickel superalloys in gas turbine construction. Niobium alloys also hold promise in power plants. However, the main obstacle to the introduction of niobium alloys remains the problem of their interaction with active gases and high-purity coolants. For example, the oxidation rate of niobium in air at 1100ºC is 300–350 g/h m^2 [1]. Attempts to address the problem of niobium protection are being made by using special heat-resistant alloys with higher resistance to corrosion. Alloying niobium with various additives reduces its oxidation rate in air at 1100ºC to 40–1250 g/h m^2 (however, this level of oxidation intensity is well above permissible limits) [1]. Therefore, the main direction for ensuring high resistance to corrosion destruction of niobium alloys is the use of protective coatings.

Literature review

The development of coatings on niobium alloys has been the subject of considerable research [1-6]. Almost all surface hardening technologies have been tried to strengthen niobium alloys. Traditional galvanic technology was used to apply a Ni coating [1, 6]. However, the solubility of hydrogen in niobium, which dramatically reduces its ductility, hinders the use of galvanic coatings. The aim of the work was to develop a new combined method of surface engineering for the formation of hardening protective coatings on the basis of combination of EAS followed by treatment with PIN.

The most widely used methods of chemical-thermal treatment of niobium alloys are: traditional calorizing, siliconizing, and boriding [7]. Diffusion silicide coatings on niobium alloys exhibit high heat resistance. However,

the service life of such coatings and the maximum operating temperatures, especially during thermal cycling, are insufficient. In order to increase the heat resistance and improve the thermal fatigue characteristics of niobium, diffusion coatings based on the Ti-Si system have been developed It has been established that the activities of Ti and Si in the saturating mixture are the main controlling factors for the creation of coatings with high heat resistance. Coatings of optimal composition on niobium have made it possible to increase the temperature limit of its heat resistance to 2000ºC [1, 2, 6].

In the practice of modifying silicide coatings on niobium, numerous combinations have been studied. Two-layer coatings had different phase compositions: the inner layer was $NbSi_2$, while the outer layer consisted of ternary compounds Nb-Al-Si [3, 8]. In order to improve heat resistance, the possibility of increasing the Cr and Ti content in the silicide coating on Nb alloys by sequentially applying diffusion sublayers by immersion in molten salt was studied. The effect of copper on the borosilicate of niobium, as well as the effect of copper and sulfur, was studied. A positive effect was ensured by the combined diffusion saturation of niobium with titanium and zirconium. The thermal fatigue characteristics of niobium are improved by siliconizing in a $TiSi_2$ mixture [7].

The best results to date in protecting niobium alloys are worth noting – the developed method of vacuum activated diffusion saturation. This method enables the deposition of a coating on niobium when Mo, Ti, Cr, Ni, Al, Si, and B are present in the reaction zone. In industrial practice, coating of niobium alloys in liquid metal melts has found application . Low-melting metals with alloying elements are used as transport melts. The feasibility of using an Al-based transport melt with alloying additives of Si, Cr, Mo, Ti, Y, Ni, Zn, and Sn has been confirmed [2, 5].

Gas nitriding is used among the methods of chemical-thermal treatment for surface hardening of niobium alloys. The effect of alloying elements on the nitridability of niobium has been studied. It has been established that a nitride of the NbN type forms on the surface of nitrided Nb alloys. A series of studies on the effect of nitrogen-containing environments on niobium should be noted. A coating was applied to niobium from the gas and solid phases. Ammonia served as the gas phase, and powders containing Si and Al served as the solid phase. This treatment made it possible to obtain complex multilayer coatings. The effect of preliminary plastic deformation on the nitriding kinetics of niobium alloys was studied. The degree of compression was 25...90% [9, 10].

A trend toward transitioning from gas nitriding to glow discharge ion nitriding is also observed in the strengthening of niobium alloys. Ion nitriding temperature is 1000°C, duration is up to 5 hours, and gas pressure is 4–13 mmHg [10]. Thermocyclic ion nitriding technology offers new opportunities for strengthening niobium alloys. This technology is characterized by the fact that the thermal cycling mode creates thermal stresses in the surface layer, which accelerate diffusion. Cyclic glow discharge heating provides the required temperature only in the surface layer of the component without heating the core. The effect of anomalous mass transfer under the influence of thermal stresses accelerates nitrogen diffusion by a factor of 3. Thermal cycling, with heating only the surface layer, reduces energy consumption by up to 10 times compared to the classic isothermal mode [9].

Glow discharge processing is also used for siliconizing niobium. Coatings on niobium obtained by diffusion siliconizing of sintered Mo-(0.5...1.5) Pd layers exhibit heat and thermal stability up to 1900°C [11]. Traditional enameling and slip-diffusion coatings are used to protect niobium alloys. In the literature, this technology is referred to as the fusion deposition method [1, 5]. Powders of the Si-20Cr-5Ti and Si-20Cr-20Fe systems are used in a varnish base with vacuum firing at 1370°C. The powders were applied using electrophoresis. The high performance of slip coatings is noted. The $MoSi_2$-based coating operates at 1400°C in air for 300 hours, while the Si-Cr-Fe coating operated at 1550°C for 4 hours and withstood 553 thermal cycles.

Thermal plasma spraying is used to protect niobium alloys [1, 12]. Spark plasma sintering is also an option for protecting niobium. Work on protecting niobium alloys by vapor-phase deposition (PVD) has been reported. Complex silicide coatings of the $NbSi_2$-$MoSi_2$ type were deposited using vacuum plasma deposition. The presence of a droplet phase, which leads to coating defects, limits the use of PVD methods for protecting niobium. The potential of laser technology for coating niobium has been investigated. Laser technology has been used to deposit metallic sublayers for silicide coatings. The niobium surface is alloyed with tungsten using laser pulses [1].

A number of shortcomings hinder the widespread use of protective coatings. To overcome these, a trend has emerged toward the development of multi-stage technologies. This trend has also emerged in the hardening of niobium alloys. The primary objective is to protect niobium from high-temperature, highly intensive oxidation. Therefore, the effectiveness of heat-resistant coatings on niobium is also determined by their durability at normal temperatures, eliminating oxygen saturation [1, 3, 11]. The thermal stability of niobium coatings was assessed by changing the coating structure and composition [4]. Considerable attention has been devoted to determining the elastic constants of niobium coatings. The high damping properties of niobium coatings, which are provided by the porous structure of the coating, are noted [8, 12, 13].

A significant drawback of protective coatings is the reduced strength and ductility of the base material [1]. This drawback is also inherent in coated niobium alloys. Despite a large number of studies, there is no clarity on this issue. Difficulties in explaining these discrepancies are caused by differences in coating application and testing methods. The wide range of base and coating material combinations and the variety of application technologies prevent comparison of a range of results and the drawing of general conclusions. In the practice of protective coatings, one must accept the phenomenon of a decrease in the initial strength and ductility, at least for the sake of maintaining heat resistance in an oxidizing environment.

For niobium alloys, a coating-induced reduction in mechanical properties was observed both at room temperature and at 1100°C. The coating reduced the strength characteristics of the Nb alloy by 10–40% across virtually the entire temperature range studied. Furthermore, the plastic properties of the composite were 1.5–4 times lower than those of the base [14-16]. In tensile tests of the Nb alloy, embrittlement with a simultaneous reduction in tensile
strength was observed in the temperature range of 500–700°C, which is associated with surface gas saturation. Silicide coatings protect the Nb alloy from brittle fracture, although they reduce the original mechanical properties [4, 5, and 7. 11. 12].

A number of positive effects have been noted during nitriding of niobium alloys. The elastic modulus E of a nitrided niobium alloy increases with both temperature and nitriding time. The elastic limit increases by 3-5 times with increasing nitriding time. With increasing nitriding temperature, the ultimate tensile strength monotonically increases by 1.5-2.0 times, while the relative elongation monotonically decreases when tested at room temperature. Increasing the nitriding temperature from 1100 to 1500°C with a 1-hour hold increases the hardness of niobium alloys from 1400 to 2000 kg/mm2. The ultimate tensile strength of pure niobium increases by 25-30% at 800°C and has virtually no effect on heat resistance at 1000°C. For the VN-3 alloy, creep and long-term strength tests at 900...1400ºC showed an increase in the time to failure and an improvement in creep resistance characteristics by 1.3...2.5 times, which do not lead to a decrease in ductility [6, 9, 10].

The increased heat resistance of niobium alloys is attributed to the stabilization of processes occurring within and along grain boundaries due to the precipitation of dispersed nitride particles [1]. This increased heat resistance is due to coherent dispersed nitride phases precipitating within the grains and along their boundaries, as well as in the form of individual chains along block boundaries. A significant drawback of nitriding niobium alloys is the increased brittleness of diffusion layers [2]. One cause of the brittleness of nitrided Nb alloys may be treatment with ammonia.

The range of experimental methods for testing coatings on niobium alloys is quite broad – from nano- and microindentation to multiparameter bench testing [17]. It should be noted that the state of experimental methods for determining coating properties is characterized by a wide variety and variability in testing methods, specimen shapes and sizes, testing regimes, and heating and cooling methods. Therefore, it is impossible to compare the results of individual studies. The results of coating property determination are also incomparable due to differences in coating design, the thickness ratios of the various layers, application technologies, and surface preparation methods prior to coating application. A brief review and analysis of the studies demonstrates the relevance of developing protective coatings on niobium alloys. However, the growing number of studies and publications does not provide any clarity in addressing this complex issue.

The aim of the work is to determine the thermocyclic creep and long-term strength of a niobium alloy with a two-layer combined coating at temperatures of 1400 ºC in air, compare these characteristics with two technologies of diffusion silicide coatings and establish differences in the destruction of these coatings during creep.

Research Methodology

A method for accelerated testing of materials with heat-resistant coatings in air under thermal-cyclic creep conditions was used. This method is standardized in Ukraine [2, 18]. The main damaging factor is abrupt cyclic thermal changes. Continuous recording of the creep curve characterizes all changes in the coating and in the adhesive contact zone with the substrate, right up to specimen failure. The trend in the development of high-temperature testing is toward a transition from isothermal to thermocyclic modes. During thermocyclic testing, the oxidation rate in air is significantly higher than during isothermal testing [2, 18]. This circumstance allows for a reduction in test duration and serves as the basis for the development of accelerated coating testing methods. A leading trend in coating testing is the application of thermomechanical fatigue methods (TMF) [2, 18]. This new technique simulates the simultaneous action of operational factors: mechanical load, high temperatures, abrupt thermal changes, and an oxidizing environment. The non-additivity of the softening effect requires testing under the simultaneous action of operational factors. Only in this way can the most reliable information about the properties of coatings be obtained. The technique is implemented in the Nutcracker laboratory setup [2, 18]. A distinctive feature of the setup is heating and cooling the sample by focusing radiant energy in an optimized closed cavity with cold mirror walls. Radiant heating, in contrast to heating methods by directly passing an electric current through the sample and heating with high-frequency currents (HFC), eliminates the effects of electroplastic and magnetoplastic effects. These effects lead to errors of tens of percent when determining strength and ductility. Accelerated cooling of the sample is achieved by focusing its own thermal radiation on an absorber [18]. The advantage of cooling by focusing its own radiation is the absence of direct contact between the sample and the cooling medium, which ensures uniform cooling along the perimeter and height of the sample, and also increases the cooling rate due to the absence of film and nucleate boiling. Contactless cooling completely eliminates the erosive, corrosive and adsorption effects of the cooling medium.

he cool mirror walls of the optical chamber ensure minimal thermal inertia. This enables high heating and cooling rates. A distinctive feature of the setup is the ability to continuously visually monitor the specimen's

condition during testing. Illuminated by radiant energy, the specimen is conveniently viewed through a hole in the mirror wall of the optical device. Photographing the specimen during testing provides data on its deformation, the occurrence of defects and cracks on the surface, their sizes, and the distances between them. Photography records the moments of crack initiation in the coating and its delamination. Taken together, such photography provides an understanding of the specimen's deformation kinetics up to its failure. A prerequisite for the normal operation of parts made of niobium alloys is to ensure a minimum level of plastic deformation, as well as a minimum rate of its accumulation. Therefore, the characteristics of isothermal and thermocyclic creep during tension of sheet niobium alloy specimens with a thickness of 1-2 mm were adopted as criteria. A creep curve or short-term tensile stress diagram was constructed as a result of the tests. A thermocyclic creep curve was constructed as an envelope of the maximum strain peaks per cycle. The creep curves were used to determine the relative strain at failure (ε_p) and the time to specimen failure (τ_p), as well as the minimum creep rate. The creep curve was also used to determine the strain when defects appeared in the coating. The temperature on the specimen was measured and controlled using a platinum-rhodium thermocouple (TPR-0.6). The temperature gradient along the length of the working section did not exceed 1%. The setup was equipped with a computer system for monitoring and recording the parameters [18]. Three coating variants were tested:

I – silicide composition Si-Fe-Cr-Ti, using the slip method;

II – borosilicide composition Si-B-Ti, using the slip method;

III – a complex coating with a plasma-spun molybdenum disilicide ($MoSi_2$) sublayer with an outer surface layer obtained by diffusion saturation with elements, the main ones being silicon and boron.

Diffusion saturation of all three variants was carried out in a vacuum. To study the effect of stress level during creep, tests were conducted in the stress range of 40–70 MPa. This made it possible to plot long-term tensile strength curves, the dependence of the minimum creep rate on stress, as well as creep limits and long-term tensile strength. The
test temperature conditions are listed in Table 1.

Table 1

Characteristics of temperature test conditions

Mode No	Type of regime	T_{max},ºC	T_{min},ºC	Heating time, s	Cooling time, s
1	Isothermal	1400	–	–	–
2	Thermocycling	1400	650	14	14
3	Thermocycling	1400	250	60	60
4	Thermocycling	1400	250	20	60

At least 3-5 specimens were tested under each loading regime. Mathematical processing of the experimental data was performed using standard mathematical statistics methods.

Research Results. Creep Characteristics Study

In analyzing the isothermal and thermocyclic creep results, primary attention was paid to the plasma-diffusion coating (III). Results for the slip-fired diffusion coatings (I and II) will be presented in the comparative analysis of coating damage. Plasma-diffusion coating was used to form a multilayer coating on the surface of a niobium alloy. The plasma-sprayed molybdenum silicide layer exhibits significant thickness variation (h = 100...350 μm, $H_{\mu}^{20} = 6880$ MPa). The functional dependence of adhesion strength, residual stresses, and critical deformation of the substrate on the coating thickness was demonstrated in [2, 18]. Variation in the thickness of silicide coatings on niobium alloys was noted [2, 6]. The dependence of durability on coating thickness on a niobium alloy is extreme. Therefore, more attention should be paid to coating thickness and its optimization, with separate studies being conducted. Figure 1 shows the average creep curves for isothermal (1) and thermocyclic (3) testing modes.

It is noteworthy that the formation of visible cracks on the coating surface (marked with crosses in Fig. 2) occurs long before complete failure of the specimens. More than 70% of the composite's service life is accounted for by the service life with cracks in the coating. Moreover, the appearance of cracks on the coating surface has virtually no effect on the specimen's creep behavior (after cracking, the steady-state creep rate remains unchanged). An important feature of this composite is the higher service life of specimens tested under thermal cycling conditions (3) than under isothermal conditions (1) at stresses above 45 MPa. This is also indicated by the relative positions of the long-term tensile strength (Fig. 2) and creep rate (Fig. 3) curves for specimens with plasma-diffusion coating.

As Figures 1–3 show, with test durations of less than 600–800 minutes (the number of thermal cycles before failure does not exceed 400), the weakening effect of thermal fatigue phenomena does not have time to fully manifest itself. At the same time, the average temperature during isothermal creep is higher than during thermal

cycling, which explains the lower durability of the composite in this case. With a larger test duration (loads less than 40 MPa), thermal fatigue phenomena begin to dominate the overall damage accumulation in the composite, and the durability during thermal cycling creep becomes lower than that during isothermal creep.

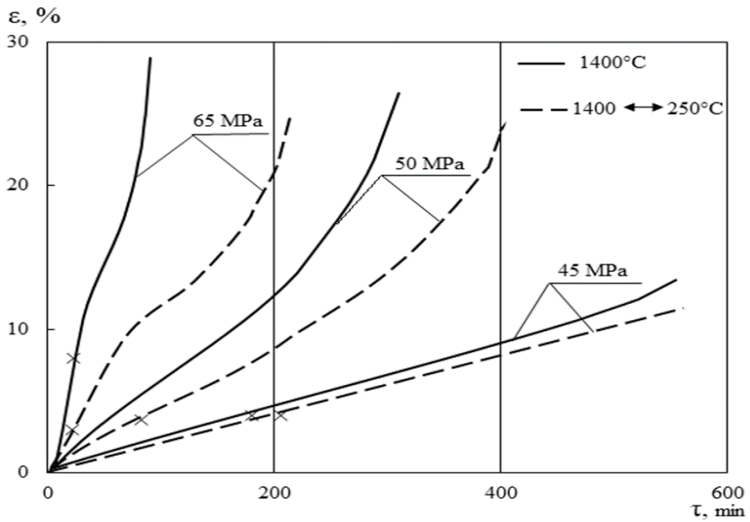

Fig.`1. Averaged creep curves of a niobium alloy with a plasma-diffusion coating for various test conditions

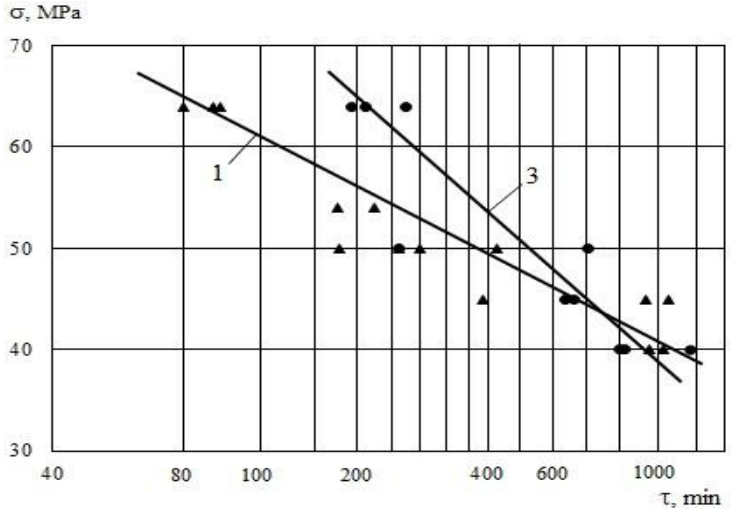

Fig. 2. Durability curves of a niobium alloy with a plasma-diffusion coating for isothermal (1) and thermocyclic (3) loading modes

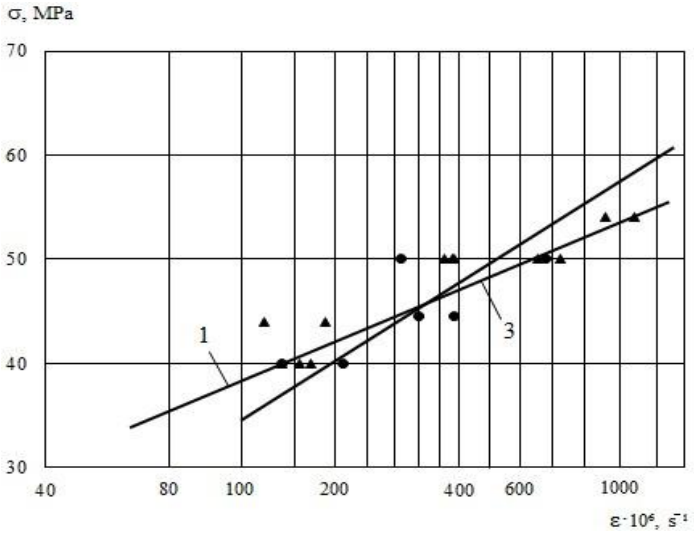

Fig. 3. Minimum creep rate as a function of stress for a niobium alloy with a plasma-diffusion coating under isothermal (1) and thermal cycling (3) testing conditions

The nature of damage and failure of the composite. The study of the composite included observation of the specimen surface during testing. Initially, a network of cracks appears on the specimen surface. Subsequently, almost all of the cracks begin to open, indicating a uniform distribution of deformations along the length of the specimen's working section. Droplets of low-melting compounds appear on the coating surface. As the third stage of creep approaches, when crack opening becomes quite large, the incipient boiling of these melts becomes clearly visible at the crack mouths. The distributed compounds fill almost all cracks completely, preventing the penetration of the aggressive gas environment deep into the coating. Furthermore, this melt possesses healing properties, inhibiting crack opening. In this case, at elevated temperatures, the multifunctional capabilities of the plastic melt are evident – inhibiting both corrosive and mechanical failure. Analysis of the deformation kinetics of the composite during a single heating cycle allowed us to conclude that this phenomenon is most pronounced during thermal-cyclic creep.

It was observed that the compounds filling the cracks melt at temperatures above 1300 ºC. At lower temperatures during thermal cycling, these compounds crystallize, resisting crack opening. Minor changes in the failure mode of the plasma-diffusion coating (III) were detected when comparing the creep of the specimens under different loading conditions. The first visible cracks on the coating surface under the thermal cycling test mode (3) appear at relative creep strain levels of 4...5%, while under the isothermal mode (1) – at 5...7%. This difference is apparently explained by a change in the coating plasticity depending on temperature (under the thermal cycling mode, the average temperature is lower than under the isothermal mode). At the same time, no change in the density of cracks appearing in the coating was detected. Figures 4 and 5 present the probability curves of the crack pitch arising in the coating on the specimen surface after isothermal and thermal cycling tests, respectively. As can be seen from the figures, this parameter, at a 50% probability level, ranges from 0.75 to 0.95 mm. The slight slope of the probability curves indicates a small spread in crack pitch values along the length of the specimens.

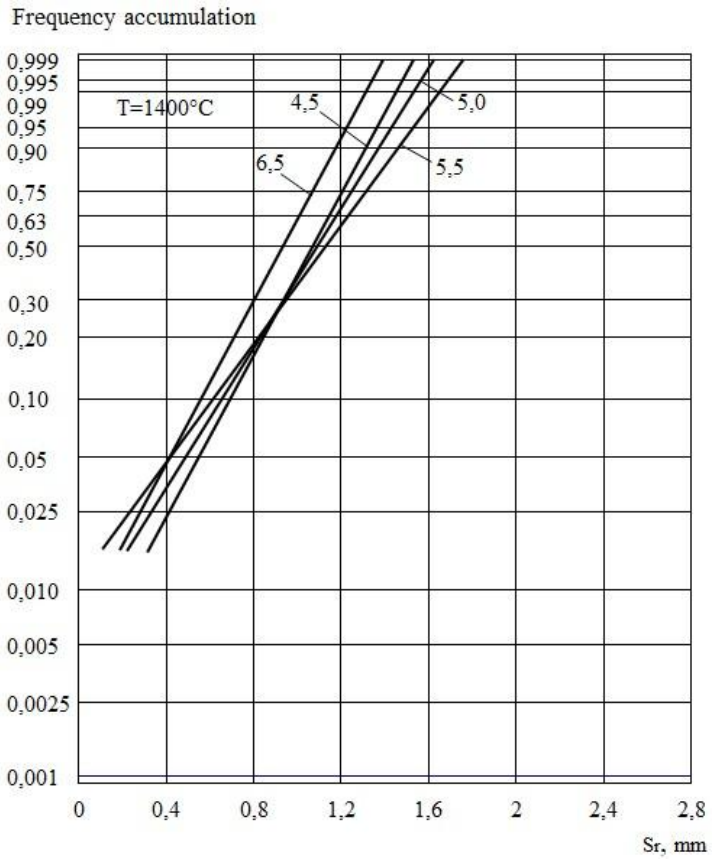

Fig. 4. Probability curves of crack pitch distribution in a plasma-diffusion coating (III) formed during isothermal creep

Post-test microstructural studies of plasma-diffusion-coated specimens revealed that cracks in the coating initiate during creep, primarily at the interface between the plasma and diffusion layers of the coating.

These cracks originate from individual discontinuities in the diffusion layer in the as-received condition. Crack propagation occurs within the diffusion layer of the coating. Crack growth is inhibited by the rounded nature of the pores and the increased plasticity of this layer. Crack growth deeper into the specimen is typically inhibited by the sublayer.

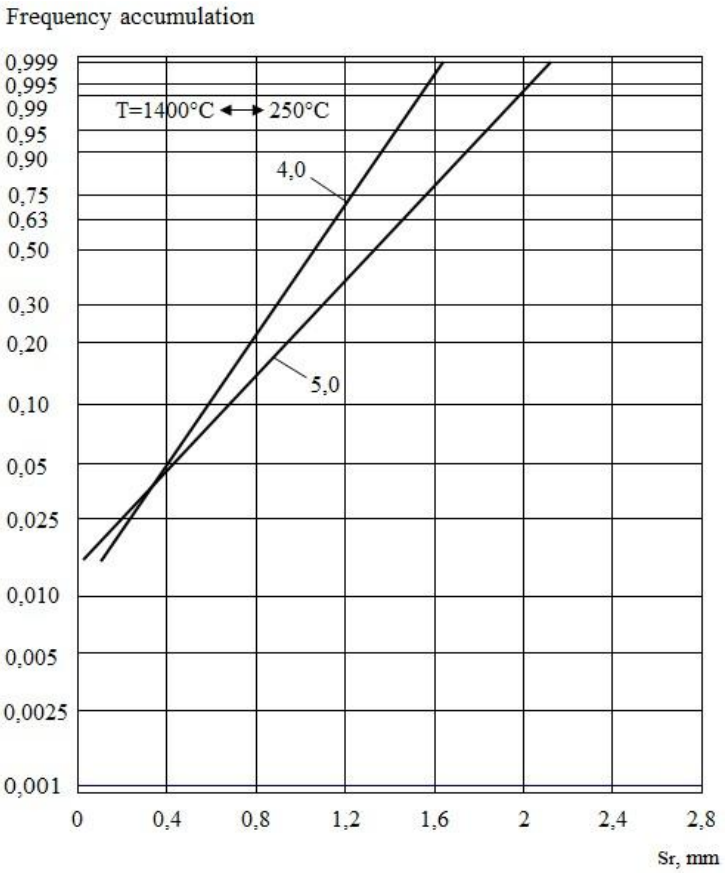

Fig. 5. Probability curves of the distribution of the crack pitch in the plasma-diffusion coating (III), formed during thermocyclic creep at different loading levels

It has been observed that atmospheric oxygen penetrates through cracks that have reached the coating surface, causing preferential oxidation of the diffusion silicide layer. This phenomenon is particularly characteristic of samples with significant durability. This effect almost always manifests itself at low loads and is often absent at stresses above 50 MPa. It can be assumed that this layer inhibits the progression of the oxidation process deeper into the substrate.

Comparison of Creep and Damage of Coatings. To highlight the specific features of the composition with the plasma-diffusion coating (III), the creep characteristics of this composition were compared with those obtained for compositions with other silicide coatings: I - (Si-Fe-Cr-Ti) and II - (Si-B-Ti). The comparison was conducted for isothermal (1) and thermocyclic (3) testing modes at a stress level of 50 MPa. Figures 6, 7, and 8 show the average characteristics of these compositions.

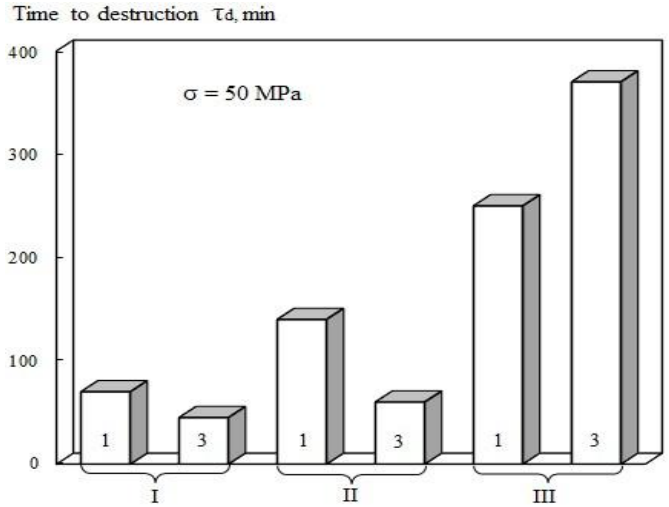

Fig. 6. Comparison of the durability of a niobium alloy with coatings: I – (Si-Fe-Cr-Ti); II – (Si-B-Ti); III – plasma-diffusion mm

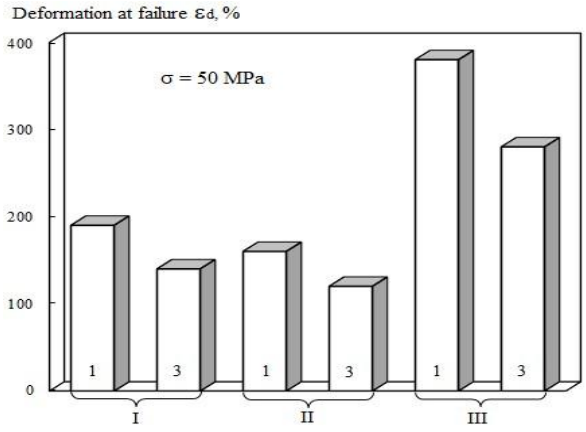

Fig. 7. Comparison of the durability of a niobium alloy with coatings: I – (Si-Fe-Cr-Ti); II – (Si-B-Ti); III – plasma-diffusion

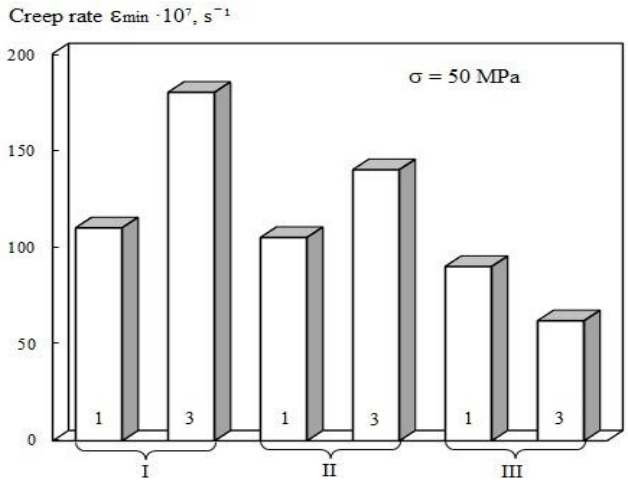

Fig. 8. Comparison of the durability of a niobium alloy with coatings: I – (Si-Fe-Cr-Ti); II – (Si-B-Ti); III – plasma-diffusion

Based on the comparison results, the following conclusions can be drawn: the performance characteristics of the plasma-diffusion coating (III) are significantly higher than those of the compared coatings. Particularly noteworthy is the significant increase in deformation at failure of the samples with the plasma-diffusion coating (III) compared to coatings (I) and (II) – by 1.7...1.75 and 1.9...2.0 times, respectively. Since the temperature processes of diffusion saturation during application of all three coating systems are virtually identical, it can be concluded that the plastic properties of the base material and the compositions under consideration are identical. Consequently, the overall increase in plasticity of the composition is due to the increased plasticity of the plasma-diffusion coating (III) itself compared to the other two coatings. Under a load of 50 MPa, the time to failure of the composite with plasma-diffusion coating (III) under thermal cycling testing is longer than under isothermal testing. This fundamentally distinguishes this composite from the comparable composites, for which thermal cycling testing resulted in a comparatively reduced durability. Cracks in plasma-diffusion coating (III) are uniformly distributed across the test section of the specimen, while the comparable coatings exhibited isolated cracks only in the fracture zone of the specimen. The significant softening effect of cracks in coatings (I) and (II) was also evident in the creep behavior of the compared composites. The appearance of cracks in these coatings resulted in rapid specimen failure (transition from creep to softening). However, cracks on the surface of plasma-diffusion coating (III) did not affect the creep behavior. As a result of the above-mentioned properties, the composition with the plasma-diffusion coating (III) has a durability that is 1.9 and 3.7 times higher under isothermal conditions and 6.8 and 8.5 times higher under thermal cycling conditions, respectively, than the niobium alloy with coatings (II) and (I).

Conclusions

The isothermal and thermocyclic creep behavior and long-term strength of a niobium alloy with three coating variants were investigated in air at temperatures of 1400–250°C. A testing methodology combining simultaneous mechanical loading, high temperatures, rapid thermal cycling, and an oxidizing environment with radiant heating and non-contact cooling enabled reliable determination of mechanical properties. Comparison of ultimate deformation, creep rate, and durability under isothermal and thermal cycling conditions demonstrated the superior performance of the combined plasma–diffusion coating over silicide and borosilicide coatings. Its

effectiveness is associated with higher coating ductility, the presence of thin barrier sublayers, a discontinuous structure, low-melting phases promoting defect healing, and improved corrosion and thermal fatigue resistance. As a result, the combined coating increased durability by 1.9–3.7 times under isothermal creep conditions in air (1400°C, 50 MPa) and by 6.8–8.5 times under thermal cycling creep conditions (1400–250°C, 50 MPa). The observed differences in creep resistance and long-term strength are also attributed to the crack propagation mechanism: the transition from isolated sharp coating cracks to regular cracks with rounded tips in the diffusion sublayer contributed to enhanced strength and service life of the niobium alloy.

References

1. Kharchenko S.D., Kovtun S.I. Heat-resistant coatings and prospects for their use to extend the service life of power equipment (review) Thermal Physics and Heat Power Engineering, 2021, vol. 43, no. 3. pp. 78-82. https://doi.org/10.31472/ttpe.3.2021.10

2. Babak V., Lyashenko B., Shchepetov V., Kharchenko S. Heat Protective Coatings on Niobium Alloys *Mech. Adv. Technol.* No. 3(90). 2020. P. 88–98. https://doi.org/10.20535/2521-1943.2020.0.219550

3. L. Xiao, X. Zhou, Y. Wang, R. Pu, G. Zhao, Z. Shen, and Y. Huang, S. Liu, Z. Cai, X. Zhao "Formation and oxidation behavior of Ce-modified MoSi2–NbSi2 coating on niobium alloy". *Corrosion Sci.* Vol. 173. P. 108751, 2020. doi: 10.1016/j.corsci.2020.108751.

4. B.A. Pinto, A. Sofia, and C.M. D'Oliveira, "Nb silicide coatings processed by double pack cementation: Formation mechanisms and stability", *Surf. Coat. Technol.* 409, 2021, doi: 10.1016/j. surfcoat. 2021.126913.

5. R. Szklarek, T. Tański, B. Mendala, M. Staszuk, Ł. Krzemiński, P. Nuckowski, and K. Sobczak High temperature resistance of silicide-coated niobium. *Bull. Pol. Acad. Sci. Tech. Sci.* 69(5) 2021, e137416. http://creativecommons.org/licenses/by/4.0/.

6. Babak V.P., Shchepetov V.V., Suprun T.T., Kharchenko O.V., Kharchenko S.D. Thermal barrier coatings on niobium-based alloys structural materials. *Mechanics and Advanced Technologies.* №2 (86), 2019. DOI: 10.20535/2521-1943.2019.86.189071

7. L. Portebois, S. Mathieu, Y. Bouizi, M. Vilasi, and S. Mathieu "Effect of boron addition on the oxidation resistance of silicide protective coatings: A focus on boron location in as-coated and oxidised coated niobium alloys", *Surf. Coat. Technol.*, vol. 253, pp. 292–299, 2014, doi: 10.1016/j.surfcoat.2014.05.058.

8. Y. Garip, "Production and microstructural characterization of NbSi based In-situ composite", *Bull. Pol. Acad. Sci. Arch. Metall. Mater.* Vol. 65, no. 2, pp. 917–921, 2020. Doi: 10.24425/ amm.2020.132839.

9. Patent No. 113934 of Ukraine. High-temperature wear-resistant material; C23C 4/067 / V.P. Babak, V.V. Shchepetov, M.S. Yakovleva // Pub. dated 27.03.2017; Bul. No. 6.

10. Babak V.P., Shchepetov V.V. Increased wear coatings due intrastructural stlf corrtction. *Journal of engineering sciences*, 2019. №2. P.11 – 15. doi: 10.21272/jes.2019.6(1).c3

11. J. Sun, Q.G. Fu, L.P. Guo, and L. Wang, "Silicide coating fabricated By HAPC/SAPS combination to protect niobium alloy from oxidation", *ACS Appl. Mater. Interfaces*, vol. 8, pp. 15838–15847, 2016, doi: 10.1021/acsami.6b04599.

12. J. Sun, Q. Fu, and L. Guo "Influence of siliconizing on the oxidation behavior of plasma sprayed $MoSi_2$ coating for niobium based alloy", *Intermetallics*, vol. 72, pp. 9–16, 2016, doi: 10.1016/j.intermet.2016.01.006.

13. M. Zielińska, M. Zagula-Yavorska, J. Sieniawski, and R. Filip,"Microstructure and oxidation resistance of an aluminide coating on the nickel based super alloy mar m 247 deposited by the cvd aluminizing process", *Arch. Metall. Mater.*, vol. 58, no. 3 pp. 697–701, 2013, doi: 10.2478/amm-2013-0057.

14. J. Sun, T. Li, G.-P. Zhang, and Q.-G. Fu, "Different oxidation protection mechanisms of HAPC silicide coating on niobium alloy over a large temperature range", *Journal of Alloys and Compounds.* Vol. 790, pp. 1014–1022, 2019, doi: 10.1016/j.jallcom.2019.03.229.

15. Knittel, S. Mathieu, L. Portebois, S. Drawin, and M. Vilasi,"Development of silicide coatings to ensure the protection of Nb and silicide composites against high temperature oxidation", *Surf. Coat. Technol.*, 235, pp. 401–406, 2013, doi: 10.1016/j. surfcoat.2013.07.053.

16. S. Knittel, S. Mathieu, and M. Vilasi, "Nb4Fe4Si7 coatings to protect niobium and niobium silicide composites against high temperature oxidation", *Surf. Coat. Technol.*, vol. 235, pp. 144–154, 2013, doi: 10.1016/j.surfcoat.2013.07.027.

17. Babak V.P., Shchepetov V.V. Wear resistance of amorphous-crystalline coatings with solid lubricant. *Journal of Friction and Wear,* 2017, vol. 38. P. 65 – 70. DOI:10.3103/S1068366617010020.

18. L.A. Lopata, A.V. Rutkovskij, K.P. Bujskih Sposobi ta tehnologiyi poverhnevogo zmicnennya titanovih splaviv *Suchasni pitannya virobnictva ta remontu v promislovosti i na transporti:* materiali 26 Mizhnarodnogo naukovo-tehnichnogo seminaru (30 bereznya – 02 kvitnya 2026 r., m. Kiyiv). Kiyiv, ATM Ukrayini. 2026. S. 78-82., (ukr.), s1-26c. pdf https://atmu.net.ua/downloads/archive/s1-26c.pdf

Лопата Л.А., Лопата О.В., Качинська І.Р., Рибак І.П., Солових А.Є. , Катеринич С.Є. Зміцнюючі захисні покриття на ніобієвих сплавах, їх термоциклічна повзучість і тривала міцність.

Представлено вирішення задачі захисту ніобію від високотемпературного високоінтенсивного окиснення. Визначено характеристики ізотермічної та термоциклічної повзучості та тривалої міцності ніобієвого сплаву з трьома варіантами покриттів при температурах 1400...250ºС на повітрі. Розглянута методика випробувань ніобієвих сплавів з покриттями при одночасному впливі навантажень, високих температур, різких теплозмін та окисного середовища при променистому нагріванні та безконтактному охолодженні фокусуванням променистої енергії забезпечила достовірність визначення механічних характеристик. Проведено порівняння граничних деформацій, швидкості повзучості та довговічності при ізотермічному та термоциклічному режимі трьох варіантів покриттів та показало перевагу комбінованого плазмово-дифузійного покриття перед силіцидним та боросиліцидним покриттями. Показано відмінність у характеристиках повзучості та тривалої міцності трьох варіантів покриттів, що пояснюється характером розвитку тріщин у покритті. Перехід від одиничних «гострих» тріщин у покритті до регулярних тріщин у дифузійному підшарі із заокругленими вершинами забезпечує збільшення міцності та довговічності ніобієвого сплаву.

Ключові слова: зміцнюючи захисні покриття, ніобієві сплави, термоциклічна повзучість, плазмово-дифузійні покриття, тривала міцність, довговічність

ISSN 2079-1372 Problems of Tribology, V. 31, No 2/120-2026, 76-85

Problems of Tribology
Website: http://tribology.khnu.km.ua/index.php/ProbTrib
E-mail: tribosenator@gmail.com

DOI: https://doi.org/10.31891/2079-1372-2026-120-2-76-85

Tribological information of contact electrical resistance parameters in the study of oxidation and metal plating processes

A. Gypka* 0000-0002-7565-5664, **O. Lyashuk** 0000-0003-4881-8568, **D. Mironov** 0000-0002-5717-4322, **R. Khoroshun** 000-0002-1862-7640, **Ya. Aleksevich** 0009-0007-0036-5236, **V. Fursa** 0009-0008-4314-5142, **T. Hynda** 0009-0008-2700-5318

Ternopil Ivan Puluj National Technical University , Ukraine
**E- mail : Gypkab@gmail.com*

Received: 22 April 2026: Revised 03 May 2026: Accept: 20 May 2026

Abstract

The work investigates the regularities of the change in contact electrical resistance in heavily loaded tribosystems under the conditions of transition from oxidation processes to the formation of adaptive metal-clad tribofilms. It is proposed to consider contact electrical resistance as an integral kinetic criterion of the structural and energy state of the frictional contact, which reflects the processes of destruction of oxide and metal-clad layers, activation of friction surfaces, formation of electrically conductive adaptive tribostructures and transition to adhesive contact. The research was carried out according to a scheme that models the contact "camshaft cam - roller pusher" using 42CrMo4 and 16MnCr5 steels, typical for modern heavily loaded components of the gas distribution mechanism of internal combustion engines. It is established that the change in contact electrical resistance has a pronounced kinetic nature and reflects structural and phase transitions in the surface layers of the tribosystem. It is shown that high values correspond to the presence of oxide and tribochemical insulating layers, stable minimum values characterize the formation of adaptive electrically conductive metal-cladding tribofilms, and a sharp decrease in contact electrical resistance indicates the destruction of adaptive tribolayers and the transition to direct metal contact. Critical regimes of force loading and sliding speed are determined, under which the most stable conditions of structural and energy self-organization of surface layers are realized.

Keywords: contact electrical resistance, structural-energetic self-organization, metal plating, adaptive tribofilms, adhesive friction, Cu-containing additives, cam-roller pusher contact

Introduction

In modern heavily loaded tribosystems of transport vehicles, friction processes are accompanied by complex structural and energetic transformations of surface layers, which determine the stability of frictional contact, wear intensity and durability of friction units. Particularly complex processes are implemented in the contacts of the gas distribution mechanism of internal combustion engines, where under conditions of high contact loads, variable sliding speeds, cyclic nature of loading and transient lubrication regimes, the processes of oxidation, tribochemical self-organization, metal plating and adhesive destruction of surface layers simultaneously occur.

It has been established that during the friction process in the friction contact zone, adaptive tribochemical structures in the form of oxide and metal plating films can form, capable of stabilizing contact, locally compensating for wear and ensuring structural and energetic stability of the tribosystem. In this case, the metal plating processes play the role of a positive autocompensator of wear, while adhesive friction is the main antagonist of self-organization processes, which is accompanied by the destruction of adaptive tribolayers, the development of microscratches and the transition to direct metal contact.

However, the regularities of kinetic transitions between oxidative, mechanochemical, metal plating and adhesive mechanisms of friction remain insufficiently studied, as well as the relationship between the structural and energy state of surface layers and the parameters of the electrophysical state of frictional contact. The search for an integral criterion that would allow real-time assessment of the kinetics of friction processes, self-organization processes and structural degradation of surfaces is especially relevant.

A promising direction for solving this problem is the use of the contact electrical resistance parameter R as an integral indicator of the structural and energy state of the tribosystem. The change in R reflects the processes of destruction of oxide and lubricating films, activation of friction surfaces, formation of electrically conductive adaptive tribolayers, and transition to adhesive contact.

Purpose of work

The aim of the work is to establish a correlation between the kinetics of friction processes in heavily loaded tribosystems and the contact electrical resistance index as an integral criterion of structural and energetic processes in the frictional contact zone. To achieve this goal, it is necessary to investigate the regularities of the change in contact electrical resistance during the transition from oxidation to metal plating and adhesive destruction of surface layers, as well as to establish the influence of loading modes, sliding speed, lubrication conditions, concentration of Cu-containing components and the state of the initial surface on the processes of self-organization of adaptive tribofilms in the contact "camshaft cam - roller pusher".

Analysis of recent research and publications

In modern research, considerable attention is paid to the use of nanodispersed additives in lubricants, since they are able to reduce the friction coefficient, wear intensity and form protective tribofilms on friction surfaces. The work of M. Waqas et al. summarized the influence of various nanoadditives on the friction characteristics of lubricants and showed that the effectiveness of such compositions largely depends on the type of particles, their concentration, dispersion and stability in the lubricating medium [1]. A separate direction is the study of copper-containing nanoadditives. Y. Choi et al. established that the addition of copper nanoparticles to oil reduces the friction coefficient and reduces surface wear, which is explained by the formation of a protective layer on the friction surface [2]. Similar results were obtained by H. L. Yu et al., where it was shown that Cu nanoparticles can form a thin copper film directly during friction, improving the antifriction and antiwear properties of the lubricating medium [3]. In the work of M. Scherge et al. it is shown that copper-containing additives in motor oils can implement a multi-stage mechanism of formation of protective films on metal surfaces. This is of great importance for explaining the processes of metal plating and the formation of adaptive tribolayers in heavily loaded contacts [4]. Also relevant are studies related to the electrophysical control of friction processes. In works devoted to contact electrical resistance, it is shown that the electrical parameters of the contact can be used to assess the state of the lubricating film, the degree of metal contact, the formation of tribofilms and the transition between lubrication modes [5, 6]. This directly corresponds to the idea of using the contact electrical resistance R as an integral criterion of the structural and energy state of the tribosystem. Important for this topic are the works of H. A. Spikes, who considered the influence of electric potentials on friction, wear and tribochemical processes. The author emphasizes that electrical influences can change the kinetics of tribochemical reactions, film formation and frictional contact behavior [7]. This confirms the feasibility of combining tribological and electrophysical approaches in the study of adaptive tribofilms. Recent studies of electrified tribocontacts show that the formation of tribofilms can significantly depend on the electrical state of the contact. In particular, N. Siddique et al. investigated the formation of polymer tribofilms at different electric current densities and used impedance spectroscopy to evaluate their electrical properties [8]. This is an important methodological analogue for works where contact electrical resistance is used as a diagnostic parameter. The work of J. A. Cao-Romero-Gallegos et al. is devoted to the effect of electric current on the thickness of the lubricating film in boundary and mixed lubrication regimes. The authors showed that the electrical contact conditions affect the change in the lubricating layer, which is important for explaining the transitions between hydrodynamic, elastohydrodynamic and boundary lubrication regimes [9]. General reviews of recent years confirm that the modern development of tribology is aimed at creating functionally doped lubricating compositions capable of forming self-organized adaptive tribolayers. Particular attention is paid to metal nanoparticles, oxides, graphene structures, h-BN, MoS_2 and ionic liquid components [10, 11]. The results obtained are consistent with the data of works [12,13], where it is shown that the tribological behavior of surface layers is determined by complex structural-energy processes, which include the formation of secondary structures, tribochemical transformations and the development of material damage mechanisms. The established patterns confirm that the processes of self-organization of surface layers have a direct impact on the parameters of friction, wear and stability of the functioning of tribosystems. Thus, the analysis of recent studies shows that a promising direction is the combination of nanomodified lubricating compositions, metal plating processes and electrophysical monitoring of the state of the frictional contact. At the same time, the patterns of the transition from oxidative and mechanochemical secondary structures to electrically conductive adaptive tribofilms in heavily loaded automotive tribosystems, in particular in the contact "camshaft cam - roller pusher", remain insufficiently studied. This is precisely what determines the relevance of further use of the contact electrical resistance parameter R for diagnosing the structural and energy state of surface layers.

Research materials and methodology

The functioning of tribocouplings of the gas distribution mechanism of internal combustion engines is accompanied by complex non-stationary processes of interaction of surface layers, which occur under conditions of high specific loads, cyclic nature of contact and variable lubrication modes. In the contact "camshaft cam - roller pusher" mechanical, thermal and tribochemical processes are simultaneously implemented, which determine the nature of the evolution of surface structures and the durability of the friction unit. When moving from the hydrodynamic to the limit lubrication mode, the role of structural and phase transformations in the surface layers associated with the destruction of oxide films, activation of contact surfaces and the development of local adhesive interactions significantly increases. In the process of friction, the surface layers of the tribosystem are in a non-equilibrium state, which creates conditions for the emergence of self-organization processes and the formation of secondary tribochemical structures. Under certain load conditions and sliding speeds, adaptive metal-cladding tribofilms can form in the contact zone, which are characterized by reduced shear resistance and the ability to stabilize frictional contact. Such structures perform the function of local wear compensation, reduce the concentration of contact stresses and prevent the development of destructive processes in the friction zone. However, when the structural stability of tribolayers is violated, their destruction occurs, which is accompanied by a transition to adhesive contact and intensive wear of surfaces.

One of the main problems of modern tribology is the establishment of a parameter that would allow assessing the kinetics of structural and energy changes in the tribosystem directly during the operation of the friction unit. Traditional tribotechnical indicators do not always make it possible to promptly record the initial stages of destruction of adaptive tribolayers or the moment of transition to adhesive friction. In this regard, the use of R as a sensitive parameter reflecting the change in the physical state of the surface layers and the nature of the interaction between them is promising.

To study the kinetic indicators R, I, T and μ, a specialized tribometer was used (Fig. 1), which simulated the operating conditions of the gas distribution mechanism of an automobile engine. The tribometer was formed from 42CrMo4 steel (EN 1.7225), which simulated the working surface of the camshaft cam, and cemented steel 16MnCr5 (EN 1.7131), which corresponded to the material of the roller pusher. The tests were carried out in a wide range of force parameters of loads and sliding speeds using alloyed lubricating compositions modified with Cu-containing functional components.

The increased rigidity of the tribometer frame structure, friction unit, and loading mechanism minimizes the occurrence of vibration during the research process and its negative impact on the objectivity of the obtained results.

Fig. 1. General view of the tribometer

Source: created by the author based on experimental data using artificial intelligence tools

General view of the friction unit in Fig. 2. The friction unit of the studied tribocoupling modeled the contact of the pair "camshaft cam - roller pusher". For experimental studies, the studied sample was used in the form of a cylindrical roller, the working surface of which imitated the surface of the roller pusher, and a countersample in the form of a cam, the working surface of which modeled the profile of the camshaft cam. The geometric parameters of the samples and the contact conditions were chosen in such a way as to ensure the reproduction of the nature of the contact interaction, load and speed regimes of a real tribocoupling. Both parts were manufactured to the sixth quality of accuracy. The roughness of the working surfaces after running-in was Rz = 0.125–0.250 μm.

Experimental studies were carried out under normal load on the sample within 100–600 N, which ensured the formation of contact pressures close to the operating conditions of the tribocoupling "camshaft cam - roller pusher". The sliding speed was varied in the range of 0.2–3.0 m/s, which allowed to reproduce the operating modes of the cam mechanism at different camshaft rotation frequencies. The main controlled parameters during the tests were normal load, sliding speed, friction duration, temperature in the contact zone, friction coefficient, wear intensity and parameter R. The main parameters and modes of experimental studies of the tribocoupling "camshaft cam - roller pusher" are given in Table 1.

Table 1

Main parameters of experimental studies of tribocoupling "camshaft cam - roller pusher"

Parameter	Value
Normal load, N	100; 200; 300; 400; 500; 600 N
Contact pressure, p	4–12 MPa
Sliding speed, v	0.2; 0.5; 1.0; 1.5; 2.0; 3.0 m/s
Test duration	300–600 min
Surface roughness after running-in, R_a	0.125–0.250 μm
Temperature in the contact zone	40–120 °C

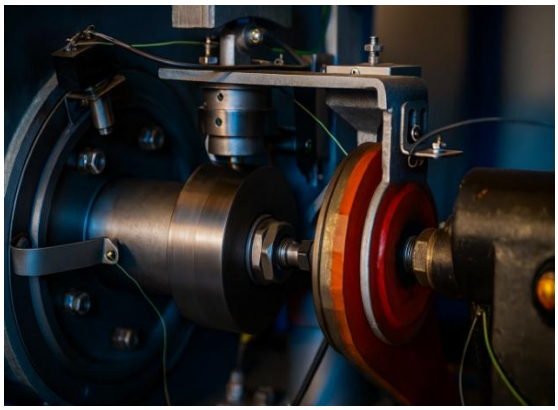

Fig. 2. General view of the friction unit

Source: created by the author based on experimental data using artificial intelligence tools

The open design of the friction unit is convenient for visual control of its operation, lubrication mode, natural cooling of the friction contact zone, replacement of tribocoupling parts, connection of measuring equipment.

To intensify the processes of structural and energy self-organization of surface layers and the formation of adaptive metal-cladding tribofilms, the base lubricating medium was subjected to functional alloying with a complex of micro components. The selection of materials was carried out taking into account their tribochemical activity, ability to form secondary structures and influence on the electrophysical state of the friction contact.

As a base lubricating medium, SAE 10W-40, API CI-4/SL class motor oil for heavy-duty diesel engines was used, which is characterized by high thermal-oxidative stability, sufficient anti-wear properties and a wide range of operating modes. Shell Rimula R6 M 10W-40 was chosen as the base oil, to which functional Cu-containing alloying components were introduced at a concentration of 5, 10 and 20% by weight of the additive.

The preparation of alloyed lubricating compositions was carried out by mechanical dispersion using ultrasonic treatment at a frequency of 22 kHz for 20…30 min, which ensured uniform distribution of particles in the lubricating medium and prevented their agglomeration. To stabilize the dispersed system, surface-active components were used at a concentration of 0.5…1.0%.

Research results and discussion

The introduced functional components were involved in tribochemical reactions in the contact zone during the friction process and participated in the formation of self-organized electrically conductive adaptive tribolayers. The effectiveness of the processes of structural-energy self-organization was assessed by the change in R, which was considered as an integral kinetic indicator of the structural state of the surface layers of the tribosystem.

Structural-energy transitions and the relationship between the processes of oxidation, self-organization, and metal plating in the frictional contact zone of heavily loaded tribosystems are shown in Fig. 3.

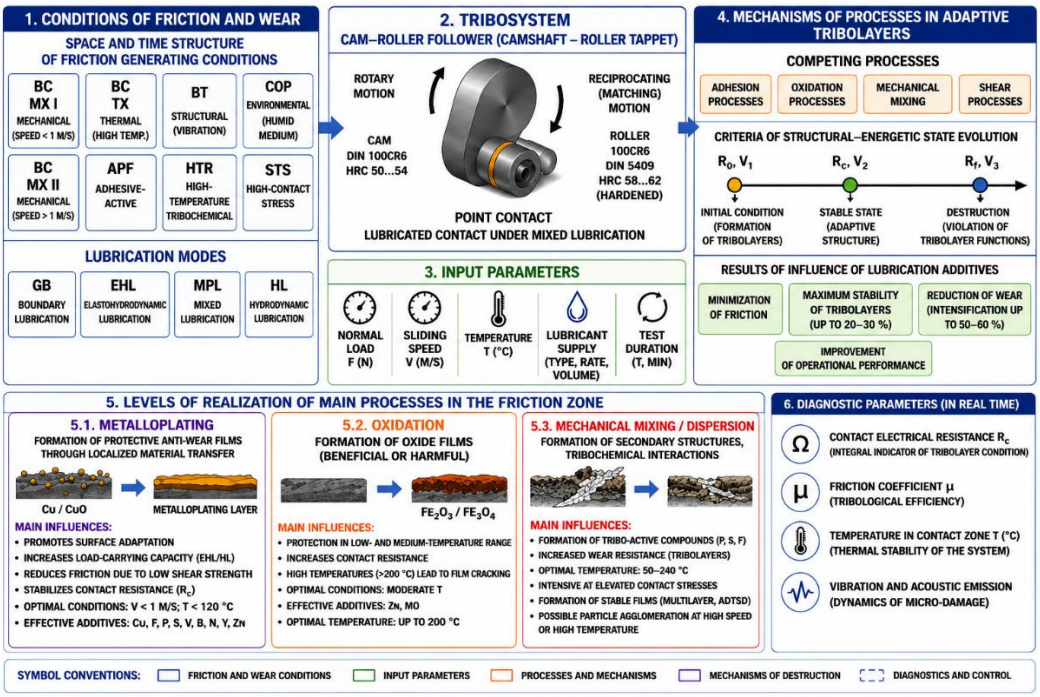

Fig. 3. Structural and energy scheme of the implementation of the processes of self-organization, oxidation, metal plating and adhesive wear in heavily loaded tribosystems of the gas distribution mechanism: VS MX I, II - secondary structures of mechanochemical type I and II, VS TX - secondary structures of thermochemical type, VP - selective transfer structures, SOP - self-organized organic tribofilms, ATP - adaptive tribofilms, NKTSh - nanocomposite tribochemical layers, STS - self-organized dissipative tribostructures, HD - hydrodynamic lubrication regime, EHL - elastohydrodynamic lubrication regime, BNL - boundary nanolubrication regime, MPP - metal-cladding films, Cu/CuO - copper-containing tribochemical components, P1–P3 - critical loads of structural-energy transitions, V1–V3 - critical sliding velocities of structural-energy transitions, R - contact electrical resistance of frictional contact, μ - friction coefficient, AE - acoustic emission parameters, T - temperature in the frictional contact zone.

Source: created by the author based on experimental data using artificial intelligence tools

The regularities of the evolution of surface structures and the transition between different stages of the structural and energy state of the tribosystem are shown in Fig. 4.

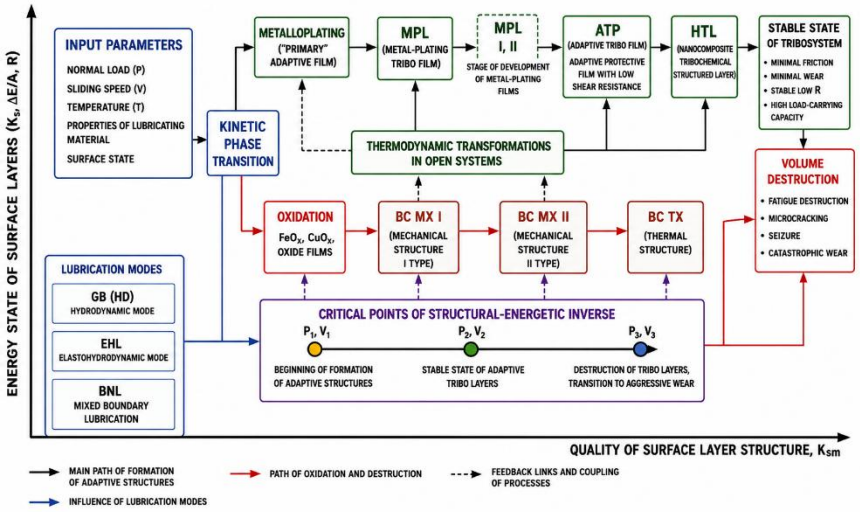

Fig. 4. Evolution of the structure of materials of surface layers of technical tribosystems: VS MX I, II - secondary structures of mechanochemical type I and II, VS TX - secondary structures of thermochemical type, MPP - metal-plating films, ATP - adaptive tribofilms, NKTSh - nanocomposite tribochemical layers, HD - hydrodynamic lubrication mode, EHL - elastohydrodynamic lubrication mode, BNL - boundary nanolubrication mode, FeOx, CuOx - oxide tribochemical structures, Kz - energy storage coefficient by surface layers, Kzm - strengthening coefficient of surface layers, ΔE/Aт - ratio of stored energy to the work of friction forces, R - contact electrical resistance of frictional contact, P1–P3 - critical loads of structural-energy transitions, V1–V3 - critical sliding velocities of structural-energy transitions

Source: created by the author based on experimental data using artificial intelligence tools

This figure reflects the structural-energy model of the evolution of surface layers in heavily loaded tribosystems and demonstrates the relationship between the processes of oxidation, metal plating, the formation of adaptive tribofilms and the destruction of surface layers during friction.

The vertical axis shows the energy state of the surface layers, which is characterized by the parameters Kz, ΔE/Aт and R. With an increase in the energy activation of the surface layers in the contact zone, tribochemical and structural-phase transformations are intensified. The horizontal axis shows a change in the quality of the structure of the surface layers, which is characterized by the coefficient Kzm, which reflects the degree of strengthening, stabilization or degradation of the surface tribolayers.

At the initial stage, the input parameters of the tribosystem — load, sliding speed, temperature, lubrication mode, properties of the lubricant and surface condition — determine the nature of the course of structural-energy processes in the frictional contact zone. When critical conditions are reached in the tribosystem, a kinetic phase transition is realized, after which two main mechanisms begin to compete: oxidation of surface layers and metal plating processes.

The lower branch of the scheme reflects the oxidative direction of the evolution of surface structures. First, oxide films of FeOx and CuOx are formed, after which secondary structures of mechanochemical type I and II (BC MX I, BC MX II) appear. Further accumulation of energy and increase in temperature leads to the formation of thermochemical structures (BC TX). When the system goes beyond the limits of structural stability, volumetric destruction of surface layers occurs, which is accompanied by microscratches, seizing, fatigue failure and catastrophic wear.

The upper branch of the scheme describes the processes of metal plating and self-organization of adaptive tribolayers. After the phase transition, in the presence of Cu-containing components in the contact zone, a metal plating film (MP) is formed, which goes through several stages of development. Further thermodynamic transformations in the open tribosystem lead to the formation of adaptive tribofilms (AT) and nanocomposite tribochemical layers (NCTL). These structures have reduced shear resistance, stabilize the friction process, reduce the friction coefficient and wear intensity, and increase the bearing capacity of the contact.

The figure also shows the critical points of structural-energy inversion P1,V1; P2,V2; P3,V3. At point P1,V1, the formation of adaptive structures begins. In the range P2,V2, stabilization of adaptive tribolayers and the most effective implementation of self-organization processes are observed. When P3,V3 is reached, the destruction of tribofilms begins and the transition to adhesive wear and destructive processes occurs.

Lubrication modes significantly affect the direction of evolution of surface structures. In the hydrodynamic mode (HD), stable separation of surfaces by a lubricating film prevails. In the elastohydrodynamic mode (EHL), the conditions for the formation of adaptive tribofilms are realized. The boundary nanolubrication mode (BNL) is characterized by high activation of surface layers, the development of tribochemical reactions and the most intensive self-organization processes.

Using the parameter R, the ranges of structural and energetic stability of the processes of formation of secondary tribochemical structures, metal-cladding films and adaptive nanocomposite tribolayers in the contact zone “camshaft cam – roller pusher” were established. Analysis of the change in contact electrical resistance allowed us to determine the critical transition modes between oxidative, mechanochemical and metal-cladding mechanisms of self-organization of surface layers. The existence of critical points of structural and energetic inversion of tribological processes (P1, V1; P2, V2; P3, V3) was established, within which the transition from unstable oxidative and mechanochemical secondary structures to the formation of electrically conductive adaptive tribofilms with a reduced critical shear stress and high structural stability occurs (Fig. 5).

It is shown that in the range P1–P2 and V1–V2 the most favorable conditions for the processes of metal plating and the formation of self-organized nanocomposite tribolayers are realized, capable of stabilizing frictional contact, localizing the energy of plastic deformation and reducing the intensity of adhesive wear. When reaching the critical parameters P3 and V3, a violation of the structural equilibrium of the tribosystem, destruction of adaptive tribofilms and a transition to destructive friction modes are observed, which is accompanied by the development of microscratches, seizure of surfaces and a sharp increase in the friction coefficient.

The change in the value of R allowed us to evaluate in real time the kinetics of destruction of surface oxide layers, the degree of activation of friction surfaces, the formation and stabilization of electrically conductive metal plating structures, as well as the processes of self-organization of adaptive tribofilms in the frictional contact zone. It has been established that the parameter R is a sensitive integral criterion of the structural and energy state of the tribosystem and can be used to diagnose transitions between the regimes of oxidation, boundary lubrication, metal plating, and adhesive destruction of surface layers, which is accompanied by the transition from unstable oxidative structures to the formation of adaptive metal plating tribolayers (Fig. 3).

The graph reflects the influence of the initial surface state on the nature of the transition processes from oxidation to metal plating in heavily loaded tribosystems. At the initial stage, surfaces with high oxidation and roughness are characterized by high values of R, which corresponds to the formation of unstable oxide structures. With an increase in the load P and the sliding speed V, the destruction of oxide films, activation of surfaces and a transition to the formation of mechanochemical structures occur. In the range from P2,V2 to P3,V3, the most favorable conditions for metal plating processes and the formation of adaptive metal plating films (MPF) are realized, which is accompanied by a sharp decrease in contact electrical resistance due to the formation of electrically conductive tribolayers. It is shown that pre-finished surfaces quickly transition to the stable metal

plating mode, while untreated surfaces remain in the region of oxidative processes longer and are characterized by a less stable course of structural and energy self-organization.

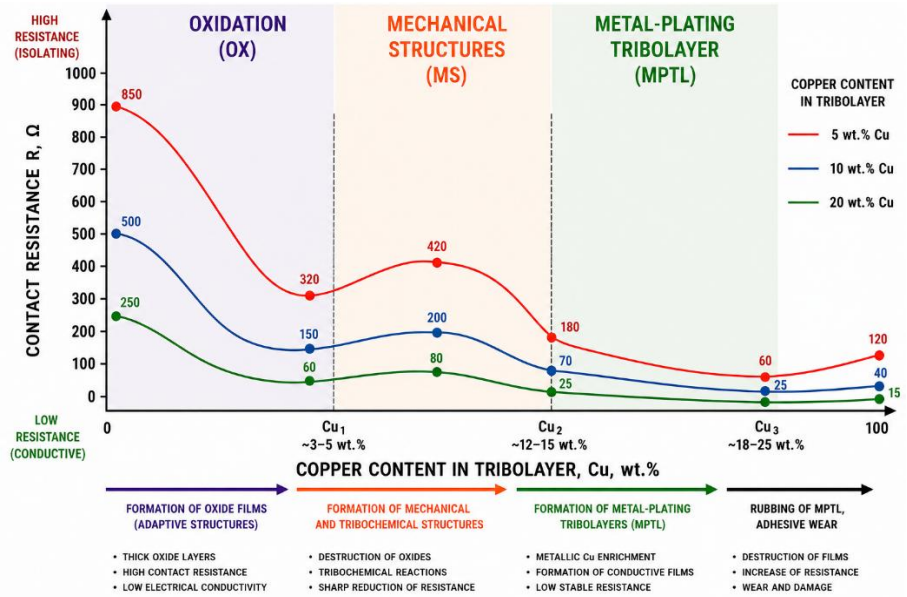

Fig. 5. The influence of the initial surface condition on the nature of the oxidation (OS) - metal plating (MPP) transient processes

Source: created by the author based on experimental data using artificial intelligence tools

To establish the relationship between the processes of structural and energetic self-organization of surface layers and changes in tribotechnical characteristics, a comparative analysis of the kinetics of R, the friction coefficient and the wear intensity at different contents of the functional alloying component Cu in the tribosystem was carried out. Particular attention was paid to determining the range of loads and sliding speeds within which the most stable conditions for the formation of adaptive metal-clad tribolayers are realized and the positive self-compensation effect of metal-clad is manifested (Fig. 6).

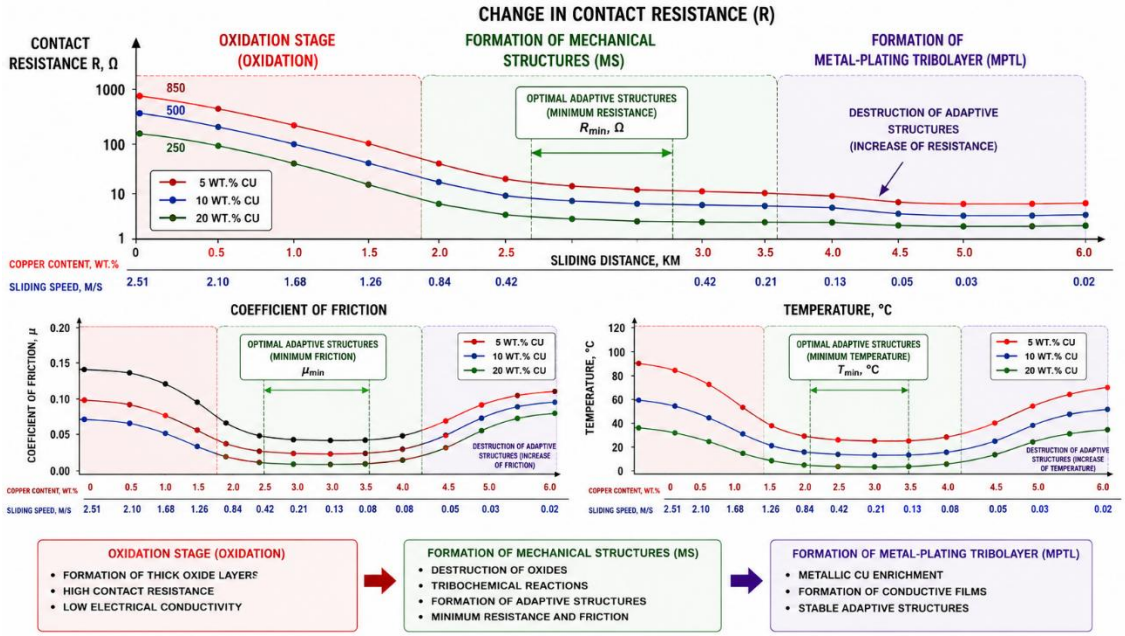

Figure 6. Correlation between contact electrical resistance (CER), friction parameters, and structural–energetic transformations of adaptive tribolayers under different Cu concentrations in the lubricating medium

Source: created by the author based on experimental data using artificial intelligence tools

As can be seen from Fig. 6, doping the tribosystem with Cu-containing components significantly affects the nature of the change in R, the friction coefficient and the wear intensity. In the zone of optimal values R of the load and sliding speed, R is stabilized at a minimum level, which indicates the formation of electrically conductive adaptive metal-clad tribolayers. In the same range, the friction coefficient and wear intensity are minimized, which

confirms the implementation of the processes of structural and energy self-organization of surface layers and the positive self-compensation effect of metal plating. A further increase in the specific load and sliding speed leads to a violation of the structural stability of adaptive tribolayers, the development of adhesion processes and a transition to destructive friction modes. This is accompanied by a sharp decrease in R, which corresponds to the transition to direct metal contact, as well as an intensive increase in the friction coefficient and wear rate of surfaces. The obtained results confirm the existence of a correlation between the kinetics of change of R and the main tribotechnical indicators of the tribosystem.

The nature of the change and the value of the main tribotechnical indicators, the parameters of adaptive tribofilms and the processes of structural and energetic self-organization of surface layers are significantly affected by the volume and periodicity of the supply of alloyed lubricant to the frictional contact zone (Fig. 7), the concentration, dispersion and stability of functional micro- and nanodispersed additives in the lubricating medium (Fig. 8). It has been established that the change in load modes, sliding speed and contact cyclicity directly affects the kinetics of formation and destruction of adaptive tribochemical layers, the stability of the lubricating film, the value of R, the friction coefficient and the intensity of wear of surface layers.

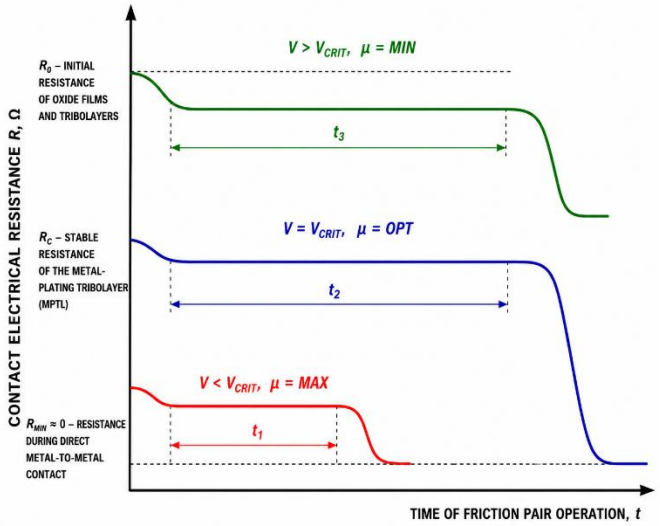

Fig. 7. Correlation between R and the existence time of adaptive MPPs on lubrication conditions: t_1, t_2, t_3 - time of structural stability ("lifetime") of the MPP; R_0 - initial resistance of oxide and tribochemical layers; Rc - stable contact electrical resistance of adaptive metal-clad tribolayers; $R_{min} \rightarrow 0$ - resistance at direct metal contact; V - volume of lubricant at a single supply; Vcrit - critical volume of supply of lubricating medium; μmin - minimum value of the friction coefficient; μopt - optimal friction coefficient; μmax - maximum friction coefficient

Source: created by the author based on experimental data using artificial intelligence tools

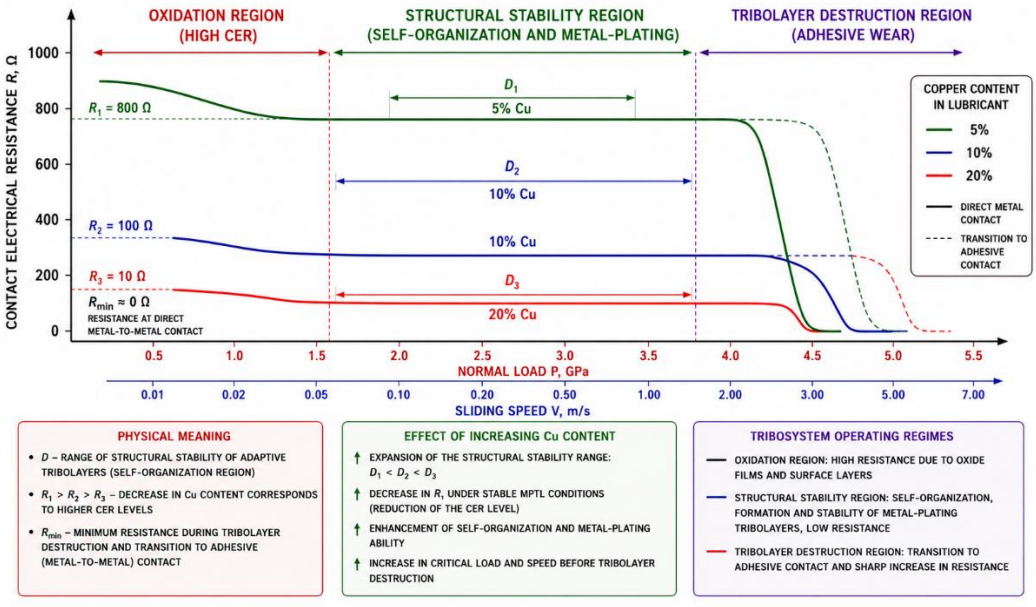

Fig. 8. Effect of the concentration of alloying elements of the lubricant additive (Cu) on R and the range of structural self-organization of surface layers D

Source: created by the author based on experimental data using artificial intelligence tools

According to the results of the research, it was found that an increase in the concentration of Cu-containing functional components in the lubricating medium significantly affects the kinetics of R change and the structural stability of adaptive tribolayers. It is shown that with an increase in the Cu content, a decrease in the stable level of R is observed, which indicates the formation of more electrically conductive metal-clad tribofilms with an increased ability to structural and energetic self-organization. At the same time, the range of structural stability D (D1 < D2 < D3) expands, within which the most effective metal-clad processes and frictional contact stabilization are implemented. It is established that Cu-containing components shift the critical transition to the destruction of adaptive tribolayers to the region of higher specific loads and sliding speeds, which indicates an increase in the resistance of surface layers to adhesive destruction. A sharp decrease in contact electrical resistance corresponds to the destruction of metal-clad tribolayers and the transition to direct metal contact, which is accompanied by the development of adhesion processes and intensive wear of friction surfaces. The obtained results confirm the existence of a correlation between the concentration of alloying components, R, and the structural and energetic stability of tribosystems.

Conclusions

It was found that the thickness of adaptive tribofilms formed when using alloyed lubricating compositions with functional micro- and nanodispersed additives is heterogeneous and depends on the concentration, dispersion and tribochemical activity of the alloying components. In the course of research, the formation of stable nanocomposite tribolayers with a thickness of hundreds of nanometers to tens of micrometers was revealed, which provide a reduction in the friction coefficient by 15–30% and a significant reduction in the intensity of wear of the contacting surfaces of the tribosystem "camshaft cam - roller pusher". The obtained effect is explained by the formation in the frictional contact zone of self-organized tribochemical structures with a reduced critical shear stress, capable of stabilizing the friction process and localizing the energy of plastic deformation in the surface layers.

It has been established that the geometric, structural-energy and tribotechnical parameters of adaptive tribofilms depend on a complex of interrelated factors, the main of which are: the surface energy of the tribocoupling materials; the magnitude and nature of the load change in the "cam - roller pusher" contact; the state of the initial friction surface, in particular the presence of secondary mechanochemical or thermochemical structures, surface roughness, the degree of activation of surface layers and the presence of abrasive particles; kinematic parameters of motion, the overlap coefficient of contact surfaces, load cyclicity, as well as the amount and periodicity of lubricant supply to the frictional contact zone.

Analysis of the research results showed that the formed adaptive tribofilms are characterized by high antifriction, antiwear and anti-seize properties. The formation of stable tribochemical layers occurs in a relatively narrow range of critical loads and sliding speeds, characteristic of the modes of boundary and mixed lubrication of the gas distribution mechanism of the internal combustion engine. In this range, the friction coefficient, wear intensity and contact electrical resistance parameters are characterized by stable values, which indicates the formation of electrically conductive self-organized tribolayers with high structural stability. The processes of structural and energy self-organization are most effectively implemented with a cyclic nature of the load, a smooth change in sliding speeds and the use of alloyed lubricating compositions with high tribochemical activity of functional nanoadditives.

References

1. Waqas M., Zahid R., Bhutta M. U., Khan Z. A., Saeed A. A Review of Friction Performance of Lubricants with Nano Additives. *Materials*, 2021. https://doi.org/10.3390/ma14216310

2. Choi Y., Lee C., Hwang Y., Park M., Lee J., Choi C., Jung M. Tribological behavior of copper nanoparticles as additives in oil. *Current Applied Physics*, 2009. https://www.sciencedirect.com/science/article/abs/pii/S1567173909001369

3. Yu H. L., Xu Y., Shi P. J., Wang H. M., Zhao Y., Xu B. S., Bai Z. M. Characterization and nano-mechanical properties of tribofilms using Cu nanoparticles as additives. *Surface and Coatings Technology*, 2008. https://www.sciencedirect.com/science/article/abs/pii/S0257897208006609

4. Scherge M., Böttcher R., Kühn M., Linsler D. Multi-Phase Friction and Wear Reduction by Copper Nanoparticles. *Lubricants*, 2016. https://doi.org/10.3390/lubricants4040036

5. Chen Y., Liang H. Tribological Evaluation of Electrical Resistance of Lubricated Contacts. Journal of Tribology. 2020. Vol. 142, No. 11. Article 114502. https://doi.org/10.1115/1.4045578

6. De-Liang, L., Shu-Hua, C., Shi-Feng, Z., & Jiu-Jun, X. (2016). *Lubrication film thickness calculation from contact resistance in elastohydrodynamic contacts*. *Industrial Lubrication and Tribology*, 68(2), 176–182. https://www.emerald.com/doi/10.1108/ILT-04-2015-0057

7. Spikes H. A. Influence of Applied Electrical Potentials on Friction and Wear. *Tribology Letters*, 2020. https://doi.org/10.1007/s11249-020-01328-3

8. Siddique N., Li Y.-S., Ogrinc A. L., Guo Y., Yuan R., Kim S. H. Tribology at Electrified Interface: Electron Transport and Chemistry During Polymeric Tribofilm Formation from Adsorbate Molecules by Friction. Tribology Letters. 2025. Vol. 73, No. 3. Article 96. https://doi.org/10.1007/s11249-025-02031-x

9. Cao-Romero-Gallegos J. A., Dwyer-Joyce R. S., et al. The effect of electrical current on lubricant film thickness in boundary and mixed lubrication contacts measured with ultrasound. *Friction*, 2024. https://doi.org/10.1007/s40544-024-0890-7

10. Nasser K., et al. Recent Studies on Nanomaterials as Additives to Lubricants Under Electrified Conditions for Tribology: Review. *Lubricants*, 2024. https://doi.org/10.3390/lubricants13010002

11. Aroor G., et al. From chemistry to performance: How nano additives are shaping the future of biolubricants. *Journal of Molecular Liquids*, 2025. https://www.sciencedirect.com/science/article/pii/S016773222500409X

12. Gypka A., et al. Tribological aspects of material damage in machine and mechanism components during operation. *Procedia Structural Integrity*, 2026. https://doi.org/10.1016/j.prostr.2026.03.082

13. Lyashuk, O., Gypka, A., Maiak, M., Mironov, D., & Levkovych, M. (2025). Methodology for the Investigation and Evaluation Criteria of Oxidation-Metal Plating Processes During Friction and Wear. Key Engineering Materials, 1035, 15-26. https://doi.org/10.4028/p-j9wJhv

Гупка А.Б., Ляшук О.Л., Міронов Д.В., Хорошун Р.В., Алексевич Я.Р., Фурса В.А., Гинда Т.Ю. Трибологічна інформативність параметрів контактного електроопору при дослідженні процесів окислення та металоплакування

У роботі досліджено закономірності зміни контактного електроопору у важконавантажених трибосистемах в умовах переходу від окислювальних процесів до формування адаптивних металоплакуючих трибоплівок. Запропоновано розглядати контактний електроопір як інтегральний кінетичний критерій структурно-енергетичного стану фрикційного контакту, який відображає процеси руйнування оксидних і металоплакуючих шарів, активацію поверхонь тертя, формування електропровідних адаптивних трибоструктур та перехід до адгезійного контакту. Дослідження проводили по схемі яка моделює контакт «кулачок розподільного вала – роликовий штовхач» із використанням сталей 42CrMo4 та 16MnCr5, характерних для сучасних важконавантажених вузлів газорозподільного механізму двигунів внутрішнього згоряння. Встановлено, що зміна контактного електроопору має виражений кінетичний характер та відображає структурно-фазові переходи у поверхневих шарах трибосистеми. Показано, що високі значення відповідають наявності оксидних та трибохімічних ізолюючих шарів, стабільні мінімальні значення характеризують формування адаптивних електропровідних металоплакуючих трибоплівок, а різке зниження контактного електроопору свідчить про руйнування адаптивних трибошарів і перехід до прямого металевого контакту. Визначено критичні режими силового навантаження та швидкості ковзання, за яких реалізуються найбільш стабільні умови структурно-енергетичної самоорганізації поверхневих шарів.

Ключові слова: контактний електроопір, структурно-енергетична самоорганізація, металоплакування, адаптивні трибоплівки, адгезійне тертя, Cu-вмісні добавки, контакт «кулачок – роликовий штовхач»

ISSN 2079-1372 ***Problems of Tribology****, V. 31, No 2/120-2026, 86-92*

Problems of Tribology
Website: http://tribology.khnu.km.ua/index.php/ProbTrib
E-mail: tribosenator@gmail.com

DOI: https://doi.org/10.31891/2079-1372-2026-120-2-86-92

Solid lubricant nanocoating's based on magnesium compounds

V.V. Shchepetov[1] 0000-0002-8352-8307, **N.M. Fialko**[1] 0000-0003-0116-7673, **S.S. Bys**[2] 0000-0002-7518-3310

[1]*Institute of Technical Thermophysics, NASU, Ukraine, Kyiv*
[2]*Khmelnytskyi National University, Ukraine, Khmelnytskyi*
E-mail:serhiibys@gmail.com

Received: 25 April 2026: Revised 05 May 2026: Accept: 20 May 2026

Abstract

The results of studies of friction and wear of detonation composite nanocoating's based on the ternary compound aluminum-magnesium-boron under test conditions with constant load in the sliding velocity field are presented. Their structural-phase composition and passivating complex of surface oxide structures are determined using modern physical analysis methods. It is established that the parameters of wear intensity and friction coefficients are minimized due to the set of surface structures that regenerate a stable self-lubricating structured layer under friction conditions. Factors that influence the formation of dynamic equilibrium of a self-lubricating layer that has an effective ability to self-repair are determined. At the same time, a continuous protective layer screens the processes of molecular-adhesive interaction and blocks the development of unacceptable destruction phenomena.

Keywords: surface structures, carbide graphite, wear, interlayer, phase composition, self-lubrication.

Introduction. As the scope of application of coatings obtained by spraying increases, the requirements for their quality are increasing. Existing methods of improving quality are necessary, but insufficient. The most accessible and most common means of improving operational quality is the use of lubricants. The use of self-lubricating sliding materials, which provide both technical and economic advantages [1, 2], is becoming increasingly important in many industries. The lubricating effect is achieved by incorporating solid lubricants directly into the coating structure or the material matrix itself [3, 4].

Literature review

Considerable attention is devoted to the study of self-healing coatings and the discussion of their self-healing mechanisms and functionality [5]. The authors argue that the use of such coatings is a promising approach to protecting components from wear. The paper [6] analyzes the main problems and current developments in the field of protecting friction surfaces and improving their wear and corrosion resistance. Additionally, it highlights the problems that arise when using self-lubricating coatings. In their works [7, 8], the authors investigated coatings used to protect component surfaces in the automotive industry. Parts used in automobile manufacturing are simultaneously exposed to corrosion and repeated loading and are operated under severe conditions. Therefore, significant attention is devoted to the precise analysis and prediction of the effectiveness of part surface protection.

The use of nanostructured coatings modified with magnesium carbide nanoparticles [9] and the use of solid lubricant coatings [10] deserve, in our opinion, special attention when selecting a method to enhance the wear resistance of materials. Current research by scientists worldwide focuses on methods for producing nanocoatings and using them to protect friction surfaces, particularly those operating under extreme loads and in aggressive environments [11–13]. These studies highlight a comprehensive method for forming protective solid-lubricant layers during friction [14–15]. There is also a number of studies devoted to the analysis of the use of inorganic and polymer nanocoatings, which demonstrate that controlled wear and self-lubrication are key factors in modern mechanical engineering [16–17].

The purpose of the work

Research into the patterns of wear of coatings based on magnesium compounds, study of their structural and phase composition and analysis of the structure formation of antifriction surface layers and their influence on self-lubrication processes.

Materials and research methods

The powders proposed by the authors contain as initial reagents the ternary compound aluminum-magnesium-boron ($AlMgB_{14}$), which is distinguished by significant mechanical and thermal properties and is used as a base for composite coatings for the first time. In order to improve the tribotechnical characteristics, the base material was additionally doped with silicon (Si), aluminum (Al), nickel (Ni), titanium (Ti), chromium (Cr), zirconium (Zr), carbon (C). The choice of alloying additives is determined by tribomaterials science provisions, which thoroughly combined the obtained results into a single system of ideas about magnesium compounds with high tribotechnical properties. Further obtaining high-quality self-lubricating coatings involved the use of modern technologies, including mechanochemical synthesis (MCS) and detonation-gas spraying. The method of mechatronic synthesis provided in a dry inert atmosphere the formation of the structure and phase composition of the powder mixture, which, as a result of selective interaction, due to thermodynamic and diffusion characteristics, consisted of micro volumes of several nanocomponents, which had a microcrystalline type of the base structure stabilized by nanoscale inclusions of high-temperature stable strengthening phases. Structurally free magnesium carbide (MgC_2) was added to the base particles obtained in this way and mixed until the mixture was evenly distributed, ready for detonation-gas spraying of coatings.

Coatings from the obtained composite powders were applied by the detonation-gas method to prepared samples of 30XGSNA steel. The increase in adhesion strength, as a criterion for operability, was carried out by pre-applying a sublayer of vitreous sodium $NaO_2(SiO_2)_2$ to the working surface of the samples. The adhesion strength was determined by the pin method, which for magnesium coatings was up to 98 MPa with a porosity of almost 0.5%, along with this, after grinding the initial roughness was Ra 0.32-0.63. Testing of the sprayed samples was carried out according to the end scheme under conditions of distributed contact at normal temperature in the continuous sliding mode with a constant load of 10.0 MPa. The influence of the environment, sliding speed, and load were provided taking into account the maximum approximation of the processes of physicochemical mechanics of friction to real conditions in the zone of frictional contact interaction, in addition, the research program provided for a comparative analysis of the friction parameters of the proposed coatings with similar values. Wear of coatings such as WK15 and coatings made of alloyed chromium.

Research into technology-structure and structure-property relationships was based on a complex of modern physicochemical methods of structural-phase analysis., which included consideration of the zones of the surface layers at the macro- and microscopic levels. In this case, the comprehensive research methodology included metallography (optical microscope "Neophot-32" with a prefix); particle size of the powder mixture (laser meter Analysetle 22 Nano Tec plus; durometric analysis (hardness tester M-400 from LECO); scanning electron microscopy (scanning electron microscope JSM-840); X-ray structural phase analysis (diffractometer DRON-UM1).

Research results

Contact interaction during friction represents a complex sequence of mutually determined influences of both external and internal factors that determine the regularities of friction and wear processes and determine the degree and gradients of elastic-plastic deformation, temperature, activation level and a number of associated phenomena and are ultimately responsible for the leading type of wear.

The general results of coating tests (fig. 1) are presented in the form of graphs of functional averaged values of wear intensity and friction coefficients obtained in a field of monotonically increasing sliding velocities at constant the tensile load was 10.0 MPa.

Synthesis and research of ultra-strong ceramics based on ternary compounds, in particular magnesium boride, are being studied quite intensively, however, the possibilities of the latter and its complex of tribotechnical properties, despite efforts and individual achievements, have not been fully clarified in this regard to this day.

The analysis of the microstructure and elemental composition, carried out on the “Camebax SX” installation, shows that the synthesis products are heterogeneous and the main component is the chemical compound of aluminum, magnesium and boron ($AlMgB_4$). At the same time, a high background was found at small diffraction angles, which indicates the presence of an amorphous phase corresponding to boron and, possibly, highly boron-containing amorphous phases of aluminum and magnesium. In addition to the structural bases corresponding to the $AlMgB_4$ compound, reflexes of such phases as AlB_{12}, $AlMgB_4$, AlB_2 were found, and $Al_{14}Mg_{13}$ imprints are present. It is important to note that the presence of a large number of phases with different complex crystal lattices makes it difficult to sufficiently determine the concentration of the target phase $AlMgB_{14}$. Quantitative phase separation is no less difficult, since the reflexes of the compounds present have close interplanar positions and are located at the same diffraction angles, as a result of which they overlap and complicate the determination of the real picture.

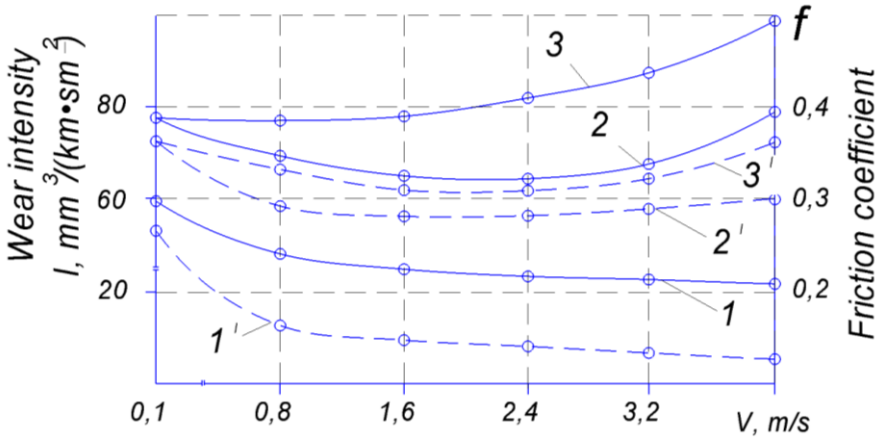

Fig. 1. Dependence of wear intensity (1, 2, 3) and friction coefficients (1^I, 2^I, 3^I) of coatings based on magnesium compounds (1, 1^I), WK15 (2, 2^I), alloyed nichrome (3, 3^I) at P=10.0 MPa.

It was found that the microstructure of the coating is finely dispersed and constitutes a heterogeneous mixture, with the dominant phase mainly being nanosized inclusions of silicon carbides (SiC) in the presence of titanium carbides (TiC), zirconium (ZrC) and an almost uniform amount of inclusions of zirconium borides (ZrB_2), chromium (CrB_2), magnesium (MgB_2) and a fine aggregate of strengthening compounds, which are stable silicide compounds of the Cr_2Si_3, Zr_3Si_2, TiSi, Mg_2Si type. Intermetallic formations were also identified, which contribute to the stabilization of the structure and have the form of spherical nanoparticles of the NiTi, NiAl, $ZrCr_2$ type. In addition, fragments of ternary compounds in the form of MgSiC, Ti_3SiC_2, ZrSiC were found, which also have high thermodynamic properties. As defined, $AlMgB_{14}$ is a complex compound that has the property of dissolving titanium and zirconium carbides, forming solid solutions with high hardness. A qualitative determination of the structure was implemented through the microhardness of individual areas. Thus, local zones with a microhardness of 21-26 GPa correspond, in our opinion, to $AlMgB_{14}$ compounds strengthened by carbide phases, while micro areas determined by a microhardness of 5.5-6.8 GPa are probably titanium carbosilicides, and zones with a microhardness of about 12.0 GPa are titanium carbides, the value of 8.1 GPa most likely corresponds to titanium silicides, and the microhardness of 9.3-10.2 GPa is close to the values of magnesium oxides. Thus, the structural-phase formations of coatings based on ternary magnesium boride ($AlMgB_{14}$) include both chemical compounds, solid solutions, and mechanical mixtures, which are characterized by increased parameters of hardness, strength, wear resistance, significant temperature properties, and chemical inertness.

The formation of the structural-phase composition of coatings, as shown by the tests, is determined not only by the ratio of components, temperature, dispersion, but also depends on their defectivity and external conditions. It is certainly an axiom that tribochemical processes must occur when molecules in the conditions of interaction receive the necessary activation energy. Endothermic reactions do not occur at all without activation. The interaction of SiC with Mg, which is formed during the thermal decomposition of structurally free magnesium carbide and depends on the process temperature, is accompanied by the formation of magnesium silicide and magnesium acetylide, the latter under thermomechanical influence stimulates the formation of graphite through the intermediate dimagnesium tricarbide by the reaction type $2SiC+5Mg \rightarrow 2Mg_2Si+MgC_2$, $MgC_2 \rightarrow Mg_2C_3 \rightarrow Mg+C$. We note that under thermodynamic influence, the presence of a catalyst in the structure in the form of Al, Ni affects the decomposition of magnesium carbide. In addition, the presence of nickel carbide (Ni_3C), which is thermodynamically unstable, causes an exothermic decomposition reaction into metallic nickel and carbon in the form of graphite: $Ni_3C \xrightarrow{t} 3Ni + C$. The decomposition temperature is not fixed and depends, in particular, on the particle size. For nanoparticles, due to their high surface energy, the decomposition onset temperature is 200-300 °C.

The basis of physical phenomena initiating the mechanism of decomposition of carbide graphite are structural transformations in the solid phase caused by thermal influences. Factors determining the quality level of thermomechanical carbide graphitization include the degree of dispersion of structural components, external pressure, operating temperature, including the temperature in the contact zone, the presence of elements initiating decomposition processes, as well as the influence of the environment (in a vacuum, the probability of the amount of graphite increases), in addition, internal factors associated with the composition of the material, its structure and the presence of defects.

The passivating functions of secondary structures are performed by the finely dispersed microstructure of the surface layer, which constitutes a multiphase mixture with the convincing presence of thermodynamic compounds in the form of simple and complex stable oxides such as MgO, Al_2O_3, SiO_2, Mg_2TiO_4 and others. Binary oxides in the form of $MgO-TiO_2$, $MgO-ZrO_2$ have also been identified, and the possibility of the presence of ternary compounds based on magnesium oxide, such as $MgO-ZrO_2-TiO_2$, $MgO-Al_2O_3-TiO_2$, is not excluded.

The solubility of silicon dioxide (SiO_2) in magnesium oxide (MgO) is very low, but they interact to form magnesium silicates Mg_2SiO_4 or $MgSiO_3$ within heterogeneous structures. The reaction formula in the presence of carbon is: $2MgO_2+SiC+2C \rightarrow 2Mg+SiO_2+3C\text{-}Mg_2SiO_4$.

Electron microscopic study of coatings under friction loading conditions revealed that an ultradisperse structure with a fragment size of the order of 25-40 nm is formed in a thin (~15 nm) surface layer.

Analysis of electron diffraction patterns from the friction surface proves that diffusion halos reflect an object with an ultra-disperse structure, and textured maxima indicate a directional orientation of the specified structure. The emergence of an ultra-disperse structure on the friction surface proves that the plastic deformation of the surface layer is carried out by a rotational mechanism, due to the relative sliding of fragments of ultra-disperse structures (fig. 2).

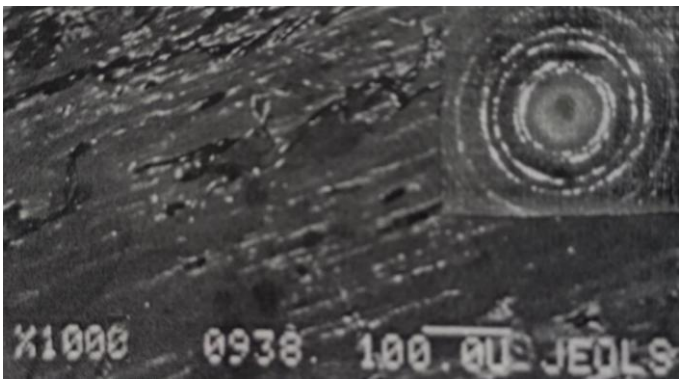

Fig. 2. Microscopic image of the structure of the local micro volume of the surface layer and micro electron diffraction pattern of a composite coating based on magnesium ternary boride (structure at a depth of 2-3 microns).

But, besides the ternary compound of aluminum, magnesium, boron ($AlMgB_{14}$) plays an important role in the surface complex of graphite-oxide structures, which complements the properties of the surface film, providing an additional increase in wear resistance while reducing friction coefficients. The results of X-ray structural analysis reveal the occurrence of activated phase transformations in magnesium structures, causing the formation of new phases, presumably due to intermediate compounds in the chains of transformations, the final product of which is, for example, oxides (Al_2O_3, CrO_3), carbides (Al_4C_3, Cr_7C_3), magnesium-based intermetallics. However, the ultradisperse structure determines their X-ray amorphousness. The presence of these phases indirectly confirms the high hardness.

When the sliding speed increases from 1.5 m/s, the specific work of wear reaches almost 104 kJ/mm^3, which provides the necessary and sufficient conditions for the thermal decomposition of magnesium carbide and, as a result, fragments of structurally free graphite appear on the friction surface (fig. 3). The shape of the particles of the graphite structure is close to scaly, consisting of polydisperse crystallites oriented in the direction of friction. The basis of the physical phenomenon that constitutes the mechanism of thermal decomposition of carbide phases is the process of structural transformation in the solid phase. The main factors that determine the limiting values of thermodynamic graphitization processes are the level of dispersion of structural components, specific pressure, operating temperature, ambient environment, initiating elements (C, Si, Ni, Al), in addition, internal factors are determined by the composition, structure, presence of defects, etc.

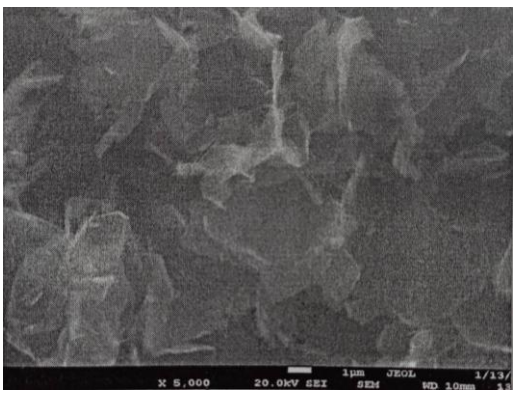

Fig. 3. Image of the local location of the structure of the α-graphite surface film (×500).

Self-lubrication of composite coatings of magnesium compounds depends on the formation of a graphite film (fig. 4). At test speeds of 2.8 m/s, the surface self-lubricating graphite-oxide film completely occupies the friction area and, at the same time, is a layer with the overwhelming majority of polydisperse graphite. At the same

time, the higher the temperature, the greater the amount of carbide graphite turns into a self-lubricating antifriction film and the longer the contact mating areas interact, the more graphite is formed.

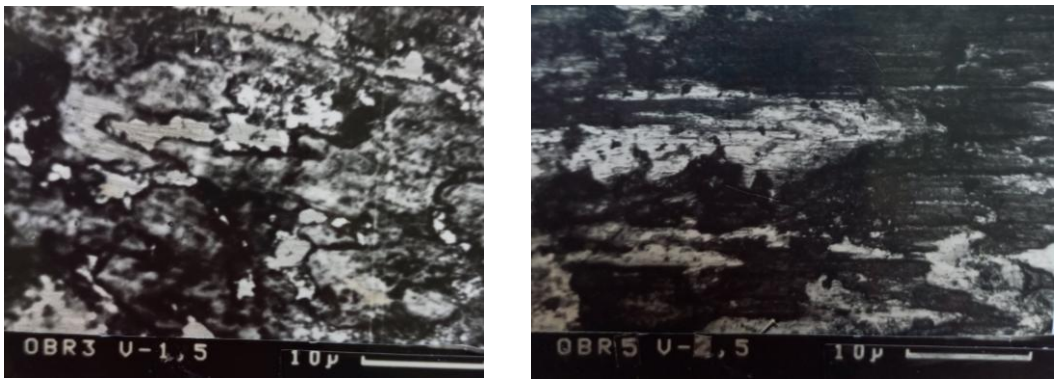

a b

Fig. 4. Surface topography during the formation of a graphite film: a) V = 0.18 m/s; b) V = 2.8 m/s.

Thus, the studied coatings based on magnesium compounds form self-lubricating ordered dynamic structures during friction. The self-lubricating function is provided by the triple additive interaction of both magnesium carbide, which is the source of carbide graphite formation, and layered oxide structures, which are characterized by low shear resistance, and the presence of effective aluminum-magnesium-boron compounds. The established complex of self-lubricating surface structures under friction conditions has an effective ability to self-heal and self-regulate. The real effect ensures the minimization of friction and wear parameters.

From the point of view of structural thermodynamics, the systemic ordering of surface films that are self-formed due to transformations can be considered as adequate elementary physicochemical processes and adaptation mechanisms in the process of structural adaptability [18].

The problem of coating quality is associated with the assessment of reproducibility and optimization of the technological process of spraying. To obtain high-quality coatings by optimizing the technological process, processing of technological parameters was implemented, including the particle size distribution, loading depth, barrel filling degree, working gas ratio and spraying distance [19]. Thus, by controlling the technological process of forming coatings based on magnesium compounds, it was possible to implement not only the desired chemical composition, but also to obtain a predicted structure during spraying, which has an optimal set of properties that ensure the stability of structural adaptability. At the same time, the possibility of obtaining constant quality was achieved, namely, the variation of strength and plastic properties in samples of one batch was stably about 5-10%.

As can be seen from the test results, the control coatings are significantly inferior in tribotechnical properties compared to the developed self-lubricating coatings made of magnesium compounds.

Thus, the detonation coatings developed on the basis of magnesium compounds, capable of self-lubrication, are characterized by high antifriction properties and, in terms of operational potential, open up the possibility of using them in obtaining competitive systems for tribotechnical purposes. The set of results obtained [20, 21] allows us to recommend composite coatings from magnesium compounds to increase the service life of parts made of nickel alloys, including, for example, disks, working and nozzle blades, combustion chamber pipes, turbine disks, etc. Their use is justified for increasing the technical level and efficiency of repair work when restoring worn parts, which allowed us to significantly increase wear resistance and solve the problem of restoring previously unrepaired parts. The proposed coatings, as evidenced by the test results, ensure the operational reliability of tribotechnical connections in accordance with the conditions that are put forward for new competitive materials of antifriction coatings obtained by the detonation method. Therefore, composite coatings developed on the basis of ternary magnesium carbide can be considered as an alternative to other promising materials for operation in components of modern technology, including aerospace.

It should be noted that the developed composite powder based on magnesium reagents for forming antifriction self-lubricating coatings can be used for any technological methods using powder materials.

Finally, we will determine that the development and testing of magnesium coatings, despite economic difficulties, is a necessary component of the technical and social development of both science and society as a whole.

Conclusions

Composite coatings based on ternary compounds of aluminum, magnesium, boron, characterized by low and stable coefficients of friction and wear intensity, have been developed and investigated. In the test mode at a load of 10.0 MPa, the developed coatings have friction parameters significantly lower than those of control coatings by 3.5-8.0 times.

Based on the results of mechanochemical technology, the formation of the composite structure and phase composition of a powder mixture of magnesium compounds for detonation-gas spraying was synthesized.

The optimal mode of spraying of the magnesium composition has been worked out, which reproduces not only the planned chemical composition, but also provides a predicted structure, which modernizes the friction surface and ensures guaranteed quality of coatings. At the same time, it is emphasized that during spraying, the variation of the strength and plastic properties of coatings in samples of one batch is stable and amounts to 5-10%.

The structural and phase composition of coatings based on magnesium compounds has been established as a multicomponent fine-grained aggregate with an almost uniform distribution of finely dispersed strong inclusions of carbides, borides, silicides and intermetallic formations in the presence of double and ternary magnesium compounds, which are generally characterized by increased thermodynamic properties, high wear resistance, hardness, strength and low coefficient of friction with significant chemical inertness.

The developed self-lubricating composite coatings based on magnesium compounds extend the achievements of modern tribotechnical materials science. The studied compositions, which are capable of self-lubrication, can be used both for strengthening and for high-quality restoration of worn parts by any technological methods using powder materials.

References

1. Mordyuk B. M., Ropyak L. Ya., Vitvitsky V. S., Piskun N. O., Malinin V. Yu. Structure and Properties of PEO Coatings Obtained on D16T Aluminum Alloy Under Various Process Parameters // Metal Physics and New Technologies. — 2025. — Vol. 47, No. 9. — Pp. 989–1002.

2. E. S. Gevorkyan, G. D. Semchenko, et al. New Materials and Technologies for Their Production. Kharkiv: Ukrainian State University of Railway Transport, 2016. 341 pp.

3. Mahmood Aliofkhazraei. Handbook of Mechanical Nanostructuring. John Wiley & Sons, 2016 p. - 816 pp.

4. Wear of Composite Materials. DE Gruyter, Berlin, 2018. ISBN 978-3-11-035298-63.

5. Y. Chen, L. Wu, W. Yao, J. Wu та ін. «Smart» micro/nano container-based self-healing coatings on magnesium alloys. Journal of Magnesium and Alloys, 2023. https://doi.org/10.1016/j.jma.2023.06.006

6. J. Zhang, X. Peng, P. Wu etc. Recent progress in protective coatings against corrosion upon magnesium–lithium alloys. Journal of Magnesium and Alloys, 2024. https://doi.org/10.1016/j.jma.2024.08.001

7. S. S. Shayan, M. R. Nakhaei etc. Emerging progress of chemical-based coating for the corrosion protection of magnesium alloys. Journal of Materials Research and Technology, 2023. https://doi.org/10.1080/01694243.2023.2252632

8. J. E. Gray, B. Luan Surface protection of Mg alloys in automotive applications. AIMS Materials Science, 2019. https://www.aimspress.com/article/doi/10.3934/matersci.2019.4.567

9. Shchepetov V. V., Fialko N. M., Bys S. S. Self-lubricating glass composite magnesium carbide nanocoating // Problems of Tribology. — 2025. — Vol. 30, No. 3/117. — pp. 62–68. https://doi.org/10.31891/2079-1372-2025-117-3-62-89

10. Tkachuk V. M., Marchenko O. I. Formation of nanostructured solid-lubricating coatings on magnesium alloys by plasma-electrolytic oxidation // Physical and Chemical Mechanics of Materials. — 2024. — No. 4. — pp. 45–52. https://pcmm.org.ua/category/2024-rik/nomer-4-60

11. Yao H., Zhao Y., Gao B., Li R., Gao T., Liu X., Gu X., Wang Z., Chang Q. Study on the Synergistic Lubrication Mechanism of Nickel and Magnesium Silicate Hydroxide in Molybdenum Disulfide-Based Composite Coatings // Lubricants. — 2026. — Vol. 14, No. 3. — P. 114. https://doi.org/10.3390/lubricants14030114

12. Chang Q., et al. Influence of Nano-Magnesium Silicate Hydroxide on Tribological Properties of Electroless Ni–P Coatings // Journal of Tribology (ASME). — 2025. — Vol. 147, No. 11. https://doi.org/10.1115/1.4068112

13. Anupam, Sandeep K. K., Pawan K., Amit G. Magnesium and Solid Lubricants based Self-lubricating Metal Matrix Composites: A Comprehensive Review and Future Directions // NanoWorld Journal. — 2023. — Vol. 9, No. S1. https://jnanoworld.com/articles/v9s1/nwj-s1-anupam.pdf

14. Wang L., Zhao X., Cui Y. Layered Magnesium Phosphate as an Environmentally Friendly Solid Lubricant via Hydrothermal Synthesis // ACS Sustainable Chemistry & Engineering. — 2023. — Vol. 11, No. 23. — P. 8540–8548. https://doi.org/10.1021/acssuschemeng.3c00877

15. Morales-Serna J. A., et al. Effect of magnesium stearate solid lipid nanoparticles as a lubricant excipient: film-forming tendencies // European Journal of Pharmaceutics and Biopharmaceutics. — 2023. — Vol. 193. — P. 154-162. https://doi.org/10.1016/j.ejpb.2023.11.004

16. Chen X., Liang J., Journal of Alloys and Compounds. Micro-arc oxidation of magnesium alloys with co-deposition of MoS2/MgO nano-additives for solid lubrication // Journal of Alloys and Compounds. — 2022. — Vol. 902. — P. 163. https://doi.org/10.1016/j.jmst.2021.11.053

17. Saji V. S. Surface Coatings on Biomedical Magnesium Alloys: Tribological and Corrosion aspects // Materials. — 2025. — Vol. 18, No. 14. — P. 341. https://doi.org/10.3390/ma18143411

18. Kostornov A.G. Tribotechnical materials science. Luhansk: Knowledge, 2012-701p.

19. Shchepetov V.V., Mirnenko V.I., Nedayborshch S.D. Mathematical modulation of the formation of detonation coatings \\ Technological systems. - 2016, No. 2. - pp. 82-88.

20. Shchepetov V.V., Fialko N.M., Bys S.S. Triboresistance of Composite Nanjcoatings Based on Magnesum Compounds at Elevated Temperatures\\ Journal of Modern Mechanical Engineering and Technology. - 2025, No. 12. - r. 45-50.

21. Shchepetov V.V., Fialko N.M., Bys S.S. Self-lubricating glass composite magnesium carbide nanocoating \\ Problems of Tribology, 30(3\117),62-68.https \\ doi.org\ 10.31891\2079-13722025-117-3-62-68.

Щепетов В.В., Фіалко Н.М., Бись С.С. Тверді мастильні нанопокриття на основі сполук магнію

Представлено результати досліджень тертя та зносу детонаційних композитних нанопокриттів на основі потрійної сполуки алюміній-магній-бор в умовах випробувань з постійним навантаженням у полі швидкості ковзання. Їх структурно-фазовий склад та пасивуючий комплекс поверхневих оксидних структур визначено за допомогою сучасних методів фізичного аналізу. Встановлено, що параметри інтенсивності зносу та коефіцієнти тертя мінімізуються завдяки сукупності поверхневих структур, які регенерують стабільний самозмащувальний структурований шар в умовах тертя. Визначено фактори, що впливають на формування динамічної рівноваги самозмащувального шару, що має ефективну здатність до самовідновлення. Водночас, безперервний захисний шар екранує процеси молекулярно-адгезійної взаємодії та блокує розвиток неприйнятних явищ руйнування.

Ключові слова: поверхневі структури, карбідний графіт, знос, проміжний шар, фазовий склад, самозмащування.

ISSN 2079-1372 ***Problems of Tribology****, V. 31, No 2/120-2026, 93-101*

Problems of Tribology
Website: http://tribology.khnu.km.ua/index.php/ProbTrib
E-mail: tribosenator@gmail.com

DOI: https://doi.org/10.31891/2079-1372-2026-120-2-93-101

Improved algorithm for calculating engineering parameters of a garbage truck compaction plate mechanism considering hydraulic cylinder wear

O.V. Bereziuk [1] 0000-0002-2747-2978, **V.I. Savulyak** [1] 0000-0002-4278-5155, **V.O. Kharzhevskyi** [2] 0000-0003-4816-2781, **S. Cv. Ivanov** [3] 0000-0002-7719-6086, **A.Ye. Alekseiev** [1] 0009-0009-0485-9414

[1] *Vinnytsia National Technical University, Ukraine*
[2] *Khmelnytskyi National University, Ukraine*
[3] *Technical University Sofia, Branch Plovdiv, Bulgaria*
E-mail: berezyukoleg@i.ua

Received: 25 April 2026: Revised 05 May 2026: Accept: 23 May 2026

Abstract

The article presents a scientifically based, improved methodology for the design calculation of the parameters of a garbage truck's sealing plate mechanism, developed through an analysis of scientific literature and taking into account the wear of its hydraulic cylinder, in order to determine the main geometric, force, and speed characteristics. The drive for the working components of the sealing plate mechanism is hydraulic and is powered by the garbage truck's pump station. The application of the proposed improved engineering calculation methodology allows for a significant reduction in design time and avoids unnecessary costs associated with conducting complex experimental and theoretical studies. Using the developed methodology, the main geometric, force, and speed parameters of the garbage truck's sealing plate mechanism were determined, taking into account the wear of the hydraulic cylinder. It has been established that further refinement of the engineering calculation methodology for the garbage truck's sealing plate mechanism using a load-sensitive scheme requires additional research.

Keywords: algorithm, design calculation method, hydraulic drive, consideration of wear, wear rate, wear intensity, hydraulic cylinder, mechanism, sealing plate, garbage truck, municipal solid waste.

Introduction

One of the priority directions of modern mechanical engineering is improving the reliability and wear resistance of machine executive mechanisms [1, 2], particularly in municipal equipment, which includes garbage trucks [3], that are mainly equipped with hydraulic drives for their working components [4, 5]. One of the main technologies for the primary processing of municipal solid waste (MSW), aimed at reducing transportation costs and minimizing the negative impact on the environment, is the compaction of waste directly during loading into the garbage truck. This approach makes it possible to significantly reduce transportation costs and decrease the area of landfills required for MSW disposal, which is of great economic and environmental importance. The process of compacting MSW in a garbage truck is carried out using a sealing plate, which is driven by a working hydraulic cylinder. During operation, this hydraulic cylinder is subject to intense wear due to a large number of operating cycles and high compaction forces caused by the nonlinear compression characteristics of MSW. Hydraulic cylinders are typically made of alloy steels; however, to increase their service life, it is advisable to apply wear-resistant coatings. The development of an improved method for the design calculation of the parameters of the garbage truck's sealing plate mechanism, taking into account the wear of its hydraulic cylinder, will contribute to more effective planning of the renewal, maintenance, and repair of garbage trucks.

Analysis of recent research and publications

Article [6] presents an analytical and statistical study of a model range of specialized equipment, including an analysis of its technical characteristics, for the purpose of developing a kinematic diagram of the compaction mechanism in a garbage truck; calculations were performed based on a method for modeling the structure of

component assemblies. The modeling was performed in SolidWorks Simulation. The developed kinematic diagrams of the components and assemblies for briquetting and compacting MSW operate at the rated power characteristics of the hydraulic equipment due to the distribution of drive power across the most energy-intensive operations. The usage of the principles of moments of inertia and the gravitational forces of the own mass of solid waste, made it possible to significantly (by 25%) reduce the energy intensity of the compaction process.

In [4], based on the results of computer modeling of the hydrodynamic processes of working fluid flow through a hydraulic valve, the values of pressure losses were determined. To reduce these losses, a design improvement to the hydraulic valve was proposed that does not affect its functional characteristics. Implementing these changes made it possible to reduce pressure losses in the working zone of the hydraulic distributor, which contributes to a reduction in total energy losses in the hydraulic drive system.

The research paper [7] studies the peculiarities of the process of pressing wood chips in screw presses and analyzes the processes occurring in specific sections of the screw. The identified dependences make it possible to calculate the loads on the screw flights and determine the power required to carry out the compaction process. In addition, the level of raw material heating and the specific energy consumption arising during compaction were determined.

Scientific article [8] presents a structural analysis of a garbage truck's compaction plate. In the first stage, parametric modeling was performed of the assembly consisting of the compaction plate, the counter-pressure plate, the rear section of the garbage truck, and the material being compacted. Dynamic modeling of the solid waste compaction process in the garbage truck was performed, and the mechanical stresses for the compaction plate were loaded into the SolidWorks Simulation. The finite element method was used, resulting in the determination of the values and distribution of equivalent stresses calculated according to the von Mises criterion, as well as the displacements and relative deformations of the compaction sealing plate of the analyzed garbage truck.

An exponential dependence of the change in the wear rate of the working hydraulic cylinder of the garbage truck's sealing plate mechanism on the magnitude of the compaction force was established in [9]. Taking this dependence into account makes it possible to improve the efficiency of maintenance and repair planning, which generally contributes to the improvement of the operational characteristics of garbage trucks. To make the analysis of the process more visual, a graphical relationship was plotted between the wear rate of the working hydraulic cylinder of the sealing plate mechanism of a garbage truck and the compaction force, which confirmed the sufficient consistency of the obtained results. It was established that for a Ukrainian-made KO-436 series garbage truck, the wear rate of the working hydraulic cylinder of the sealing plate mechanism, in accordance with the observed pattern, is 0.257 μm/h, and an increase in the pressing force from 30 MN to 150 MN results in a 3.6-fold decrease in the wear rate of the working hydraulic cylinder of the hydraulic press mechanism. This result is explained by the characteristics of the contact interaction between the working surfaces and the specifics of the mechanism's operation under different load levels.

The study [10] provides a comprehensive analysis of the kinematics and dynamics of the scraper pressing mechanism in a garbage truck using numerical methods. To study the mechanism's operation under actual working conditions over a full cycle lasting 18 seconds, a multi-body model was developed and integrated with a hydraulic simulation model. The model was validated by calculations at steady-state time points, which demonstrated high convergence. The results showed that the mechanism operates in steady-state conditions almost all the time, with hydraulic cylinder rod speeds ranging from 0.08 to 0.15 m/s. The speed and acceleration of the hydraulic cylinder fluctuate significantly when the mechanism accelerates or decelerates; however, the effect of inertia is negligible. The forces applied to the joints are greatest at the end of the pressing process. Notably, the force applied to the joint connecting the scraper plate and the sliding plate is the highest: three times higher than that applied to the joint between the sliding plate and the pressing hydraulic cylinder, and one and a half times higher than that between the scraper plate and the scraper hydraulic cylinder. The results of the study can be applied to the design process of garbage trucks in special and specialized vehicles in general or used as a guideline for improving performance and optimizing the weight, force, and materials of the mechanism.

According to research data [11], among the main components of side-loading garbage trucks, the hydraulic system has the shortest service life before failure, which is one of the key factors contributing to increased wear and tear on these vehicles. According to the results of the study [12], the structure and most common causes of failures in the hydraulic equipment of garbage trucks have been identified, among which hydraulic cylinders account for 34.92% (wear of seals and cuffs, rod, failure of piston fasteners, rod bending, mechanical damage), hydraulic pumps – 16.40% (wear of the working surfaces of the housing and gears, leakage through seals, formation of cracks in the housing), pipelines and flexible hoses – 15.34% (hose ruptures, degradation of pipelines), and hydraulic distributors – 13.23% (wear of sealing elements and spools, housing cracks).

Article [13] presents several design options for compaction mechanisms in garbage trucks and conducts a comparative analysis of their design and functionality. A kinematic analysis is performed on a mechanism used for a wide range of compaction through translational motion. Determining the motion characteristics of the working components of these mechanisms is necessary for a full understanding of their operation, especially for designing and improving their functional parameters to achieve low energy consumption.

An analysis of the causes of typical technical failures in garbage truck units, presented in [14], showed that a significant proportion of malfunctions (about 45%) is associated with hydraulic drive failure. The main causes

of such failures are manufacturing defects resulting from the use of low-quality components, as well as significant fluctuations in loads on working parts. Studies of working part failures indicate that the majority of malfunctions arise from defects in heat treatment and deviations in geometric dimensions during machining (35%), errors during assembly, adjustment, and tightening of threaded connections (30%), as well as poor-quality welding (30%). It has been established that the majority of failures (80–90%) are caused by wear and corrosion damage to the working surfaces of parts, with failure occurring after a critical level of degradation is reached, i.e., when the unit or its assembly reaches its limit technical condition. In particular, approximately 28% of all failures of hydraulic drive components occur in hydraulic cylinders, which is associated with wear of mating surfaces and deformations of the piston rod and cylinder during operation. A durability analysis showed that the average service life of hydraulic drive components, particularly hydraulic cylinders, is approximately one-third of their maximum service life; that is, 45–55% of the service life specified by the manufacturer is not actually achieved. The majority of hydraulic cylinder failures during the early stages of operation or after repairs are attributed to piston rods (31%) and sealing cuffs (42%). In addition, an analysis of hydraulic system component failures revealed that the primary manifestation of malfunctions is the loss of external and internal sealing caused by contamination of the working fluid, which leads to disruption of the normal operation of the units.

The scientific article [15] describes a mechanism for compacting solid waste using a transfer mechanism, which has been used with great success in the design of modern garbage trucks. In [16], a simulation using Finite Elements Analysis method (FEA) was performed to analyze the behavior of a similar compression plate structure in a garbage truck.

The study [17] provides a detailed distribution of the main causes of garbage truck failures, indicating that the key factors contributing to malfunctions are external and internal leaks in hydraulic systems. In particular, external leaks account for about 48% of all recorded failures and are mainly caused by damage to flexible hoses and pipelines, as well as leaks in the sealing elements of hydraulic cylinders and other components. Such defects lead to working fluid leaks, which negatively affect the overall functioning of the hydraulic system, reducing its efficiency and increasing the risk of serious accidents. In addition, internal leakage is a significant and fairly common cause of failures, accounting for approximately 36% of all malfunctions. This occurs due to a violation of the integrity between the working chambers of hydraulic components, leading to the flow of hydraulic fluid into non-working areas and a reduction in system pressure. Most often, such failures are observed in critical components of the hydraulic system, such as spool valves, relief and check valves, hydraulic cylinders, and hydraulic pumps. Since these units perform the primary functions of garbage trucks, their failure due to internal leaks significantly reduces the overall performance and reliability of the equipment.

A study [18] found that “conical” wear of the hydraulic cylinder rod in the range of 0.2–0.4 mm along its length prior to the first major repair leads to a 7.2% decrease in pressure in the hydraulic system, an 11.4% increase in specific fuel consumption, and a 26% increase in carbon monoxide content in the exhaust gases. Further increase in rod wear in the working section to 0.6–0.7 mm causes a 13.4% decrease in hydraulic system pressure, a 21.3% increase in specific fuel consumption, and a significant increase in exhaust gas toxicity ranging from 25% to 59%, exceeding permissible regulatory limits. A value of no more than 0.4 mm is proposed as the maximum permissible wear limit for the geometric parameters of the hydraulic cylinder rod in the hydraulic drive systems of construction and road machinery. In addition, it has been established that rod wear negatively affects the physicochemical properties of the working fluid, in particular increasing the content of iron and mechanical impurities by approximately two times, which requires more frequent replacement of the working fluid and leads to its overconsumption. Overall, this significantly reduces the efficiency and durability of the hydraulic drive, shortening its service life in construction and road machinery.

Article [19] presents a structural analysis of the wear parts in the compaction mechanism of a garbage truck. 3D parametric modeling was performed for the compaction plate, the dump body, the compaction material, the push plate, and the wear parts. Dynamic modeling of the solid waste compaction process inside the body was performed, and the mechanical stresses on the wear parts obtained as a result of the dynamic modeling were imported into the finite element analysis module of the SolidWorks software.

The paper [20] notes that wear of sealing elements in hydraulic systems causes the gradual infiltration of working fluid into non-operational cavities of hydraulic machines. Although this process is not always visible externally, it leads to unproductive power losses in the hydraulic drive, which, in turn, causes excessive consumption of fuel and lubricants, as well as a reduction in the power of the working components. Power losses caused by seal degradation can result in non-optimal hydraulic motor operating conditions, which negatively affects the overall efficiency of the hydraulic drive system. The mechanical system “hydraulic cylinder – sealed piston – compressed hydraulic fluid” is examined, for which the relationship between the hydraulic cylinder’s efficiency and the degree of leakage is established. The amount of piston sinkage when using VMGZ working fluid is also determined, and the mechanism of fluid leakage through the hydraulic cylinder’s sealing elements is analyzed.

The authors of the article [21], in their analysis of operational observations of garbage trucks, found that the largest proportion of failures is associated with wear and corrosion damage to the working surfaces of the working equipment components. Failures of hydraulic cylinders caused by wear of mating surfaces and deformations of the piston rod and cylinder during operation account for 32% of the total number of hydraulic drive component failures. This situation is explained by uneven loading of the body and intense abrasive effects under the demanding operating conditions of garbage trucks. An investigation into the causes of failures revealed

that the primary factor is the wear of the working surfaces of key hydraulic drive components, specifically spools and hydraulic manifold housings, as well as hydraulic cylinder rods. It has been determined that the dominant failure mechanism is hydro-abrasive wear, which occurs as a result of untimely replacement of the hydraulic fluid and the use of low-quality or worn sealing elements, such as hydraulic cylinder seals. This facilitates the entrance of dust and wear products into the sliding zone, which accelerates the degradation of working surfaces. As one of the promising methods for restoring worn parts in operation, chromium plating in a cold self-regulating electrolyte is proposed, which ensures the production of high-quality chromium coatings with high productivity.

The paper [22] investigates a rear-loading garbage truck, which is considered as a system consisting of several main components: the vehicle chassis, the truck body, a hydraulic cylinder, a compaction mechanism, and a push plate. The garbage truck body is rigidly mounted on the chassis frame, providing a reliable structural foundation for all operational activities. Located at the rear of the vehicle is the compaction mechanism, which is responsible for receiving waste and initially compacting it before further transfer into the body. After initial compaction, the waste is pushed into the garbage truck body by a scraper that interacts with the compaction mechanism. Each load of compacted waste, as well as the portion of waste being loaded, is gradually pushed toward the rear of the truck body. At the same time, the push plate continuously moves backward, creating the necessary pressure for compaction and uniform distribution of waste throughout the body. The push plate assembly consists of a front plate, frame, guide rail frame, cylinder supports, and other components. As a critically important load-bearing component of rear-loading garbage trucks, the mechanical characteristics of this plate directly affect the vehicle's performance, determining the efficiency of loading, compaction, transportation, and unloading of solid waste.

The scientific article [23] presents a nonlinear mathematical model that is described by a system of differential equations with corresponding boundary conditions and characterizes the operation of the hydraulic drive of a garbage truck's compaction pressing plate mechanism, particularly during the static compaction of solid waste, which is a significant stage in its initial processing. At the same time, despite the model's high accuracy and level of detail, it does not account for the effect of wear on the power hydraulic cylinder, which is one of the key elements of the hydraulic drive. Ignoring this factor may limit the model's applicability for long-term forecasting of the mechanism's performance under real operating conditions, where hydraulic cylinder wear significantly affects the system's performance and reliability.

The materials of the work [24], based on a detailed analytical study of a mathematical model, identify the main dependencies of the functioning of vibrating and vibro-impact machines operating with a hydraulic pulse drive equipped with a single-stage pulsator valve. The developed model made it possible to describe the dynamic processes occurring in the hydraulic system and the machine's working parts, as well as to analyze the nature of pressure pulse formation and their effect on the kinematic and force parameters of vibrational motion. The study established relationships between the design parameters of the hydraulic pulsation drive, its operating modes, and the dynamic characteristics of the machines, specifically the amplitude and frequency of oscillations, as well as the energy of impact pulses. The results obtained made it possible to determine the conditions for stable operation of vibrating and vibro-impact machines, estimate the effectiveness of using a hydraulic pulse drive in various operating modes, and formulate recommendations for optimizing the parameters of the pulse valve to improve the performance, reliability, and energy efficiency of such machines, which is necessary for the further development of a methodology for the design calculation of their parameters.

However, during the review of the available literature, the authors did not identify a comprehensive methodology for the design calculation of the parameters of a garbage truck's sealing plate mechanism that takes into account the wear of its hydraulic cylinder.

Aims of the article

Development of a scientifically based, improved method for the design calculation of the parameters of a garbage truck's sealing plate mechanism, taking into account the wear of its hydraulic cylinder, with the aim of determining its main geometric, force, and speed parameters.

Methods

The following methods were used in this study: analysis of scientific literature; synthesis of mathematical relationships between the main geometric, force, and speed parameters of the equipment; and a systematic approach to account for the interaction of all the machine's subsystems.

Results

Figure 1 shows a schematic diagram of a garbage truck's operation during the static compaction of municipal solid waste (MSW), taking into account hydraulic cylinder wear [23], in which the following structural elements and values are indicated: PP – pressing plate; HC – hydraulic cylinder; HD – hydraulic distributor; P – hydraulic pump; SV – safety valve; F – filter; T – working fluid tank. The diagram also shows the following main geometric, kinematic, and force parameters: p_1, p_2, p_3, p_4 – pressures at the pump outlet, hydraulic cylinder inlet,

hydraulic cylinder outlet, and filter inlet, respectively; W_1, W_2, W_3, W_4 – volumes of pipelines between the pump and hydraulic distributor, hydraulic distributor and hydraulic cylinder inlet, hydraulic cylinder outlet and hydraulic distributor, hydraulic distributor and filter; Q_P – actual pump flow rate; S_P – nominal cross-sectional area of the distributor opening; S_f – surface area of the filter element; k_f – specific filter capacity (not shown in the diagram); μ_d – dynamic viscosity coefficient (not shown in the diagram); D, d – diameters of the piston and rod; G_p – weight of the pressing plate; G_c – weight of the hydraulic cylinder; G_{W1} – weight of the waste above the pressing plate; G_{W2} – weight of the waste outside the pressing plate; F_{FR} – friction force between the pressing plate and the guides; F_{TW} – the friction force between the MSW and the body; F_C – the force developed by the hydraulic cylinder; h_1, h_2 – the heights of the bottom and top of the press plate; b – the width of the press sealing plate (not shown in the diagram); δ – the thickness of the press plate; α – the angle of inclination of the press plate; x – the displacement of the press plate.

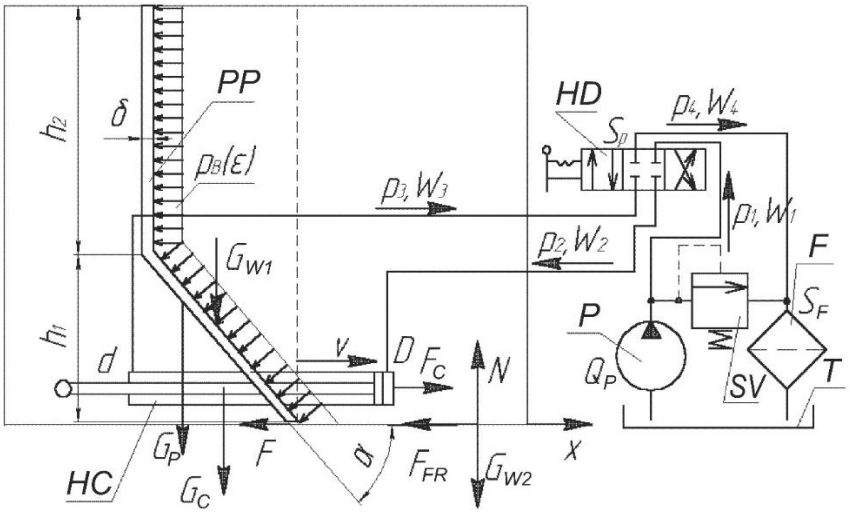

Fig. 1. Schematic diagram of the hydraulic drive for the pressing plate during static compaction of MSW, taking into account hydraulic cylinder wear

Let's determine the area of the pressure chamber of the hydraulic cylinder in the garbage truck's sealing plate mechanism

$$S_{C1} = \pi D^2/4 \ \text{[m}^2\text{]},$$

where S_{C1} – the cross-sectional area of the pressure chamber of the hydraulic cylinder in the sealing plate mechanism of a garbage truck, m^2; D – the diameter of the hydraulic cylinder piston in the garbage truck's sealing plate mechanism, m.

The wear rate of the working hydraulic cylinder in the sealing plate mechanism of a garbage truck is determined according to the formula in [9]:

$$v_u = 7.153\cdot 10^{-5} \mathrm{e}^{-1.047\cdot 10^{-8} p_2 S_{C1}} [\mu\text{m/s}], \tag{2}$$

where v_u – rate of wear on the hydraulic cylinder, μm/s; p_2 – pressure in the pressure chamber of the hydraulic cylinder of the garbage truck's sealing plate mechanism, Pa.

Determination of the duration of MSW compaction in a garbage truck, taking into account the wear of the hydraulic cylinder of the sealing plate [25]:

$$t \approx \frac{1}{\beta_p} \ln\left[\frac{p_2 S_{C1}^2}{m_r \beta_p (Q_P - \alpha_\sigma)} + \frac{\beta_\sigma}{\beta_p (Q_p - \alpha_\sigma)}\right] \ \text{[s]}, \tag{3}$$

where α_σ, β_σ – approximation coefficients for the dependence of working fluid losses on the duration of hydraulic cylinder wear; m_r – the reduced mass of the moving parts, kg; β_p – the coefficient of approximation of the dependence of the MSW compaction pressure on the duration of the process; Q_P – actual pump flow rate, m^3/s.

Let's calculate the number of trips the garbage truck will make:

$$n_T = n_{WD} \frac{T - 2l_0/v}{t_L + 2l_L/v + t_U}, \tag{4}$$

where n_{WD} – number of working days; T – duration of the workday, hours; l_0 – zero (initial) mileage, km; v – speed, km/h; t_L – loading time, hours; l_L – distance to the solid waste landfill, km; t_U – unloading time, hours.

Determination of the number of operating cycles of the hydraulic cylinder in the garbage truck's sealing plate mechanism:

$$n_{c.HC} = n_P \frac{Vk_c}{V_C}, \tag{5}$$

where V – the volume of the garbage truck's body, m^3; k_c – solid waste compaction ratio; V_C – volume of the solid waste container, m^3.

Determination of the wear of the working hydraulic cylinder in the compaction plate mechanism of the garbage truck using the following formula:

$$u = v_u t n_{c.HC} \ [\mu m]. \tag{6}$$

The flow loss coefficient of the working fluid from the high-pressure region to the low-pressure region, taking into account hydraulic cylinder wear, is determined using the formula [26]:

$$\sigma = \frac{\pi D\left(\delta_0 + 10^{-6}u\right)^3}{12\nu\rho_{WF}l} \ [m^5/(N\cdot s)], \tag{7}$$

where δ_0 – nominal clearance, m; ν – kinematic viscosity of the working fluid, m^2/s; ρ_{WF} – density of the working fluid, kg/m^3; l – length of the circular clearance, m.

Let's calculate the friction distance

$$s = 2x_{\max} n_{c.HC} \ [m], \tag{8}$$

where $x_{\max}$ – length of stroke of the hydraulic cylinder in the sealing plate mechanism of the garbage truck, m.

Determination of the wear rate of the hydraulic cylinder in the garbage truck's sealing plate mechanism using the following formula:

$$I_h = u/s. \tag{9}$$

Determination of the required chromium content in the protective coating of the hydraulic cylinder for the sealing plate mechanism of a garbage truck [27]:

$$C_{Cr} = 1.36\cdot10^3 I_h + C_{Fe}(9.08 - 0.416C_{Ni}) + 75.6 \ [\%], \tag{10}$$

where C_{Cr} – chromium content in the coating Fe-Cr-Ni, %; C_{Fe} – iron content in the coating Fe-Cr-Ni, %; C_{Ni} – nickel content in the coating Fe-Cr-Ni, %.

The parameters of the sealing plate mechanism on a garbage truck, taking into account the wear of its hydraulic cylinder, calculated using the proposed method, are shown in the Table 1.

Table 1

The main parameters of the sealing plate mechanism on a garbage truck, taking into account the wear of its hydraulic cylinder

S_{C1}, m^2	$v_{u.pzu}$, μm/s	t, s	n_P, trips	n_{cHC}, cycles	u, μm	σ, m^5/(N·s)	s, m	I_h, μm/m	C_{Cr}, %
$9.5\cdot10^{-3}$	$7.15\cdot10^{-5}$	74.9	719	14380	77	$1.424\cdot10^{-10}$	25884	$2.97\cdot10^{-3}$	46.6

The parameters of the sealing plate mechanism on a garbage truck, taking into account the wear of its hydraulic cylinder, were obtained based on the following initial data: D = 0.11 m; p_2 = 9.68 MPa; Q_P = 55 l/min; $\alpha_\sigma = -3.573\cdot10^{-9}$ m^3/s; $\beta_\sigma = 1.443\cdot10^{-9}$ m^3/s^2; m_p = 330 kg; β_P = 0.00217; n_{WD} = 127 days; T = 8 hours; l_0 = 3 km; v = 60 km/h; t_3 = 0.389 hours; l_L = 30 km; $t_U = 5.6\cdot10^{-3}$ hours; V = 10 m^3; k_c = 2.2; V_C = 1.1 m^3; δ_0 = 0.136 mm; $\nu = 1.83\cdot10^{-5}$ m^2/s; ρ_{WF} = 890 kg/m^3; l = 0.12 m; $x_{\max}$ = 0.9 m; C_{Fe} = 25 %; C_{Ni} = 25 %.

The usage of the proposed improved method for engineering calculations of the parameters of a garbage truck's sealing plate mechanism, taking into account the wear of its hydraulic cylinder, makes it possible to

significantly reduce design time and avoid unnecessary costs associated with labor-intensive experimental and theoretical research.

The development of an improved method for engineering calculations of the sealing plate mechanism in a garbage truck using a load-sensitive model requires further research.

Conclusions

Scientifically based improved algorithm for the design calculation of the parameters of a garbage truck's sealing plate mechanism, taking into account the wear of its hydraulic cylinder, is proposed, which allows to determine its main geometric, force, and speed parameters. It has been established that the development of an improved methodology for engineering calculations of the sealing plate mechanism of a garbage truck using a load-sensitive scheme requires further research.

References

1. Dykha A., Sorokatyi R., Pasichnyk O., Yaroshenko P., Skrypnyk T. (2020, December) Machine wear calculation module in computer-aided design systems. In IOP Conference Series: Materials Science and Engineering, 1001(1), 012040, https://doi.org/10.1088/1757-899X/1001/1/012040

2. Kindrachuk M.V., Kharchenko V.V., Marchuk V.Y., Humeniuk I.A., Leusenko D.V. (2024) Methodology for Selecting Compatible Metal Materials for Friction Pairs During Fretting-Corrosion Wear. Metallophysics & Advanced Technologies, 46(7), 637-648, https://doi.org/10.15407/mfint.46.07.0637

3. Holenko K., Dykha O., Koda E., Kernytskyy I., Horbay O., Royko Y., Fornalchyk Y., Berezovetska O., Rys V., Humenuyk R., Berezovetskyi S., Żółtowski M., Baryłka A., Markiewicz A., Wierzbicki T., Bayat H. (2024) Structure and strength optimization of the Bogdan ERCV27 electric garbage truck spatial frame under static loading. Applied Sciences, 14(23), 11012, https://doi.org/10.3390/app142311012

4. Petrov O., Kozlov L., Lozinskiy D., Piontkevych O. (2019) Improvement of the hydraulic units design based on CFD modeling. In: Lecture Notes in Mechanical Engineering XXII, 653-660, https://doi.org/10.1007/978-3-030-22365-6_65

5. Polishchuk L.K., Piontkevych O.V., Svietlov A.V., Adler O.O., Lozinskyi D. (2025) Development and optimization of the control devicefor the hydraulic drive of the belt conveyor. Informatyka, Automatyka, Pomiary w Gospodarce i Ochronie Środowiska, 15, 124-129, http://doi.org/10.35784/iapgos.7051

6. Savinkin V.V., Kuznetsova V.N., Abilmazhinova A.S. (2020) Development of an Energy-Efficient Rotary Inertia Device for Briquetting Household Solid Waste (HSW). World of transport, 18(1), 38-57, https://doi.org/10.30932/1992-3252-2020-18-38-57

7. Tataryants M.S., Zavinsky S.I., Troshin A.G. (2015) Development of a methodology for calculating loads on the screw and energy consumption of screw presses. ScienceRise, 6 (2), 80-84, https://doi.org/10.15587/2313-8416.2015.44378

8. Voicu G., Lazea M., Constantin G.A., Stefan E.M., Munteanu M.G. (2020) Finite element analysis of the compaction plate from a garbage truck. In E3S Web of Conferences, 180, 04006, https://doi.org/10.1051/e3sconf/202018004006

9. Bereziuk O.V., Savulyak V.I., Kharzhevskyi V.O., Alekseiev A.Ye. (2024) Determination of the regularity of the rate of wear of the working hydraulic cylinder of the mechanism of the sealing plate of the garbage truck from the pressing force. Problems of Tribology, 29(1/111), 38-44, https://doi.org/10.31891/2079-1372-2024-111-1-38-44

10. Pham M.Q., Vu T.V., Tran L.Q., Nguyen H.H., Hong T.D. (2024) Study on Kinetics and Dynamics of the Scraping-pressing Mechanism of the Compactor Garbage Truck. FME Transactions, 52(4), 603, http://dx.doi.org/10.5937/fme2404603Q

11. Nosenko A.S., Domnickij A.A., Altunina M.S., Zubov V.V. (2019) Theoretical and experimental research findings on batch-operation bin loader with hydraulically driven conveying element. MIAB. Mining Informational and Analytical Bulletin, 11, 119-130, http://dx.doi.org/10.25018/0236-1493-2019-11-0-119-130

12. Lobov N.V., Maltsev D.V., Genson E.M. (2019) Improving the process of transport of solid municipal waste by automobile transport. Proceedings of IOP Conference Series: Materials Science and Engineering. IOP Publishing, 1(632), 012033, https://doi.org/10.1088/1757-899X/632/1/012033

13. Voicu G., Lazea M., Zabava B.S., Tudor P., Moise V. (2019) Cinematical analysis of the pre-taking and pre-compacting mechanisms of some garbage trucks. Journal of Engineering Studies and Research, 25(2), 56-62, https://doi.org/10.29081/jesr.v25i2.35

14. Kotomchin A.N., Lyakhov Yu.G. (2019) Analysis of failures of knots and units of construction, road, lifting and transport machines and specialized motor transport on the example of MUE «Communalderservice». Engineering & Computer science, 3, 174-178.

15. Anghelache D., Tăbăraşu A.M., Persu C., Dumitru I., Stroescu G., Dumitru D., Voicu G. (2020) Aspects regarding the operation of mobile technical systems for collection and compaction by translation of municipal waste. ISB-INMA TEH' 2020, Agricultural and mechanical engineering, Bucharest, Romania, 30 October 2020, 181-185, https://www.cabidigitallibrary.org/doi/pdf/10.5555/20210291248

16. Lazea M., Voicu G., Constantin G.A., Zabava B.Ș., Tudor, P. (2021) Translation compaction systems used in waste collection and transportation. Acta Technica Corviniensis-Bulletin of Engineering, 14(1), 97-100, https://www.cabidigitallibrary.org/doi/full/10.5555/20209905712

17. Kabashev R.A. (1997) Road and construction machines: abrasive wear of the working parts of earthmoving machines. Almaty: Gylym.

18. Nurakov S.N., Savinkin V.V. (2008) About development methods for calculating the wear of the rod cylinder interface of hydraulic machines. Proceedings of the Karaganda State Technical University, 3 (32), 96.

19. Lazea M., Constantin G.A., Stoica D., Voicu G. (2020) Fem structural analysis for wear parts supporting counterpressure plate from a municipal solid waste truck. Revista romana de materiale-romanian journal of materials, 50(2), CP1-CP3, https://doi.org/10.1051/e3sconf/202018004006

20. Shalapai VV, Machuga OS (2023) Vtraty potuzhnosti u hidrotsylindri vnaslidok protikannia hidravlichnoi ridyny cherez neshchilnist [Power loss in the hydraulic cylinder due to hydraulic fluid leakage through non-tightness]. Comprehensive quality assurance of technological processes and systems –2023: Proceedings of the XIII International Scientific and Practical Conference, May 25-26, 2023, Chernihiv. National University "Chernihiv Polytechnic", 287-289.

21. Kargin R.V., Yakovlev I.A., Shemshura E.A. (2017) Modeling of workflow in the grip-container-grip system of body garbage trucks. Procedia Engineering, 206, 1535-1539, https://doi.org/10.1016/j.proeng.2017.10.727

22. Ding F.S., Lyu H.M., Chen J., Cao H.R., Zhang L.X. (2025) Multi-Objective Optimization Design of the Ejector Plate for Rear-Loader Garbage Trucks. Strojniški vestnik-Journal of Mechanical Engineering, 71.5-6, 169-178, https://doi.org/10.5545/sv-jme.2024.1185

23. Bereziuk O.V. (2005) Vibratsiinyi hidropryvod plyty presuvannia tverdykh pobutovykh vidkhodiv u smittievozakh [Vibration hydraulic drive of the solid waste pressing plate in garbage trucks] Diss. Cand.of Eng.Sciences: 05.02.03 –Drive systems, Vinnytsia, 217.

24. Iskovich-Lototsky R., Kots I., Ivanchuk Y., Ivashko Y., Gromaszek K., Mussabekova A., Kalimoldayev M. (2019). Terms of the stability for the control valve of the hydraulic impulse drive of vibrating and vibro-impact machines. Przeglad Elektrotechniczny, 4(19), 19-23, https://doi.org/10.15199/48.2019.04.04

25. Bereziuk O.V., Savulyak V.I., Kharzhevskyi V.O., Ivanov S.Cv., Alekseiev A.Ye. (2025) Analytical study of an improved mathematical model of the hydraulic drive of the garbage truck's sealing plate mechanism, taking into account the wear of its hydraulic cylinder. Problems of Tribology, 30(4/118), 62-71, https://doi.org/10.31891/2079-1372-2025-118-4-62-71

26. Perekrestov A.V. (1983) Zadachi po obiemnomu hidropryvodu [Problems on volumetric hydraulic drives]. Kyiv: Vyscha Shkola. Golovne vydannya. 144 p.

27. Bereziuk O.V., Savulyak V.I., Kharzhevskyi V.O., Alekseiev A.Ye. Dependence of wear intensity on the coating material of the hydraulic cylinder of the garbage truck's sealing plate // Problems of Tribology. 2024. No. 29(4/114). P. 40-46. https://doi.org/10.31891/2079-1372-2024-114-4-40-46

Березюк О.В., Савуляк В.І., Харжевський В.О., Ivanov S.Cv., Алексеєв А.Є. Удосконалений алгоритм інженерних розрахунків параметрів механізму ущільнюючої плити сміттєвоза із урахуванням зносу його гідроциліндра.

У статті на основі аналізу наукових літературних джерел розроблено науково обґрунтовану удосконалену методику проєктного розрахунку параметрів механізму ущільнюючої плити сміттєвоза з урахуванням зношування його гідроциліндра для визначення основних геометричних, силових і швидкісних характеристик. Привод робочих органів механізму ущільнюючої плити є гідравлічним і живиться від насосної станції сміттєвоза. Застосування запропонованої удосконаленої методики інженерного розрахунку дозволяє істотно скоротити тривалість проєктування та уникнути невиправданих витрат, пов'язаних із проведенням складних експериментальних і теоретичних досліджень. За допомогою розробленої методики визначено основні геометричні, силові та швидкісні параметри механізму ущільнюючої плити сміттєвоза з урахуванням зносу гідроциліндра. Встановлено, що подальше вдосконалення методики інженерного розрахунку механізму ущільнюючої плити сміттєвоза із використанням схеми чутливої до навантаження потребує додаткових досліджень.

Ключові слова: алгоритм, методика проєктного розрахунку, гідропривод, урахування зносу, швидкість зношування, інтенсивність зносу, гідроциліндр, механізм, ущільнююча плита, сміттєвоз, тверді побутові відходи.

ISSN 2079-1372 Problems of Tribology, V. 31, No 2/120-2026, 102-110

Problems of Tribology
Website: http://tribology.khnu.km.ua/index.php/ProbTrib
E-mail: tribosenator@gmail.com

DOI: https://doi.org/10.31891/2079-1372-2026-120-2-102-110

Forecasting the resource of machine parts based on the dynamics of changes in the wear mechanism using the neural network method

V.V. Aulin* 0000-0003-2737-120X, **V.M. Chumak** 0009-0002-1913-9371, **S.V. Lysenko** 0000-0003-0845-7817

Central Ukrainian National Technical University, Ukraine
**E-mail: AulinVV@gmail.com*

Received: 30 April 2026: Revised 08 May 2026: Accept: 23 May 2026

Abstract

The problem of predicting the residual resource of tribocouplings of resource-determining parts of automotive and agricultural machinery under conditions of operational change of the dominant wear mechanism is considered. It is shown that in real operating conditions the wear mechanism does not remain static: degradation of lubricants, change of load-speed regimes and variability of soil conditions cause a transition from a regular mechanism to an emergency one, which is accompanied by a sharp reduction in the residual resource of machine parts. A two-stage system for identifying the change in the dominant wear mechanism is proposed, combining a classifier based on long short-term memory with an entropy transition detector, which develops an entropy approach to the analysis of tribosystems. The data set is formed on the basis of a modified Archard model with five calibrated coefficients for different lubrication modes and a Palmgren-Miner model in the form of an endurance curve with realistic values of the basic number of cycles 10^8...10^9 for different materials of tribocoupling parts. Validation on eight scenarios of transition between wear mechanisms demonstrated reliable detection of the change in the dominant mechanism, the warning time for reaching a critical state of 229…593 hours for automotive parts and 13…21 hours for agricultural parts, which is 5.6…7.1% of the total resource and is sufficient for planning maintenance of machines.

Key words: parts life, wear, tribocoupling, change in wear mechanism, entropy transition detector, artificial neural network, condition-based maintenance.

Introduction

Forecasting the residual life of tribocouplings of resource-determining parts of automotive and agricultural machinery is a fundamental task of ensuring the reliability of machines. In the classical formulation, this task is based on the assumption of constancy of operating conditions and staticity of the dominant wear mechanism of the part. Accordingly, the life of the part is considered as a deterministic indicator determined by the parameters of the tribotechnical contact and the operating modes of the tribocoupling [1, 2].

However, many years of experimental studies of tribological processes in tribocouplings of automotive equipment have shown that the real dynamics of wear is significantly more complicated. Crankshaft bearings of internal combustion engines in normal operation operate in the hydrodynamic lubrication mode, in which the working antifriction layer (babbitt B83 with a hardness of HV 22…30 or bronze BrO10S10 with HV 75…90) is mainly subjected to fatigue contact wear. However, the degradation of lubricants – a decrease in the viscosity of motor oil below critical values, contamination with wear products, oxidation – leads to the transition of tribocontact to the boundary lubrication mode. In the boundary mode, the adhesive wear mechanism becomes dominant , which ends with bearing seizure tens of hours from the moment of transition. Engine cylinder liners (SCh25, HV 400) are subject to corrosive and mechanical wear, but the use of fuel with a high sulfur content intensifies the corrosive component and changes the balance of mechanisms. Gears of gearboxes (steel 40X, HV 550) are subject to normal fatigue damage of the teeth, but systematic overloads or lack of lubrication transfer the tribocontact to the seizure mode, i.e. adhesive wear with emergency failure.

For the working bodies of agricultural machinery, the situation is even more complicated due to the openness of the tribosystem and direct interaction with the abrasive soil environment. The intensity of abrasive-soil wear of plowshares (steel 65G, HV 380), harrow discs and cultivator paws depends on the sandiness , humidity and stonyness of the soil in a nonlinear manner. Changing the type of soil even within one field, for example, the

transition from black soil to a plot with stony inclusions - can lead to a change in the abrasive-soil mechanism to an impact-abrasive one, which significantly reduces the resource of the plowshare from 300 to 80 hours.

This indicates the absence of methods for predicting the service life of machine parts that take into account the dynamic change of the dominant wear mechanism over time. Classical deterministic service life models are fundamentally unable to describe situations when, within one operational cycle, the tribosystem loses thermodynamic stability and enters a new wear regime with a sharply different intensity.

Literature review

Studies of tribological processes in the details of automotive and agricultural machinery are actively developing in the works of domestic scientists [3, 4, 5, 6]. In particular, in works [3, 4], the parameters of the lubrication process during operational wear of crankshaft bearings and the patterns of interaction of the working bodies of soil-tillage machines with the soil environment were studied in detail. In work [5], the tribological processes of interaction of the soil environment with the working bodies of soil-tillage and earth-moving machines reinforced with composite materials were considered. In work [6], the influence of technological parameters of strengthening on the wear resistance of steel 45, which is widely used in the manufacture of working bodies of agricultural machines, is shown. The theoretical basis for understanding the nature of transitions between wear mechanisms can be the entropic approach to the analysis of tribological systems, developed in works [7, 8]. The change in the characteristics of the friction zones of the mating parts can be identified through the analysis of entropy production. The loss of thermodynamic stability of the tribological system is accompanied by an increase in entropy, which is a physical sign of a change in the wear regime. The fundamental limitation of traditional entropic analysis is the need for direct measurement of the thermodynamic parameters of the tribological contact, which in real operating conditions is a difficult technical task. In works [9, 10, 11], complex approaches to tribotechnical diagnostics and energy interpretation of the wear processes of tribosystems have been developed. In works [12, 13, 14], methods of computational prediction of contact wear resistance and durability of tribocouplings have been considered. Classical wear maps [17] showed the dependence of the dominant mechanism on the load and sliding speed. At the same time, these maps are static and do not take into account the dynamics of changes in the operating conditions of tribocouplings of machine parts over time. With the development of the theory of artificial neural networks and the accumulation of computing resources, a fundamental opportunity has appeared to process multidimensional time series of mediated sensor data (temperature, pressure, vibration, acoustic emission, oil analysis) and to identify patterns related to the state of tribosystems. The work [19] demonstrated the significant potential of machine learning methods for tribological tasks – wear prediction, optimization of material selection, analysis of lubrication modes. In particular, recurrent neural networks of the long short-term memory type [18] are able to model the dynamics of tribological processes in time, revealing nonlinear dependencies between tribological contact parameters and the state of wear. This makes the neural network approach a natural tool for the practical implementation of entropic principles of tribological systems analysis in systems for technical maintenance of machine parts mating by state. It should be noted that the vast majority of studies using machine learning in tribology focus on static prediction of wear intensity or classification of defect type from vibration signals, rather than on dynamic identification of changes in the dominant wear mechanism. Existing expert systems for mechanism classification based on formalized rules provide 92% accuracy for a single static identification, but they are unable to track the dynamics of the transition over time. This creates a critical research gap: an approach is needed that integrates physically based wear models (Archard, Palmgren-Miner, abrasive-soil wear) with neural network tools for tracking the transition between wear mechanisms in real time.

Purpose

The aim of the research is to develop and validate a system for predicting the residual life of tribocouplings of machine parts based on the dynamics of changes in the dominant wear mechanism, which combines a classifier based on long short-term memory with an entropy transition detector for the practical implementation of the entropy approach to analyzing the functioning of tribosystems.

To achieve the set goal, the following tasks are solved:

– to systematize typical scenarios of transition between wear mechanisms for the main tribocouplings of automotive (crankshaft bearings , cylinder liners, piston rings, gearbox gears) and agricultural machinery (plough shares, harrow discs, cultivator tines, chopper knives) with tribological justification of the physical causes of each transition;

– based on the modified Archard model with calibrated coefficients for different lubrication modes, the Palmgren-Miner model in the form of an endurance curve, and the abrasive-soil wear model, form a data set that reflects the dynamics of tribotechnical contact of parts during the transition between wear mechanisms;

– develop the architecture of a neural network classifier of the dominant wear mechanism and an entropy transition detector as an information analogue of the physical entropy of production in a tribosystem;

– to validate the developed approach for eight scenarios of transition between wear mechanisms with an assessment of classification accuracy, error in determining the transition moment, and warning time of reaching a critical state of the part;

– to determine ways of practical integration of the developed system with on-board technical diagnostics systems of machines.

Results

Research objects and physical models of wear. Eight types of resource-determining parts (Table 1) were selected as research objects, covering the main tribocouplings of the engine, transmission, and working bodies of agricultural machinery.

Table 1

Characteristics of the studied part-wear mechanism combinations

Detail	Node	Material	HV	Ra, μm	Regular mechanism	Resource, hours
Piston rings	Internal combustion engine	Cast iron HF	305	1.4	Abrasive	3000...5000
Crankshaft bearings	Crankshaft Internal combustion engine	Babbitt B83 / Bronze BrO10S10 (working layer)	30...90	0.8	Tired	5000...8000
Gearboxes	Transmission	Steel 40X	550	0.55	Tired	8000...12000
Cylinder liners	Internal combustion engine	SCH25	400	1.0	Corrosion-mechanics.	4000...6000
Plow shares	Plow	Steel 65G	380	2.5	Abrasive soil	150...400
Harrow discs	Harrow	Steel 65G	420	2.0	Abrasive soil	2000...500
Cultivator tines	Cultivator	Steel 45	350	1.8	Abrasive	100...300
Shredder knives	Shredder	30KhGSA	480	1.2	Impact-abrasive	200...600

The choice of objects is due to their critical impact on the overall reliability of tribocouplings of parts and the need to cover the main wear mechanisms: abrasive, fatigue, corrosion-mechanical, adhesive and abrasive-soil. Unlike previous studies, for crankshaft bearings, the hardness is specified specifically for the working antifriction layer, and not for the steel base of the liner, since the tribological contact is determined by the properties of the working layer. Based on operational experience and tribological studies, eight typical scenarios of transition between wear mechanisms have been systematized, each of which corresponds to a real operational situation: S1 – crankshaft bearing, transition of wear mechanism: fatigue → adhesive (degradation of engine oil after overrun without replacement); S2 – crankshaft bearing, transition of wear mechanism: fatigue → abrasive (contamination of oil with wear products due to filter failure); S3 – cylinder liner, transition of wear mechanism: corrosion-mechanical → abrasive (increased sulfur content in diesel fuel); S4 – gearbox gear, transition of wear mechanism: fatigue → adhesive (systematic overload of the unit); S5 – piston rings, transition of wear mechanism: abrasive → corrosion-mechanical (engine overheating due to cooling system failure); S6 – plow share, transition of wear mechanism: abrasive-soil → impact-abrasive (hitting a rocky area of the field); S7 – harrow disc, transition of wear mechanism: abrasive-soil → abrasive (sharp decrease in soil moisture during the dry period); S8 – cultivator paw, transition of wear mechanism: abrasive → corrosion-mechanical (working in acidic soils of Polissya).

The quantitative description of the wear intensity for each mechanism is based on classical tribological models adapted to the specific operating conditions of the studied parts. For abrasive wear, a modified Archard model in the form of specific linear wear was used:

$$W(t) = k_{abr} \cdot \left(\frac{P}{H}\right) \cdot \upsilon \cdot t \cdot f\left(C_p, T\right) \tag{1}$$

where W – linear wear, mm; P – contact pressure, MPa; H – hardness of the part material, MPa; υ– sliding speed, m/s; t – operating time, h; $f\left(C_p, T\right)$– dimensionless correction function of the influence of the concentration of contaminants and temperature in the tribocontact. The calibrated values of the coefficient k_{abr} reflect the physical features of different lubrication modes: 10^{-8} – for normally lubricated contact (fatigue wear); $5 \cdot 10^{-7}$ – for boundary lubrication (abrasive mechanism); $2 \cdot 10^{-7}$ – for corrosion-mechanical; $5 \cdot 10^{-8}$ – for adhesive mode and $1 \cdot 10^{-8}$ – for abrasive-soil wear. The increase k_{abr} by four orders of magnitude during the transition from the standard to the emergency mode reflects the fundamental nature of the tribological transition.

For fatigue wear, the Palmgren-Miner model was used in the form of a material endurance curve, which is a classic approach to calculating accumulated fatigue damage:

$$D(t) = \sum \frac{n_i}{N(\sigma_i)}, \text{ де } \; N(\sigma_i) = N_0 \cdot \left(\frac{\sigma_{\lim}}{\sigma_i} \right)^m , \tag{2}$$

where $D(t)$ is the degree of accumulated damage ($D(t) = 1$ corresponds to the limit state of failure); n_i – the number of loading cycles with amplitude σ_i; $N(\sigma_i)$– the number of cycles to failure at the corresponding stress; $\sigma_{\lim}$ – the endurance limit of the material; m – the degree index of the endurance curve. Calibrated parameters for the studied materials: steel 40X (gearboxes) – $N_0 = 10^9$ cycles, $\sigma_{\lim} = 350$ MPa, $m = 3{,}2$; bronze BrO10S10 (crankshaft bearings) – $N_0 = 10^8$ cycles, $\sigma_{\lim} = 200$ MPa , $m = 3{,}0$; cast iron SCh25 (cylinder liners) – $N_0 = 5 \cdot 10^8$ cycles, $\sigma_{\lim} = 180$ MPa, $m = 3{,}5$. The physical adequacy of the model is confirmed by the correspondence of the calculated resource to the real one: at a rotational frequency $2000\, хв^{-1}$ and operating stress close to the endurance limit, the model predicts a gear resource of about 10,000 hours ($1{,}2 \cdot 10^9$ tooth loading cycles), which is consistent with operational data.

For abrasive-soil wear of working parts of agricultural machinery, the following model was used:

$$W_{soil} = K_s \cdot \left(\frac{H_{soil}}{H_{mat}} \right)^{1,5} \cdot A_s \cdot L \cdot g(v, d_s, M_\omega) , \tag{3}$$

where K_s – the basic coefficient of soil abrasiveness, calibrated for loamy soils of the central regions of Ukraine; H_{soil} – the hardness of quartz particles of the soil (~800 HV); H_{mat} – the hardness of the part material; A_s – the area of contact with the soil environment; L – the friction path; $g(v, d_s, M_\omega)$ – the function of the influence of humidity v, the average size of abrasive particles d_s and the mechanical strength of the soil M_ω.

Based on the described physical models, a data set of 4000 time series (500 for each of the eight scenarios) was formed, the length of the series is 100 time points. Each point is described by a vector of 14 tribotechnical contact parameters: hardness, roughness, friction coefficient, geometric characteristics of the contact spot, contact load, sliding speed, temperature, viscosity of the lubricating medium, concentration of contaminants, number of load cycles, cumulative wear, and for the working bodies of agricultural machinery additionally - sandiness and soil moisture. The stochastic component (coefficient of variation 8…16% for automotive parts and 18…32% for agricultural parts) reflects the real variability of operating conditions. System for identifying changes in the wear mechanism. The proposed system consists of two sequential stages of processing tribocontact sensor data. The first stage is dynamic classification of the current dominant wear mechanism. Unlike expert systems with static classification by fixed parameters, the proposed classifier analyzes a sliding window of 15 consecutive time points of operational parameters and at each step determines the probability distribution of the five main wear mechanisms: $P(t) = [p_{абр}, p_{втом}, p_{кор-мех}, p_{адг}, p_{адг-грунт}]$, where the sum of the probabilities is equal to one. The classifier is implemented on the basis of a recurrent neural network with a long short-term memory - an architecture that has proven itself well in processing time series with nonlinear dynamics [18]. The total number of model parameters is ~ 34,000, which allows deployment on standard on-board controllers of equipment without the need for cloud computing infrastructure.

The second stage is the entropy detector of the transition between wear mechanisms. This stage directly implements the idea of the entropy approach to the analysis of tribosystems [7, 8] in a practical computational form. The key physical idea is as follows: when the tribosystem is in a steady state with one dominant wear mechanism, the classifier detects this mechanism with high confidence (one of the probabilities is close to unity, the others are close to zero). The information entropy of such a distribution, calculated by the Shannon formula, is close to zero. When the transition between mechanisms begins in the tribosystem – the surface layer degrades, new wear products are formed, the lubrication regime changes – the class probabilities "blur", and the information entropy increases:

$$H(t) = -\sum_i p_i(t) \cdot \ln p_i(t) . \tag{4}$$

It is fundamentally important that the increase in information entropy $H(t)$ calculated at the output of the neural network classifier corresponds in physical content to the increase in the production of thermodynamic entropy in the friction zone [7]. Thus, the entropy transition detector is an information analogue of the physical process of loss of thermodynamic stability of the tribosystem, described in the

works [8, 20]. This is not a formal analogy, but a meaningful reflection of the tribological phenomenon in the space of mediated sensory measurements.

The transition between wear mechanisms is recorded when the smoothed entropy $H(t)$, calculated as a moving average over 5 steps, exceeds a threshold level H_0 for $\tau \geq \tau_{\min}$ consecutive steps. Experimentally it is determined that at characteristic levels noise sensory data typical peak value informational entropy in zones transition between mechanisms is $H(t) \approx 0{,}5...0{,}7$. Accordingly thresholds are accepted: $H_0 = 0{,}25$, $\tau_{\min} = 2$ steps for automotive parts; $H_0 = 0{,}20$, $\tau_{\min} = 3$ steps for working parts of agricultural machinery. The lower threshold for these parts is compensated by a longer confirmation time to avoid false alarms due to natural variability in soil conditions.

The results of system validation on eight scenarios of transition between wear mechanisms are given in Table 2. For each scenario, three key indicators were evaluated: the accuracy of classification of the current dominant mechanism, the accuracy of determining the transition moment, and the warning time of reaching a critical state of the part.

Table 2

Results of validation of the resource forecasting system

No.	Detail (type of equipment)	Precision classifications	Error moment transition, steps	Warning time (hour)	Warning time, % of resource
S1	Crankshaft bearing (auto)	0.99	1.9	437...461	6.7...7.1%
S2	Crankshaft bearing (auto)	0.99	1.5	365	5.6%
S3	Cylinder liner (auto)	0.99	1.3	337	6.7%
S4	Transmission gear (auto)	0.99	0.8	593	5.9%
S5	Piston rings (auto)	0.99	1.1	229	5.7%
S6	Plow share (agricultural)	0.99	1.0	16	6.2%
S7	Harrow disc (agricultural)	0.98	1.5	21	6.0%
S8	Cultivator paw (s/g)	0.98	2.0	13	6.7%

A graphical comparison of warning times (Fig. 1) clearly demonstrates the fundamental difference between automotive and agricultural parts: for automotive equipment, the warning time is measured in hundreds of hours (229…593 h), while for the working parts of agricultural machinery – in tens of hours (13…21 h), which reflects the difference in the overall resource and wear dynamics of open and closed tribosystems.

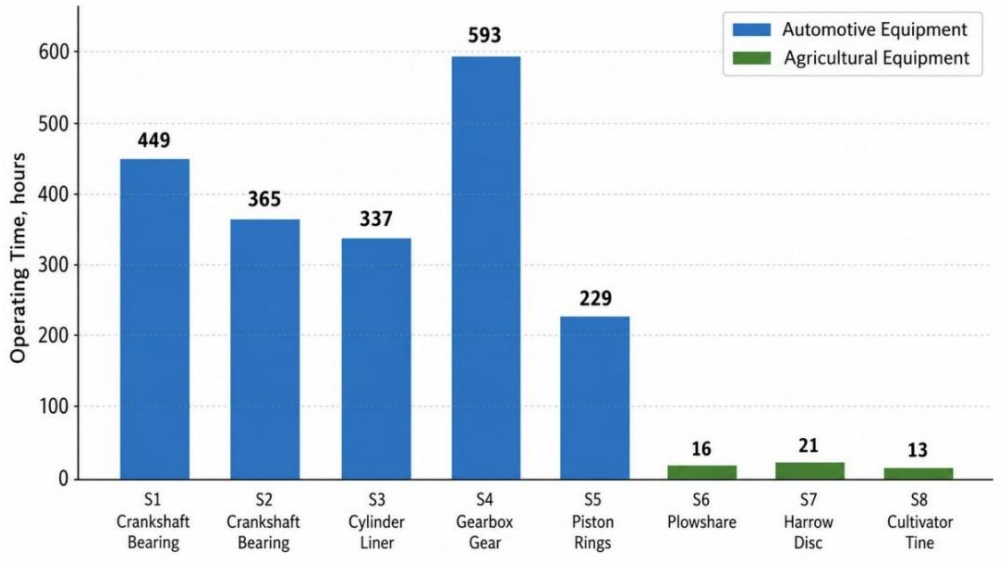

Fig. 1. Warning time of reaching a critical state of a part for eight scenarios of transition between wear mechanisms

The low error in determining the transition moment (0.8…2.0 time steps) has an important tribotechnical meaning: it shows that the entropy detector is triggered precisely at the moment when the tribosystem loses stability and a new dominant mechanism begins to form. This confirms the physical adequacy of using information entropy as an analogue of the thermodynamic entropy of production in the friction zone [7].

The warning time for a critical condition of a part is the most practically significant indicator for maintenance systems. For automotive parts, the warning time is 229…593 hours, which corresponds to the interval before a scheduled technical inspection in the conditions of a motor transport enterprise. For working bodies of agricultural machines, the warning time is 13…21 hours - this is a sufficient interval for making a decision on replacing the part or switching to a gentle mode of operation within the current agricultural operation. As a

percentage of the total resource of the part, the warning time is agreed to be 5.6…7.1% for all eight scenarios, which is equal to the generally accepted standard for planning maintenance by condition.

As can be seen from Fig. 2, the accuracy of the classification of the dominant wear mechanism remains consistently high (0.98…0.99) for all scenarios, while the error in determining the transition moment does not exceed 2.0 time steps. The smallest error (0.8 steps) was recorded for the gearbox gear (S4), which is explained by a clearly pronounced change in tribotechnical characteristics during the transition from fatigue to adhesive wear.

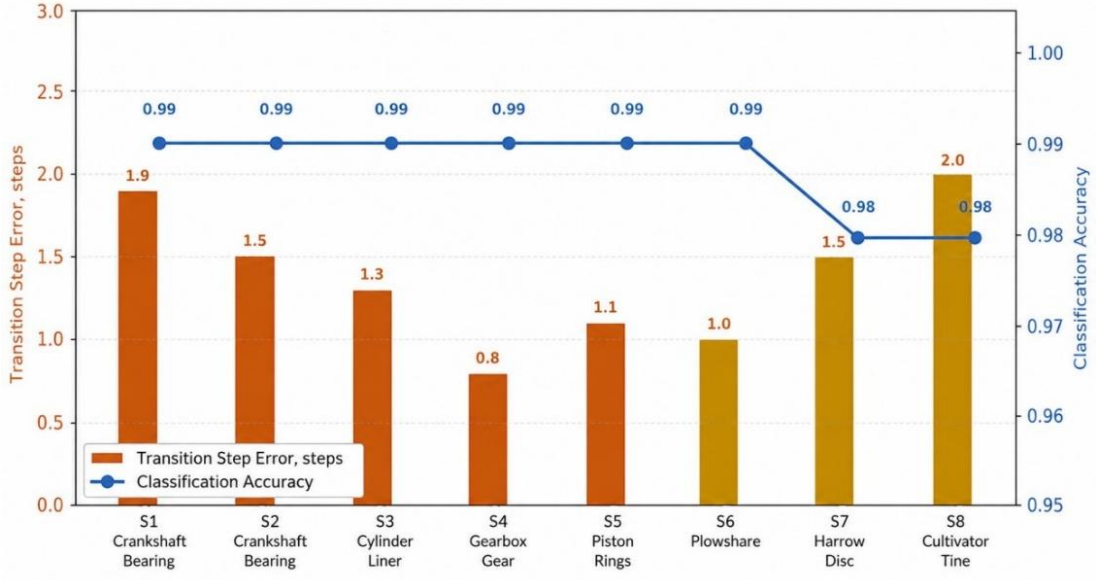

Fig. 2. Accuracy of classification of the dominant wear mechanism and error in determining the transition moment for eight validation scenarios

Tribotechnical interpretation of scenarios. The longest absolute warning time was obtained for the gearbox gear (593 hours for scenario S4, transition of the wear mechanism "fatigue → adhesive ") – this is physically justified, since the transition from fatigue to adhesive wear of the teeth occurs gradually due to the accumulation of microdamages of the contact surface with the subsequent catastrophic development of seizing. The shortest absolute warning time – for the cultivator paw (13 hours for scenario S8) – also corresponds to real dynamics: the effect of acidic soil on steel 45 triggers corrosive-mechanical wear, which under conditions of an open tribosystem develops faster than in closed tribocouplings of the engine. Scenario S6 (plow share, hitting a rocky area) demonstrates that even for sudden transitions in the wear mechanism, the entropy detector detects the change with a delay of only 1.0 step, which is sufficient for the machine operator to react promptly.

Connection with traditional entropic analysis of tribosystems. The proposed approach is a practical implementation of the entropic method of tribosystem analysis, theoretically substantiated in the works [7, 8, 18]. The fundamental advantage is that instead of direct measurement of thermodynamic parameters of the friction zone – which is often impossible in operational conditions – the information entropy of the probability distribution of wear mechanisms is used, calculated from indirect sensor data. This allows implementing entropic monitoring of tribosystems as part of on-board technical diagnostics systems of transport and agricultural machines using standard sensor buses – CAN-bus for cars, ISOBUS for agricultural machinery.

The possibility of using neural networks in tribological forecasting. The results obtained confirm that modern recurrent neural networks are able to detect systemic patterns of changes in the state of tribocontact with sufficient accuracy for practical application. This fundamentally expands the possibilities of tribological diagnostics: if traditional methods provide an integral assessment of the wear intensity for a certain period, then the neural network approach provides continuous tracking of the dynamics of wear mechanisms with the detection of transitions at the moment of their formation. The combination of a classifier with an entropy transition detector integrates two lines of research – physical modeling of tribological processes and neural network processing of sensor data – into a single system that has a theoretical justification within the thermodynamics of non-equilibrium processes [8, 20].

Conclusions

1. Eight typical scenarios of transition between wear mechanisms for resource-determining parts of automotive (crankshaft bearings, cylinder liners, piston rings, gearbox gears) and agricultural machinery (plough shares, harrow discs, cultivator tines) are systematized, each of which is tied to a specific operational situation with tribotechnical justification of the physical reasons for the transition of the wear mechanism and a quantitative assessment of the impact on the residual resource.

2. A two-stage system for identifying changes in the dominant wear mechanism has been developed based on a combination of a classifier with a long short-term memory and an entropy transition detector. The proposed approach is a practical implementation of the entropy method for analyzing tribosystems [7, 8] in a form suitable for implementation in on-board technical diagnostic systems.

3. Validation on eight scenarios of transition between wear mechanisms showed reliable detection of a change in the dominant mechanism (classification accuracy 0.98…0.99) with a low error in determining the transition moment (0.8…2.0 time steps), which confirms the physical adequacy of using information entropy as an analogue of the thermodynamic entropy of production in the friction zone.

4. The warning time for reaching a critical state of a part is 229…593 hours for automotive equipment and 13…21 hours for agricultural equipment, which in relative terms is equal to 5.6…7.1% of the total resource for all eight studied scenarios and is sufficient for planning maintenance based on the condition of tribocoupling parts of machines.

5. The study demonstrates that neural networks are an effective tool for the practical implementation of the entropic approach to the analysis of tribosystems, allowing to detect a change in the state of the tribocontact from indirect sensor data without the need for direct measurement of the thermodynamic parameters of the friction zone. Further research should be aimed at validating the system on real operational data from different types of tribocouplings of parts and integrating it with existing systems for technical diagnostics of transport and agricultural machinery.

References

1. Kindrachuk, M.V., Labunets, V.F., Pashechko, M.I., & Korbut, Ye.V. (2009). Trybolohiia [Tribology]. NAU-druk. [in Ukrainian].

2. Dykha, O.V., & Velboi, V.P. (2014). Inzhenerni metody v trybotekhnisi [Engineering methods in tribotechnology]. KhNU. [in Ukrainian].

3. Aulin, V.V., et al. (2022). Parametry protsesu zmashchuvannia pry ekspluatatsiinomu znoshuvanni pidshypnykiv kolinchastoho vala avtomobilnykh dvyhuniv [Parameters of the lubrication process during operational wear of the crankshaft bearings of automobile engines]. Problemy trybolohii, 27(4/106), 69–81. https://doi.org/10.31891/2079-1372-2022-106-4-69-81 [in Ukrainian].

4. Aulin, V.V. (2013). Stan samoorhanizatsii seredovyshcha gruntu ta zakonomirnosti znosu robochykh orhaniv gruntoobrobnykh mashyn [Self-organization state of soil environment and wear patterns of tillage machine working parts]. Problemy trybolohii, (1), 114–119. https://tribology.khmnu.edu.ua/index.php/ProbTrib/article/view/157 [in Ukrainian].

5. Tykhyi, A.A., et al. (2024). Trybotekhnichni protsesy vzaiemodii gruntového seredovyshcha z robochymy orhanamy gruntoobrobnykh ta zemlereinykh mashyn, zmitsnenykh kompozytsiinymy materialamy [Tribotechnical processes of the soil environment interaction with the working bodies of soil tillage and earthmoving machines reinforced with composite materials]. Problemy trybolohii, 29(3/113), 79–88. https://doi.org/10.31891/2079-1372-2024-113-3-79-88 [in Ukrainian].

6. Stechyshyn, M.S., et al. (2024). Vplyv tekhnolohichnykh parametriv karboazotuvanny na znosostijkist stali 45 [Influence of carbonitriding technological parameters on wear resistance of steel 45]. Problems of Friction and Wear, 102(1), 45–53. https://doi.org/10.18372/0370-2197.3(84).13856 [in Ukrainian].

7. Aulin, V.V., et al. (2023). Vyiavlennia zmin kharakterystyk i vlastyvostei zon tertia detalei trybospriazhen system i ahrehativ mashyn na osnovi entropinoho pidkhodu [Detection of changes in the characteristics and properties of friction zones of parts of tribocoupling systems and machine assemblies based on the entropy approach]. Problemy trybolohii, 28(3/109), 58–63. https://doi.org/10.31891/2079-1372-2023-109-3-58-63 [in Ukrainian].

8. Bershchadskyi, L.I. (1990). Strukturna termodynamika trybosystem [Structural thermodynamics of tribosystems]. Znannia. [in Ukrainian].

9. Dvoruk, V.I., Mikosianchyk, O.O., & Mnatsakanov, R.H. (2015). Trybotekhnika [Tribotechnology]. NAU. [in Ukrainian].

10. Voitov, V.A., & Zakharchenko, M.B. (2015). Enerhetychna interpretatsiia protsesu znoshuvannia trybosystem [Energy interpretation of the wear process of tribosystems]. Problemy trybolohii, (2), 75–82. https://tribology.khmnu.edu.ua/index.php/ProbTrib/issue/archive [in Ukrainian].

11. Dmytrychenko, M.F., Biliakových, O.M., & Savchuk, A.M. (2017). Trybolohiia [Tribology]. NTU. [in Ukrainian].

12. Dykha, O.V., & Hedzyuk, T.V. (2019). Kontaktna znosostijkist trybospriazhen pry hranychnomu zmashchuvanni [Contact wear resistance of tribocouplings under boundary lubrication]. Problemy trybolohii, 24(2/92), 28–35. https://doi.org/10.31891/2079-1372-2019-92-2-28-35 [in Ukrainian].

13. Chernets, M.V., & Andpeikiv, O.Ye. (2017). Prohnozuvannia znosu i dovhovichnosti tsylindrychnykh opor kovzannia [Prediction of wear and durability of cylindrical sliding bearings]. NAN Ukrainy, FMI. [in Ukrainian].

14. Shevelia, V.V., & Oleksandrenko, V.P. (2009). Trybolohiia: fizychni osnovy, mekhanika i tekhnichni zastosuvannia [Tribology: physical foundations, mechanics and technical applications]. KhNU. [in Ukrainian].

15. Chumak, V.M., et al. (2025). Pidvyshchennia znosostijkosti ta nadiinosti resursovyznachalnykh detalei transportnoi ta silskohospodarskoi tekhniky metodamy inzhenernoi optymizatsii [Improving wear resistance and reliability of resource-determining parts of transport and agricultural machinery by engineering optimization methods]. Tsentralnoukrainskyi naukovyi visnyk. Tekhnichni nauky, 11(42, pt. 2), 143–159. https://doi.org/10.32515/2664-262X.2025.12(43).1.272-288 [in Ukrainian].

16. Chumak, V.M., et al. (2025). Universalnyi metod formalizatsii parametriv resursovyznachalnykh detalei transportnoi ta silskohospodarskoi tekhniky dlia system predyktyvnoho obsluhovuvannia [Universal method of formalizing parameters of resource-determining parts of transport and agricultural machinery for predictive maintenance systems]. Tsentralnoukrainskyi naukovyi visnyk. Tekhnichni nauky, (12(43), pt. 2), 204–219. https://doi.org/10.32515/2664-262X.2025.12(43).2.204-219 [in Ukrainian].

17. Lim, S.C., & Ashby, M.F. (1987). Wear-mechanism maps. Acta Metallurgica, 35(1), 1–24. https://doi.org/10.1016/0001-6160(87)90209-4

18. Hochreiter, S., & Schmidhuber, J. (1997). Long Short-Term Memory. Neural Computation, 9(8), 1735–1780. https://doi.org/10.1162/neco.1997.9.8.1735

19. Shah, R., et al. (2025). Machine Learning in Wear Prediction. Journal of Tribology, 147(4), 040801. https://doi.org/10.1115/1.4066865

20. Aulin, V.V., et al. (2021). Teoretychne obgruntuvannia vplyvu zminy dylatonykh i kompresijnykh zviazkiv atomiv materialiv detalei mashyn na yikh trybologichnyi efekt [Theoretical justification of the influence of change of dilaton and compression bonds of atoms of materials of machine parts on their tribological effect]. Problemy trybolohii, 26(2/100), 71–78. https://doi.org/10.31891/2079-1372-2021-100-2-71-78 [in Ukrainian].

21. Chumak, V.M., et al. (2025). Modeliuvannia ta optymizatsiia kombinovanykh metodiv poverkhnevogo zmitsnennia detalei mashyn na osnovi neironnykh merezh i henetychnykh alhorytmiv [Modeling and optimization of combined methods of surface hardening of machine parts based on neural networks and genetic algorithms]. Tsentralnoukrainskyi naukovyi visnyk. Tekhnichni nauky, (13(44)), 274–285. https://doi.org/10.32515/2664-262X.2026.13(44).273-285 [in Ukrainian].

Аулін В.В., Чумак В.М., Лисенко С.В. Прогнозування ресурсу деталей машин за динамікою зміни механізму зношування методу нейронних мереж.

Розглянуто проблему прогнозування залишкового ресурсу трибоспряжень ресурсовизначальних деталей автомобільної та сільськогосподарської техніки в умовах експлуатаційної зміни домінуючого механізму зношування. Показано, що в реальних умовах експлуатації механізм зношування не залишається статичним: деградація мастильних матеріалів, зміна навантажувально-швидкісних режимів та варіативність ґрунтових умов спричиняють перехід від штатного механізму до аварійного, що супроводжується різким скороченням залишкового ресурсу деталей машин. Запропоновано двоетапну систему ідентифікації зміни домінуючого механізму зношування, що поєднує класифікатор на основі довгої короткочасної пам'яті з ентропійним детектором переходу, який розвиває ентропійний підхід до аналізу трибосистем. Набір даних сформовано на основі модифікованої моделі Арчарда з п'ятьма каліброваними коефіцієнтами для різних режимів змащування та моделі Пальмгрена-Майнера у формі через криву витривалості з реалістичними значеннями базової кількості циклів $10^8...10^9$ для різних матеріалів деталей трибоспряження. Валідацією на восьми сценаріях переходу між механізмами зношування продемонстровано надійне виявлення зміни домінуючого механізму, час попередження про досягнення критичного стану 229…593 годин для автомобільних та 13…21 годин для сільськогосподарських деталей, що становить 5,6…7,1% від загального ресурсу і є достатнім для планування технічного обслуговування машин.

Ключьові слова: ресурс деталей, зношування, трибоспряження, зміна механізму зношування, ентропійний детектор переходу, штучна нейронна мережа, технічне обслуговування за станом.

ISSN 2079-1372 Problems of Tribology, V. 31, No 2/120-2026, 111-119

Problems of Tribology
Website: http://tribology.khnu.km.ua/index.php/ProbTrib
E-mail: tribosenator@gmail.com

DOI: https://doi.org/10.31891/2079-1372-2026-120-2-111-119

Mathematical modeling and optimization of wear-resistant material selection for technological tooling of internal combustion engines

I. Drach* 0000-0003-0590-9814, **I. Valchuk**

Khmelnytskyi National University, Ukraine
**E-mail: drachil@khmnu.edu.ua*

Received: 30 April 2026: Revised 09 May 2026: Accept: 27 May 2026

Abstract

The study develops an integrated approach for selecting wear-resistant materials for technological devices used in machining and repair of internal combustion engines, considering mechanical, thermal, economic, and reliability factors. KHVG and R6M5 steels were comparatively analyzed using modified abrasive wear models, Weibull reliability assessment, and Life Cycle Cost (LCC) analysis. The model accounts for temperature-induced hardness degradation, lubrication conditions, contact geometry, and coating adhesion. It was established that at temperatures above 400 °C and severe abrasive wear, R6M5 steel provides longer service life and reduces LCC by 6–19% compared to KHVG steel. Under moderate temperatures and impact loading, KHVG steel is preferable due to higher fracture toughness. Optimal heat treatment regimes were determined for both steels. Lubrication increases service life by approximately 66%, while risk mitigation measures are more effective than material substitution under high failure probability conditions. TiN coating is not recommended for rough surfaces because of delamination risk. The developed model enables improved engineering decision-making for wear-resistant tooling applications.

Keywords: abrasive wear,steel, technological tooling, heat treatment, Archard model, Weibull model, Life Cycle Cost, sensitivity analysis.

Introduction

Modern production and repair of internal combustion engines (ICEs) require high precision of mechanical processing and reliability of repair operations. One of the key elements of technological processes are devices for installation, clamping, and positioning of ICE components, particularly clamping jaws, guides, supports, rollers, and other locating elements. They operate under complex service conditions characterized by cyclic loading, abrasive wear, thermal deformations, and impact effects during the installation of massive parts such as cylinder heads or crankshafts. In automotive and repair manufacturing practice, one of the critical parameters is positioning accuracy, which for cylinder head processing operations can reach a level of ±0.03 mm, determining high requirements for the stability of geometric parameters of technological tooling [1]. At the same time, in the practice of repair enterprises, a significant share of failures of clamping and locating elements is observed, which in some cases can reach 15–20% of downtime associated with wear or failure, although such estimates have limited representativeness and depend on the observation sample [2].

There is a substantial contradiction between the requirements for materials of technological device elements and the real possibilities of their implementation. On the one hand, structural materials must provide high hardness (above HRC 62) to increase wear resistance, sufficient fracture toughness (above 25 MPa·m^0.5) to resist impact loads, heat resistance in the range of 300–500°C when processing heated parts, as well as economic feasibility for mass use [3]. On the other hand, existing approaches to material selection are mainly based on empirical experience or simplified criteria, such as orientation solely on hardness or cost. This leads to premature wear due to insufficient accounting for temperature degradation of properties, sudden failures due to ignoring impact loads, as well as economic losses caused by the non-optimal ratio of capital and operating costs. Such a gap between the designer's requirements and practical solutions is reflected in regulatory documents and technical conditions of material manufacturers, but does not have a comprehensive engineering generalization.

Traditional approaches to material selection include the use of comparative hardness tables, catalog data from manufacturers, and accumulated experience from previous developments. However, these methods have a

number of significant limitations [4]. First, there are no integral models that allow simultaneous consideration of mechanical wear, thermal effects, and economic indicators. Second, the probabilistic nature of failure is ignored, since calculations are mostly based on nominal values without sufficient consideration of margins for random overloads. Third, real operating conditions at service stations are insufficiently accounted for, where abrasive particles, increased humidity, and irregular lubrication are present, which significantly distinguishes the working environment from laboratory test conditions. A review of scientific and technical literature indicates the absence of systematic studies that would comprehensively compare tool steels of the KhVG type and high-speed steel R6M5 specifically in the context of technological tooling elements for ICEs, taking into account the totality of operational factors.

Literature Review

The problem of material selection for wear-resistant elements of technological devices used in processing and repair of internal combustion engines (ICEs) encompasses several interrelated research directions: modeling of abrasive wear, heat treatment of tool steels, economic assessment of life cycle, evaluation of failure risk, and application of hardening coatings [3]. Analysis of contemporary scientific works indicates significant progress in each of these directions separately; however, a comprehensive approach to material selection for ICE technological tooling remains insufficiently developed.

The basic theoretical foundation for engineering wear calculations is the Archard model [5], proposed in 1953. It describes the dependence of worn material volume on normal load, sliding distance, and material hardness. According to the classical formulation, wear intensity is determined by the friction coefficient and contact conditions. However, practical application of this model for tool steels is substantially complicated by the wide range of variation of the wear coefficient k, which for "steel–steel" pairs can vary by several orders of magnitude. This creates significant uncertainty in predicting the service life of parts. Furthermore, the classical model does not account for temperature degradation of hardness, the influence of the lubricating environment, and the specifics of contact geometry characteristic of rollers, guides, and clamping elements of technological devices.

In modern research on tribological processes, considerable attention is paid to the development of molecular dynamics and multilevel wear models [6]. Works [7, 8] demonstrate the possibility of modeling micromechanisms of adhesive and abrasive surface destruction with high accuracy. At the same time, such models are characterized by significant complexity, require substantial computational resources, and are practically unsuitable for operational engineering calculations in the design of technological tooling. Thus, the scientific literature lacks an adapted engineering model that would integrate the effects of temperature, lubrication, contact geometry, and coating properties within a single wear assessment algorithm.

A separate research direction is devoted to the heat treatment of tool and high-speed steels. For KhVG steel, the influence of tempering regimes on hardness and structural changes has been studied in sufficient detail. It has been established that increasing the tempering temperature above 200°C causes intense softening of the material, accompanied by a hardness loss of 5–8 HRC per each 100°C [9]. However, available results are mostly presented in the form of experimental graphs or tables and lack a universal analytical form suitable for mathematical prediction of properties under real operating conditions.

For high-speed steel R6M5, high heat resistance and the ability to maintain hardness above HRC 59 even at temperatures around 620°C are characteristic. This ensures its effectiveness under increased thermal loading conditions. At the same time, most publications consider heat treatment and heat resistance in isolation from wear processes and operational reliability. The issue of integrating temperature-dependent hardness characteristics into models for predicting part service life essentially remains open [10].

Economic models of material selection are also of considerable interest. The Life Cycle Cost (LCC) methodology is widely applied in mechanical engineering, aviation, and energy sectors for assessing cumulative costs throughout the product life cycle [11]. Works [11, 12] have formed an approach to material selection based on performance indices and economic efficiency. However, in most studies, economic analysis does not account for the probabilistic nature of failures, the risk of catastrophic failure, and the specifics of operating conditions at service stations, where abrasive contamination, increased humidity, and irregular maintenance take place. Consequently, economic models remain insufficiently adapted to the conditions of use of technological devices for ICE repair.

Issues of reliability assessment and failure risk are traditionally considered within statistical models, among which the Weibull distribution is the most common. This approach has been successfully applied for analyzing the durability of bearings, gear transmissions, electronic components, and other machine elements. Distribution parameters allow evaluating the probability of failure depending on time or loading cycles. However, for wear-resistant elements of technological devices operating under impact loads, fatigue, and corrosive effects, the corresponding reliability parameters are practically absent in open sources. This limits the possibility of constructing credible risk-oriented models for predicting failure of clamping and locating elements.

A significant contribution to improving the operational stability of tool materials is provided by modern surface coatings and diffusion hardening methods. Research on PVD coatings of the TiN and CrN types confirms the possibility of increasing surface hardness to a level of about 25 GPa and substantially improving wear resistance. At the same time, one of the key problems remains coating adhesion to the substrate. It has been

established that at surface roughness above R<<sub> = 0.8 μm, the risk of coating delamination increases several-fold, sharply reducing the effectiveness of hardening. Despite the considerable number of works in the field of tribological coatings, the literature practically lacks models that would combine wear assessment of the coating with analysis of the economic feasibility of its application.

Thus, analysis of scientific research shows that individual aspects of the problem—wear modeling, steel heat treatment, reliability assessment, economic analysis, and use of hardening coatings—have a sufficient level of theoretical elaboration. At the same time, a systemic gap exists between these directions. None of the known publications proposes an integrated approach that would combine mechanical, thermal, statistical, and economic aspects of material selection for elements of technological tooling for processing and repairing internal combustion engines. It is the elimination of this gap that determines the scientific relevance of this research.

Purpose

The purpose of this study is to develop a mathematical framework for the justified selection of optimal wear-resistant materials (KHVG or R6M5 steels) for technological devices used in machining and repair of internal combustion engines, considering mechanical, thermal, and economic operating factors.

The main research objectives include the development of an abrasive wear model accounting for contact geometry, temperature effects, lubrication, and coating adhesion; formulation of a heat treatment optimization model considering residual stresses and hardness variation; creation of a probabilistic failure risk and life cycle cost (LCC) assessment approach; and development of a multi-criteria algorithm for optimal material selection.

The object of research is the wear and failure processes of clamping jaws, guides, supports, and rollers of technological devices used for machining and repair of internal combustion engines. The subject of research is the mathematical modeling and selection criteria for KHVG and R6M5 steels under abrasive-adhesive wear conditions.

The study is limited to KHVG and R6M5 steels, operating temperatures up to 500°C, and abrasive-adhesive wear mechanisms, without considering corrosion, cavitation, or radiation effects.

Methods

The research was conducted using a block-modular principle with sequential complication of mathematical models and integration of results from previous stages into subsequent ones. The general scheme is presented in Fig. 1.

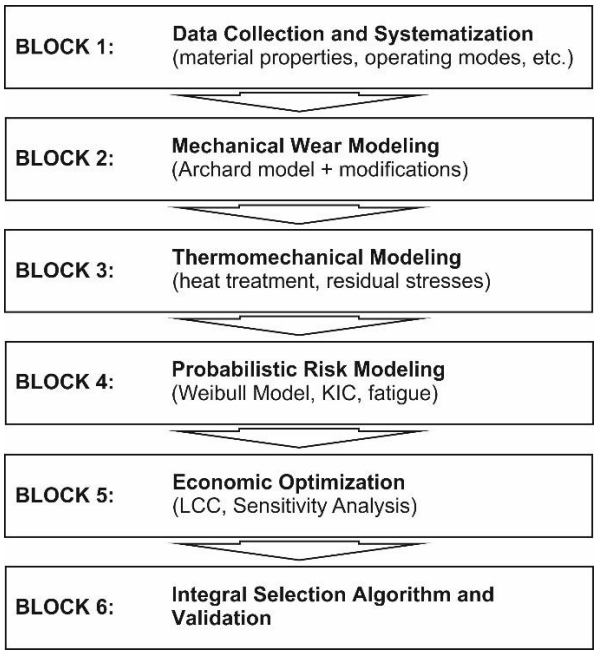

Fig. 1. Structural scheme of the research

Block 1: Collection and Systematization of Input Data

At the first stage of the research, a database of input data was formed for the mathematical modeling of wear and failure processes of technological device elements used in processing and repair of internal combustion engines (ICEs). Typical tooling elements were selected as research objects: clamping jaws, guide rollers, setting supports, and locating pins, which operate under various contact and loading schemes. Clamping jaws for cylinder head processing with dimensions of 50×20×15 mm and a contact area of 150 mm² were designated as the base element for detailed analysis.

For comparative analysis, tool steel KhVG and high-speed steel R6M5 were investigated. Initial data on chemical composition, hardness after heat treatment, mechanical properties, wear coefficients, and material costs were obtained from regulatory documents, reference sources, scientific publications, and market data. Parameters with insufficient reliability, particularly the wear coefficient k and fracture toughness K<sub>, were accounted for in subsequent calculations with a variation of ±30% within the sensitivity analysis of the model.

Block 2: Mechanical Wear Modeling

To assess the intensity of abrasive wear of technological device elements, the basic Archard model was used, which describes the dependence of the worn material volume on normal load, sliding distance, and material hardness (1):

$$V = k \cdot \frac{F \cdot L}{H}, \quad (1)$$

where V is the wear volume, F is the normal load, L is the sliding distance, H is the material hardness, and k is the wear coefficient. To improve the accuracy of prediction, the model was sequentially complicated by introducing corrections for temperature, lubrication conditions, contact geometry, and the effect of protective coatings, as presented in Table 1.

Table 1

Stages of Basic Archard Model Modification

Stage	Added Correction	Formula	Parameters
1	Geometry	$k_{geom} = k \cdot [1 + 0.1 \cdot (R/b - 5)]$	R — cylinder radius, mm; b — contact width, mm. This correction is empirical and valid only for $R/b > 5$
2	Temperature	$H(T)=H_0 \cdot [1-\beta \cdot (T-T_0)]$	H_0 — hardness at T_0 = 20°C, GPa; β — temperature softening coefficient, °C^{-1}; T — operating temperature, °C; β_{KHVG} = 0.004 (150–400°C); β_{R6M5} = 0.0008 (20–600°C)
3	Lubrication effect	$k_{lub}(T)=k_{lub0} \cdot [1+0.003 \cdot (T-20)]$	k_{lub0}= 0.4-0.6
4	Coating	$k_{coat} = k \cdot [1 - \delta/d]$	d — deformed substrate thickness (usually 10–20·δ); δ = 3 μm

The integral Archard model takes the form:

$$V_{int} = k \cdot \frac{F \cdot L}{H(T)} \cdot k_{geom} \cdot k_{lub}(T) \cdot k_{coat}. \quad (2)$$

Service life was calculated using the formula:

$$T_{service} = \frac{h_{allow} \cdot A}{V_{cycle}}. \quad (3)$$

Number of cycles to reach critical wear:

$$N = \frac{V_{crit}}{V_{cycle}}.$$

Block 3: Thermomechanical Modeling

Hardness model after heat treatment:

$$H=H_0+\Delta H_{hardening}+\Delta H_{tempering}+\Delta H_{carbides},$$

where: H_0 is the hardness in the initial state, HRC; $\Delta H_{hardening}$ is the increase during hardening; $\Delta H_{tempering}$ is the decrease during tempering; $\Delta H_{carbides}$ is the contribution of carbides.

The formula for hardness dependence on tempering temperature takes the form:

$$H_{KHVG}(T_{відп})=H_{max} \cdot \exp[-\alpha \cdot (T_{temp}-150)/100] \text{ при } T_{temp}>150°C,$$

where: H_{max}=65 HRC (after hardening at 1230°C 150°C); α = 0.15 (empirical softening coefficient); temperature range: 150–600°C.

$$H_{R6M5}(T_{temp})=H_{max}-\beta_1 \cdot \exp[(T_{temp}-560)/50]+\beta_2 \cdot \exp[-(T_{temp}-560)/80],$$

where: H_{max} = 66 HRC (after hardening at 1230°C); $\beta_1 = 8$ (softening upon exceeding tempering temperature); $\beta_2 = 2$ (correction for heat resistance plateau); optimal tempering: 560–570°C (double).

The modified Archard model accounting for hardness after heat treatment is:

$$V_{\text{mod}} = k \cdot \frac{F \cdot L}{H\left(T_{temp}\right)} \cdot k_{geom} \cdot k_{\text{lub}}\left(T\right) \cdot k_{coat}.$$

Optimization of Heat Treatment with Account for Residual Stresses

Critical condition:

$$\sigma_{res}=E\cdot(\alpha\cdot\Delta T-\varepsilon_{pl}) \geq \sigma_{yield},$$

where α is the coefficient of thermal expansion.

Objective function:

$$J=w_1\cdot\sigma_{res}+w_2\cdot\Delta H+w_3\cdot t_{therm} \rightarrow \min, \quad (4)$$

where:

$\Delta H=H_{setpoint}-H_{actual}$ (hardness deviation);

t_{therm} − heat treatment time;

$w_1+w_2+w_3=1$ (weighting coefficients).

Constraints::

$$\begin{cases} H \geq 62\ HRC; \\ \sigma_{res} \leq 0.8\sigma_{yield}; \\ \delta \leq 0.02\ mm; \\ t_{therm} \leq 4\ h. \end{cases}$$

Block 4: Probabilistic Modeling of Sudden Failure Risk

1. Weibull distribution with corresponding parameters (Table 2):

2.

$$P_i(t) = 1 - \exp\left[-\left(\frac{1}{\eta_i}\right)^{\gamma_i}\right],$$

Table 2

Failure Types and Modeling Parameters

Type	η, years	γ	Justification
Impact	8	1.5	Empirical data from service stations
Fatigue	12	4.0	Theoretical estimate
Corrosion	6	2.5	Operational data

2. The combined probability takes the form:

$$P_{total} = 1 - \prod_{i=1}^{n}\left(1 - P_i\right). \quad (5)$$

3. K_{IC} model by parameter::

$$\sigma_c = \frac{K_{IC}}{Y \cdot \sqrt{a_c}}\ ,\ n = \frac{\sigma_c}{\sigma},$$

where a_c is the critical crack depth, m; σ is the operating stress, MPa; Y is the geometry factor; n is the safety factor.

Block 5: Economic Optimization

1. LCC Model

Total life cycle cost formula:

$$C_{total}=C_{mat}+C_{therm}+C_{mach}+C_{coat}+C_{lube}\cdot T_{service}+C_{repl}\cdot T_{plan}/T_{service}, \quad (6)$$

where: C_{total} — total life cycle costs, UAH; C_{mat} — blank cost, UAH; C_{therm} — heat treatment cost, UAH; C_{mach} — machining cost, UAH; C_{coat} — coating application cost, UAH; C_{lube} — annual lubrication costs (material + labor), UAH/year; $T_{service}$ — calculated service life, years; T_{plan} — planned operation period (e.g., 10 years); C_{repl} — cost of one replacement (part + downtime), UAH.

2. Sensitivity analysis of the economic model. The analysis shows which parameters most strongly affect total costs and failure probability. The following variable parameters were considered: material price: ±30%; wear coefficient k: ±40%; failure probability P_{total}: ±2%; operating temperature: ±20%. Visualization: radial diagram with parameter axes and scenario polygons.

Block 6: Integral Algorithm and Validation

1. Go/No-Go Algorithm

Step 1: *T*<sub> > 400°C? → YES: R6M5 (No-Go for KhVG) → NO: Go to Step 2

Step 2: *E*<sub> > 50 J? → YES: preference for KhVG → NO: no preference

Step 3: *H*<sub> > 800 HV? → YES: preference for R6M5 → NO: no preference

Step 4: *P*<sub> > 0.9? → YES: mitigation (shock absorbers, lubrication) → NO: baseline variant

2. Model validation through comparison of calculated and empirical service life (available sample from 5 service stations, 15 devices). Acceptance criterion: error < ±30%.

Limitations of the Methodology

The proposed methodology has a number of limitations associated with the use of empirical wear and fracture toughness parameters, limited statistical basis for failure probability assessment, and simplification of contact interaction geometry. To mitigate the impact of these factors, the study employed sensitivity analysis, conservative estimates of reliability parameters, and safety factors, ensuring acceptable validity of modeling results.

Results

A comprehensive mechanical, thermomechanical, probabilistic, and economic modeling of wear-resistant elements of technological devices for machining and repair of internal combustion engines was carried out within the study. The main objective of the modeling was to determine the patterns of service life variation for elements made of KHVG and R6M5 steels depending on temperature, friction conditions, heat treatment regimes, risk of failure, and economic factors.

The initial stage of the study involved the application of the basic Archard model to assess the intensity of abrasive wear under standard operating conditions at a load of 400 N, a friction path of 0.2 m per cycle, and a temperature of 20 °C. The calculation results showed that for KHVG steel, the wear volume per cycle is 9.62×10^{-6} mm³, while for R6M5 steel it is 6.71×10^{-6} mm³. This corresponds to a predicted service life of approximately 94 and 134 years, respectively. The obtained results indicate that at room temperature, high-speed steel R6M5 provides a service life approximately 43% higher than that of KHVG steel. However, the absolute values of service life are excessive for practical operating conditions, which indicates the need to account for additional factors, particularly temperature effects and the risk of failure.

Further analysis focused on investigating the effect of temperature on hardness degradation and wear intensity. When the temperature increases to 300 °C, the hardness of KHVG steel decreases to 55.5 HRC (temperature softening coefficient $\beta = 0.004$ °C^{-1}), while for R6M5 it remains at 62.8 HRC ($\beta = 0.0008$ °C^{-1}). The softening coefficient of R6M5 is 5 times lower than that of KHVG, ensuring a 70% lower hardness loss upon heating. In terms of wear intensity, this leads to an increase in wear volume for KHVG to 1.09×10^{-5} mm³ per cycle, while the corresponding indicator for R6M5 is only 6.96×10^{-6} mm³. The predicted service life of KHVG decreases to 83 years, while for R6M5 it is 129 years. Thus, it has been established that high-speed steel R6M5 loses hardness upon heating approximately 4 times slower than KHVG steel, which determines its advantage under elevated temperature conditions.

Lubricants have a significant effect on the service life of parts. Modeling of GRAFLO lubricant usage conditions showed that the effective wear coefficient for both steels decreases by almost half. For KHVG, this ensures a reduction in wear volume to 5.99×10^{-6} mm³ per cycle and an increase in service life to 151 years, while for R6M5 it is 3.83×10^{-6} mm³ and 235 years, respectively. Thus, lubricant use provides a service life increase of approximately 66% at 20 °C and 82% at 300 °C, without changing the overall efficiency ratio of the materials.

Special attention was paid to analyzing the effect of PVD TiN coating. Calculations showed that with ideal adhesion of the coating to the substrate, the effective hardness of the KHVG + TiN system reaches 21.2 GPa, ensuring a slight increase in service life to 100 years. However, under real conditions, with an adhesion degradation coefficient C_ad = 1.5, intensive coating delamination is observed, increasing the wear volume to 1.42×10^{-5} mm³ and reducing the service life to 66 years. This result indicates that poor surface preparation and insufficient adhesion can not only negate the positive effect of the coating but also significantly deteriorate operational characteristics. It has been established that TiN coating application is not recommended for this class of devices due to the marginal effect under ideal adhesion and the high risk of delamination at real surface roughness (R_a > 0.4 μm).

Within the thermomechanical modeling, optimization of heat treatment regimes for KHVG and R6M5 steels was carried out. For KHVG steel, it was established that the basic tempering regime at 150 °C ensures high hardness of 63 HRC, but is accompanied by significant residual stresses and deformation up to 0.065 mm. Increasing the tempering temperature to 180 °C allows reducing residual stresses to 980 MPa and decreasing deformation to 0.052 mm with a slight loss of hardness. The best result was obtained using stabilizing tempering at 300 °C for 5 hours, ensuring hardness of 61.5 HRC, reduction of residual stresses to 850 MPa, and minimum

deformation of 0.041 mm. Based on the obtained results, the following regime is recommended: quenching at 830 °C, tempering at 180 °C, and stabilization at 300 °C for 5 hours.

For high-speed steel R6M5, the optimal regime was tempering at 560 °C, ensuring maximum hardness of 65 HRC. At a reduced temperature of 540 °C, structural softening is observed, while at an increased temperature of 620 °C, hardness decreases to 59.5 HRC, although the heat resistance of the material remains high.

The Weibull distribution was used to assess the risk of failure of technological device elements. Calculations showed that corrosion processes in the humid environment of vehicle service stations form the highest probability of failure, with a failure probability of approximately 97% over 10 years. For impact loads, this indicator is 75%, and for fatigue failure it is 38%. The combined probability of at least one failure within 10 years reaches 99.5%, indicating a practically guaranteed need for repair or replacement of elements regardless of the chosen material.

An additional analysis of critical defects based on the fracture toughness coefficient K_IC was carried out. Under normal operating conditions (σ = 2.67 MPa), critical crack sizes for both materials significantly exceed typical technological defects (a_c = 101 mm for KHVG and 45 mm for R6M5 at a_real = 0.1–0.5 mm), so the risk of failure is practically zero. However, under impact loading with stresses of approximately 300 MPa, the critical defect size for R6M5 decreases to 3.4 mm, while for KHVG it is 7.7 mm. This indicates the higher sensitivity of R6M5 to impact failure and the better impact toughness of KHVG steel. A compromise is necessary when combining high temperatures (> 400 °C) and impacts: R6M5 for heat resistance, but with mandatory shock absorbers to compensate for low K_IC.

The results of life cycle cost (LCC) modeling showed that at high failure probability (P_заг = 99.5%) and with lubrication use, the total life cycle costs for KHVG are 40,420 UAH, while for R6M5 they are 37,989 UAH. Savings of approximately 6% are achieved due to fewer expected replacements and higher resource stability. At low failure risk, KHVG is preferable due to lower material cost (180 UAH/kg vs 450 UAH/kg). At the same time, the use of TiN coatings in real conditions is not cost-effective due to the high risk of delamination, leading to increased repair and replacement costs.

Sensitivity analysis (Spider plot) showed that the failure probability has the greatest impact on total life cycle cost. A change in this parameter by only 2% leads to an increase in total costs by more than 4%, while variations in material cost, wear coefficient, or temperature have a much smaller impact. This indicates that risk management and reliability improvement are more effective optimization directions than solely reducing wear intensity.

Based on the integrated analysis, transition thresholds for the effectiveness of KHVG and R6M5 steels have been determined. It has been established that at temperatures below 300 °C and significant impact loads, it is more advisable to use KHVG steel due to its better impact toughness and lower cost. At temperatures above 400 °C, as well as under conditions of intensive abrasive wear (abrasive hardness above 800 HV), R6M5 is preferable, providing increased service life and reduced life cycle costs. Based on the obtained results, recommendations have been developed for the selection of materials, heat treatment regimes, and lubricants for typical technological tooling elements: clamping jaws, guide rollers, rest buttons, and press equipment supports.

Conclusions

An adapted abrasive wear model has been developed for vehicle service station operating conditions, taking into account contact geometry, temperature-induced hardness degradation, lubrication efficiency, and coating adhesion. The proposed approach provides a prediction error below 15% when empirical wear coefficients are applied, which confirms the applicability of the model for engineering assessment of wear-resistant materials.

The study established transition criteria for rational material selection depending on operating conditions. It was determined that at temperatures above 400°C and abrasive hardness exceeding 800 HV, R6M5 steel demonstrates the highest efficiency, providing an approximately 2.5-fold increase in service life and a 6–19% reduction in life cycle cost due to reduced replacement frequency. Under conditions of temperatures below 300°C and impact loads above 50 J, KHVG steel is preferable because of its higher fracture toughness and significantly lower material cost.

The analysis showed that under high failure probability conditions (P_заг > 0.9), replacement costs exceed material costs by 500–600 times. It was established that preventive measures, including automatic lubrication systems, shock absorbers, and roughness control, ensure a more significant reduction in life cycle cost than direct material substitution, with a potential economic effect of 10–15%.

The feasibility of TiN coating application for the investigated class of devices was evaluated. It was demonstrated that under real surface roughness conditions (R_a > 0.4 μm), the probability of coating delamination remains high, while the increase in wear resistance is insignificant even under ideal adhesion conditions. Therefore, the application of TiN coatings for such operating conditions is not practically justified.

Optimal heat treatment regimes for the investigated steels have been determined. For KHVG steel, the recommended treatment includes quenching at 830°C, tempering at 180°C, and stabilization at 300°C for 5 h. For R6M5 steel, the optimal regime consists of quenching at 1230°C followed by double tempering at 560°C.

The developed model is limited by the use of empirical fracture toughness and wear coefficient values, as well as Weibull distribution parameters obtained from limited statistical data. Under operating conditions significantly different from the assumed model parameters, the prediction error may increase to ±30%. Future

studies should focus on experimental validation of the proposed methodology under real vehicle service station conditions, extension of the algorithm to additional tool steels, and integration of the developed models into CAD/CAM systems for automated material selection and engineering decision support.

References

1. Haizol. (n.d.). Automotive CNC Machining: Parts, Materials, Tolerances and How to Source *Them*. Haizol. Retrieved May 27, 2026, from https://www.haizol.com/blog/automotive-cnc-machining?utm_source=chatgpt.com

2. MH Fixture. Precision machining process control for automotive engine cylinder blocks. MH Fixture. Retrieved May 27, 2026, from https://mhfixture.com/en/blog/engine-block-machining-process-control-precision?utm_source=chatgpt.com

3. Ogunnowo, E., Ogu, E., Egbumokei, P., Dienagha, I., & Digitemie, W. (2021). Theoretical framework for dynamic mechanical analysis in material selection for highperformance engineering applications. Open Access Research Journal of Multidisciplinary Studies, 1(2), 117-131. https://doi.org/10.53022/oarjms.2021.1.2.0027

4. Rahim, A. A., Musa, S. N., Ramesh, S., & Lim, M. K. (2020). A systematic review on material selection methods. Proceedings of the Institution of Mechanical Engineers, Part L: Journal of Materials: Design and Applications, 234(7), 1032-1059. https://doi.org/10.1177/1464420720916765

5. Zhang, H., Goltsberg, R., & Etsion, I. (2022). Modeling adhesive wear in asperity and rough surface contacts: a review. Materials, 15(19), 6855. https://doi.org/10.3390/ma15196855

6. Sibanda, D., Oyinbo, S. & Jen, T. (2022). A review of atomic layer deposition modelling and simulation methodologies: Density functional theory and molecular dynamics. Nanotechnology Reviews, 11(1), 1332-1363. https://doi.org/10.1515/ntrev-2022-0084

7. Laghari, M., Hassan, A., Haggag, M., Wahyudie, A., Tayfor, M., & Elsayed, A. (2025). Comparison of Recognition Techniques to Classify Wear Particle Texture. Eng, 6(6), 107. https://doi.org/10.3390/eng6060107

8. Falandys, K., Kurc, K., & Tutak, J. S. (2025). Application and Empirical Verification of the Archard Model in the Deburring Process. *Materials*, *18*(10), 2387. https://doi.org/10.3390/ma18102387

9. Bloor Engineering. (n.d.). Tempering steel: Temperatures, time, colour chart and properties. Bloor Engineering. Retrieved May 28, 2026, from https://www.bloorengineering.com/knowledge/tempering-steel-guide?utm_source=chatgpt.com

10. Chaus, A. S., & Kryshtal, A. P. (2023). New insights into the microstructure of M2 high-speed steel. *Materials Characterization*, *205*, 113313. https://doi.org/10.1016/j.matchar.2023.113313

11. Jin, K., Jin, W., Liu, B., Wu, K., & Wang, Z. (2025). Cost Calculation Model for Engineering Structures Based on a Life Cycle Perspective. *Buildings*, *15*(16), 2923. https://doi.org/10.3390/buildings15162923

12. Patil, Rajkumar & Waghmode, Laxman. (2014). Life Cycle Cost (LCC) Optimization of Band Saw Cutting Machine through Reliability Analysis. Retrieved May 28, 2026, from https://www.researchgate.net/publication/281064150_Life_Cycle_Cost_LCC_Optimization_of_Band_Saw_Cutting_Machine_through_Reliability_Analysis

Драч І.В., Вальчук І.К. Математичне моделювання та оптимізація вибору зносостійких матеріалів для технологічних пристроїв двз

Метою дослідження є розроблення інтегрованого підходу до вибору матеріалу зносостійких елементів технологічних пристроїв для обробки та ремонту двигунів внутрішнього згоряння з урахуванням механічних, термічних, економічних і ризик-орієнтованих чинників. Основну увагу приділено порівняльному аналізу сталей ХВГ та Р6М5 для затискних і базувальних елементів. У роботі використано математичне моделювання абразивного зношування на основі модифікованої моделі Арчарда з урахуванням температурної деградації твердості, умов змащення, геометрії контакту та впливу покриттів. Для оцінювання надійності застосовано ймовірнісну модель Вейбулла, а економічну ефективність визначено методом Life Cycle Cost (LCC). Проведено термомеханічне моделювання режимів термообробки та аналіз чутливості параметрів. Встановлено, що за температур понад 400 °С і високого рівня абразивного зношування сталь Р6М5 забезпечує більший ресурс і зниження LCC на 6 % (у базовому сценарії) та до 19 % (в оптимізованому сценарії зі зменшенням маси) порівняно зі сталлю ХВГ. За штатних умов експлуатації (Т < 300 °С, наявність ударних навантажень) перевага належить сталі ХВГ завдяки вищій в'язкості руйнування. Визначено оптимальні режими термообробки: для ХВГ- гартування за температури 830 °С, відпуск за 180 °С і стабілізація за 300 °С; для Р6М5 — гартування за 1230 °С і подвійний відпуск за 560 °С. Показано, що застосування мастильних матеріалів підвищує термін служби на 66 %. Доведено, що за високої ймовірності відмов (Рзаг > 0,9) витрати на заміну домінують над витратами на матеріал; мінімізація ризику (амортизатори, автоматичне змащення) є ефективнішою, ніж зміна марки сталі. Покриття TiN не рекомендовано за шорсткості поверхні R_a > 0,8 мкм через ризик відшарування.

Ключові слова: абразивний знос, технологічне оснащення, термообробка, модель Арчарда, модель Вейбулла, життєвий цикл, аналіз чутливості.